THE PETROLOGY AND GEOCHEMISTRY OF THE UPPER CRITICAL ZONE OF THE BUSHVELD COMPLEX AT THE AMANDELBULT SECTION OF RUSTENBURG PLATINUM MINES LIMITED, NORTHWESTERN TRANSVAAL, SOUTH AFRICA.

by

MATTHEW FIELD, B.Sc Hons.

Thesis presented for the degree of Master of Science in the Department of Geology, Rhodes University, Grahamstown.

January, 1987.

DECLARATION

All the work in this thesis is the original work of the author, except where specific acknowledgement is made to the work of others

SIGNED:

Matthew Field
De Beers Geology Department
P.O. Box 47
Kimberley
8300.

January 1987.

ABSTRACT

A study of petrological and geochemical variations through the upper Critical Zone of the Bushveld Complex at Amandelbult section of R.P.M. was undertaken.

The sequence at this locality may be divided into seven "Units", two of which appear to be complete, possessing the sequence harzburgite-pyroxenite-norite-anorthosite. The other five Units lack basal, intermediate or upper members. Considerable lateral variations are apparent in this sequence, but these are restricted to the Lower Pseudo Reef-Merensky Reef interval, the same portion of the succession which is affected by pothole structures.

The single most important petrographic feature of genetic significance is the occurrence of annealed, recrystallized anorthosite immediately underlying ultramafic layers. This, together with the undulatory nature of the contact between the two rock layers, suggests that the ultramafic layer was emplaced as a hot liquid over a pre-existing, crystalline anorthosite floor, and that some remelting of this layer occurred.

Variations in the chemical make-up of constituent silicate minerals reveal a number of significant processes which may have been operative in the magma chamber prior to crystallization. Olivine grains, for instance, exhibit extremely wide chemical variations both within single layers and from one layer to the next. These variations are best explained by re-equilibration processes with spinel and base metal sulphides, rather than by wide variations in original liquidus compositions. It appears that the compositions of the initial liquids from which each basal olivine-bearing layer crystallized, were approximately similar. Variations in the iron-magnesium ratio of ortho-pyroxenes indicate well defined continuous fractionation trends in units which are considered to be complete. Magnesian compositions are recorded in ultramfic members, while increasingly iron-enriched values are recorded upwards through the sequence pyroxenite-norite-anorthosite. Plagioclase grains exhibit less well defined fractionation trends, but it is clear that an upward increase in An is encountered through individual Units. This is in direct contrast to the trend exhibited by orthopyroxene. A further feature of plagioclase grains is the considerable degree of chemical zonation exhibited by them. In cumulus grains this is commonly manifested as strongly reversed rims, while in intercumulus grains normal zoning is ubiquitous.

Whole-rock chemical variations through the succession indicate that cyclical variations occur through successive Units, but that these merely reflect changes in modal mineralogy and not liquid fractionation trends. Such trends can be shown for selected element ratios, where these elements are known to partition into a single mineral phase. Ratios of pyroxene components such as the nickel/scandium ratio, exhibit a saw-tooth pattern through successive Units, while ratios of

plagioclase components such as the strontium/alumina ratio have unique, fairly constant values for each individual Unit but different values for successive Units. The latter type of cyclicity is not always strictly confined to lithologically recognized boundaries between Units, and a slight overlap into overlying ultramafic layers is apparent.

An investigation of variations in trace element levels in a single layer in five widely separated boreholes revealed that there is some evidence for a lateral fractionation trend from the southwest (more primitive) to the northeast (more evolved), although the small number of data points available preclude definite conclusions.

There exists in the data some evidence, that the Giant Mottled Anorthosite differs chemically from the other anorthosites in the study section, and that it more closely resembles rocks of the Main Zone. This evidence is particularly apparent in variations of the chromium/aluminium ratio of orthoyroxene grains, and in the An content of plagioclase grains, both of whose trends exhibit distinct inflections at the base of this member.

The features of the succession at Amandelbult are best explained by the model of Eales et al. (in press,a), which visualizes the input of a number of pulses of new, hot liquid into a magma chamber containing the fractionated residua of previous influxes. At a critical point in time, just prior to the mafic Merensky Reef input, a large input of gabbroic liquid was intruded at high levels in the chamber. The lower portions of this liquid mixed with the residua of earlier mafic inputs, which in turn mixed with new inputs of mafic, typical Critical Zone liquids. Thus the lower portions of the study section represent mixtures of new Critical Zone liqiuds with the residua of previous such influxes, while the upper portions have the added complication of mixture with a Main Zone-type liquid. The unique chemical character of the Giant Mottled Anorthosite appears to be a direct manifestation of the influence of the Main Zone liquid.

CONTENTS.

page

CHAPTER 1: INTRODUCTION. 1
1.1 Motivation 1
1.2 Nomenclature 2
1.3 An Overview of the Bushveld Complex 4
1.3.1 Tectonic and Structural Setting 5
1.3.2 The Layered Sequence 8
1.4 The Regional Setting of Amandelbult 11
1.5 Sampling Procedures and Localities 13
CHAPTER 2: STRATIGRAPHY 14
2.1 Introduction 14
2.2 Stratigraphic Descriptions 15
2.2.1 The UG-1 Unit 15
2.2.2 The UG-2 Unit 16
2.2.3 The Lower Pseudo Unit 16
2.2.4 The Upper Pseudo Unit 17
2.2.5 The Footwall Unit 18
2.2.6 The Merensky Unit 18
2.2.7 The Bastard Unit 19
2.3 Lateral Variations and Other Stratigraphic Complications 20
2.3.1 Lateral Variations 20
2.3.2 Potholes 21
2.3.3 Iron-rich Pegmatites 23
CHAPTER 3: PETROGRAPHY 25
3.1 Introduction 25
3.2 Anorthosites 25
3.3 Norites 29
3.4 Pyroxenites 33
3.4.1 Poikilitic Pyroxenites 33
3.4.2 Pegmatoidal Pyroxenites 37
3.4.2.1 The Merensky Reef 37
3.4.2.2 The Lower Pseudo Reef 39
3.4.2.3 The UG-1 Pegmatoidal Pyroxenite 40
3.5 Harzburgites 41
3.6 Chromitites 42
CHAPTER 4: MINERALOGY 45
4.1 Introduction 45
4.2 Olivine 45
4.2.1 Fe-Mg Relationships 46
4.2.2 Ni-Olivine Relationships 48
4.2.3 Mn-Olivine Relationships 52
4.3 Pyroxenes 52
4.3.1 Introduction 52
4.3.2 Major and Minor Element Variations of Orthopyroxenes 54
4.3.3 Fe-Mg Variations in Orthopyroxenes through the Succession 58
4.3.4 Cr/Al and Cr/Ti Variations in Orthopyroxenes 59
4.3.5 Clinopyroxene 60
4.4 Plagioclase 61
4.4.1 Intercumulus Grains 62
4.4.2 Unrestrained Cumulus Grains 63
4.4.3 Restrained Cumulus Grains 64
4.4.4 Variations in Plagioclase Composition with Stratigraphic Height 65
4.5 Discussion 66

4.5.1 Causes and Implications of Chemical Zoning of Feldspars.....66
4.5.2 Cryptic Cyclical Variations in Mineral Chemistry.....67
4.5.3 The Critical Zone-Main Zone Boundary.....70
CHAPTER 5: WHOLE-ROCK GEOCHEMISTRY.....72
5.1 Major Elements.....72
5.1.1 Variation Diagrams.....73
5.1.2 Variations with Stratigraphic Height.....74
5.1.3 Normative Data.....75
5.2 Trace Elements.....76
5.2.1 Nickel, Copper and Cobalt.....77
5.2.2 Vanadium, Scandium and Zinc.....80
5.2.3 Chromium.....82
5.2.4 Strontium.....83
5.2.5 Zirconium, Yttrium and Rubidium.....83
5.3 Trace Element Variations through the UG-2 Poikilitic Pyroxenite.....84
5.4 Discussion.....86
5.4.1 Compatible Elements; Evidence for Cyclicity.....86
5.4.2 Incompatible Elements.....89
CHAPTER 6: DISCUSSION.....92
6.1 Introduction.....92
6.2 Existing Models.....92
6.2.1 The Wager and Brown (1968) Model.....92
6.2.2 Irvine's (1980) Model.....94
6.2.3 Vermaak's (1976) Model.....97
6.2.4 The Model of Irvine, Keith and Todd (1983).....99
6.2.5 The Models of Campbell et al.(1983) and Naldrett et al.(1986).....101
6.2.6 The Model of Eales, Marsh, Mitchell, De Klerk, Kruger and Field (1986; in press).....104
6.3 Evaluation of the Models.....106
6.4 Towards a Model.....111
CHAPTER 7: CONCLUSIONS.....115
APPENDIX A. X-Ray Flourescence Spectrometry.....118
APPENDIX B. Electron Microprobe Analyses.....120
REFERENCES.....123
ACKNOWLEDGEMENTS.....129

LIST OF FIGURES.

Figure 1.1. The I.U.G.S. classification scheme for gabbroic and ultramafic plutonic rocks (after Streckeisen, 1976). This scheme is used to classify the rocks of the study section, but only cumulus mineral constituents are considered.

Figure 1.2 A more rigid classification of the rocks of the upper Critical Zone at Union Section of R.P.M. (after Eales et al., in press), based on geochemical criteria. This scheme is equally applicable to the rocks at Amandelbult.

Figure 1.3a. A map showing the regional geology of the western Transvaal, and the localities of the mines referred to in the text. (After Viljoen et al.,1986)

Figure 1.3b. A map showing the surface geology of the area around Amandelbult Section of R.P.M.

Figure 1.3c. A map of the southwestern portion of Amandelbult Section, showing the outcrop of the Merensky Reef, the positions of pothole structures, and the positions of the boreholes which were sampled sampled. (Reproduced with permission of the Mine Geologist of Amandelbult Section of R.P.M.).

Figure 1.4a Logs of boreholes AD, AE and AF. The numbers marked down the right hand side of each log represent individual sample positions.

Figure 1.4b Logs of boreholes AW, AX and AZ. Note that samples were only taken from the UG-2 pyroxenite layer, and that boreholes AW and AX represent "pothole" successions.

Figure 2.1 The stratigraphic subdivision of (a) the Bushveld Complex, (b) the Rustenburg Layered Suite and (c) the study section at Amandelbult. Thicknesses of suites and zones in columns (a) and (b) are taken from SACS (1980), while those in (c) were measured in borehole cores.

Figure 2.2a Photograph showing the nature of the Giant mottled anorthosite at Union Section of R.P.M. This member is not exposed in mine workings at Amandelbult.

Figure 2.2b Photograph showing the undulatory contact of the Merensky Reef and the underlying Footwall anorthosite.

Figure 2.2c Photograph showing fine, inch-scale layering in norite below the Footwall Marker. This is at approximately the same stratigraphic position as the "stripies" horizon at Union Section.

Figure 2.2d Photograph showing the sharp, undulatory contact between the P2 middling anorthosite/leuco-

troctolite and harzburgite of the Upper Pseudo Reef. Note the bleached nature of the anorthosite in the scalloped area in the centre of the photograph. Examination of this rock in thin section revealed a recrystallized texture.

Figure 2.2e Photograph showing the irregular and sharp nature of the contact between norite and harzburgite of the Lower Pseudo Reef. Note the fragments of harzburgitic material trapped in lower parts of the norite

Figure 2.2f Photograph of the P2 middling anorthosite sandwiched between the two harzburgitic layers of the Upper pseudo Reef.

Figure 2.2g Photograph of the thin pegmatoidal pyroxenite layer underlying the UG-2 chromitite layer. The painted arrow head is on chromitite.

Figure 2.2h Photograph of the basal portions of the UG-1 chromitite at Union Section. Similar features are seen in core specimens at Amandelbult, where the UG-1 is only poorly exposed underground.

Figure 2.3 A more detailed log of the Pseudo Unit intersection of borehole AE, which shows more clearly the nature of harzburgite and olivine-bearing pyroxenite horizons of the Pseudo and Footwall Units.

Figure 2.4 This diagram shows the lateral variations of "normal" successions at Amandelbult (after Viljoen et al., 1986).

Figure 2.5 Variations in the thickness of the Merensky Reef layer at Amandelbult, and the distribution of pothole structures (after Viljoen et al., 1986).

Figure 2.6 A dip-section showing the essential features of a pothole structure, and the development of the various types of "Reefs". Here BR- Bastard Reef, MR- Merensky Reef, P-1- Upper Pseudo Reef, P-2- Lower Pseudo Reef.

Figure 2.7 The distribution of ultramafic pegmatite (dunite/pegmatoid) at Amandelbult (after Viljoen et al., 1986)

Figure 3.1a Photomicrograph of a typical mottled anorthosite, with intercumulus orthopyroxene which poikilitically enclose cumulus plagioclase grains. Note the smaller, rounded nature of the enclosed grains.

Figure 3.1b Photomicrograph of an "adcumulus anorthosite", which consists entirely of plagioclase. Note the preferred orientation of the larger grains and the cluster of smaller grains (upper right), which

Figure 3.1c Photomicrograph of the contact between harzburgite and an "annealed anorthosite". The two rock types are seperated by a thin chromitite layer (dark grains in the centre). Note the recrystallized nature of the plagioclase grains.

Figure 3.1d Photomicrograph of a resorbed olivine grain in the Footwall anorthosite of borehole AF.

Figure 3.1e Photomicrograph of a sulphide bleb (dark patch, lower right) in the Merensky anorthosite.

Figure 3.1f Photomicrograph of intercumulus magnetite (dark patches, centre right) in the Giant Mottled Anorthosite.

Figure 3.1g Photomicrograph of the P2-middling leuco-troctolite showing the presence of olivine grains, whose outer reaches contain inclusions of plagioclase.

Figure 3.1h Lower magnification photomicrograph of the P2-middling leucotroctolite, showing the predominance of cumulus plagioclase over olivine.

NOTE: The scale bar below each photomicrograph represents 1 millimetre.

Figure 3.2a Photomicrograph of a cumulus orthopyroxene grain in norite, showing a late-stage overgrowth which poikilitically encloses small plagioclase grains.

Figure 3.2b Photomicrograph of a norite, showing the occurrence of two different orthopyroxene habits.

Figure 3.2c Photomicrograph of a norite showing the poikilitic enclosure of orthoproxene and plagioclase by clinopyroxene.

Figure 3.2d Photomicrograph of cumulus orthopyroxene in norite, showing the development of fine exsolution lamallae of clinopyroxene parallel to the (100) crystallographic direction of the host grain.

Figure 3.2e Photomicrograph of a poikilitic pyroxenite, showing the interpenetration of cumulus ortho-pyroxene grains, and the nature of intercumulus plagioclase.

Figure 3.2f Photomicrograph showing the enclosure of cumulus orthopyroxene by intercumulus clinopyroxene. Note the resorbed nature the enclosed grains.

Figure 3.2g Photomicrograph of poikilitic pyroxenite under-lying a thin chromitite later. Note the presence of an extremely elongated orthopyroxene grain, whose direction of elongation parallels the base of the chromitite layer.

Figure 3.2h Photomicrograph showing a strained cumulus orthopyroxene grain, whose exsolution lamallae are kinked. Note also, that the intercumulus

plagioclase grains are polygonized, further evidence of strain.

Figure 3.3a Photomicrograph showing the presence of a myrmekitic intergrowth of quartz and plagioclase in the intercumulus assemblage of poikilitic pyroxene.

Figure 3.3b Photomicrograph of a poikilitic pyroxenite, showing the presence of cumulus orthopyroxene and intercumulus plagioclase. Note also the co-existence of strained and unstrained cumulus grains.

Figure 3.3c Photomicrograph showing the presence of calcite in the intercumulus assemblage of pokilitic pyroxenite.

Figure 3.3d Photomicrograph of the pegmatoidal pyroxenite of the Merensky Reef, showing the presence of coarse olivine grains, and large intercumulus plagioclase grains.

Figure 3.3e Photomicrograph showing the enclosure of a rounded plagioclase grain in an altered cumulus olivine grain in the Merensky Reef.

Figure 3.3f Photomicrograph of a finer-grained olivine grain, showing the development of a reaction rim of clinopyroxene, in the Merensky Reef.

Figure 3.3g Photomicrograph showing a symplectic intergrowth of olivine and orthopyroxene in the Merensky Reef.

Figure 3.3h Photomicrograph of Upper Pseudo Reef harzburgite, showing the presence of cumulus olivine and orthopyroxene.

Figure 3.4a Photomicrograph of a harzburgite, showing the poikilitic enclosure olivine by orthopyroxene.

Figure 3.4b Photomicrograph of a resorbed, elongated orthopyroxene grains adjacent to a thin chromitite layer.

Figure 3.4c Photomicrograph of an un-annealed chromitite layer.

Figure 3.4d Photomicrograph of an annealed chromitite layer.

Figure 3.4e Photomicrograph of an un-annealed chromitite layer, in which stacks or chains of chromite layers can be recognized.

Figure 3.4f Photomicrograph showing the occurrence of ovoid structures which possibly describe the original outlines of orthopyroxene grains, which have since been resorbed.

Figure 3.4g Photomicrograph of a chromite inclusion orthopyroxene, around which a plagioclase halo has

developed.

Figure 3.4h Photomicrograph of an opaque grain which poikilitically encloses intercumulus plagioclase.

Figure 4.1 A stratigraphic log showing the positions of samples which were analysed by electron microprobe, and the mineral species which were analysed.

Figure 4.2 A plot of mole percentage Fo in olivine, against a stratigraphic log. Here P-1, P-2 and MR refer to Lower Pseudo, Upper Pseudo and Merensky Reef respectively.

Figure 4.3 A plot of Fo mole percent against NiO for olivine grains. In (a) each individual analysis is plotted, and in (b) averged analyses for each sample are plotted. The error bars in (b) represent one standard deviation. Symbols: stars - Merensky Reef; solid triangles - P2 middling; open triangles - P2 marker (base of Footwall Unit); open circles - base of UG-2 Unit; solid circles - Upper Pseudo Reef, upper layer; solid squares - Upper Pseudo Reef, lower layer; open squares - Lower Pseudo Reef

Figure 4.4 A plot of Fo mole percent against MnO for olivine grains. Each data point represents an average per sample, and error bars one standard deviation. Symbols are the same as for figure 4.3.

Figure 4.5 The pyroxene quadrilateral, showing averaged compositions per sample. Superimposed on the diagram are the fractionation trends of Atkins (1969).

Figure 4.6 Variation diagrams in which major and minor element compositions (as weight percentages) of orthopyroxenes are plotted against MgO. Each data point represents a single analysis, except where such points are very close to one another.

Figure 4.7 Variations in orthopyroxene chemistry plotted against a stratigraphic column. In (a) the MMF (atomic Mg/Mg+Fe) ratio is plotted for each individual analysis. In (b) and (c) averaged Cr/Al and Cr/Ti are plotted, where the error bars represent one standard deviation.

Figure 4.8 Clinopyroxene composition, represented by En mole percent (Mg/Mg+Fe+Ca), and Wo (Ca/Mg+Fe+Ca). Here each individual analysis is plotted.

Figure 4.9 Variations in plagioclase chemistry represented on a portion of the Ab-An-Or diagram. Analyses are presented for each Unit for intercumulus and cumulus grains.

Figure 4.10 Microprobe profiles, in terms An mole percent and potassium in parts per million, across an intercumulus plagioclase grain. The profile represents

a complete profile from grain rim to grain rim.

Figure 4.11 Three microprobe profiles across cumulus plagioclase grains, in terms of An mole percent and potassium. In (a) an anorthitic core is rimmed by a more albitic margin. In (b) a reversed anorthitic margin is evident at both ends. In (c) a strongly anorthitic margin is apparent on one margin only.

Figure 4.12 A plot of plagioclase analyses, in terms of An mole percent, against a stratigraphic log. Here squares represent intercumulus grains, circles cumulus unrestrained grains, and triangles cumulus restrained grains. Open symbols represent grain margins, and solid symbols grain cores.

Figure 5.1 Variation diagrams in which major element concentrations are plotted against MgO.

Figure 5.2 Variations in major element oxide levels through the stratigraphic column.

Figure 5.3 Variations in normative constituents. In (a) the relative variations of the four major normative constituents are presented. In (b) variations in the level of Sr in normative plagioclase are shown.

Figure 5.4 Varaition diagrams of trace elements, plotted against MgO.

Figure 5.5 Variations in trace element levels through boreholes AE and AF.

Figure 5.6 Trace element varaitions through the poikilitic pyroxenite of the UG-2 Unit. Symbols for the five boreholes are; AE- solid triangles, AF- solid squares, AW- open circles, AX- solid circles, and AZ- open triangles.

Figure 5.7 Variations of selected trace element ratios through the UG-2 pokilitic pyroxenite. The symbols are the same as for figure 5.6.

Figure 5.8 Plan-diagrams of Amandelbult showing averaged Ni/Sc and Co/Sc values for the UG-2 poikilitic pyroxenite in each of five boreholes. These values only reflect samples which do not contain olivine, chromite, or base metal sulphides.

Figure 5.9 Geochemical variations through the succession which indicate cyclicity. In (a), the $Sr/Al_2O_3^*$ ratio is designed to eliminate the presence of Al in pyroxene (see text for details), so that the ratio indicates variations in plagioclase components. In (b) and (c) variations reflect changes in pyroxene components.

Figure 5.10 A plot of MgO against Sr for the Footwall, Merensky and Bastard Units, which shows that a unique linear trend can be defined for norite and anorthosite rocks of each Unit.

Figure 6.1 A conceptual model which describes the seqeunce of events which led to the formation of the study section. Refer to the text for details.

LIST OF TABLES.

Table 4.1 Averaged olivine analyses for each of the olivine-bearing samples which were sampled. The analyses show weight percentage concentrations of element oxides, the number of cations, based on 4 oxygens, and the number of analyses used in the average (N).

Table 4.2 Averaged orthopyroxene analyses for each sample. The analyses show weight percentage concentrations of element oxides, the number of cations based 6 oxygens, and the number of analyses in the average (N).

Table 4.3 Averaged clinopyroxene analyses. The analyses show weight percent concentrations of element oxides, the number of cations based on 6 cations, and the number of analyses in the average (N).

Table 4.4 Representative plagioclase analyses. The analyses show weight percent concentrations of element oxides and the number of cations, based on 32 oxygens. Analysis codes are: R- rim of grain, C- core of grain and RS- restrained grain.

Table 5.1 Whole-rock analyses for samples from borehole AE. These include major elements, without H2O- and LOI, as well as trace elements.

Table 5.2 C.I.P.W. weight percent norms for samples from borehole AE. The normative mineral codes are;

Ap - apatite	En - enstatite
Il - ilmenite	Fs - ferrosilite
Or - orthoclase	Wo - wollastonite
An - anorthite	Hy - hypersthene
Ab - albite	Q - quartz
C - corundum	Fo - forsterite
Mt - magnetite	Fa - fayalite
Di - diopside	MgNo is the magnesium number.

Table 5.3 Trace element analyses for boreholes AF, AW, AX and AZ.

Table 5.4 Some distribution coefficient data, taken from the literature.

CHAPTER 1 : INTRODUCTION.

1.1 Motivation.

In recent years considerable research has been conducted on rocks of the Bushveld Complex in the western and northwestern Transvaal, by staff and postgraduate students of the Geology Department at Rhodes University. This work has concentrated largely on aspects of the layered rocks of the upper Critical Zone and intrusive ultramafic pegmatites at the Rustenburg and Union Sections of Rustenburg Platinum Mines Limited (R.P.M.). The only previous work on petrographical and geochemical aspects of a similar sequence of upper Critical Zone rocks at the Amandelbult Section of R.P.M. was conducted by Scoon (1985), whose main theme was ultramafic pegmatites. Therefore, a more intensive investigation of these rocks was desirable, to gain greater insight into variations which occur within this compartment of the Complex. This thesis was written to document such an investigation. The project was carried out as part of the Council for Scientific and Industrial Research's Cooperative Scientific Project on the Bushveld Complex. The long-term aim of this project is to document the geology and geochemistry of the Complex as extensively as possible, and to use the data so gained to arrive at a genetic model which satisfactorily explains most of the features of the Complex, but in particular the origin of Merensky Reef-type platinium group element mineral deposits.

1.2 Nomenclature.

At the outset of this chapter it is necessary to review the terminology of layered igneous rocks. Much of the pioneering work in this field was done on the Skaergaard intrusion of Greenland, by workers such as Wager, Brown and Wadsworth (1960). Their interpretation of the layering which is developed in this intrusion, is that it formed as a direct result of crystals nucleating and then settling out of the host liquid to form layers on the floor of the magma chamber, in a sedimentary fashion, under the influence of gravity. These crystals were referred to as "cumulus" crystals, while any melt which might have become trapped between them was called intercumulus, and any minerals which subsequently crystallized from the intercumulus melt would therefore be postcumulus minerals. This became known as the cumulus theory.

In more recent investigations many workers have seriously questioned the validity of gravity settling as the dominant mechanism for the formation of layered intrusions. Foremost amongst these were Campbell (1978), McBirney and Noyes (1979) and Morse (1979). One of their most serious objections was that the density of plagioclase is too low for it to sink in basaltic liquids. The terminology introduced by Wager et al. (1960), has however become entrenched in descriptions of layered rocks. Irvine (1982), in a review of terminology for layered intrusions, recommended that the terminolgy introduced

by Wager et al. (op.cit.) be retained, and that it be used in a non-genetic sense.

A cumulate rock is defined (Irvine, 1982) as an igneous rock characterized by a cumulus framework of touching mineral grains that were evidently formed and concentrated primarily through fractional crystallization. The fractionated crystals are called cumulus crystals. They are typically subhedral to euhedral in habit and are cemented together by texturally younger postcumulus material. This material appears to have crystallized from the intercumulus liquid which occupied the interstices of the cumulus framework. In orthocumulate rocks there is abundant (25-20%) postcumulus material and the cumulus minerals should ideally exhibit many of their original crystallization forms. Mesocumulates have less postcumulus material (7-25%) and cumulus grains should adjoin in part along mutual interference boundaries developed through overgrowth. Adcumulates have only minor discrete postcumulus material (0-7%), and mutual interference boundaries between cumulus grains must be common.

The nomenclature used in the naming of the rocks of the study section is based on that proposed by the I.U.G.S. (International Union of Geological Sciences) subcommission on the systematics of igneous rocks for gabbroic and ultramafic rocks (Streckeisen, 1976) presented in figure 1.1. The nomenclature adopted here however, considers only the cumulus constituents of each rock in the main name. For example, a rock consisting of cumulus orthopyroxene and cumulus olivine could be called

Figure 1.1. The I.U.G.S. classification scheme for gabbroic and ultramafic plutonic rocks (after Streckeisen, 1976). This scheme is used to classify the rocks of the study section, but only cumulus mineral constituents are considered.

Figure 1.2 A more rigid classification of the rocks of the upper Critical Zone at Union Section of R.P.M. (after Eales et al., in press), based on geochemical criteria. This scheme is equally applicable to the rocks at Amandelbult.

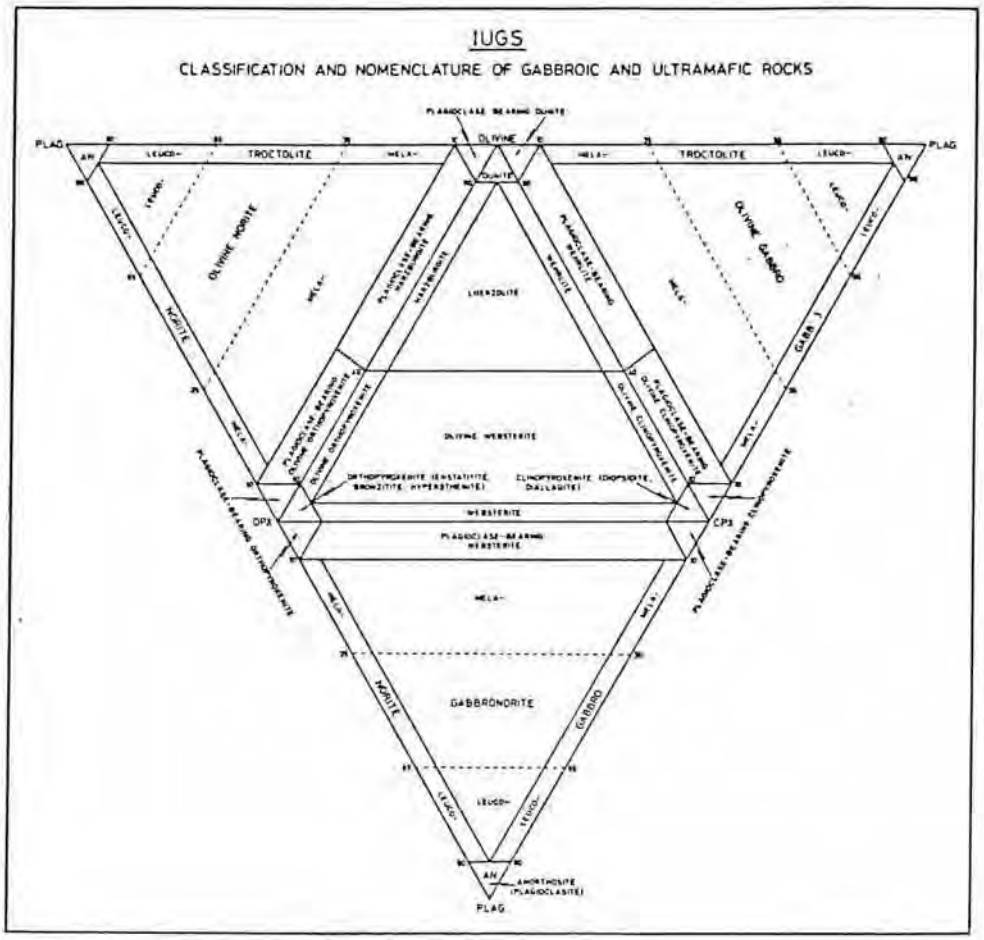

Figure 1.1

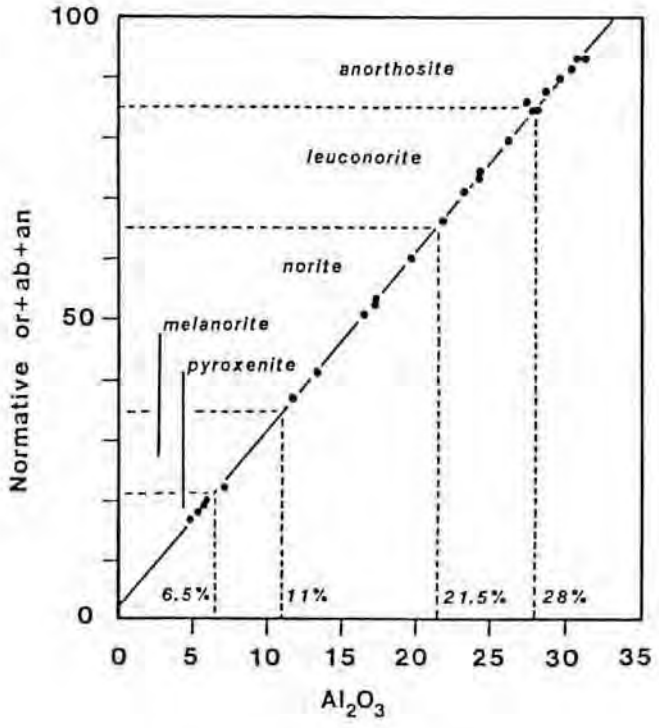

Figure 1.2

either a harzburgite or an olivine orthopyroxenite depending on the relative proportions of these two phases present in the rock. Certain modifiers are introduced here to broaden the classification. For example, if a rock contains a large modal proportion of postcumulus feldspar, it may be referred to as a feldspathic pyroxenite. Norites exhibit a wide compositional range which is based upon varing proportions of cumulus plagioclase and orthopyroxene, and it is convenient therefore to divide them into three groups based on their relative proportions of dark (orthopyroxene) and light (plagioclase) coloured minerals into leuco-, meso- and melano- members. For the sake of brevity the prefix "meso-" is usually dropped. Textural terms may also be used to modify rock names, and here the terms "poikilitic" and "pegmatoidal" are most commonly used to distinguish two varieties of pyroxenite. Another term which has become entrenched in the literature is "mottled", which has been used to describe certain anorthosites which contain large oikocrysts of pyroxene which impart a mottled appearance to the rock. Eales et al. (in press) have shown that this nomenclature can be more rigidly defined on a chemical basis, and their classification is presented in figure 1.2.

1.3 An Overview of the Bushveld Complex.

The Bushveld Complex is a large body of igneous rock, whose east-west and north-south diameters are approximately 400 km and 200km respectively. It was intruded into the sediments of the Transvaal Sequence between 2095 and 1670 million years ago

(Tankard et al., 1982), and consists of a wide diversity of rock types, ranging from ultramafic dunites and peridotites, through mafic gabbros, norites and anorthosites to felsic granites and granophyres. Hall, a pioneering worker, suggested in 1932 that the Complex is made up of five megascopic components, namely; a volcanic phase represented by the volcanics of the Pretoria Group; a sill phase represented by various satellite intrusions of gabbro, diorite and diabase found around the periphery of the Complex; an epicrustal phase, the Rooiberg felsites; a main plutonic phase making up the layered rocks; and a late plutonic phase represented by the Bushveld granites. Although there is some doubt about the relationship between the Pretoria Group volcanics and the Complex, the other phases are clearly recognizable. Their relative chronologies, particularly that of the Rooiberg felsites, are still not clear however.

1.3.1 Tectonic and Structural Setting.

The Bushveld Complex intrudes the the predominantly sedimentary sequence of the Transvaal Group. The Transvaal basin was just one of a number of sedimentary basins which formed on the Archaean Kaapvaal craton during Proterozoic times. Prior to the intrusion of the Complex, this cratonic region had been subjected to a considerable number of ultramafic igneous events, including the komatiitic lava flows of the Onverwacht, intrusion of plutonic complexes such the Usushwana, Mambula and Muldersdrif, the extrusion of Dominion Group andesites and the

massive outpourings of Ventersdorp lava. Even within the Transvaal sequence itself magmatic activity in the form of the Hekpoort andesites and Dullstroom basalts, is evident. It is clear therefore, that the Bushveld Complex does not represent an isolated igneous event.

The mode of intrusion of the Bushveld Complex has been widely debated. Early interpretations by Hall (1932) suggested that the Complex was intruded as a single, large lopolith. This theory has been dismissed in more recent years, particularly since the results of a number of geophysical surveys have became available. Truter (1955) was the first to suggest that the Complex consists of a number of separate compartments, and this was supported by the results of the gravity survey of Smit et al. (1960), and later by numerous other surveys, including those of inter alia, Walraven and Darracott (1976) and Molyneaux and Klinkert (1978). This division of the Complex into four seperate compartments, namely the far-western, western, eastern and northern is still favoured today (Lee and Sharpe, 1986).

Structurally, the Bushveld Complex was intruded into a terrain that is dominated by east-northeast and north-northwest trends. Tectonic movements along these trends are thought have been important in the development of the successive sedimentary basins which formed on the Kaapvaal craton, and in particular, they are thought to have been responsible for the southeast to northwest migration of the depositional axes of the successive

basins. Lee and Sharpe (op.cit.), who used Landsat images to aid structural interpretation, defined six structural domains in the host rocks of the Bushveld Complex, each of which contains a unique set of lineaments. In most of these domains the lineaments are apparently related to other major structural features such as the Johannesburg Dome or Pilansberg Alkaline Complex.

A number of theories have been proposed in order to explain the position and form of the Complex. Hamilton (1970) and Rhodes (1975) suggested a meteorite impact origin, but since no direct evidence can be found to prove this, the theory has not been greatly favoured. Van Biljon (1976) related the Bushveld to plate-tectonic theory, and suggested that the eastern and western lobes were once joined, and have since been separated by a spreading-centre. Pretorius (1973), in a comprehensive treatment of the Archaean and Proterozoic structure of southern Africa, suggested a that concentric pattern of tectonic domains is centred around central Zimbabwe, and that a number of radially disposed upwarps diverge from this nucleus. The Great Dyke parallels one of these upwarps, while its extensions bisect the long axis of the Bushveld Complex in the south and, it may be linked up with the younger East African Rift system in the north. This evidence suggests that the Complex may have been intruded along a deep-seated fracture system. Hunter (1976) proposed that the emplacement of the Complex occured in response to compression which induced horizontal stresses, but that these were not due to basinal subsidence alone (Hunter and Hamilton, 1978). Sharpe and Snyman (1980) developed a hypothesis

based on thin-elastic plate theory, and on a study of deformation in the Kaapvaal Craton during Transvaal sedimentation. They suggest that the intrusion of satellite diabase sills occured in response to depression of Transvaal sediments in a domain of horizontal compression. Further subsidence lead to the intrusion of the Complex proper along zones of shear failure. In addition it is suggested that the feeders of the Complex lie on two elliptical traces which represent two large-scale inverted conic fractures. These are thought to have originated as a result of brittle failure of the crust brought about by mantle diapirism. Lee and Sharpe (1986) could find no evidence to suggest that the location and form of the Bushveld Complex were influenced by deep-seated crustal fractures, and instead they point out two important observations. Firstly, that the the locus of the Transvaal basin, the Bushveld Complex and the greatest development of Bushveld granite lie along the Great Dyke-Bushveld lineament, and secondly that all the feeders of the eastern compartment of the Complex lie along a prominent 010o trend, while the two feeders of the western compartment lie on a prominent 165o lineament. The former observation is thought to represent a single waxing and waning asthenospheric bulge, while the latter emphasizes the importance of local structural factors.

1.3.2 The Layered Sequence.

The rocks constituting the study section cannot be considered in isolation from the enormous thickness of underlying and overlying layered rocks, as these are in stratigraphic

continuity with them, and their genesis is likely to be intimately interwoven with those of the study section. It is therefore necessary to consider briefly the megascopic characteristics of the layered suite. These rocks constitute Hall's (1932) Main Plutonic Phase, or in more recent terminology, the Rustenburg Layered Suite (S.A.C.S., 1980). The subdivision of this Suite has undergone numerous changes in the past 50 years (see S.A.C.S., 1980, p 234), of which the informal subdivision of S.A.C.S. (1980) is adopted in this thesis. As a direct result of poor outcrop in the western Transvaal, most stratigraphic descriptions of the layered succession have been made on exposures in the eastern compartment, and although megascopic similarities exist between the two lobes their consanguinuity cannot be assumed. It was for this reason that the following descriptions are restricted to those features which have been observed in outcrop in the western lobe.

The Marginal, Lower and lower Critical Zones are best known from the region west of the Pilansberg. Here the Marginal Zone rocks, which overlie metamorphosed Transvaal sediments, are 800 metres thick and can be divided into five cyclic units (Engelbrecht, 1985), each consisting of olivine norite, gabbroic norite and norite or websterite. The Lower Zone consists largely of interlayered olivine norite, norite, and bronzitite, with minor dunite and harzburgite layers. It has been described by Engelbrecht (op.cit.) as a zone of low plagioclase content. It is approximately 1000 metres thick.

The base of the Critical Zone is defined by the first occurrence of a significant chromitite layer, the LG-1 chromitite. The Critical Zone is interspersed with a variable number of these layers, which have been divided into three groups, the Lower Group (LG), the Middle Group (MG) and the Upper Group (UG) chromitites. In the western Bushveld eight LG, four MG and two UG chromitite layers have been recognized. Apart from chromitites the Critical Zone consists largely of bronzitite and harzburgite layers in its lower regions, while above the MG-2 chromitite, rocks bearing cumulus plagioclase, such as norites and anorthosites begin to dominate. It is within this upper portion of the Critical Zone that the present study section is located.

The boundary between the Critical and Main Zones is somewhat debatable and uncertainty exists as to where it should be placed. Some authors, such as Kruger (1983), place it above the Merensky Reef, while others, such as Eales et al. (in press,a), provide strong geochemical evidence for it to be placed at the top of the Bastard Unit. Tankard et al. (1982) define the Main Zone as those rocks which contain cumulus clinopyroxene and lack chromite. This zone contains a great thickness (2700-4400 metres, S.A.C.S.,1980) of interlayered norite, gabbro and anorthosite.

The Upper Zone is characterized by the occurrence of three distinctive cumulus minerals, namely magnetite, apatite and fayalitic olivine, each of which has been used to define a

different subzone. Subzone A contains numerous composite magnetitite layers overlain by magnetite gabbro, while Subzone B is dominated by troctolite and Subzone C contains cumulus apatite in troctolite layers. The uppermost layer of this Zone appears to be the most highly evolved lithology in the layered succession as it consists of a hornblende-bearing diorite, which contains interstitial alkali feldspar and quartz (Tankard et al., 1982).

1.4 The Regional Setting of Amandelbult.

Amandelbult Section of R.P.M. is situated 100 km north of Rustenburg and 40 km south of Thabazimbi in the northwestern Transvaal (see Fig.1.3a). The mine includes portions of the farms Elandsfontein 386KQ, Schildpadnest 385KQ, Zwartkop 369KQ, Amandelbult 383KQ, Middellaagte 328KQ, Elandskuil 378 KQ and Haakdoorndrift 374KQ (Fig.1.3b). Geologically, it occupies a discrete suboutcrop of upper Critical and Main Zone rocks which strike approximately northeast, and dip on average at 22 degrees towards the southeast. Outcrop of upper Critical Zone rocks is poor, their topographical expression being that of a flat plain which is covered by a 3 metre thick layer of black turf. Main Zone gabbros outcrop as large pointed hills (pyramids) to the southeast, while Lower Critical Zone pyroxenites constitute Swartkop hill to the northwest. The Upper Zone rocks are also poorly exposed, but their weathering gives rise to characteristic red soils, from which their presence may be inferred.

Figure 1.3a. A map showing the regional geology of the western Transvaal, and the localities of the mines referred to in the text. (After Viljoen et al., 1986)

Figure 1.3b. A map showing the surface geology of the area around Amandelbult Section of R.P.M.

Figure 1.3c. A map of the southwestern portion of Amandelbult Section, showing the outcrop of the Merensky Reef, the positions of pothole structures, and the positions of the boreholes which were samlped sampled. (Reproduced with permission of the Mine Geologist of Amandelbult Section of R.P.M.).

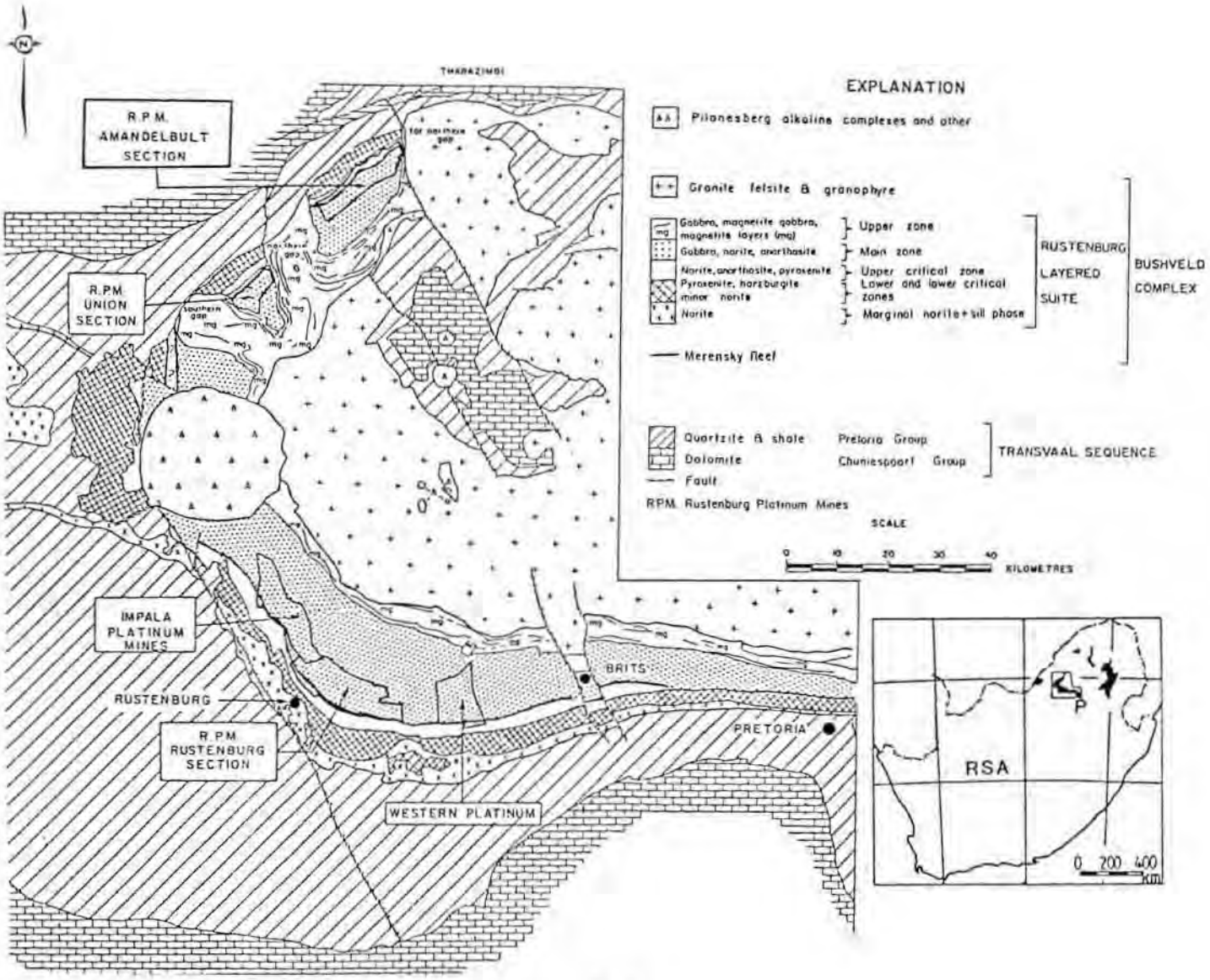
THABAZIMBI
R.P.M. AMANDELBULT SECTION
R.P.M. UNION SECTION
IMPALA PLATINUM MINES
RUSTENBURG
R.P.M. RUSTENBURG SECTION
WESTERN PLATINUM
BRITS
PRETORIA
EXPLANATION
Pilanesberg alkaline complexes and other
Granite felsite & granophyre
Gabbro, magnetite gabbro, magnetite layers (mg)
Upper zone
Gabbro, norite, anorthosite
Main zone
Norite, anorthosite, pyroxenite
Upper critical zone
Pyroxenite, harzburgite minor norite
Lower and lower critical zones
Norite
Marginal norite + sill phase
RUSTENBURG LAYERED SUITE
BUSHVELD COMPLEX
Merensky Reef
Quartzite & shale
Pretoria Group
Dolomite
Chuniespoort Group
TRANSVAAL SEQUENCE
Fault
RPM Rustenburg Platinum Mines
SCALE
0 10 20 30 40 KILOMETRES
RSA
0 200 400 km

Figure 1.3a

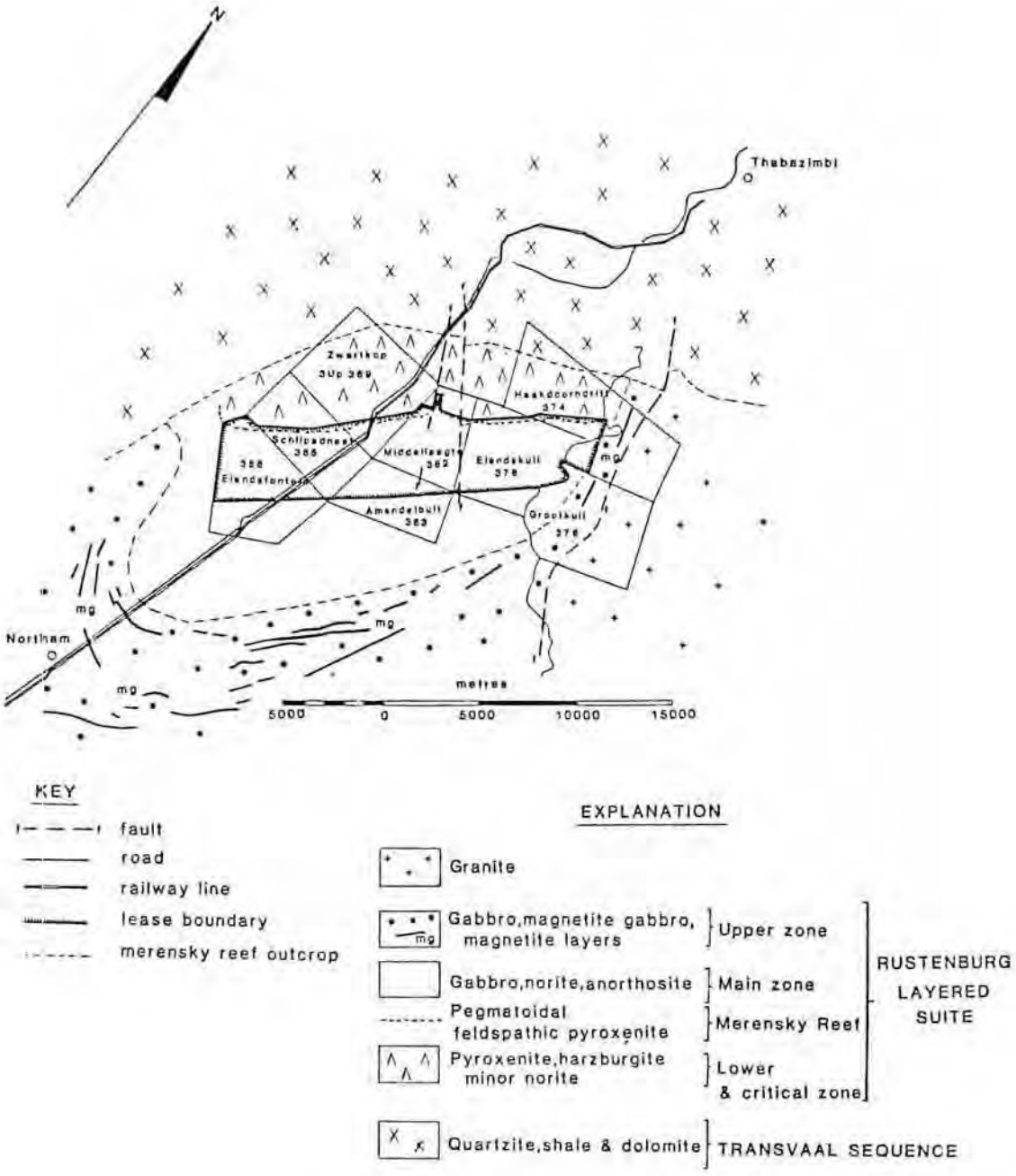
N
Thabazimbi
Zwartkop
3Up 369
Haakdoornkuil
374
Schilpadnest
368
Middelkraal
372
Elandskuil
378
mg
368
Elandsfontein
Amandelbult
383
Grootkuil
376
mg
mg
Northam
mg
metres
5000
0
5000
10000
15000
KEY
fault
road
railway line
lease boundary
merensky reef outcrop
EXPLANATION
Granite
Gabbro,magnetite gabbro, magnetite layers
Upper zone
Gabbro,norite,anorthosite
Main zone
Pegmatoidal feldspathic pyroxenite
Merensky Reef
Pyroxenite,harzburgite minor norite
Lower & critical zone
RUSTENBURG LAYERED SUITE
Quartzite,shale & dolomite
TRANSVAAL SEQUENCE

Figure 1.3b

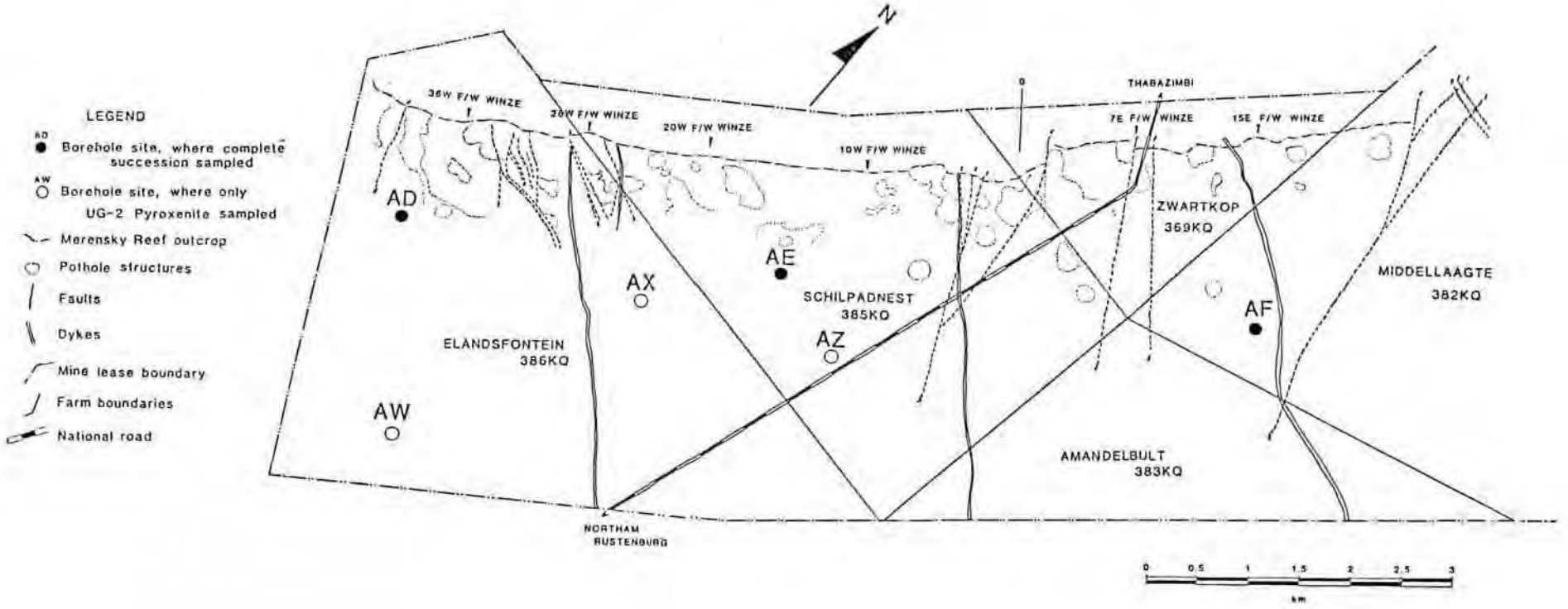
LEGEND
AD Borehole site, where complete succession sampled
AW Borehole site, where only UG-2 Pyroxenite sampled
Merensky Reef outcrop
Pothole structures
Faults
Dykes
Mine lease boundary
Farm boundaries
National road
N
36W F/W WINZE
30W F/W WINZE
20W F/W WINZE
10W F/W WINZE
0
THABAZIMBI
7E F/W WINZE
15E F/W WINZE
AD
AE
AX
AZ
AW
AF
ZWARTKOP
369KQ
SCHILPADNEST
385KQ
ELANDSFONTEIN
386KQ
MIDDELLAAGTE
382KQ
AMANDELBULT
383KQ
NORTHAM
RUSTENBURG
0 0.5 1 1.5 2 2.5 3
km

Figure 1.3c

The upper Critical and Main Zone rocks at Amandelbult are terminated along strike in the northeast and southwest, as at Union Section, by enigmatic features known as "gaps". In these regions Upper Zone rocks appear to transgress those of the upper Critical and Main Zones, and a dramatic change in strike is witnessed. The "northern gap" separates the upper Critical Zone rocks at Amandelbult and their equivalents at Union Section, while the "far northern gap" at the northeastern extremity of Amandelbult has the same effect, although no continuation of Critical Zone rocks is known further to the northeast.

A large number of faults transgress the succession, and while most of them have minor displacements (throws of around 5 metres, Viljoen et al., 1986), a few, such as those bounding the Middelaagte graben, may have throws of up to 530 metres (Viljoen et al., op.cit.). Most of the faults, as well as a large number of cross-cutting dykes, trend in a northwesterly direction. The dykes are of various affinities, and although no detailed investigation of them has been undertaken, both doleritic and kimberlitic varieties have been recognized. The latter type is thought to be related to the nearby Pilansberg Alkaline Complex, while the former may be either of Waterberg or Karoo age.

1.5 Sampling Procedures and Localities.

In all, samples were taken from six borehole cores, whose surface positions are indicated on figure 1.3c. In boreholes AD, AE and AF, the succession from just above the Giant Mottled Anorthosite to just below the UG-1 chromitite (see figure 2.1), an interval of 125 metres, was sampled at approximately two metre intervals. In boreholes AW, AX and AZ, the ten metre-thick horizon between the lower Pseudo Reef and the UG-2 chromitite was sampled at one metre intervals. All these sampling positions are indicated on their respective borehole logs in figure 1.4. The original numbers of these boreholes are EL-15, SKN-19, ML-30, EL-17, SKN-19 and EL-18 for AD, AE, AF, AW, AX and AZ respectively.

In each case a sample consisted of a 30cm length of core, which was broken into three roughly equal parts. The outer two thirds were combined and crushed together to a fine pulp, which was used to manufacture pressed powder briquettes and fusion discs for X.R.F whole-rock analyses (see appendix A). The inner third was retained as a handspecimen, from which thin sections and microprobe sections were cut. In a few cases, samples were taken across lithological contacts. Here the outer two thirds were crushed as separate samples, and labelled as "A" and "B" respectively. The inner third, which usually contained the contact, was retained, and in most cases thin- and microprobe sections were cut across the lithological contact. A large sample of Merensky Reef was taken from an underground exposure. It is labelled AE-MR.

Figure 1.4a Logs of boreholes AD, AE and AF. The numbers marked down the right hand side of each log represent individual sample positions.

Figure 1.4b Logs of boreholes AW, AX and AZ. Note that samples were only taken from the UG-2 pyroxenite layer, and that boreholes AW and AX represent "pothole" successions.

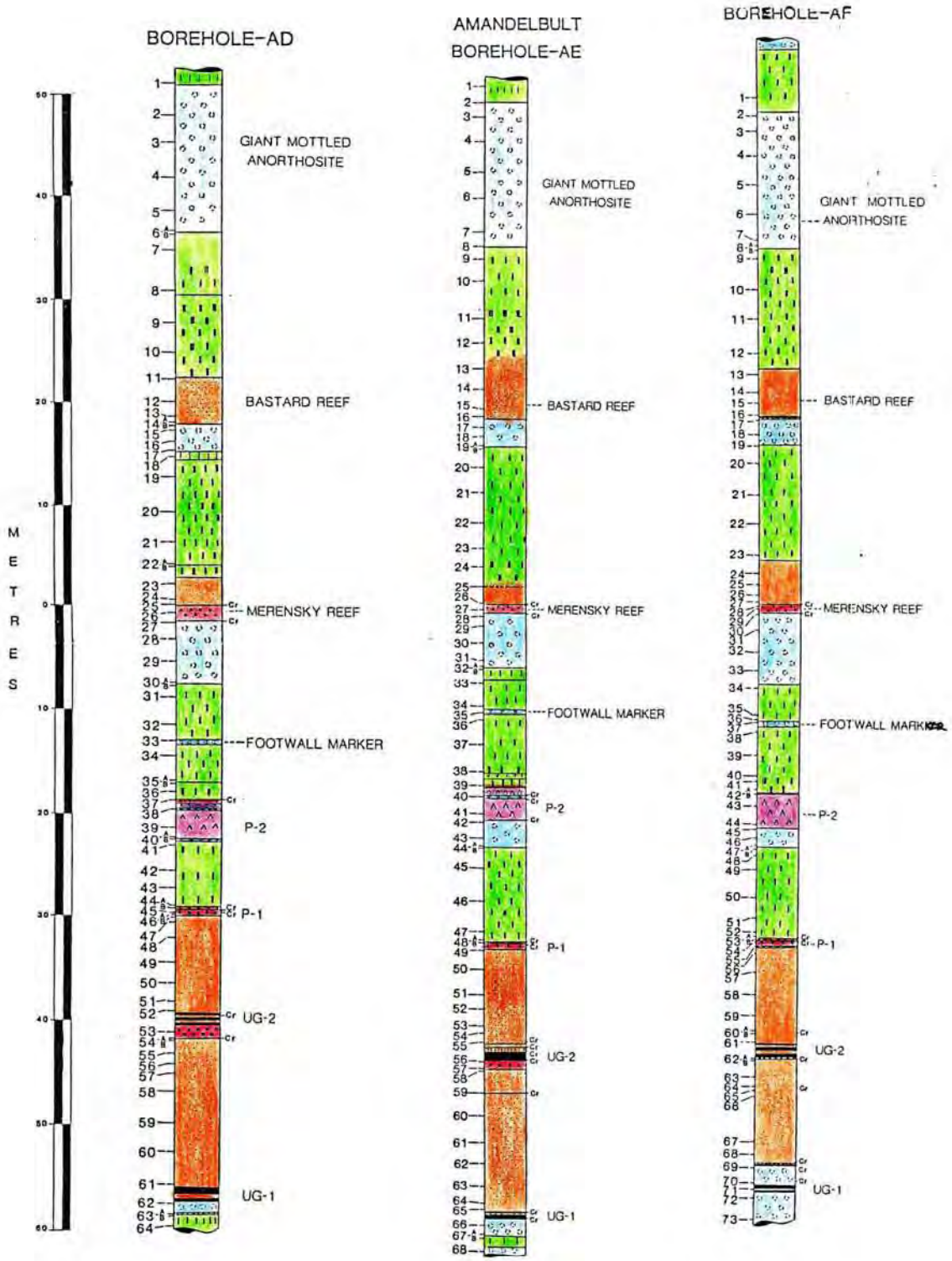
METRES
BOREHOLE-AD
GIANT MOTTLED ANORTHOSITE
BASTARD REEF
MERENSKY REEF
FOOTWALL MARKER
P-2
P-1
UG-2
UG-1
AMANDELBULT
BOREHOLE-AE
GIANT MOTTLED ANORTHOSITE
BASTARD REEF
MERENSKY REEF
FOOTWALL MARKER
P-2
P-1
UG-2
UG-1
BOREHOLE-AF
GIANT MOTTLED ANORTHOSITE
BASTARD REEF
MERENSKY REEF
FOOTWALL MARKER
P-2
P-1
UG-2
UG-1

Figure 1.4a

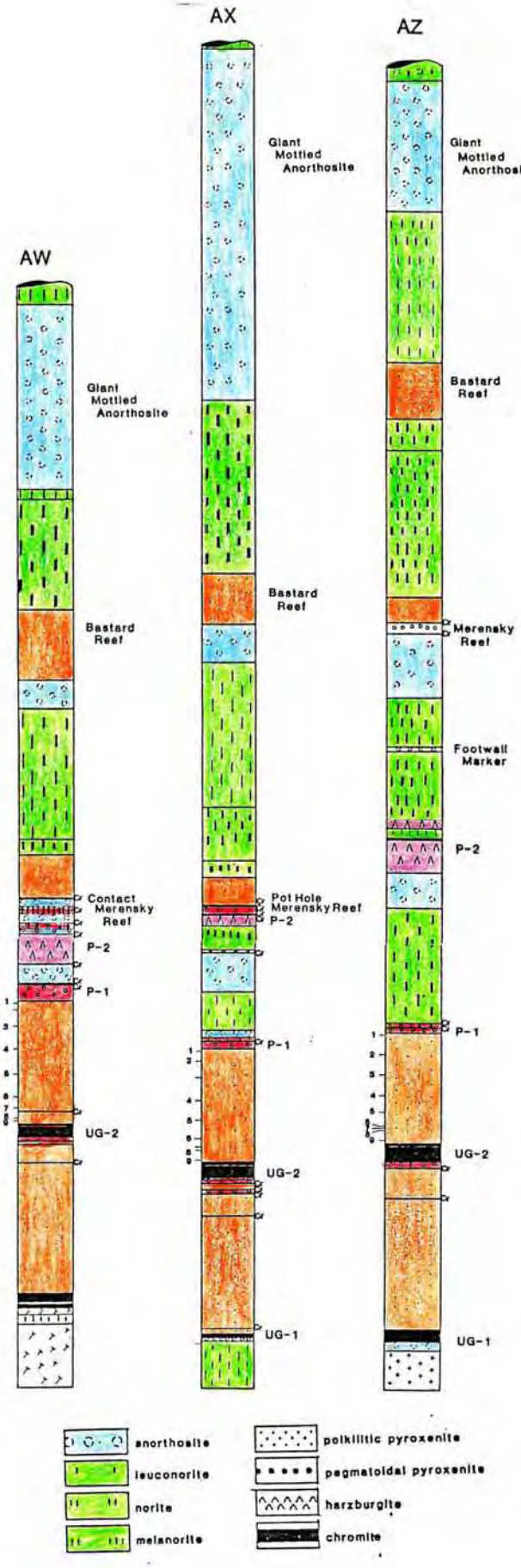
AW
AX
AZ
Giant Mottled Anorthosite
Bastard Reef
Contact Merensky Reef
P-2
P-1
UG-2
Pot Hole Merensky Reef
UG-1
Merensky Reef
Footwall Marker
anorthosite
leuconorite
norite
melanorite
poikilitic pyroxenite
pegmatoidal pyroxenite
harzburgite
chromite

Figure 1.4b

Figure 2.1 The stratigraphic subdivision of (a) the Bushveld Complex, (b) the Rustenburg Layered Suite and (c) the study section at Amandelbult. Thicknesses of suites and zones in columns (a) and (b) are taken from S.A.C.S. (1980), while those in (c) were measured in borehole cores.

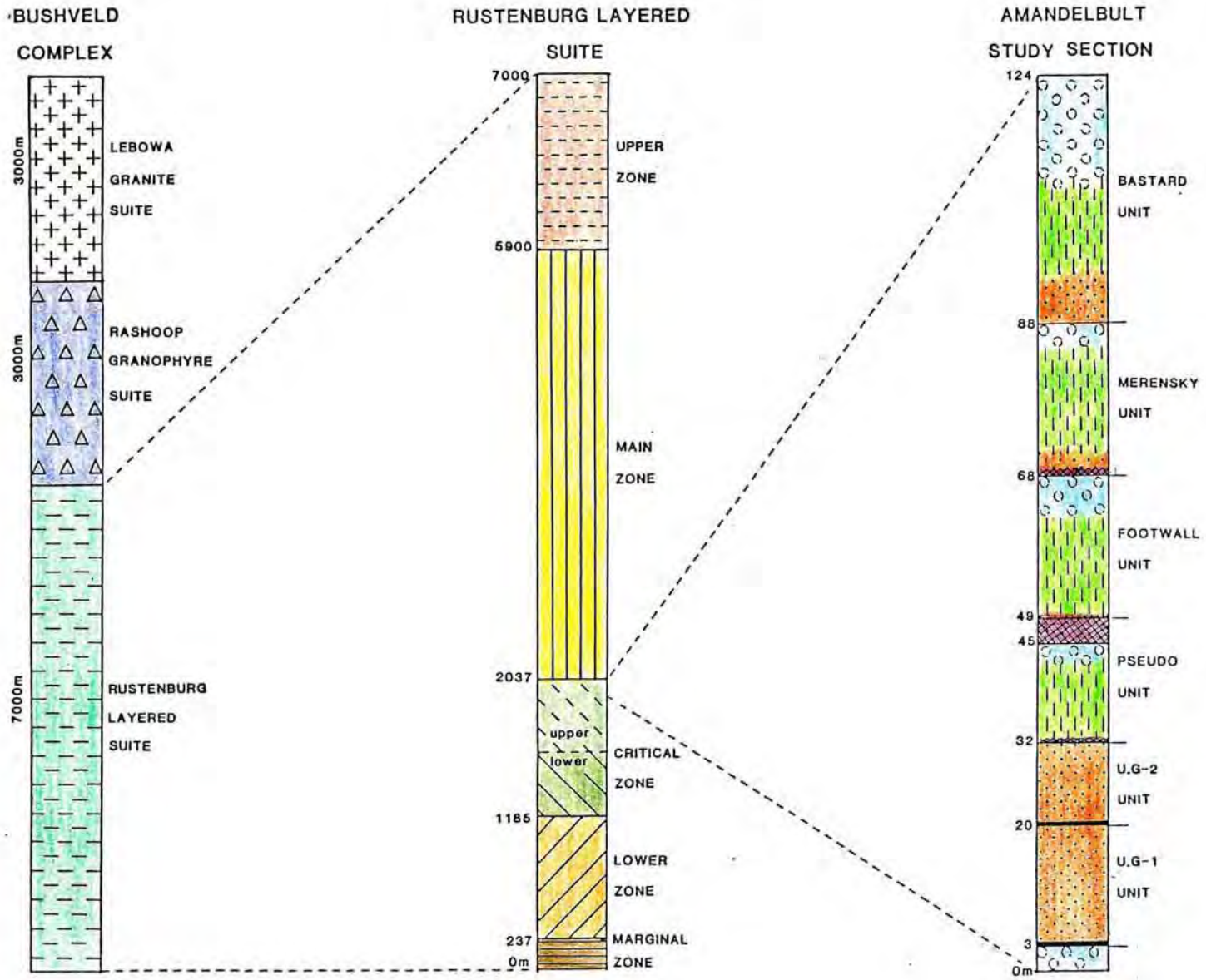
BUSHVELD
COMPLEX
3000m
LEBOWA
GRANITE
SUITE
3000m
RASHOOP
GRANOPHYRE
SUITE
7000m
RUSTENBURG
LAYERED
SUITE
RUSTENBURG LAYERED
SUITE
7000
UPPER
ZONE
5900
MAIN
ZONE
2037
upper
lower
CRITICAL
ZONE
1185
LOWER
ZONE
237
MARGINAL
ZONE
0m
AMANDELBULT
STUDY SECTION
124
BASTARD
UNIT
88
MERENSKY
UNIT
68
FOOTWALL
UNIT
49
45
PSEUDO
UNIT
32
U.G-2
UNIT
20
U.G-1
UNIT
3
0m

Figure 2.1

CHAPTER 2: STRATIGRAPHY

2.1 Introduction

The Bushveld Complex has been divided into three lithostratigraphic suites by the South African Committee for Stratigraphy (S.A.C.S., 1980), namely the Rustenburg Layered Suite, the Rashoop Granophyre Suite and Lebowa Granite Suite. Of these only the Rustenburg Layered Suite is pertinent to the present study. The subdivision of this group of lithologies has undergone numerous changes over the past fifty years. The most recent re-classification of Bushveld stratigraphy (by S.A.C.S., 1980), places the rocks of the present study section in the Mathlagame Norite-Anorthosite of the Rustenburg Layered Suite. The old classification of Cameron (1971) has, however, remained in use, and has been adopted by S.A.C.S. (1980) as an informal subdivision. In this context the rocks of the study section form part of the upper Critical Zone, the subdivision which is adopted in this thesis (see figure 2.1).

Figure 2.1 shows that the stratigraphic section at Amandelbult has been subdivided into a number of recognizable "Units". These Units, ideally, have a mafic lithology at their base, which grades upwards into more felsic members. Some, however, appear to have been truncated, while others appear to lack intermediate, or lowermost members of the ideal sequence. It is for this reason that these apparently repetitive units are not refered to as "Cyclic Units".

2.2 Stratigraphic Descriptions

At least seven repetitive units can be recognized in the upper Critical Zone succession at Amandelbult Section of R.P.M., namely; (from the bottom upwards), the UG-1, UG-2, Lower Pseudo, Upper Pseudo, Footwall, Merensky and Bastard Units respectively. Each of these Units is described separately below, while an idealized column is given in figure 2.1.

2.2.1 The UG-1 Unit

The UG-1 Unit consists of a basal chromitite layer which is overlain by a poikilitic pyroxenite. The basal chromitite (the UG-1 chromitite) is usually a composite layer 0.7 to 1.5 metres thick, but it intermittently splits and penetrates the underlying anorthosite causing the formation of lenses of anorthosite in chromitite and stringers of chromitite in the anorthosite (see figure 2.2h). The association of anorthosite with chromitite is characteristic of the UG-1 throughout the Complex, and is particularly well known from the famous Dwars River section in the Eastern Transvaal. The overlying pyroxenite is a fine grained poikilitic bronzitite which is usually 15 metres thick. A persistent 2 cm-thick chromitite layer is developed approximately 10 metres above the UG-1 chromitite, while a second such layer separates the poikilitic pyroxenite from the topmost layer of the unit, a 1-metre thick pegmatoidal pyroxenite (see figure 2.2g).

2.2.2 The UG-2 Unit

This unit is similar to the UG-1 in that it consists of a basal chromitite overlain by pyroxenite. The UG-2 chromitite differs from the UG-1 in that it is not a single layer, but consists of a lower "main seam" with two or three overlying "leader seams". The latter are separated from the main seam by thin layers of poikilitic pyroxenite. The main seam is between 60 and 80 cm thick, while the leaders are considerably thinner (10 cm). The leader seams and the upper parts of the main seam are easily distinguished from other chromitites as they contain large clots of pyroxene, which gives them a spotted appearance. The remainder of the unit consists of 10 metres of poikilitic pyroxenite. The lowermost metre of the pyroxenite may contain cumulus olivine grains, whereas the remainder of it is a fairly uniform bronzitite.

2.2.3 The Lower Pseudo Unit

This unit sharply overlies the UG-2 pyroxenite, commencing with 65 cm of olivine-bearing feldspathic pegmatoidal pyroxenite (the Lower Pseudo Reef), which is separated from the overlying harzburgite by a 0.5 cm thick chromitite band. The harzburgite, which is 20 cm thick, is itself overlain by a thin chromitite of 0.5 cm. The remainder of the unit consists of norite (10 m) which grades upwards into anorthosite (3 m thick). The contact between the harzburgite and norite is sharp but undulatory, and "flames" of harzburgite can be seen protruding into the norite (see figure 2.2e).

2.2.4 The Upper Pseudo unit

The Upper Pseudo Unit represents one of the most complex horizons encountered in the Critical Zone of the Bushveld Complex (Viljoen et al., 1986). In the southwestern section of the mine, this unit consists of a basal chromitite (2-3 cm thick) overlain by a feldspathic harzburgite (2 metres thick), which itself is overlain by a thin chromitite (1 cm). These lithologies are overlain by an anorthositic layer known as the P-2 middling. The basal part of this layer consist of pure plagioclase rock but this grades upwards into a leucotroctolite which may itself grade upwards into a mottled anorthosite (see figure 2.2f). The P-2 middling is sharply overlain by a second harzburgite layer 1-2 metres thick. This unit is collectively known as the Upper Pseudo Reef. In the north-eastern section of the mine the P-2 middling is no longer present and the Upper Pseudo unit consists of a composite feldspathic harzburgite layer with a basal chromitite.

The Upper Pseudo Unit is enigmatic, as it consists of mafic (harzburgite) and felsic (anorthosite) endmembers of typical Critical Zone rocks, but lacks any intermediate members such as pyroxenites and norites. Furthermore, correlation with upper Critical Zone rocks at other mines in the western lobe of the Complex is complicated by this horizon. A more detailed section of this portion of the succession is shown in figure 2.3.

Figure 2.2a Photograph showing the nature of the Giant mottled anorthosite at Union Section of R.P.M. This member is not exposed in mine workings at Amandelbult.

Figure 2.2b Photograph showing the undulatory contact of the Merensky Reef and the underlying Footwall anorthosite.

Figure 2.2c Photograph showing fine, inch-scale layering in norite below the Footwall Marker. This is at approximately the same stratigraphic position as the "strepies" horizon at Union Section.

Figure 2.2d Photograph showing the sharp, undulatory contact between the P2 middling anorthosite/leucotroctolite and harzburgite of the Upper Pseudo Reef. Note the bleached nature of the anorthoosite in the scalloped area in the centre of the photograph. Examination of this rock in thin section revealed a recrystallized texture.

Figure 2.2e Photograph showing the irregular and sharp nature of the contact between norite and harzurgite of the Lower Pseudo Reef. Note the fragments of harzburgitic material trapped in lower parts of the norite.

Figure 2.2f Photograph of the P2 middling anorthosite sandwiched between the two harzburgitic layers of the Upper pseudo Reef.

Figure 2.2g Photograph of the thin pegmatoidal pyroxenite layer underlying the UG-2 chromitite layer. The painted arrow head is on chromitite.

Figure 2.2h Photograph of the basal portions of the UG-1 chromitite at Union Section. Similar features are seen in core specimens at Amandelbult, where the UG-1 is only poorly exposed underground.

a

b

c

d

e

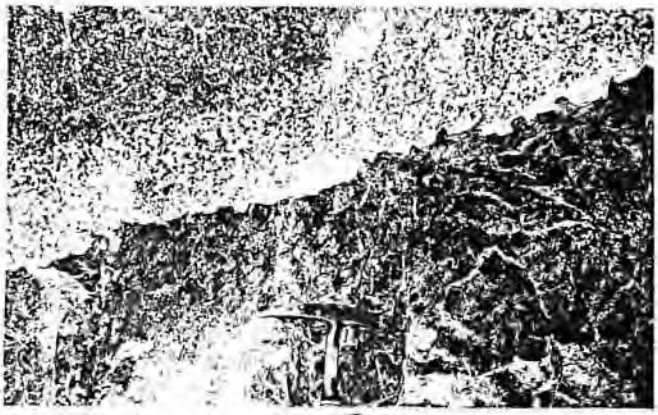

f

g

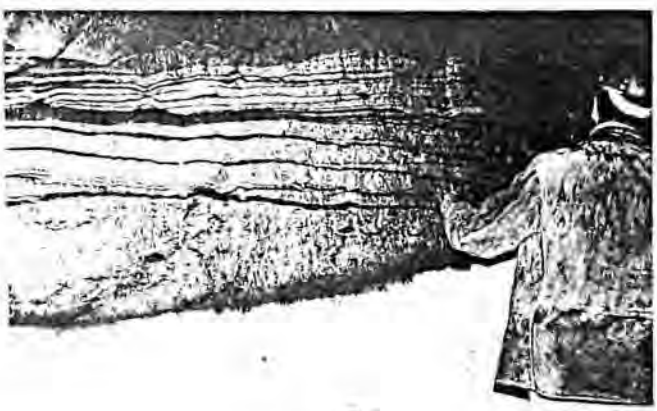

h

Figure 2.3 A more detailed log of the Pseudo Unit intersection of borehole AE, which shows more clearly the nature of harzburgite and olivine-bearing pyroxenite horizons of the Pseudo and Footwall Units.

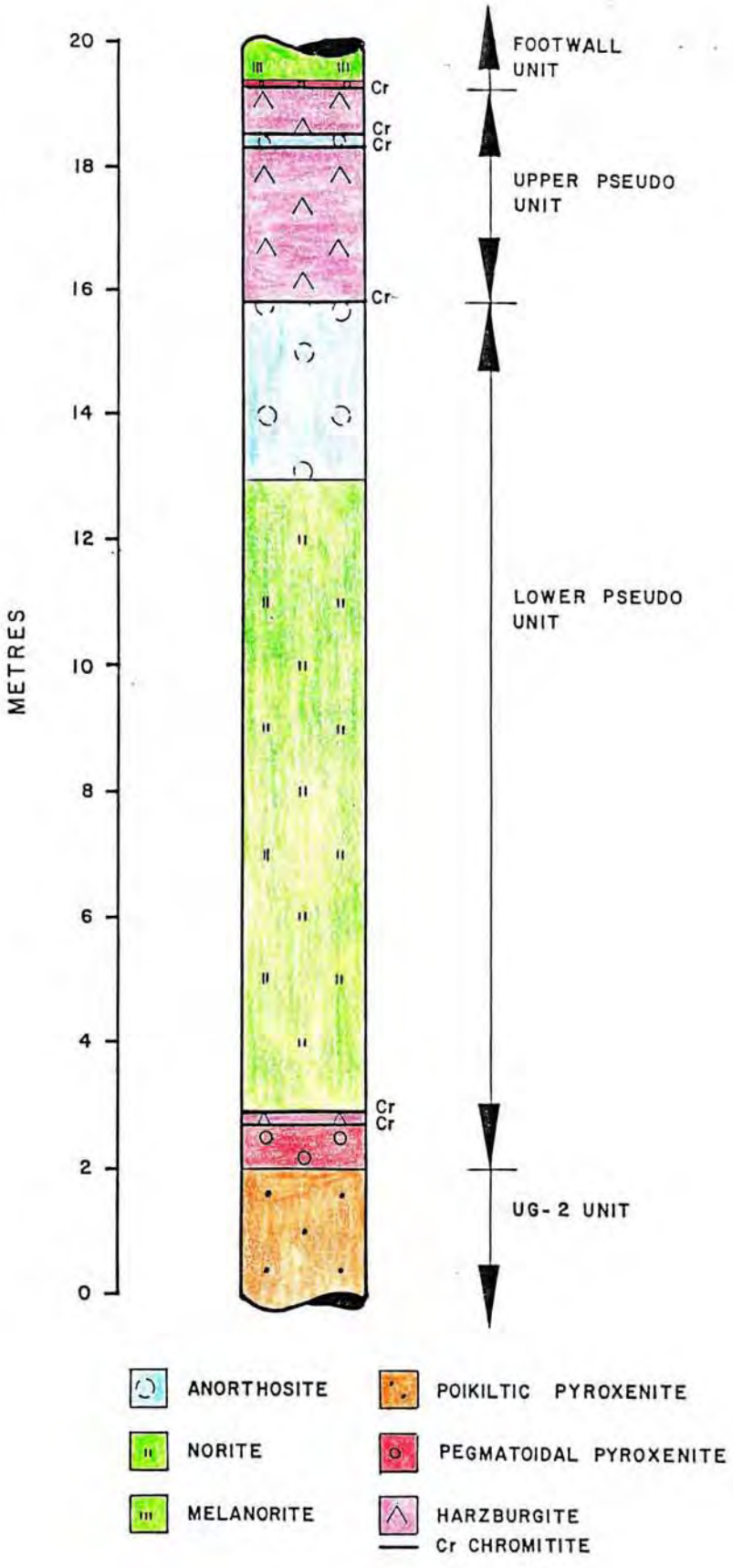
METRES
20
18
16
14
12
10
8
6
4
2
0
Cr
Cr
Cr
Cr
Cr
Cr
FOOTWALL UNIT
UPPER PSEUDO UNIT
LOWER PSEUDO UNIT
UG-2 UNIT
ANORTHOSITE
NORITE
MELANORITE
POIKILTIC PYROXENITE
PEGMATOIDAL PYROXENITE
HARZBURGITE
Cr CHROMITITE

Figure 2.3

2.2.5 The Footwall Unit

Generally, the Footwall Unit conforms well with the definition of a typical cyclic unit (Irvine, 1982). It commences with a thin chromitite layer (0.5 cm thick), which is followed upwards by a thin layer (6 cm) of olivine-bearing feldspathic pegmatoidal pyroxenite. The latter lithology grades upwards into melanorite, norite and mottled anorthosite. A complication in this ideal crystallization sequence is the development of a persistent, 50 cm thick layer of mottled anorthosite within the norite layer, known as the Footwall Marker. Both the upper and lower contacts of this horizon are gradational over a few centimetres, while the norite immediately below the Footwall Marker has an extremely well devoloped "inch-scale" layering, similar to that observed in the "strepies" horizon at Union Section (De Klerk, 1982) (figure 2.2c). It should also be noted that this Unit lacks a poikilitic pyroxenite member, and therefore does not represent a complete Unit in the strictest sense.

2.2.6 The Merensky Unit

The Merensky unit is regarded by Vermaak (1976) as one of the most complete cyclic units in the Critical Zone of the Complex. It commences with a thin chromitite layer (1 cm thick) which forms a sharp, but wavy (undulatory) contact with the underlying Footwall anorthosite (figure 2.2b). This is then

followed by an olivine-bearing feldspathic pegmatitic pyroxenite or harzburgite, which is in turn overlain by a thin (1 cm) chromitite. This group , i.e chromitite + pegmatoid + chromitite, constitutes the economically important "Merensky Reef", which is the world's largest producer of platinum group elements (P.G.E), as well as significant quantities of copper, nickel,cobalt and gold.

The upper chromitite is overlain by poikilitic pyroxenite, which grades upwards into melanorite, norite and mottled anorthosite. The total thickness of the unit is variable, averaging around 20 metres.

2.2.7 The Bastard Unit

This is the second of Vermaak's (op.cit) complete cyclic units, and although it megascopically resembles the Merensky Unit, there are important differences between the two. Firstly, the Bastard Unit does not contain any significant concentrations of chromite; secondly, olivine does not occur as a cumulus mineral, at Amandelbult; thirdly, no pegmatoidal rock occurs at the base of the Unit; and fourthly, it is very poorly mineralized (in terms of P.G.E.), even though abundant sulphide blebs may be present in the basal member, a poikilitic pyroxenite, known as the Bastard Reef. The poikilitic pyroxenite grades upwards into melanorite, norite and finally mottled anorthosite (see figure 2.3h). The Bastard Unit mottled anorthosite is a particularly striking member as it contains very large oikocrysts of ortho- and clino- pyroxene (up to

5cm), and consequently it is referred to as the "Giant Mottled Anorthosite". It is a persistent marker horizon, and its top contact with overlying norite may be used as an approximation of the Critical Zone - Main Zone boundary.

2.3 Lateral Variations and Other Stratigraphic Complications

2.3.1 Lateral Variations

A number of workers (eg., De Klerk,1982) have distinguished "normal" and "potholed" stratigraphic successions in the Bushveld Complex, where "normal" successions are those which have not been affected by "potholes" (see the following section, 2.4.3). In this section lateral variations in normal successions will be considered.

Lateral variations are most pronounced in the northeastern sectors of the mine. A large area of the southwestern sector, i.e., from 43W to 12W (see Map fig 1.3c), which includes boreholes AD, AE, AW, AX, and AZ, exhibits a normal succession which closely resembles that described in the preceding sections (2.2.1 to 2.2.7). It is between the 12W and 11W winzes that the first lateral changes become evident, where the P-2 middling anorthosite thins out, and the two harzburgite layers of the Upper Pseudo Unit coalesce. This succession is maintained as far east as the 15E winze, and matches that observed in borehole AF.

Figure 2.4 This diagram shows the lateral variations of "normal" successions at Amandelbult (after Viljoen et al., 1986).

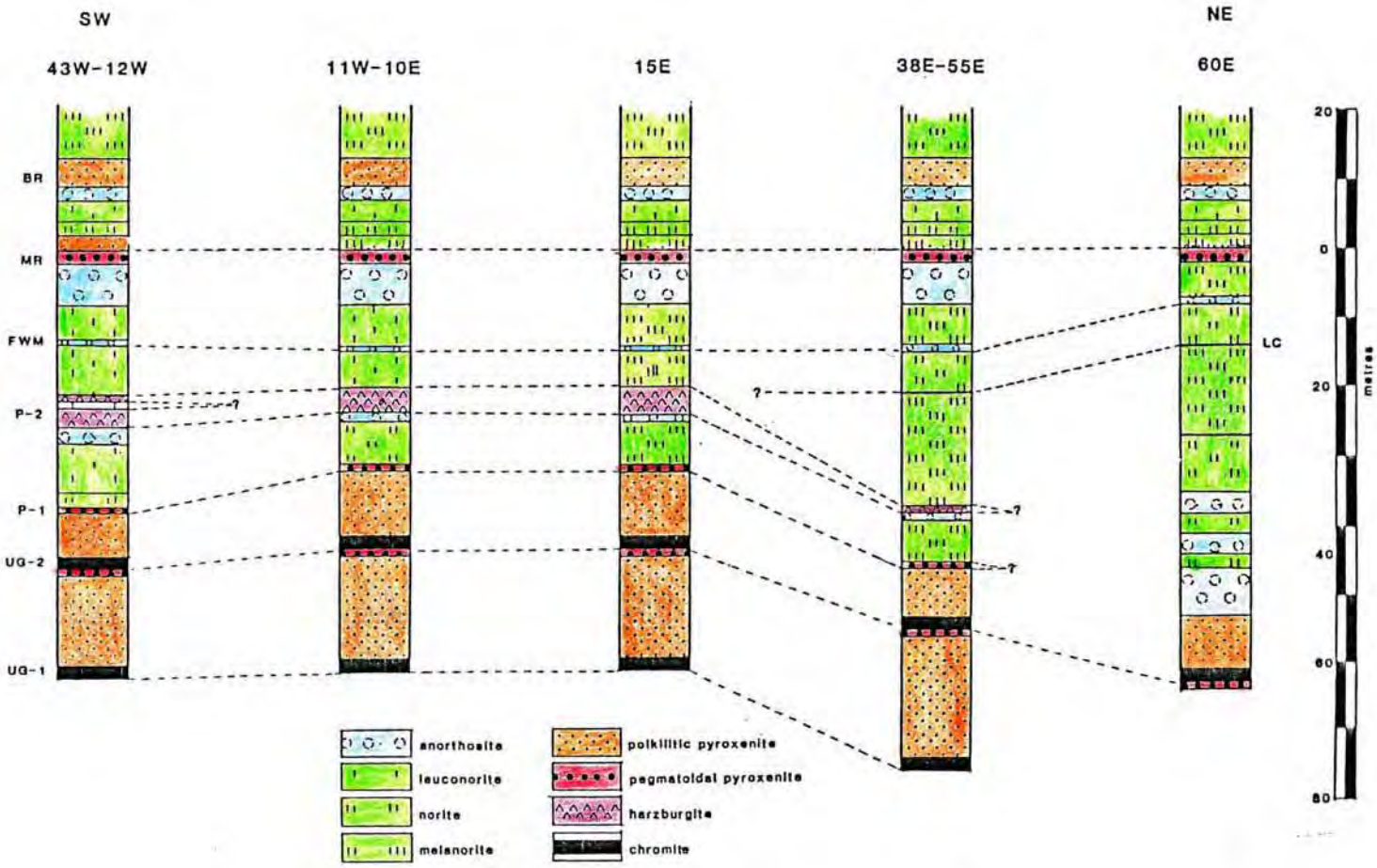
SW
NE
43W-12W
11W-10E
15E
38E-55E
60E
BR
MR
FWM
P-2
P-1
UG-2
UG-1
LC
?
anorthosite
leuconorite
norite
melanorite
poikilitic pyroxenite
pegmatoidal pyroxenite
harzburgite
chromite
20
0
20
40
60
80
metres

Figure 2.4

To the east of the 15E winze the Upper Pseudo reef thins dramatically, and its overlying chromitite is seen to part from the harzburgite layer and to transgress the overlying norites to a preferred height, after which it maintains a fairly constant stratigraphic position below the lower Merensky chromitite. Where this chromitite is in this disposition, it is known colloquially as the "Lone Chrome" chromitite (Cilliers, pers comm). In the extreme northeastern sector of the mine, i.e. east of 55E, the succession changes considerably. Here, neither the Lower or Upper Pseudo Reefs is developed, while the immediate footwall of the Merensky Reef is melanorite, instead of anorthosite. The Footwall Marker, however maintains its previous stratigraphic position. In the stratigraphic positions previously occupied by the harzburgitic Pseudo Reefs, several alternating layers of mottled anorthosite and norite occur. These variations are summarized in figure 2.4. It is also important to note that the lateral stratigraphic changes appear to be limited to the succession between the upper contact of the UG-2 Unit and the lower contact of the Merensky Unit.

2.3.2 Potholes

Potholes are amongst the most enigmatic features of the layered rocks of the Bushveld Complex. They are slump-like structures which commonly affect the Merensky Reef horizon, and consequently have a great bearing on mining operations. In a pothole, normal Merensky Reef plunges sharply downwards, and in so doing transgresses its immediate footwall, usually coming to

rest on the upper Pseudo Reef. In plan view a pothole is circular to elliptical in shape, varying in diameter from a few tens of metres to a kilometre or more. Their distribution at Amandelbult is shown in figure 2.5.

The more important features of potholes are best seen in a dip section (figure 2.6), from which it can be seen that as a pothole is approached , the Merensky Reef becomes progressively thinner, until at the edge of the pothole the pegmatoidal portion of the reef wedges out completely and the upper and lower Merensky chromitites coalesce. This coalesence results in the formation of "contact-type" reef. The edge of the pothole is defined as that point at which the contact-type reef begins to transgress the Footwall Unit (Viljoen et al.,1986). Those layers which overlie normal Reef are warped into the pothole, with immediate hangingwall members being affected to a greater extent than those which are higher up in the succession.

"Pothole-type" Reef is developed where contact-type Reef comes to rest upon the Upper Pseudo Reef. This Reef is usually a pegmatoidal feldspathic pyroxenite, similar to normal Merensky Reef. It is separated from the Upper Pseudo Reef by a thin chromitite, while a chromitite separates it from overlying poikilitic pyroxenite. It can be seen from figure 2.6 that it is possible for the pothole to reach the Footwall Marker, but no pegmatoid is developed where this is the case. It is also possible for a pothole to transgress the upper harzburgite

Figure 2.5 Variations in the thickness of the Merensky Reef layer at Amandelbult, and the distribution of pothole structures (after Viljoen et al., 1986).

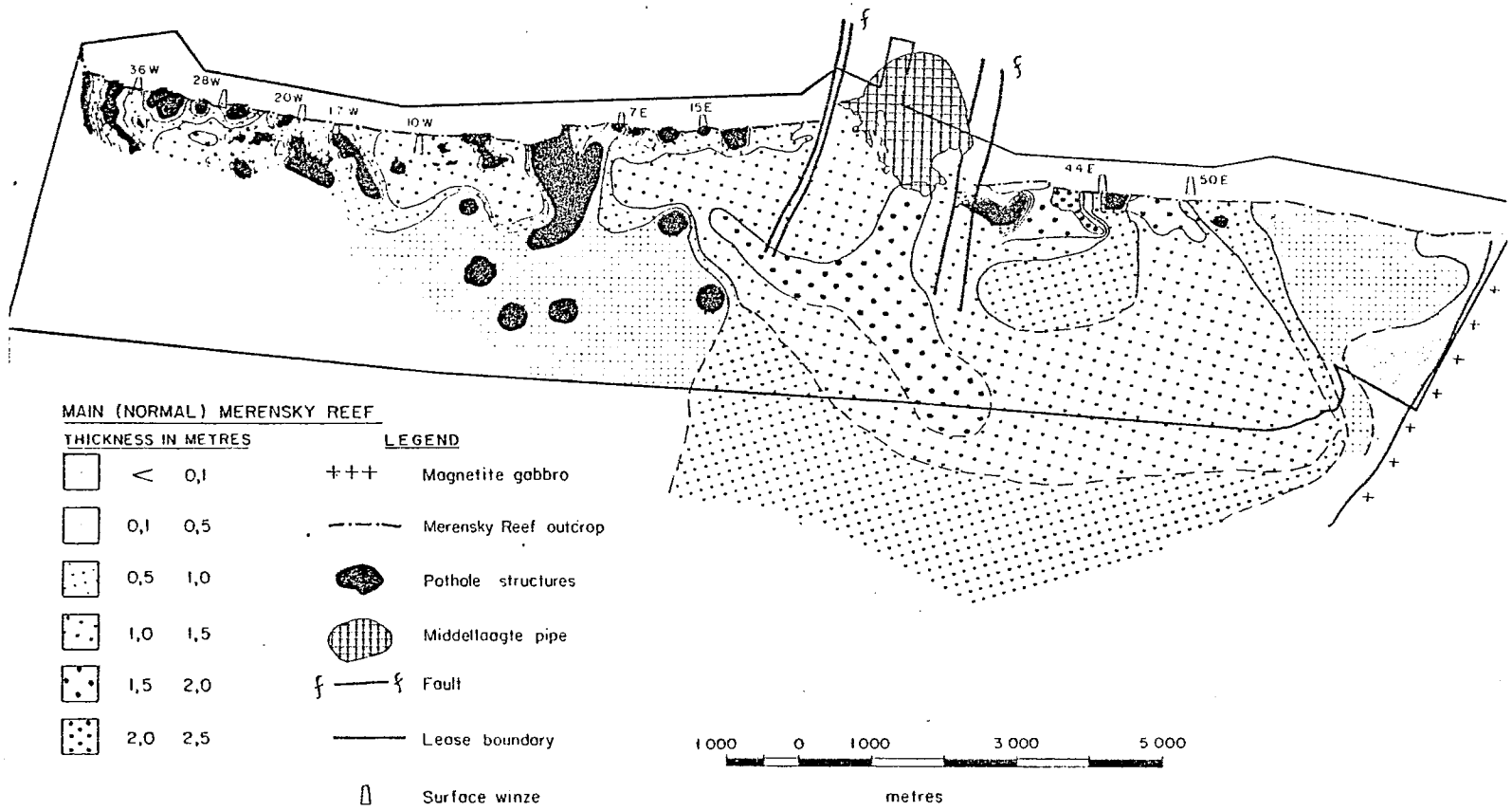
36W
28W
20W
17W
10W
7E
15E
44E
50E
MAIN (NORMAL) MERENSKY REEF
THICKNESS IN METRES
LEGEND
< 0,1
0,1 0,5
0,5 1,0
1,0 1,5
1,5 2,0
2,0 2,5
Magnetite gabbro
Merensky Reef outcrop
Pothole structures
Middellaagte pipe
Fault
Lease boundary
Surface winze
1 000 0 1000 3 000 5 000
metres

Figure 2.5

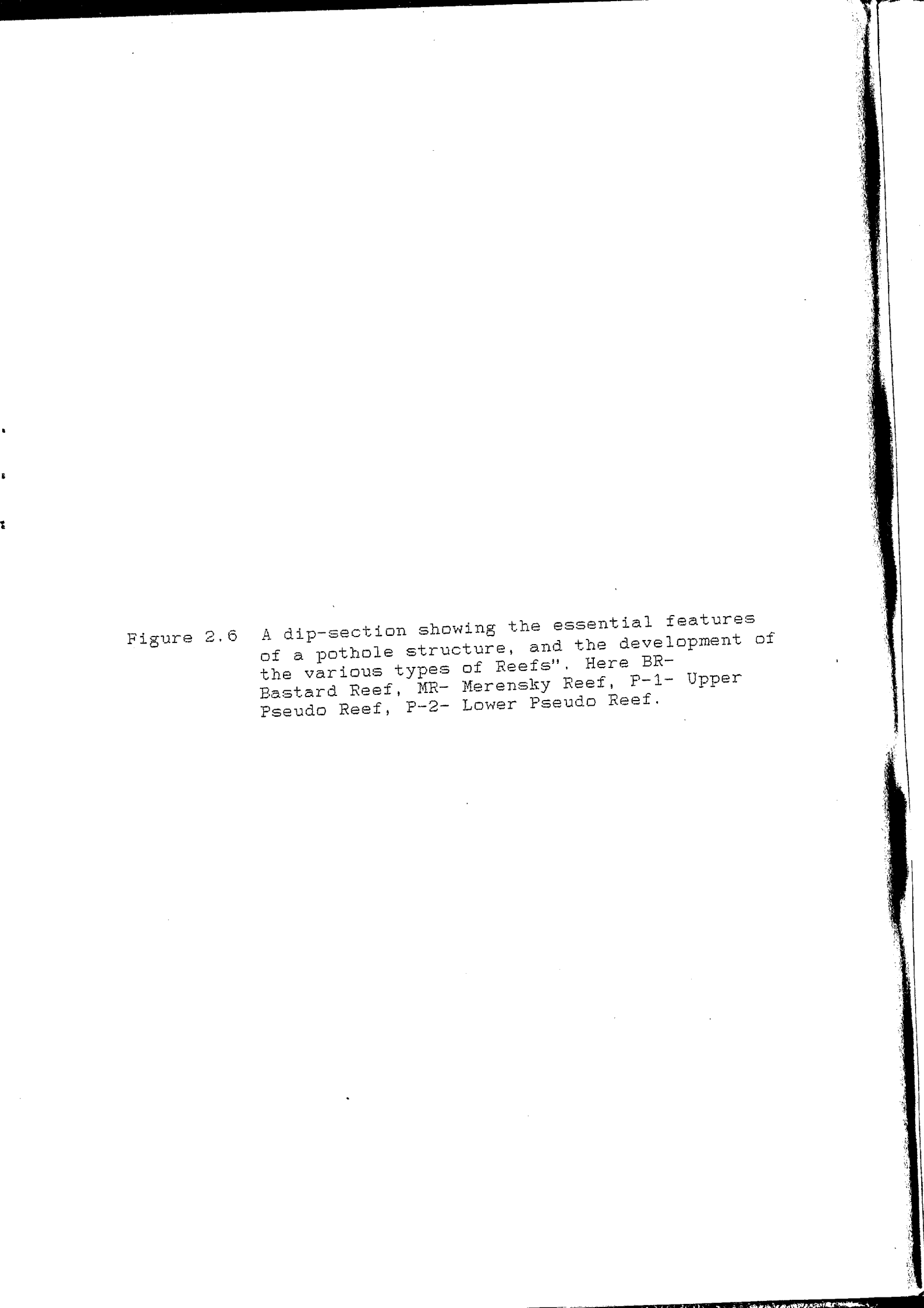

Figure 2.6 A dip-section showing the essential features of a pothole structure, and the development of the various types of Reefs". Here BR- Bastard Reef, MR- Merensky Reef, P-1- Upper Pseudo Reef, P-2- Lower Pseudo Reef.

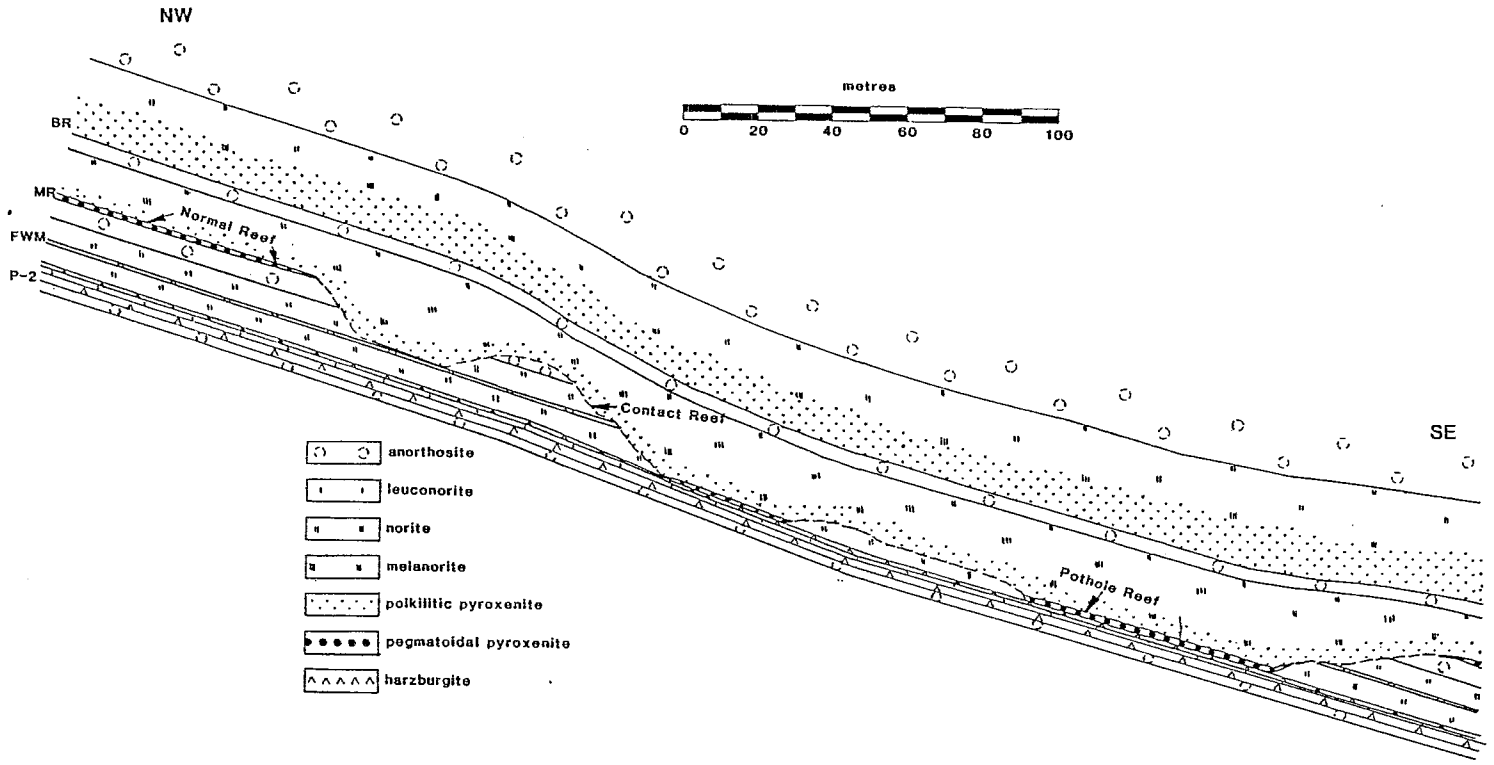
NW
SE
metres
0
20
40
60
80
100
BR
MR
FWM
P-2
Normal Reef
Contact Reef
Pothole Reef
anorthosite
leuconorite
norite
melanorite
poikilitic pyroxenite
pegmatoidal pyroxenite
harzburgite

Figure 2.6

layer of the Upper Pseudo Unit and to reach the lower harzburgite. Although potholes have been seen to transgress the Pseudo Reef at Union Section (De Klerk, pers.comm) to date none has been observed to breach the Upper Pseudo Reef at Amandelbult (Viljoen et al.,1986).

As far as mineralization is concerned, both contact-type and pothole-type Reefs are mineralized. The former type is seldom mined because of its irregularity, but the latter often contains grades higher than that of normal Reef, and is thus regarded as favourable for exploitation (Viljoen et al, op.cit.).

2.2.3 Iron-rich Pegmatites.

The presence of these bodies further complicates the stratigraphy of the Critical Zone. They are seldom exposed at surface and are known only from underground exposures and their pronounced surface magnetic anomalies (Scoon,1985). They vary in size from the large Middellaagte Pipe, which has a long axis of 2 km (Viljoen et al, op.cit.), to small bodies measuring a few metres across. Their distribution at Amandelbult is shown in Figure 2.7.

The pegmatites are generally dark coloured and range in composition from pure hortonolite dunites to wehrlites and websterites (Scoon,1985), which may contain significant proportions of magnetite, sulphides and platinum group elements.

Figure 2.7 The distribution of ultramafic pegmatite (dunite/pegmatoid) at Amandelbult (after Viljoen et al.,1986)

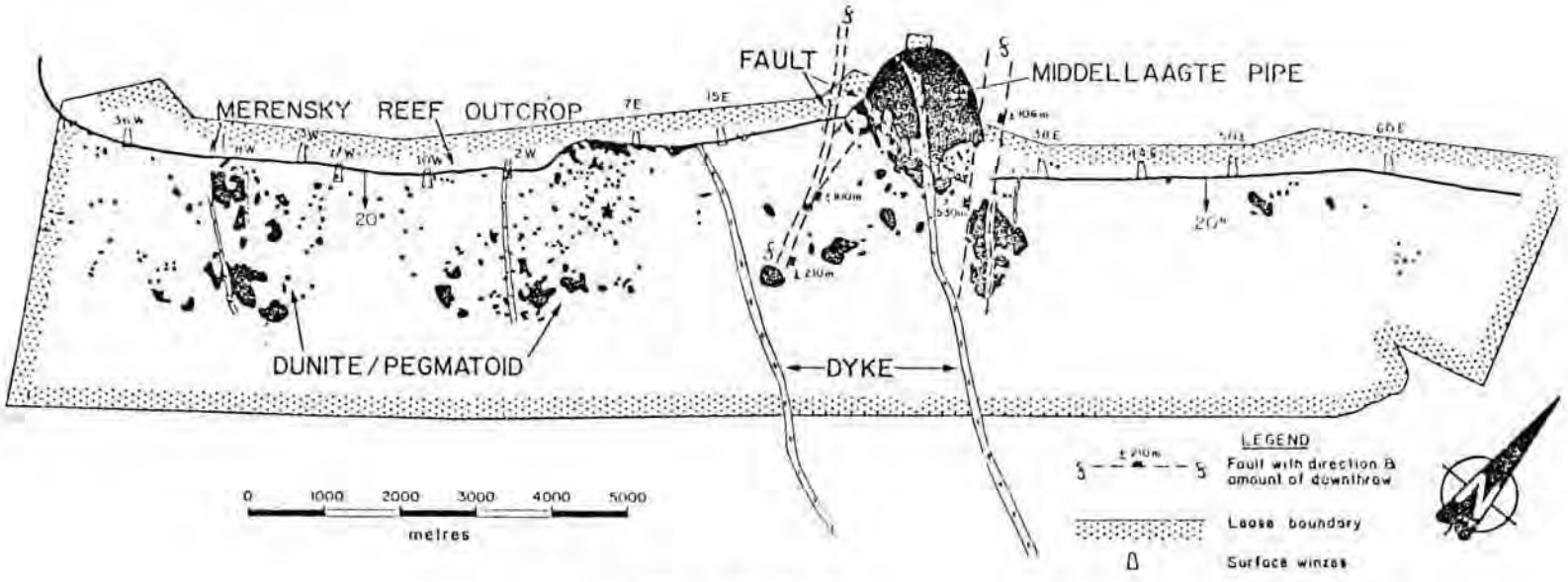
FAULT
MIDDELLAAGTE PIPE
MERENSKY REEF OUTCROP
7E
15E
20°
20°
DUNITE/PEGMATOID
DYKE
0
1000
2000
3000
4000
5000
metres
LEGEND
Fault with direction & amount of downthrow
Loose boundary
Surface winzes

Figure 2.7

Their effect on the succession is particularly pronounced in the upper Critical Zone, where they have replaced certain lithologies. Replacement is particularly pronounced in rocks of anorthositic affinity, but is not restricted to them. Where replacement has occurred the original lithology may be difficult to recognize, while the only horizon which appears to escape total replacement is the Upper Pseudo Reef (Viljoen et al., op.cit.). Scoon (1985) has observed that where the Merensky Reef has been replaced, the P.G.E. values are maintained. The origin of these pegmatoidal bodies is beyond the scope of this investigation and the reader is referred to Phillips (1984), Scoon (1985) and Viljoen and Scoon (1985).

CHAPTER 3: PETROGRAPHY

3.1 Introduction.

Petrographic studies were carried out on a suite of 280 thin sections which are representative of samples taken from all six boreholes (see Chapter 1). This meant that a large number of samples of each rock type were examined, which in turn meant that a large measure of generalization was required in their descriptions if excessive length was to be avoided. However, similarities and differences of individual rock types in different Units have been noted. Each individual rock type, as defined by the nomenclature laid out in Chapter 1, is described separately below.

3.2 Anorthosites.

Anorthosites are defined as those rocks which contain plagioclase as their sole cumulus constituent, while common postcumulus phases include clinopyroxene and orthopyroxene. Rare postcumulus phases are biotite, olivine, base-metal sulphides and magnetite. These rocks usually constitute the uppermost layers of cyclic units, but they may also occur as discrete layers within norites, as for example the Footwall Marker, or between harzburgite layers, as for example the P-2 Middling. A unique association is that of anorthosite with chromitite at the base of the UG-1 chromitite layer.

Petrographically, three varieties of anorthosite can be recognized, namely "mottled", "adcumulus" and "annealed" anorthosites. Mottled anorthosites are characterized by the occurrence of large oikocrysts of postcumulus clino- and orthopyroxene which poikilitically enclose some plagioclase grains. These oikocrysts are extremely variable in both size and distribution, while the relative proportions of pyroxene and plagioclase in any one thin section are dependent on the chance intersection of a "mottle", and are therefore unlikely to be representative of the rock as a whole. A feature of the plagioclase in these rocks is that those grains which are poikilitically enclosed by pyroxene are somewhat different to those which are not. The latter are usually subhedral, large (1-4 mm in length), distinctly zoned and appear to have their long axes preferentially oriented, while those that are encapsulated within pyroxenes are often smaller (less than 1 mm), subhedral to rounded in habit, less obviously zoned and randomly oriented (see figure 3.1a).

"Adcumulus" anorthosites contain very little (less than 7 percent) postcumulus material. They are often equigranular, with grain sizes between 2 and 4 mm, while the long axes of plagioclase grains show a moderate to strong preferred orientation. Occasional aggregates of small (0.5-1 mm), equidimensional plagioclase grains appear to disrupt the layering (see Figure 3.1b). Oscillatory zoning is a particularly distinctive feature of the larger oriented plagioclase grains and up to four zones can be recognized in single grains in thin section. This zoning may be taken as evidence for late

stage overgrowth of feldspar components onto primocryst plagioclase grains. "Annealed" anorthosites usually occur as localized thin selvages along contacts between mottled or adcumulus anorthosites and more mafic rocks, such as harzburgites and pyroxenites. In underground exposures and in core specimens they appear as milky white bands separating such lithologies (see Figure 2.2d). In thin section these rocks are characterized by the occurrence of plagioclase grains which are equidimensional, and grain boundaries which meet in near perfect triple junctions of 120 degrees. This suggests that they have been recrystallized. Furthermore these grains do not appear to be zoned, while any preferred orientation has been destroyed, and they do not appear to contain any true postcumulus material, although some olivine and pyroxene grains from overlying lithologies may be incorporated within them. Figure 3.1c is a photomicrograph of such an annealed anorthosite. The three petrographic varieties of anorthosite described above need not constitute entire anorthosite layers, indeed they seldom do, the norm being a gradation of one into another.

Accessory phases in anorthosites include biotite, chromite, olivine, base-metal sulphides and magnetite. Biotite often occurs as fine needles which are preferentially oriented parallel to exsolution lamellae in pyroxene oikocrysts, or as large flakes in close association with pyroxene, chromite or magnetite grains. Chromite is most common in the anorthosite comprising the footwall of the UG-1 chromitite layer, where

Figure 3.1a Photomicrograph of a typical mottled anorthosite, with intercumulus orthopyroxene which poikilitically enclose cumulus plagioclase grains. Note the smaller, rounded nature of the enclosed grains.

Figure 3.1b Photomicrograph of an "adcumulus anorthosite", which consists entirely of plagioclase. Note the preffered orientation of the larger grains and the cluster of smaller grains (upper right), which disrupt the layering.

Figure 3.1c Photomicrograph of the contact between harzburgite and an "annealed anorthosite". The two rock types are seperated by a thin chromitite layer (dark grains in the centre). Note the recrystallized nature of the plagioclase grains.

Figure 3.1d Photomicrograph of a resorbed olivine grain in the Footwall anorthosite of borehole AF.

Figure 3.1e Photomicrograph of a sulphide bleb (dark patch, lower right) in the Merensky anorthosite.

Figure 3.1f Photomicrograph of intercumulus magnetite (dark patches, centre right) in the Giant Mottled Anorthosite.

Figure 3.1g Photomicrograph of the P2-middling leuco-troctolite showing the presence of olivine grains, whose outer reaches contain inclusions of plagioclase.

Figure 3.1h Lower magnification photomicrograph of the P2-middling leucotroctolite, showing the predominance of cumulus plagioclase over olivine.

NOTE: The scale bar below each photomicrograph represents 1 millimetre.

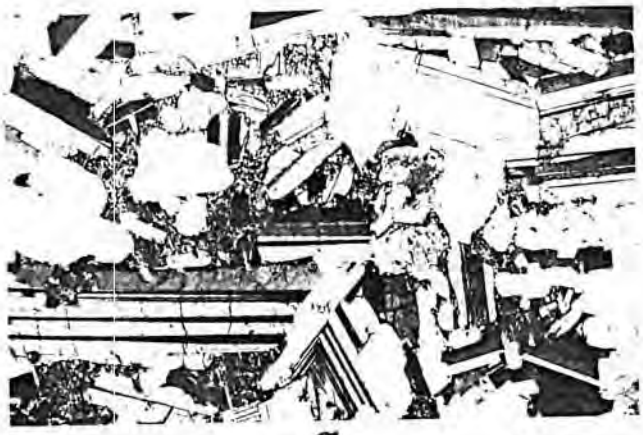

a

b

c

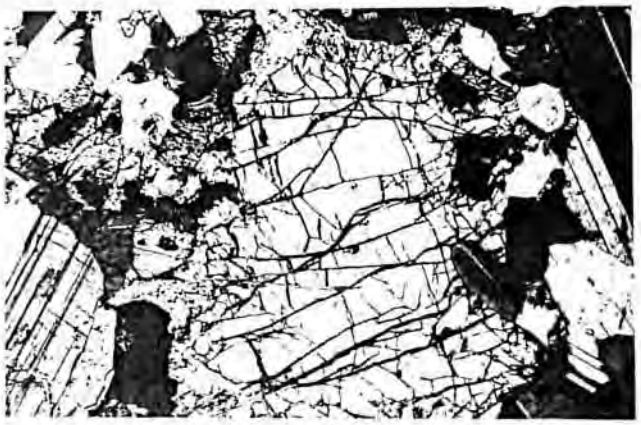

d

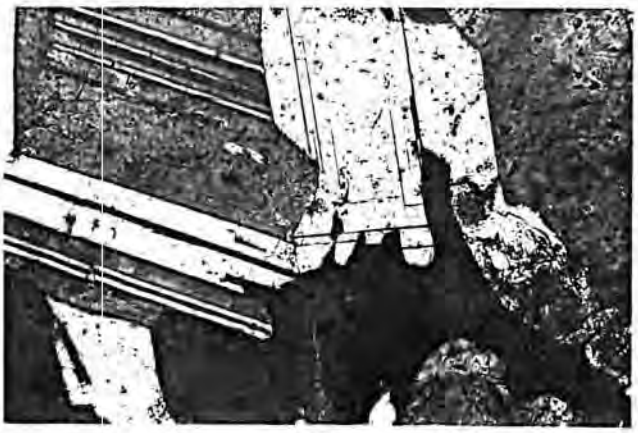

e

f

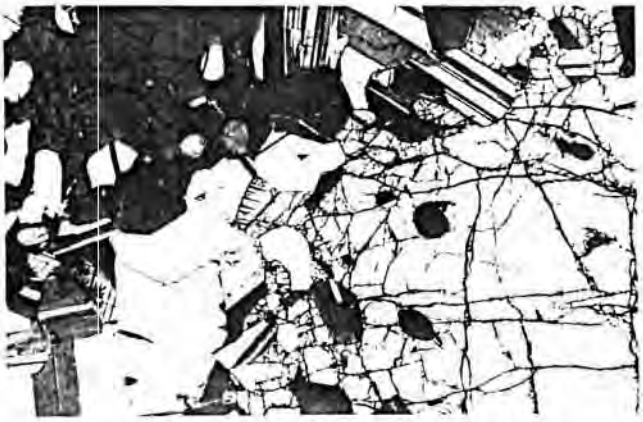

g

h

large concentrations of euhedral grains form stringers or bands of chromitite. This mineral can also be found in other anorthosites as well, where it occurs as tiny (0.1 mm) euhedral grains, commonly at plagioclase grain boundaries. Olivine is a rare constituent in anorthosites, but a few resorbed grains were found in the Footwall anorthosite in borehole AF. where they are mantled by a rim of reaction magnetite and orthopyroxene (see Figure 3.1d). Base-metal sulphides are frequently encountered in anorthosites underlying mafic layers such as the Bastard, Merensky, and Upper Pseudo Reef horizons. Here they occur as anhedral blebs in pore spaces between cumulus plagioclase grains. Because they are restricted to the uppermost contact regions of anorthosites, it likely that they originate from the overlying mafic layers. Sample AE-16 is a particularly good example of an anorthosite containing sulphide blebs (see figure 3.1e). Apart from being an alteration phase of olivine, magnetite may occur as a discrete postcumulus phase in the Bastard (Giant Mottled) anorthosite (see Figure 3.1f).

The P-2 Middling anorthosite may contain a troctolitic layer in which large clots of olivine are to be found in a predominantly plagioclase rock. This olivine may be both cumulus and postcumulus in nature, as the centers of the grains do not appear to be indented by feldspar, while the outer regions of the grains poikilitically enclose small plagioclase laths. This suggests an original cumulus grain onto which late-stage growth was added. Figure 3.1g is a photomicrograph of this rock.

Late stage deuteric alteration of anorthosites is generally limited to that which occurs along, and adjacent to pervasive veins and cracks which transgress the rock. This alteration usually results in the saussuritization of plagioclase and the replacement of pyroxene by a felted intergrowth of chlorite and sericite. Olivine, where it is present, appears to be most affected, being altered to serpentine, magnetite and bowlingite and/or iddingsite.

3.3 Norites

Norites contain both orthopyroxene and plagioclase as cumulus mineral constituents. The relative abundance of these two mineral phases is extremely variable, and may vary systematically with stratigraphic height in some units. For these reasons it is convenient to divide norites into three subtypes, namely, leuconorite, norite (or mesonorite) and melanorite. In this regard the proposal of Scoon (1985), that the three subtypes be defined in terms of their modal percentages of orthopyroxene, is adopted. Thus leuconorites contains less than 30 percent, norites between 30 and 70, and melanorites more than 70 percent cumulus orthopyroxene respectively. It is important to note here that a number of synonyms for these varieties are to be found in the literature. For example, Vermaak (1976) uses the name "spotted anorthosite" for leuconorite, while Viljoen et al. (1986) use "anorthositic norite" and "pyroxenitic norite" as synonyms for

"leuconorite" and "melanorite" respectively. The former author's classification is not justifiable in terms of that laid out at the begining of this chapter, as the "spots" of spotted anorthosites are aggregates of cumulus orthopyroxene, and the rock should therefore be termed a norite.

Norites are to be found in the Bastard, Merensky, Footwall and Lower Pseudo units, where they are often the dominant rock type (volumetrically). There is often a gradation between poikilitic pyroxenite and melanorite at the base, and less commonly between leuconorite and anorthosite at the top of these units. A feature of the contact between leuconorite and mottled anorthosite in the Footwall Unit, is the development of two dark, pyroxene-rich bands (5-10 cm thick) separating the two lithologies. Within the norites themselves there is often a gradation from melanorite at the base through norite to leuconorite. The relative thicknesses of these three subtypes vary, but mesonorite usually is dominant. The norite layer of the Lower Pseudo Unit is unusual in that it does not have a melanoritic base, and mesonorite overlies harzburgite.

In thin section it can be seen that pyroxene grain morphology is extremely variable. In the leuconorites the cumulus nature of primocryst orthopyroxene grains is often obscured by late-stage overgrowths, which also poikilitically enclose some plagioclase grains and thus impart a mottle-like aspect to the rock (see figure 3.2a). The cumulus core however, is revealed where such grains are in contact and mutual interference boundaries are developed between them. In meso- and mela-

norites interference boundaries are more common, and late-stage overgrowths less common. Where orthopyroxene grains are unaffected by late-stage overgrowth two dominant grain forms are obvious, namely a stumpy, prismatic, equidimensional habit, and an elongated lath-like habit, in which the length:breadth ratio of the grains is around 3:1 (see figure 3.2b). There does not appear to be any systematic correlation between the occurrence of the two forms and stratigraphic position.

Plagioclase grain morphology in norites is not unlike that in anorthosites, and two distinctive populations can be recognized, namely a population of small, sometimes rounded grains which are enclosed in oikocrysts of pyroxene, and larger subhedral to euhedral grains which are oriented in a preferred direction. In pyroxene-dominated lithologies a subophitic relationship is commonly developed between plagioclase and orthopyroxene, while there is also a tendency for small plagioclase grains to be clustered around the peripheries of larger orthopyroxene grains (Figure 3.2c).

Clinopyroxene is a common minor constituent of norites, in which it may be found in at least four distinctly different habits. Most commonly it occurs as large oikocrysts which poikilitically enclose both plagioclase and orthopyroxene. These poikilocrysts are randomly distributed, and are present in all the different norite layers. Clinopyroxene may also be found as reaction rims around some orthopyroxene grains, where

it apparently is the product of a reaction between orthopyroxene and plagioclase (Wells, 1952). Thirdly, this mineral is found as exsolution lamellae and blebs in orthopyroxene, where the lamellae are parallel to the (100) crystal face of the host (see figure 3.2d). It is also possible that some of the rims previously mentioned are the result of the migration of exsolved material beyond the confines of the host grain. This could be particularly true where such rims are in optical continuity with exsolution lamellae. A more rare occurence of clinopyroxene is where it has formed symplectic intergrowths with orthopyroxene. Wells (1952) recognized similar features, and concluded that the lack of normal crystal faces in these intergrowths could be taken as evidence for their co-crystallization. If this is so it means that orthopyroxene crystallized over an extended time-period.

Minor phases in these rocks include olivine, biotite and chromite. Olivine occurs only in the Footwall norite, and in most cases it is restricted to the lower portions of the layer. In borehole AF, however, widely scattered, partially resorbed olivine grains occur above the Footwall Marker. Biotite is present in most thin sections where it is usually closely associated with pyroxene grains, but it also occurs as larger postcumulus grains filling interstitial spaces between cumulus grains. Chromite is an accessory component of norites, and generally occurs as small (0.05-0.1 mm), euhedral, widely scattered grains.

Most norites which were examined in thin section are fresh,

Figure 3.2a Photomicrograph of a cumulus orthopyroxene grain in norite, showing a late-stage overgrowth which poikilitically encloses small plagioclase grains.

Figure 3.2b Photomicrograph of a norite, showing the occurrence of two different orthopyroxene habits.

Figure 3.2c Photomicrograph of a norite showing the poikilitic enclosure of orthoproxene and plagioclase by clinopyroxene.

Figure 3.2d Photomicrograph of cumulus orthopyroxene in norite, showing the development of fine exsolution lamallae of clinopyroxene parallel to the (100) crystallographic direction of the host grain.

Figure 3.2e Photomicrograph of a poikilitic pyroxenite, showing the interpenetration of cumulus orthopyroxene grains, and the nature of intercumulus plagioclase.

Figure 3.2f Photomicrograph showing the enclosure of cumulus orthopyroxene by intercumulus clinopyroxene. Note the resorbed nature the enclosed grains.

Figure 3.2g Photomicrograph of poikilitic pyroxenite under-lying a thin chromitite later. Note the presence of an extremely elongated orthopyroxene grain, whose direction of elongation parallels the base of the chromitite layer.

Figure 3.2h Photomicrograph showing a strained cumulus orthopyroxene grain, whose exsolution lamallae are kinked. Note also, that the intercumulus plagioclase grains are polygonized, further evidence of strain.

NOTE: The scale bar below each photomicrograph represents 1 millimetre.

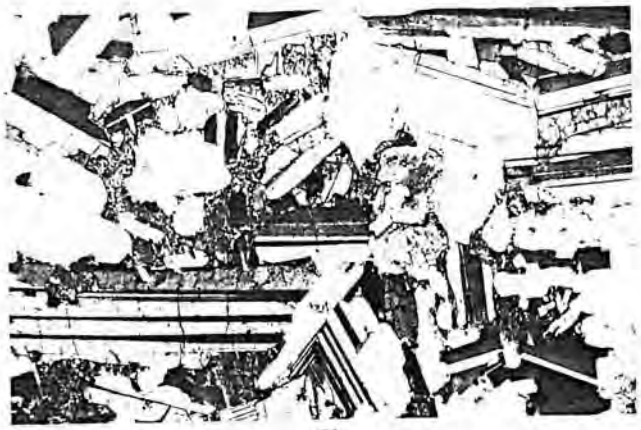

a

b

c

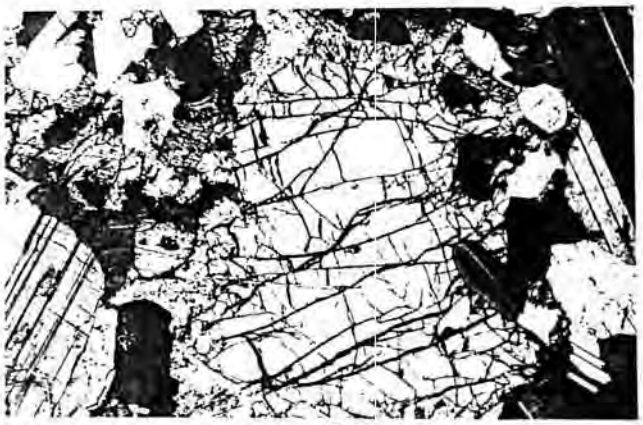

d

e

f

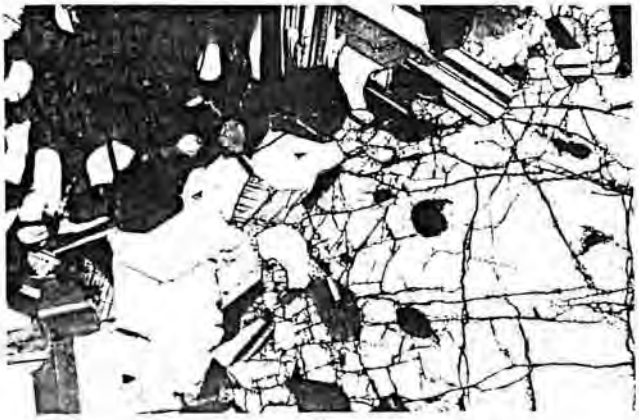

g

h

with alteration being restricted to crosscutting veins and their immediate surroundings.

3.4 Pyroxenites

These rocks have orthopyroxene (>90%) as their dominant cumulus mineral phase, while olivine and chromite may be present in lesser amounts. The orthopyroxene is usually bronzite and consequently the rock is often referred to as bronzitite but the simple term "pyroxenite" is preferred here, and since cumulus clinopyroxene cumulates do not occur in the succession this term may be used unambiguously. Two distinct textural varieties of pyroxenite, namely poikilitic and pegmatoidal, can be recognized. These two varieties are considered separately below.

3.4.1 Poikilitic Pyroxenites.

These rocks are characterized by the poikilitic enclosure of fine- to medium- grained orthopyroxene crystals by postcumulus plagioclase and clinopyroxene oikocrysts. In the study section they constitute large portions of the UG-1 and UG-2 Units, while in the Merensky and Bastard Units they form prominent horizons at or near the base. Significantly, they are absent from the Footwall Unit.

The cumulus orthopyroxene grains are variable in both size and morphology, and although they are generally euhedral to

subhedral in habit, two distinct crystal forms can be recognized. Firstly, there are stumpy, prismatic grains whose dimensions are roughly equidimensional, and secondly there is a population of lath-like grains, whose length/breadth ratios average around 3:1. Some exceptional individuals have ratios of 9:1. These elongated individuals are often located near small chromitite layers, and it may be significant that their long axes are oriented parallel to the bases of these layers (see Figure 3.2g and 3.4f). The subhedral nature of many orthopyroxene grains is brought about by a number of interactions and reactions. A common feature is to find interlocking orthopyroxene laths, in which one grain appears to penetrate another (see Fig.3.2e). Secondly, where orthopyroxene grains are enclosed by clinopyroxene oikocrysts, the former grains have a rounded appearance, suggestive of a reaction relationship between them (see Figure 3.2f). A third phenomenon, which has previously been described by Eales and Reynolds (1986) is the occurence of embayments of plagioclase into orthopyroxene wherever this mineral is in contact with chromian spinel. This is attributed by these authors to the following reaction;

Mg-Al spinel + Opx + liquid = Fe-Cr spinel + Plag + liquid.

This reaction likewise may explains the occurrence of halos of plagioclase which surround inclusions of chromite in orthopyroxene (see Figure 3.4b). Many orthopyroxene grains contain fine, closely spaced exsolution lamellae and blebs of clinopyroxene, which are arranged parallel to the (100) plane

of the host grain. Two features of these lamellae are particularly noteworthy. Firstly, it is apparent that not all orthopyroxene grains in a thin section contain such lamellae; and secondly, a number of these grains have been strained, and consequently their exsolution lamellae have been kinked (see figure 3.2h). Of particular interest in the latter case is that not all grains in a particular thin section have kinked lamellae, and orthopyroxene grains with kinked lamellae may coexist alongside others which do not appear to have suffered any strain.

Plagioclase is the dominant postcumulus phase in these rocks, and in many cases it may contribute 10 percent or more to the rock's mode. In such cases the rock is referred to as a feldspathic poikilitic pyroxenite. Individual plagioclase grains are generally large (>5mm), and poikilitically enclose both orthopyroxene and chromite grains, and in many grains distinct zoning is disernable. In some grains zoning may be obscured by strain effects, while in other specimens strain has led to the recrystallization or polygonization of large grains into a number of smaller individuals. These may easily be confused with cumulus grains (see Fig 3.2h). The postcumulus nature of plagioclase is best confirmed by its presence in myrmekitic intergrowths with quartz (Fig.3.3a).

Clinopyroxene is a subordinate, but important postcumulus phase, which occurs as large, sporadic oikocrysts enclosing cumulus orthopyroxene and chromite grains, as well as postcumulus plagioclase. This means that it is an extremely late

crystallization-product in these rocks. However, some grains appear to possess cumulus affinities as well, such as well developed crystal faces and rational interference boundaries with orthopyroxene grains. This is indicative of an extended crystallization period. Other postcumulus phases include biotite, quartz, an opaque phase and calcite. Biotite is clearly recognizable as an intercumulus precipitate, and although it generally does not constitute more than 5 percent of the rock's mode, it may be locally more common, particularly in the UG-1 pyroxenite, where it may be the product of a late crystallizing, vapour-enriched liquid. The occurrence of quartz in the postcumulus assemblage has also been documented by Vermaak and Hendriks (1976) and De Klerk (1982). In these rocks this mineral is sparsely developed, and individual grains seldom exceed 0.1 mm in diameter. Similarly calcite occurs as small discrete anhedral grains, whose habit negates any suggestion that it is an alteration product of some other primary phase, (see Fig. 3.3c), although it may be of hydrothermal origin. There is some evidence to suggest that an opaque phase, possibly a spinel, may have crystallized from the postcumulus liquid. In figure 3.4h an opaque grain which partially encloses part of a postcumulus plagioclase grain can be seen.

The poikilitic pyroxenites from the different units are similar in most macroscopic features, including grain size and mineral composition. The UG-2 pyroxenite however, is the only horizon which contains olivine, and here it occurs only at the

Figure 3.3a Photomicrograph showing the presence of a myrmekitic intergrowth of quartz and plagioclase in the intercumulus assemblage of poikilitic pyroxenite.

Figure 3.3b Photomicrograph of a poikilitic pyroxenite, showing the presence of cumulus orthopyroxene and intercumulus plagioclase. Note also the coexistence of strained and unstrained cumulus grains.

Figure 3.3c Photomicrograph showing the presence of calcite in the intercumulus assemblage of pokilitic pyroxenite.

Figure 3.3d Photomicrograph of the pegmatoidal pyroxenite of the Merensky Reef, showing the presence of coarse olivine grains, and large intercumulus plagioclase grains.

Figure 3.3e Photomicrograph showing the enclosure of a rounded plagioclase grain in an altered cumulus olivine grain in the Merensky Reef.

Figure 3.3f Photomicrograph of a finer-grained olivine grain, showing the development of a reaction rim of clinopyroxene, in the Merensky Reef.

Figure 3.3g Photomicrograph showing a symplectic intergrowth of olivine and orthopyroxene in the Merensky Reef.

Figure 3.3h Photomicrograph of Upper Pseudo Reef harzburgite, showing the presence of cumulus olivine and orthopyroxene.

NOTE: The scale bar below each photomicrograph represents 1 millimetre.

a

b

c

d

e

f

g

h

base of this layer. The UG-1 and UG-2 poikilitic pyroxenites contain a considerably greater proportion of scattered, accessory chromian spinel grains than their Merensky and Bastard Unit counterparts.

3.4.2 Pegmatoidal Pyroxenites.

These rocks, whose main cumulus constituent is orthopyroxene, may also contain significant proportions of olivine and chromite, as well as large postcumulus grains of plagioclase and clinopyroxene, while base metal sulphides are a common accessory phase. As their name implies, they are extremely coarse grained rocks, a characteristic which makes them difficult to describe from thin sections of conventional size. Pegmatoidal pyroxenites are present in the study section in the platiniferous Merensky Reef, the lowermost few centimetres of the Footwall Unit, the Lower Pseudo Reef and the immediate footwall of the UG-2 chromitite (or UG-1 pegmatoidal pyroxenite). Each of these occurrences is considered separately below.

3.4.2.1 The Merensky Reef.

This horizon is bounded on both upper and lower surfaces by thin chromitite layers, and it is texturally a most inhomogeneous layer. In general, it can be considered to be an olivine-bearing pegmatoidal pyroxenite, and while Vermaak and Hendriks (1976) give an average modal composition of:-

orthopyroxene	65.2 percent
feldspar	18.8 percent

clinopyroxene 12.9 percent
olivine 2.7 percent

for Rustenburg and Union Sections, the Amandelbult variety would appear to contain a greater modal proportion of olivine. Megascopically, that is in underground exposures, the central and lower portions of the Reef contain more olivine than the upper parts. The proportion of intercumulus space between cumulus grains may be great, and is largely filled by large postcumulus plagioclase grains (see figure 3.3d), while large clinopyroxene and biotite grains may also be locally common. The poikilitic enclosure of a number of cumulus grains by a single postcumulus phase is a common feature of this lithology. Smaller postcumulus grains of base-metal sulphides and quartz complete the intercumulus assemblage. A feature that does not appear to have been satisfactorily explained is the manner in which the cumulus grains are widely separated within the intercumulus phases. This renders it difficult to accept that the cumulus phases ever occurred as packed aggregates of grains between which the intercumulus liquid crystallized merely as an "infill".

The inter-relationships between the various mineral phases are particularly complex in this rock, and often obscured by late stage deuteric alteration of cumulus grains. The mineral species most affected by alteration is olivine, which is often pervaded by thick veins of serpentine, chlorite and magnetite. In some cases this alteration has resulted in the total replacement of the grain (see figures 3.3e and f). Pyroxene and feldspar grains are less affected, but some sericitiztion and saussurization of these phases can be seen in places.

Vermaak and Hendriks (op.cit) recognized a bimodality in grain size distribution of olivines and pyroxenes in the Reef, a feature which is readily recognizable in the rocks of this study section as well. Figure 3.3f (sample AF-28) shows typical examples of the finer grained variety of olivine, while figure 3.3d exhibits typically larger grains. Some rounded anhedral olivine grains are separated from postcumulus feldspar by a rind of clinopyroxene, while in other instances subhedral grains of olivine are in direct contact with postcumulus feldspar and no "reaction rim" of clinopyroxene is developed between the two phases. Furthermore some olivine grains may themselves contain rounded inclusions of plagioclase (Figure 3.3e). The relationship between orthopyroxene and olivine is also apparently incongruous, as in some cases a grain of the former phase may poikilitically enclose an olivine grain, (Figure 3.3g) while in the same thin section a symplectic intergrowth of the two may be seen. A further complication is a situation where rational grain boundaries between the two phases are developed.

3.4.2.2 The Lower Pseudo Reef

This thin horizon may resemble the Merensky Reef, although grains may not be as large. Large orthopyroxene grains dominate the cumulus assemblage, but olivine grains are not uncommon. These latter grains are of two recognizable types. Firstly, there are large anhedral grains which are intergrown with orthopyroxene, the interface between them consisting of

cuspate - lobate projections of one into the other; and secondly there are subhedral grains which may be poikilitically enclosed in either orthopyroxene, clinopyroxene or plagioclase. Those olivine grains enclosed by orthopyroxene are usually rimmed by a rind of clinopyroxene. Chromite is a common accessory cumulus phase.

The postcumulus assemblage is dominated by plagioclase, with lesser amounts of clinopyroxene and biotite being present. Generally, the contribution of plagioclase to the overall mode of the rock seldom exceeds ten percent.

3.4.2.3 The UG-1 Pegmatoidal Pyroxenite.

This horizon is totally devoid of olivine and the cumulus assemblage consists mostly of orthopyroxene with accessory chromite. Plagioclase is the dominant postcumulus phase, with lesser amounts of clinopyroxene and biotite being represented. Although the orthopyroxene grains in this horizon are larger than those found in poikilitic pyroxenites, the extremely large grains (more than 2cm) found in other pegmatoidal pyroxenites are not represented here. Nevertheless, this member is distincly coarser grained than the underlying poikilitic pyroxenite, and therefore warrants distinction from other pyroxenite layers.

3.5 Harzburgites.

Harzburgites are those rocks which contain both olivine and orthopyroxene as cumulus phases, and in which the former species is dominant. In the upper Critical Zone at Amandelbult these rocks are minor layers, restricted to the Pseudo Reef horizons. The harzburgites are medium grained, melanocratic rocks which often contain significant quantities of intercumulus plagioclase. This results in an essentially dark-coloured rock with a spotted white appearance, for which the name "tarentaal" (guineafowl) has been coined by the miners.

The upper Pseudo Reef horizon in the western portions of the mine consists of two harzburgite layers which are separated by an anorthositic to leucotroctolitic layer (the P2-middling). The two harzburgitic layers are very similar in appearance, consisting of subhedral olivine and subhedral to anhedral orthopyroxene cumulate grains. Where these two mineral species are in contact, embayments of one into the other are a common feature, which is suggestive of disequilibrium between them (see figure 3.4a). Less common is the poikilitic enclosure of orthopyroxene by olivine. Apart from postcumulus plagioclase, the occurrence of large clinopyroxene oikocrysts is a feature of these rocks, and chadacrysts of olivine and orthopyroxene are commonly enclosed by it. Biotite is a less common postcumulus phase.

The alteration of mafic mineral phases in harzburgites has a

Figure 3.4a Photomicrograph of a harzburgite, showing the poikilitic enclosure olivine by orthopyroxene.

Figure 3.4b Photomicrograph of a resorbed, elongated orthopyroxene grains adjacent to a thin chromitite layer.

Figure 3.4c Photomicrograph of an un-annealed chromitite layer.

Figure 3.4d Photomicrograph of an annealed chromitite layer.

Figure 3.4e Photomicrograph of an un-annealed chromitite layer, in which stacks or chains of chromite layers can be recognized.

Figure 3.4f Photomicrograph showing the occurrence of ovoid structures which possibly describe the original outlines of orthopyroxene grains, which have since been resorbed.

Figure 3.4g Photomicrograph of a chromite inclusion orthopyroxene, around which a plagioclase halo has developed.

Figure 3.4h Photomicrograph of an opaque grain which poikilitically encloses intercumulus plagioclase.

NOTE: The scale bar below each photomicrograph represents 1 millimetre.

a

b

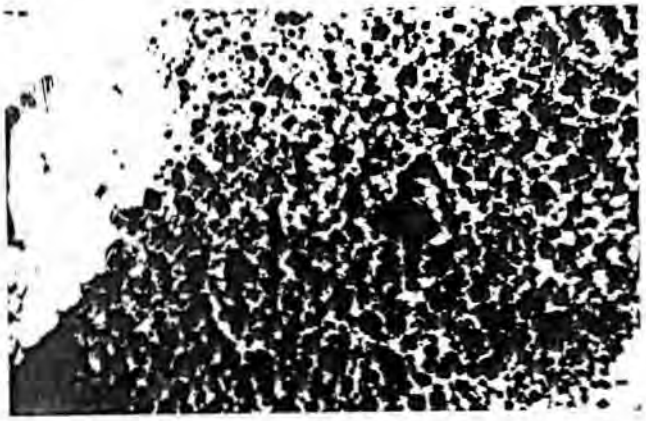

c

d

e

f

g

h

profound influence on the appearance of the rock. The most notable effect is the breakdown of olivine which yields an array of alteration products, such as serpentine, magnetite and iddingsite-bowlingite intergrowths. Pyroxene and feldspar are less affected and are only mildly altered. In some rocks alteration leads the the total breakdown of all primary phases.

3.6 Chromitites.

Chromitite is a rock which consists almost entirely of chromian spinel. In the Critical Zone of the Bushveld Complex a large number of such layers have been described, and they have been assigned to three main groups, namely the Lower (LG), Middle (MG) and Upper (UG). All of those intersected in the study section are from the Upper Group. The thickest of these are the UG-1 and UG-2, which, were not sampled because of restrictions imposed by the mine management. However, a number of smaller chromitites were sampled. These occur at the following positions;

i. between the P2 harzburgite and P2-middling anorthosite-leucotroctolite;

ii. between the P2 harzburgite and the P1 anorthosite;

iii. between the Lower Pseudo Reef (P1) and the UG-2 poikilitic pyroxenite;

iv. the chromitite which is half a metre above the main

UG-2 chromitite, in the UG-2 poikilitic pyroxenite

v. a thin layer approximately 4 metres below the UG-2 leader, in the UG-1 poikilitic pyroxenite;

vi. various layers, closely related to the UG-1 in both the UG-1 poikilitic pyroxenite, and the underlying UG-1 Footwall anorthosite.

In broad terms the chromitites can be described in terms of two end-member textural varieties. The more primitive end member consists of an aggregate of individually recognizable grains with intercumulus plagioclase, while the most evolved type has chromite grains which have coalesced and annealed to such a degree that individual cumulus grains are no longer recognizable. Figures 3.4c and d, illustrate typical examples of such endmembers. Any intermediate texture between these endmembers may be preserved.

Eales and Reynolds (1986) describe a number of textural features of chromitites at Union Section. Some of these are recognizable at Amandelbult as well. Firstly, there is a wide range in the sizes of chromite grains, and where they are scattered, they are small (0.05-0.1 mm), but where they have coalesced they are considerably larger (up to 1 mm). In some layers small grains form the base of the layer, while the largest grains tend to be found in the centres and at the tops of layers. This is a feature which must lead one seriously to question gravity-settling as a viable mechanism for their presence. In some relatively un-annealed chromitites, grains

appear to have been stacked on top of one another to form long columns (see Figure 3.4e). In places these columns may bifurcate to form branches. This feature is attributed by Eales and Reynolds (op.cit) to in-situ growth and to be inimical to the hypothesis of growth by cumulus deposition. Another feature which was noted by these authors, is the occurrence of ovoids formed by scattered chromite grains which are surrounded by orthopyroxene grains (Fig.3.4g). Furthermore , as has been previosly noted, many chromite grains that have been enclosed within, or that grew adjacent to, orthopyroxene grains, are surrounded by a halo of plagioclase. This reaction relationship may also explain the occurrence of arrangements of chromite grains which mimic the original euhedral shapes of orthopyroxene grains, which have since been totally replaced by intercumulus plagioclase (Figure 3.4d).

The chromitites of the Pseudo Reef horizons are generally very thin (0.5cm), and discontinuous. The Merensky pegmatoid is bounded on both surfaces by thin un-annealed chromitites. The uppermost of these is the last significant accumulation of chromite in the study section. In spite of the recognition of a chromitite layer at the base of the Bastard Reef, by Viljoen et. al.(1986) no such layer was encountered in any of the borehole cores that were sampled, and nor was it seen in underground exposures by the author.

CHAPTER4: MINERALOGY

4.1 Introduction

The majority of rocks in the study section consist of varying proportions of two main mineral types, namely orthopyroxene and plagioclase. Olivine and chromite are major constituents only in discrete layers. Chemical variations of the three abovementioned silicate phases were investigated by electron microprobe analysis using a Jeol 733 superprobe with crystal spectrometers. The analyses were performed on highly polished thin sections taken from regularly spaced samples through borehole AE. These samples include all nine olivine-bearing members as well as 32 other samples. The stratigraphic positions of the samples, and the minerals that were analysed in each are represented in figure 4.1, while the experimental conditions used for each type of analysis are summarized in Appendix B.

4.2 Olivine.

Olivine is an orthosilicate, whose structure is made up of independent SiO_4 tetrahedra which are linked by divalent cations in six-fold co-ordination (Deer et al., 1982). The ferromagnesian olivines, of which the Bushveld variety is an example, show a complete solid solution series between forsterite (Mg_2SiO_4) and fayalite (Fe_2SiO_4) in which complete diadochy exists between Mg^{2+} and Fe^{2+} (Deer et al. op.cit). In iron-rich members Mn and Ca may replace Mg and Fe, while at the magnesium end of the spectrum Ni may substitute for these ions.

Figure 4.1 A stratigraphic log showing the positions of samples which were analysed by electron microprobe, and the mineral species which were analysed.

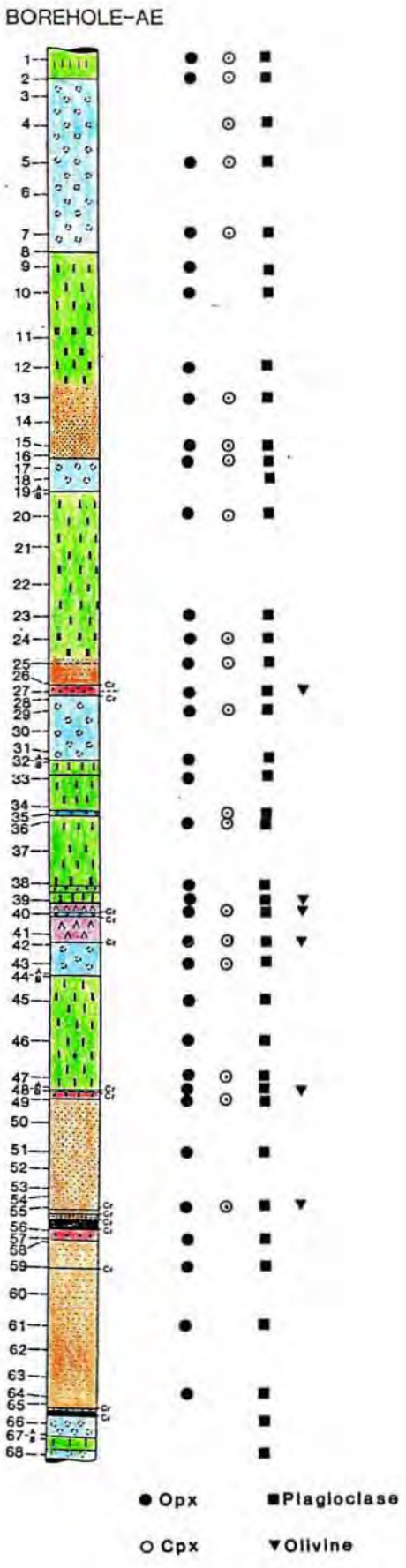

Figure 4.1

Table 4.1 Averaged olivine analyses for each of the olivine-bearing samples which were sampled. The analyses show weight percentage concentrations of element oxides, the number of cations, based on 4 oxygens, and the number of analyses used in the average (N).

TABLE 4.1 OLIVINE ANALYSES BY MICROPROBE

Sample Number:	AE-MR	AE-39.4	AE-39.5	AE-39.6	AE-40.1
Oxides					
SiO_2	39.55	40.75	39.85	39.90	40.01
FeO	18.52	14.06	16.91	17.92	15.68
MnO	0.22	0.19	0.22	0.26	0.20
NiO	0.32	0.33	0.32	0.29	0.31
MgO	41.40	45.60	43.37	41.62	43.54
CaO	0.02	0.02	0.01	0.02	0.01
Total	100.06	101.03	100.69	100.00	99.96
Cations					
Si^{4+}	1.0099	1.0073	1.0029	1.0145	1.0086
Fe^{2+}	0.3950	0.2912	0.3556	0.3810	0.3349
Mn^{2+}	0.0040	0.0040	0.0040	0.0057	0.0044
Ni^{2+}	0.0088	0.0060	0.0065	0.0058	0.0064
Mg^{2+}	1.5742	1.6630	1.6270	1.5781	1.6369
Ca^{2+}	0.0005	0.0004	0.0003	0.0004	0.0002
N	9	7	5	3	5

Sample Number:	AE-40.2	AE-42	AE-48	AE-55
Oxides				
SiO_2	40.15	40.13	40.11	39.90
FeO	16.95	16.87	16.57	18.69
MnO	0.21	0.22	0.19	0.23
NiO	0.32	0.34	0.35	0.35
MgO	43.23	42.38	43.44	41.16
CaO	0.02	0.02	0.01	0.02
Total	100.88	99.97	100.68	100.38
Cations				
Si^{4+}	1.0075	1.0157	1.0070	1.0144
Fe^{2+}	0.3557	0.3571	0.3480	0.3973
Mn^{2+}	0.0044	0.0048	0.0041	0.0050
Ni^{2+}	0.0064	0.0069	0.0071	0.0072
Mg^{2+}	1.6278	1.5993	1.6263	1.5611
Ca^{2+}	0.0006	0.0005	0.0003	0.0007
N	5	4	6	5

At Amandelbult, olivine occurs in thin pyroxenite and harzburgite layers at the base of each of the Merensky, Footwall, Lower Pseudo and UG-2 units, while in the Upper Pseudo Unit it occurs in a thicker harzburgite layer as well as in the thin leucotroctolitic P-2 middling layer. It is absent from the UG-1 and Bastard Units. 115 olivine analyses were performed on grains from nine thin sections. Averaged analyses for each sample are listed in Table 4.1

4.2.1 Fe-Mg Relationships.

Olivine may be regarded as an important genetic indicator mineral because it is generally one of the first minerals to crystallize from mafic liquids. As a result of the complete solid solution series which exists between Mg_2SiO_4 and Fe_2SiO_4, the measured Mg/Fe ratio of the mineral may give some clue as to the mafic nature of the liquid from which they crystallized, provided that its chemistry has not been altered subsequent to crystallization. In cumulate rocks, where whole-rock analyses cannot be equated with original liquid compositions, olivine chemistry may be the only possible indication of the nature of that original liquid.

The Mg-Fe relationship in olivine is conventionally expressed as a Fo (forsterite) value, which is the atomic $Mg/(Mg+Fe^{2+})$ ratio. A plot of these values against a stratigraphic column in figure 4.2. shows that a fair degree of variation is prevalent both within individual layers and between successive olivine-bearing layers. It could be said that there is a general upward increase in Fo with height in the column

Figure 4.2 A plot of mole percentage Fo in olivine, against a stratigraphic log. Here P-1, P-2 and MR refer to Lower Pseudo, Upper Pseudo and Merensky Reef respectively.

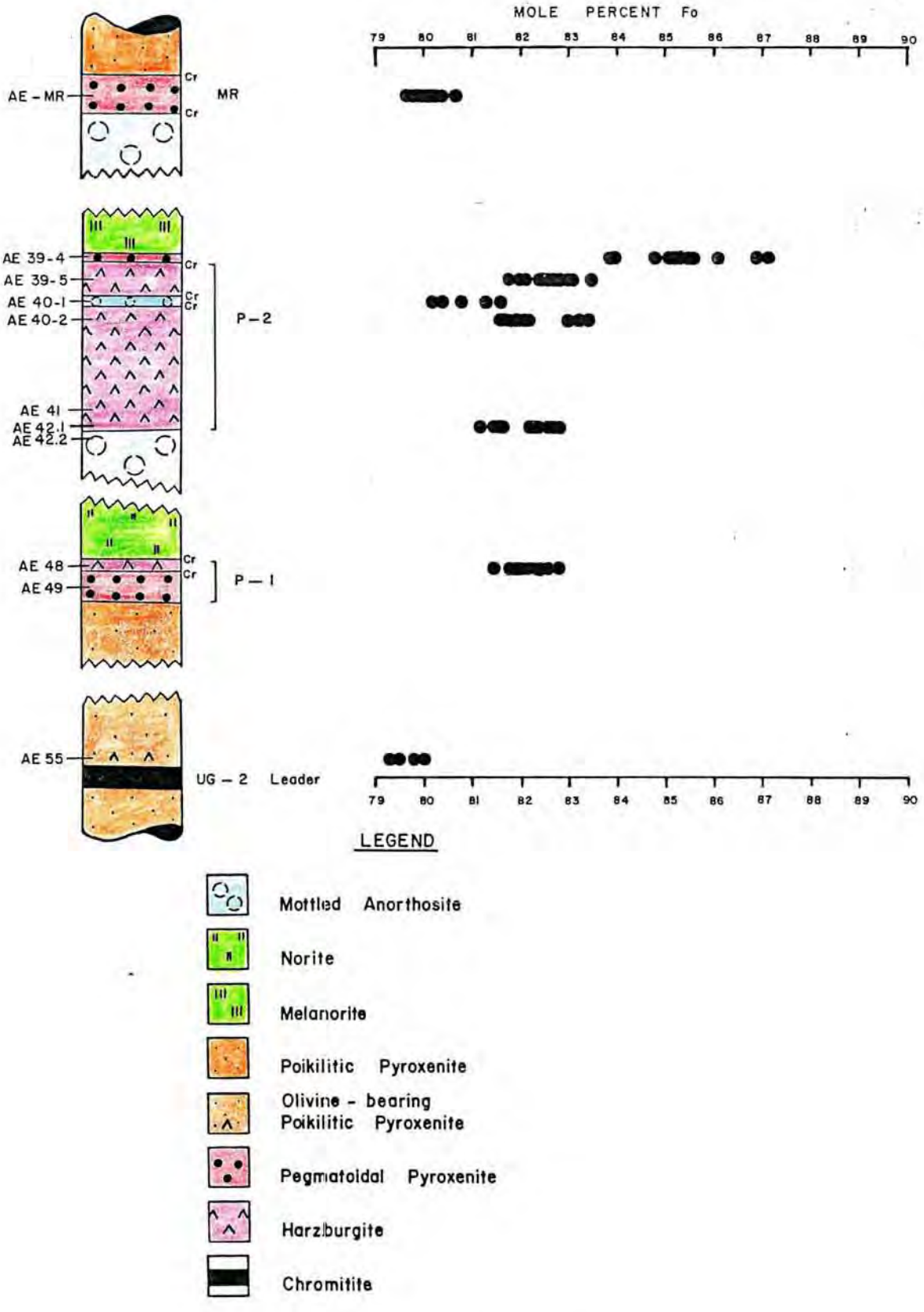
MOLE PERCENT Fo
79 80 81 82 83 84 85 86 87 88 89 90
AE - MR
Cr
Cr
MR
AE 39-4
AE 39-5
AE 40-1
AE 40-2
AE 41
AE 42.1
AE 42.2
Cr
Cr
Cr
P - 2
AE 48
AE 49
Cr
Cr
P - 1
AE 55
UG - 2
Leader
79 80 81 82 83 84 85 86 87 88 89 90
LEGEND
Mottled Anorthosite
Norite
Melanorite
Poikilitic Pyroxenite
Olivine - bearing Poikilitic Pyroxenite
Pegmatoidal Pyroxenite
Harzburgite
Chromitite

Figure 4.2

between the basal portions of the UG-2 Unit (Fo $_{79.3-80.0}$) through the Lower Pseudo Reef (Fo $_{81.5-82.6}$), to the Upper Pseudo Reef (Fo $_{81.8 \text{ to } 83.4}$), with the highest value of Fo $_{89}$, being attained in the olivine-bearing pegmatoidal pyroxenite of the Footwall Unit (the P2 Marker). The olivines of the P2 middling leucotroctolite have lower Fo values (80.4 to 81.6) than their equivalents in both enveloping harzburgite layers of the Upper Pseudo Reef. The olivines of the Merensky Reef, which has the highest stratigraphic occurrence of olivine in the study area, have low Fo values of 79.7 to 80.4. In each of the olivine-bearing layers no significant chemical zonation could be detected in individual grains, so that the ranges in compositions evident in figure 4.2, reflect grain-to-grain variations.

In the light of this mineral's early position in the crystallization sequence, it could be suggested that each of the olivine-bearing layers between the UG-2 and Footwall Units represents the crystallization of increasingly magnesian liquids. Before accepting this possibility however, it is necessary to consider factors which may have influenced the composition of olivine. Since chromite is a fairly common accessory cumulus phase in harzburgites and olivine-bearing pyroxenites, and since it also an early crystallizing phase from mafic liquids, olivine-spinel interactions may have important genetic implications. Jackson (1969) and Evans and Wright (1972) assumed that liquidus equilibrium between olivine and spinel is maintained at sub-solidus temperatures, and further that the partitioning of Fe and Mg between the two species could be used as the basis for a geothermometer. Roeder et al.(1979) subsequently re-evaluated the olivine-

spinel geothermometer, and showed convincingly that subsolidus re-equilibration is indeed possible between the two mineral species, particularly in plutonic rocks which remain at elevated temperatures for long periods. This means that the Fe in olivine is likely to be exchanged for Mg in spinel, with the result that the Fo value of olivine is modified and no longer is representative of the grain's original liquidus composition. It is indeed significant therefore that the sample which yielded values of Fo_{87} contains a 2 cm thick chromitite layer, whilst the Merensky Reef and P2 middling samples, which have lower Fo values, contain little or no chromite grains. Furthermore, if the lowest measured Fo values for each sample are taken as the best approximations of liquidus compositions, a far narrower range ($Fo_{79.3-81.8}$) is described. This indicates, that each new liquid input, from which each succesive olivine-bearing layers crystallized, was problably of a similar composition.

4.2.2 Ni-Olivine Relationships.

The partitioning of Ni between olivine crystals and their coexisting liquid has been regarded by some authors, for example Ringwood (1956), as being of some genetic significance. Deer et al. (1982) regard the partition data with some circumspection, as it has been shown, for example by Hart and Davis (1978), that partition coefficients are dependent on a number of factors including temperature, pressure and bulk composition. Nevertheless, Scoon (1985) and Scoon and De Klerk (in press) have shown that successive olivine-bearing layers at Union and Amandelbult Sections are

Figure 4.3 A plot of Fo mole percent against NiO for olivine grains. In (a) each individual analysis is plotted, and in (b) averged analyses for each sample are plotted. The error bars in (b) represent one standard deviation. Symbols: stars - Merensky Reef; solid triangles - P2 middling; open triangles - P2 marker (base of Footwall Unit); open circles - base of UG-2 Unit; solid circles - Upper Pseudo Reef, upper layer; solid squares - Upper Pseudo Reef, lower layer; open squares - Lower Pseudo Reef.

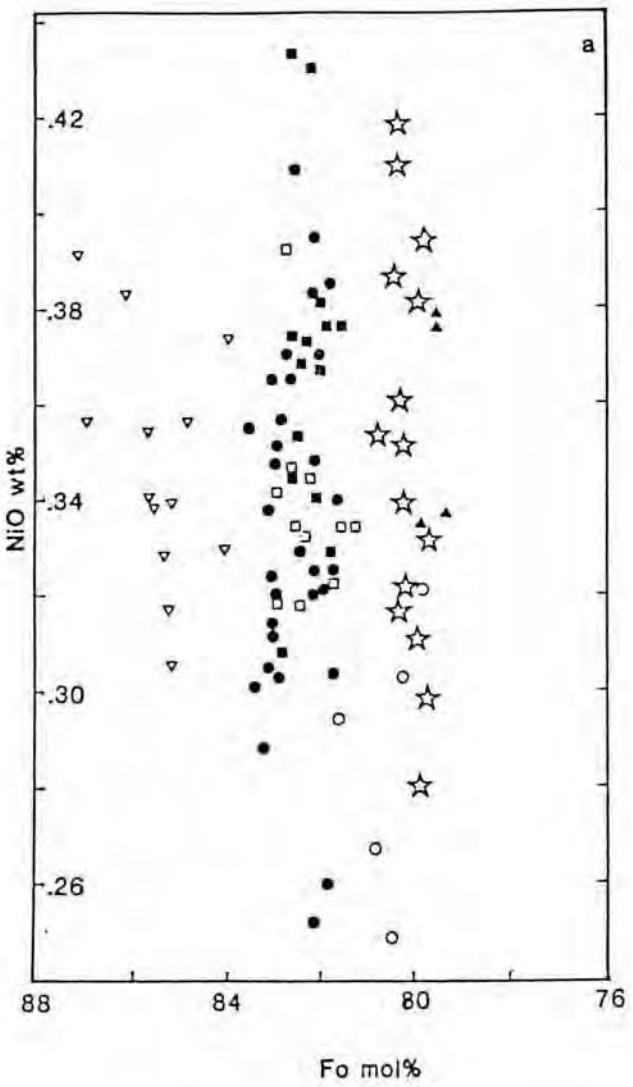
a
.42
.38
.34
.30
.26
NiO wt%
88
84
80
76
Fo mol%

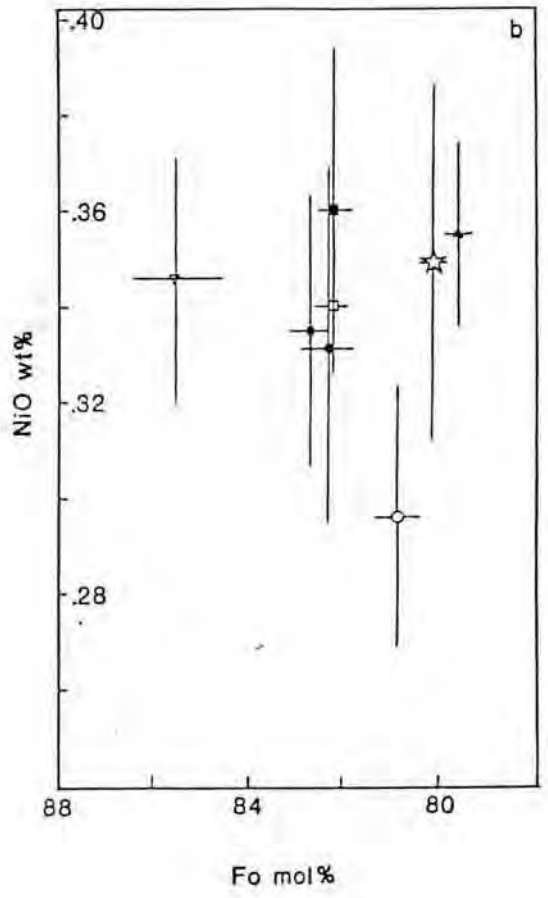
b
.40
.36
.32
.28
NiO wt%
88
84
80
Fo mol%

Figure 4.3

uniquely characterized by the Ni/Mg ratios of their constituent olivine grains.

In an attempt to see if this characterization could be reproduced by the data of this study, Ni weight percentages are plotted against Fo in figures 4.3a and b. In the first diagram each individual analysis was plotted, and the resultant diagram (figure 4.3a) shows that each layer is poorly characterized. The individuality of each layer is somewhat clearer in figure 4.3b, where the anlyses have been averaged for each sample and standard deviations calculated. Five groupings can be recognized in figure 4.3b, namely;

(i) the Footwall pegmatoidal pyroxenite,

(ii) the Merensky Reef,

(iii) the P-2 middling leucotroctolite,

(iv) the basal, olivine-bearing portion of the UG-2 poikilitic pyroxenite and,

(v) the remainder of the Upper and Lower Pseudo Reef layers.

This diagram (figure 4.3b) may be somewhat misleading, for the differences between layers is brought about more by differences in Fo content, which have been shown to be artificial (with respect to initial liquidus compositions), rather than by real differences between the Ni contents of olivine grains in each different layer.

A further feature of figure 4.3a is the the wide range in Ni concentrations exhibited by olivine grains from individual

layers. This feature has previously been recognized by Scoon and De Klerk (in press) for the Merensky Reef at Union Section, and by Barnes and Naldrett (1985) in the J-M (Howland) Reef of the Stillwater Complex. The latter authors ascribe this to equilibration between sulphides and olivine. Early workers, such as Wager and Mitchell (1951) showed that Ni is preferentially incorporated into Mg-rich olivine. Later work on synthetic systems by Ringwood (1956), showed that pure Ni_2SiO_4 has a lower melting point than pure Mg_2SiO_4, so that early olivine crystals should theoretically have lower Ni/Mg ratios than the liquids from which they crystallized. This contrast in behaviour between natural and synthetic systems was ascribed by Ringwood (op.cit) to the presence of Fe^{2+} in natural systems, so that Ni would replace Fe rather than Mg. Others, for example Burns and Fyfe (1966) and Irvine (1974) attribute the high Ni/Mg ratio of early olivines to a higher proportion of octahedrally co-ordinated sites (for which Ni has a high affinity) in olivine than in the host liquid. Barnes and Naldrett (1985) showed that a linear correlation exists between NiO and FeO for olivines of the J-M Reef, and further that olivines in the Reef have both higher NiO and FeO than those beyond its confines. They attribute this phenomenon to re-equilibration between olivines and Ni-bearing sulphides during magma mixing. Their model will be considered in more detail in Chapter 6, and it is sufficient to point out here that a new magma batch, enriched with immiscible sulphide droplets is required to mix with a more evolved magma which is crystallizing olivine. Through turbulent mixing, the olivines from the old batch come into contact with sulphide droplets from the new magma. Those grains which make contact exchange

ions, with Ni being transfered from sulphide to olivine. A whole array of olivine grains, possessing a wide variety of Ni concentrations is produced through the effectiveness of the contact they make with the sulphide droplets.

This model may be used to explain the high variability of Ni concentrations in the olivines of the study section as well, but the paucity of olivine grains in the remainder of the succession, particularly in sulphide-free rocks makes the hypothesis difficult to test. If the variable Ni content of olivines is brought about by re-equilibration with sulphides, then the characterization of individual layers through Ni/Mg ratios is purely artificial, and in no way reflects significant differences between the compositions of initial liquids.

Figure 4.4 A plot of Fo mole percent against MnO for olivine grains. Each data point represents an average per sample, and error bars one standard deviation. Symbols are the same as for figure 4.3.

Figure 4.5 The pyroxene quadrilateral, showing averaged compositions per sample. Superimposed on the diagram are the fractionation trends of Atkins (1969).

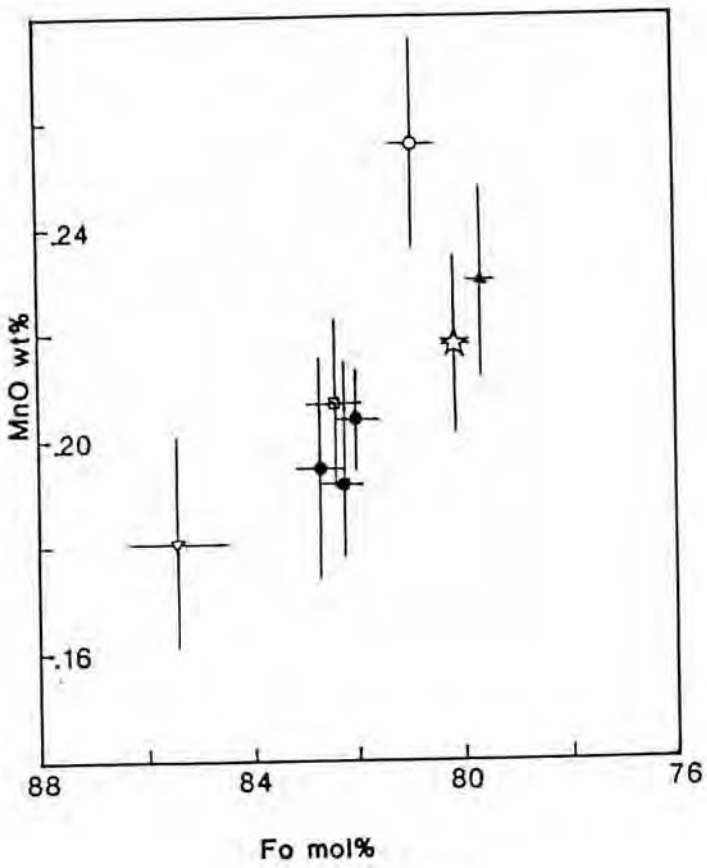

Figure 4.4

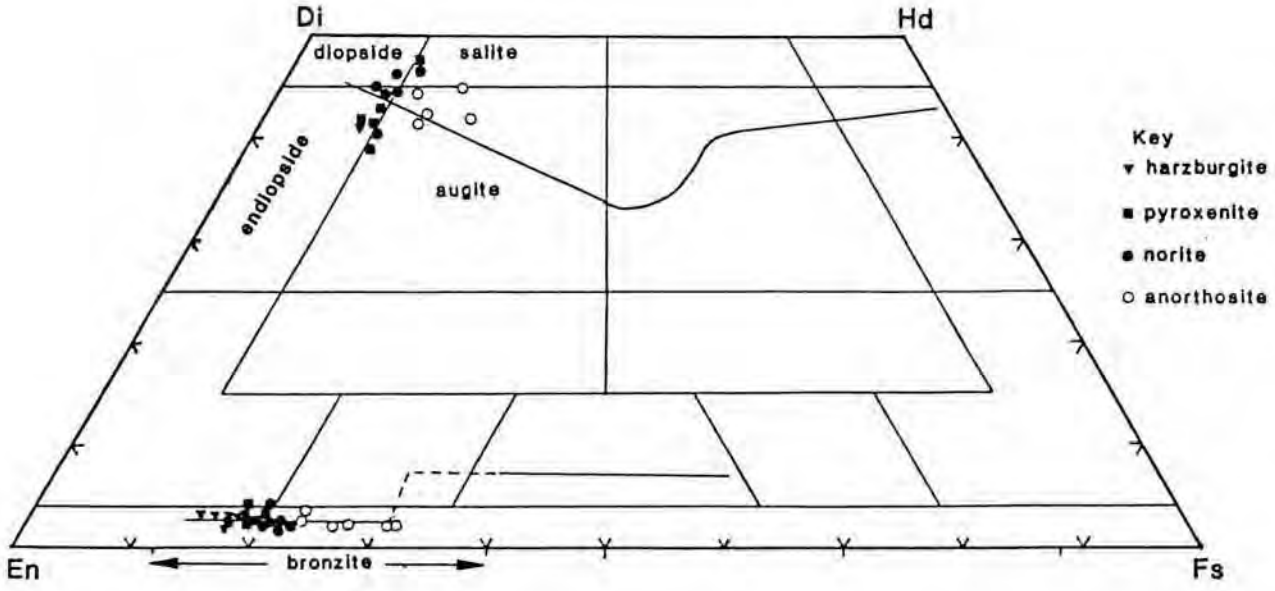

Figure 4.5

4.2.3 Mn-Olivine Relationships.

Manganese may substitute for the (Mg,Fe^{2+}) group in olivine, particularly if the olivine is relatively Fe-enriched (Deer et al., 1982). The Mn concentrations of olivines in the study section vary from 0.14 to 0.28 weight percent, while a plot of MnO against Fo content, in figure 4.4, reveals that most of the layers have narrow ranges of MnO contents. Here again, only the Pseudo Reef horizons may be grouped together, while all the other layers plot as separate entities. Furthermore, a near-linear inverse correlation between Fo and MnO is apparent, with only the P2 middling olivines deviating greatly from the trend. The linear sequence does not, however, follow the stratigraphic sequence.

To summarize, the olivines of the study section exhibit fairly wide chemical variations. These variations do not appear to represent differences in liquidus compositions, as sub-solidus equilibration with spinel has affected their Fe-Mg ratios, while re-equilibration with sulphides may be invoked to explain wide variations in Ni contents.

4.3 Pyroxenes

4.3.1. Introduction

Pyroxenes are the most abundant ferromagnesian silicate mineral phase in the rocks of the study section, and both ortho- and clino- varieties are represented. Orthopyroxene, occurs mainly as a cumulus phase, but it may also be an intercumulus mineral in anorthosites. Clinopyroxene occurs

exclusively as an intercumulus phase and it is present, albeit sporadically, in all the different rock types represented in the succession.

Pyroxenes may be expressed chemically by the general formula $[(M2)(M1)(Si,Al)_2O_6]$, where in orthopyroxenes the M1 and M2 sites are occupied almost exclusively by Fe^{2+} and Mg^{2+} cations, while in clinopyroxenes the M2 site is generally occupied by Ca^{2+}. Other elements which may substitute into the M-sites, include Ti, Al, Mn, Cr, Na and Ni (Deer et al.,1978). A further feature of pyroxenes is that trivalent and tetravalent cations may substitute for divalent ones in the M-sites, provided that the extra charge is compensated for in the (Si,Al) group by the substitution of Al^{3+} for Si^{4+}. This means that Al may be present both in M-sites as well as the tetrahedral sites.

The essential feature of pyroxene structure is the linkage of SiO_4 tetrahedra by the sharing of two corners of the tetrahedron to form continuous $n(SiO_3)$ chains. These chains are linked laterally by M1 and M2 cations. The former lie between the apices of SiO_3 chains, whereas the latter lie between their bases. Co-ordination around M1 is regular octahedral, whereas around M2 co-ordination is dependent on the nature of the M2 cation. If it is Mg, the co-ordination is six-fold, whereas it is eight-fold for Ca and Na (Deer et al., 1963).

A feature of the pyroxenes from plutonic environments is the development of exsolution features. These come about as a result of high-temperature orthopyroxene being capable of

Table 4.2 Averaged orthopyroxene analyses for each sample. The analyses show weight percentage concentrations of element oxides, the number of cations based 6 oxygens, and the number of analyses in the average (N).

TABLE 4.2. ORTHOPYROXENE ANALYSES BY MICROPROBE

Sample Number:	AE-1	AE-2	AE-5	AE-7	AE-9	AE-10	AE-12
Oxides							
SiO_2	53.75	53.89	53.84	54.16	54.62	55.07	55.58
TiO_2	0.36	0.28	0.28	0.26	0.31	0.28	0.19
Al_2O_3	0.73	0.83	0.70	0.86	1.01	1.09	1.24
FeO	20.29	19.67	19.43	17.53	14.80	12.89	11.12
Cr_2O_3	0.08	0.10	0.09	0.11	0.22	0.29	0.26
MnO	0.34	0.37	0.39	0.37	0.31	0.29	0.25
NiO	0.05	0.04	0.07	0.05	0.08	0.10	0.09
MgO	23.34	23.68	23.81	25.40	27.13	28.71	29.73
CaO	1.18	1.13	1.13	1.22	1.34	1.20	1.03
Na_2O	0.04	0.01	0.02	0.02	0.02	0.02	0.01
Total	100.14	100.00	99.77	99.98	99.84	99.93	99.50
Cations							
Si^{4+}	1.9807	1.9823	1.9841	1.9745	1.9699	1.9663	1.9735
Ti^{4+}	0.0099	0.0078	0.0078	0.0072	0.0085	0.0076	0.0050
Al^{3+}	0.0318	0.0358	0.0304	0.0371	0.0427	0.0458	0.0518
Fe^{2+}	0.6252	0.6051	0.5988	0.5345	0.4465	0.3850	0.3303
Cr^{3+}	0.0022	0.0030	0.0027	0.0031	0.0062	0.0082	0.0074
Mn^{2+}	0.0106	0.0114	0.0122	0.0115	0.0094	0.0086	0.0075
Ni^{2+}	0.0015	0.0012	0.0022	0.0014	0.0023	0.0028	0.0025
Mg^{2+}	1.2827	1.2987	1.3083	1.3807	1.4591	1.5282	1.5743
Ca^{2+}	0.0464	0.0446	0.0446	0.0475	0.0517	0.0460	0.0391
Na^{1+}	0.0027	0.0008	0.0012	0.0013	0.0013	0.0013	0.0009
N	6	5	3	3	8	5	5

Sample Number:	AE-13	AE-15	AE-16	AE-20	AE-23	AE-24	AE-25
Oxides							
SiO_2	55.61	55.40	54.76	54.77	54.90	55.39	55.30
TiO_2	0.25	0.25	0.19	0.20	0.21	0.19	0.15
Al_2O_3	1.28	1.16	1.30	1.19	1.09	1.32	1.61
FeO	11.43	11.85	14.96	14.94	13.61	13.30	12.49
Cr_2O_3	0.27	0.25	0.29	0.26	0.22	0.27	0.28
MnO	0.25	0.21	0.31	0.31	0.26	0.28	0.27
NiO	0.07	0.08	0.14	0.08	0.10	0.10	0.08
MgO	29.72	28.95	27.02	27.12	27.85	28.51	28.62
CaO	1.12	1.41	1.85	1.38	1.34	1.25	1.57
Na_2O	0.01	0.05	0.02	0.02	0.03	0.02	0.03
Total	100.02	99.61	100.84	100.27	99.61	100.63	100.40
Cations							
Si^{4+}	1.9681	1.9739	1.9601	1.9677	1.9727	1.9662	1.9617
Ti^{4+}	0.0065	0.0066	0.0051	0.0054	0.0057	0.0049	0.0041
Al^{3+}	0.0534	0.0488	0.0540	0.0504	0.0462	0.0554	0.0674
Fe^{2+}	0.3384	0.3532	0.4478	0.4489	0.4090	0.3949	0.3707
Cr^{3+}	0.0074	0.0071	0.0082	0.0074	0.0061	0.0076	0.0079
Mn^{2+}	0.0076	0.0063	0.0094	0.0094	0.0080	0.0085	0.0081
Ni^{2+}	0.0019	0.0024	0.0040	0.0023	0.0027	0.0029	0.0022
Mg^{2+}	1.5684	1.5378	1.4421	1.4528	1.4920	1.5088	1.5138
Ca^{2+}	0.0426	0.0538	0.0710	0.0531	0.0517	0.0476	0.0598
Na^{1+}	0.0010	0.0032	0.0014	0.0014	0.0023	0.0013	0.0018
N	5	6	4	5	5	5	5

94 22 c

Sample Number:	AE-MR	AE-29	AE-32	AE-33	AE-36	AE-38	AE-39.4
Oxides							
SiO_2	54.38	54.98	55.15	55.30	55.61	55.99	55.47
TiO_2	0.28	0.24	0.33	0.26	0.22	0.16	0.17
Al_2O_3	1.66	1.20	1.11	1.01	1.30	1.61	1.62
FeO	11.83	14.65	14.60	13.84	11.78	11.08	9.53
Cr_2O_3	0.23	0.26	0.28	0.19	0.30	0.28	0.32
MnO	0.28	0.32	0.31	0.29	0.25	0.24	0.27
NiO	0.07	0.07	0.05	0.08	0.09	0.06	0.12
MgO	28.74	27.39	27.49	28.16	29.13	29.98	30.36
CaO	1.52	1.40	1.43	1.09	1.54	1.25	1.67
Na_2O	0.03	0.02	0.02	0.01	0.02	0.02	0.03
Total	99.02	100.54	100.77	100.23	100.25	100.67	99.56
Cations							
Si^{4+}	1.9529	1.9672	1.8962	1.9743	1.9691	1.9649	1.9598
Ti^{4+}	0.0075	0.0064	0.0084	0.0070	0.0059	0.0042	0.0045
Al^{3+}	0.0702	0.0505	0.0448	0.0425	0.0541	0.0664	0.0675
Fe^{2+}	0.3553	0.4383	0.4199	0.4131	0.3488	0.3252	0.2816
Cr^{3+}	0.0066	0.0075	0.0075	0.0053	0.0085	0.0079	0.0089
Mn^{2+}	0.0084	0.0098	0.0089	0.0088	0.0075	0.0072	0.0081
Ni^{2+}	0.0021	0.0021	0.0014	0.0022	0.0027	0.0016	0.0034
Mg^{2+}	1.5389	1.4613	1.4095	1.4994	1.5378	1.5686	1.5994
Ca^{2+}	0.0583	0.0536	0.0526	0.0416	0.0585	0.0470	0.0632
Na^{+}	0.0019	0.0017	0.0013	0.0009	0.0013	0.0014	0.0021
N	4	5	10	3	5	6	2

Sample Number:	AE-39.5	AE-40.1	AE-40.2	AE-42	AE-43	AE-45	AE-46
Oxides							
SiO_2	55.25	55.24	55.99	55.33	54.80	55.17	54.91
TiO_2	0.17	0.25	0.16	0.10	0.30	0.27	0.36
Al_2O_3	1.65	1.54	1.61	1.70	0.98	1.02	1.12
FeO	10.19	10.96	11.08	10.68	16.46	14.55	13.16
Cr_2O_3	0.26	0.32	0.28	0.32	0.23	0.24	0.26
MnO	0.24	0.25	0.24	0.23	0.35	0.32	0.28
NiO	0.06	0.09	0.06	0.07	0.03	0.07	0.04
MgO	30.01	29.80	29.98	29.65	26.45	27.65	27.85
CaO	1.58	1.59	1.25	1.49	0.93	1.14	1.52
Na_2O	0.04	0.03	0.02	0.03	0.01	0.01	0.02
Total	99.45	100.07	100.67	99.60	100.54	100.43	99.53
Cations							
Si^{4+}	1.9588	1.9545	1.9649	1.9619	1.9738	1.9729	1.9715
Ti^{4+}	0.0045	0.0067	0.0042	0.0027	0.0082	0.0072	0.0098
Al^{3+}	0.0690	0.0643	0.0664	0.0710	0.0414	0.0431	0.0476
Fe^{2+}	0.3021	0.3242	0.3252	0.3167	0.4959	0.4352	0.3952
Cr^{3+}	0.0073	0.0090	0.0079	0.0090	0.0066	0.0069	0.0074
Mn^{2+}	0.0072	0.0076	0.0072	0.0069	0.0106	0.0097	0.0084
Ni^{2+}	0.0017	0.0025	0.0016	0.0020	0.0008	0.0019	0.0011
Mg^{2+}	1.5864	1.5722	1.5686	1.5676	1.4205	1.4743	1.4909
Ca^{2+}	0.0600	0.0601	0.0470	0.0566	0.0360	0.0436	0.0585
Na^{+}	0.0028	0.0020	0.0014	0.0021	0.0005	0.0006	0.0017
N	4	2	6	3	4	8	5

Sample Number:	AE-47	AE-48	AE-49	AE-51	AE-55	AE-57	AE-59
Oxides							
SiO_2	55.34	55.49	55.67	55.77	55.27	55.78	56.24
TiO_2	0.23	0.14	0.22	0.24	0.17	0.18	0.29
Al_2O_3	1.24	1.48	1.22	1.26	1.50	1.26	1.04
FeO	13.27	10.59	12.39	12.53	11.77	11.64	12.15
Cr_2O_3	0.30	0.27	0.23	0.30	0.28	0.32	0.25
MnO	0.24	0.26	0.25	0.27	0.24	0.28	0.27
NiO	0.06	0.07	0.07	0.07	0.10	0.07	0.07
MgO	28.16	30.01	29.00	28.94	28.51	28.97	29.36
CaO	1.31	1.51	1.17	1.50	2.10	1.82	1.53
Na_2O	0.02	0.01	0.02	0.04	0.05	0.03	0.02
Total	100.17	99.83	100.25	100.92	99.99	100.35	101.21
Cations							
Si^{4+}	1.9724	1.9627	1.9734	1.9679	1.9655	1.9728	1.9742
Ti^{4+}	0.0063	0.0033	0.0058	0.0064	0.0045	0.0047	0.0076
Al^{3+}	0.0520	0.0617	0.0511	0.0524	0.0629	0.0527	0.0428
Fe^{3+}	0.3955	0.3133	0.3678	0.3699	0.3501	0.3443	0.3566
Cr^{3+}	0.0085	0.0076	0.0066	0.0084	0.0079	0.0091	0.0069
Mn^{2+}	0.0073	0.0078	0.0075	0.0080	0.0073	0.0084	0.0079
Ni^{2+}	0.0017	0.0020	0.0020	0.0020	0.0029	0.0019	0.0020
Mg^{2+}	1.4968	1.5827	1.5329	1.5226	1.5118	1.5278	1.5367
Ca^{2+}	0.0500	0.0572	0.0446	0.0567	0.0800	0.0690	0.0577
Na^{+}	0.0015	0.0007	0.0017	0.0024	0.0035	0.0022	0.0016
N	5	6	5	12	4	8	7

Sample Number:	AE-61	AE-64
Oxides		
SiO_2	55.89	55.74
TiO_2	0.21	0.25
Al_2O_3	1.32	1.15
FeO	12.26	13.16
Cr_2O_3	0.30	0.30
MnO	0.27	0.27
NiO	0.08	0.08
MgO	29.08	28.83
CaO	1.61	1.54
Na_2O	0.03	0.03
Total	101.04	100.85
Cations		
Si^{4+}	1.9677	1.9734
Ti^{4+}	0.0055	0.0066
Al^{3+}	0.0546	0.0481
Fe^{3+}	0.3610	0.3897
Cr^{3+}	0.0084	0.0084
Mn^{2+}	0.0082	0.0082
Ni^{2+}	0.0022	0.0023
Mg^{2+}	1.5264	1.4956
Ca^{2+}	0.0606	0.0585
Na^{+}	0.0018	0.0022
N	12	6

incorporating a considerable proportion of Ca in its crystal lattice. With cooling however, this Ca is exsolved as very fine lamellae or blebs of clinopyroxene. In the case of lamellae this usually occurs along specific crystallographic planes, namely the [100] set of the host orthopyroxene grain. The very fine nature of these lamellae, which are approximately between 0.001 and 0.002 mm thick and 0.005mm apart, present a major problem during microprobe analysis, because it is extremely difficult to place the electron beam between them. To overcome this problem a defocussed beam of 20 microns diameter was employed, and the resultant analyses are taken to represent high-temperature, pre-exsolution compositions. Averaged orthopyroxene analyses for each sample are presented in Table 4.2.

4.3.2 Major and Minor Element Variations of Orthopyroxenes.

It is common practice to represent pyroxene analyses on the pyroxene quadrilateral diagram, on which pyroxene compositions can be classified within various fields. Figure 4.5 is such a diagram on which averaged analyses, per sample, have been plotted. In addition to these the pyroxene- fractionation trends of Atkins (1969) for the Bushveld Complex have been plotted. The orthopyroxenes of the study section fall into the "bronzite" field and lie close to Atkins' fractionation curve. Furthermore, En values can be seen to decrease through the rock sequence harzburgite- pyroxenite-norite-anorthosite. Analyses of clinopyroxenes place these minerals in four fields, namely endiopside, diopside, salite and augite. These analyses are broadly scattered around Atkins' (1969) fractionation curve, while individual rock types do not appear

Figure 4.6 Variation diagrams in which major and minor element compositions (as weight percentages) of orthopyroxenes are plotted against MgO. Each data point represents a single analysis, except where such points are very close to one another.

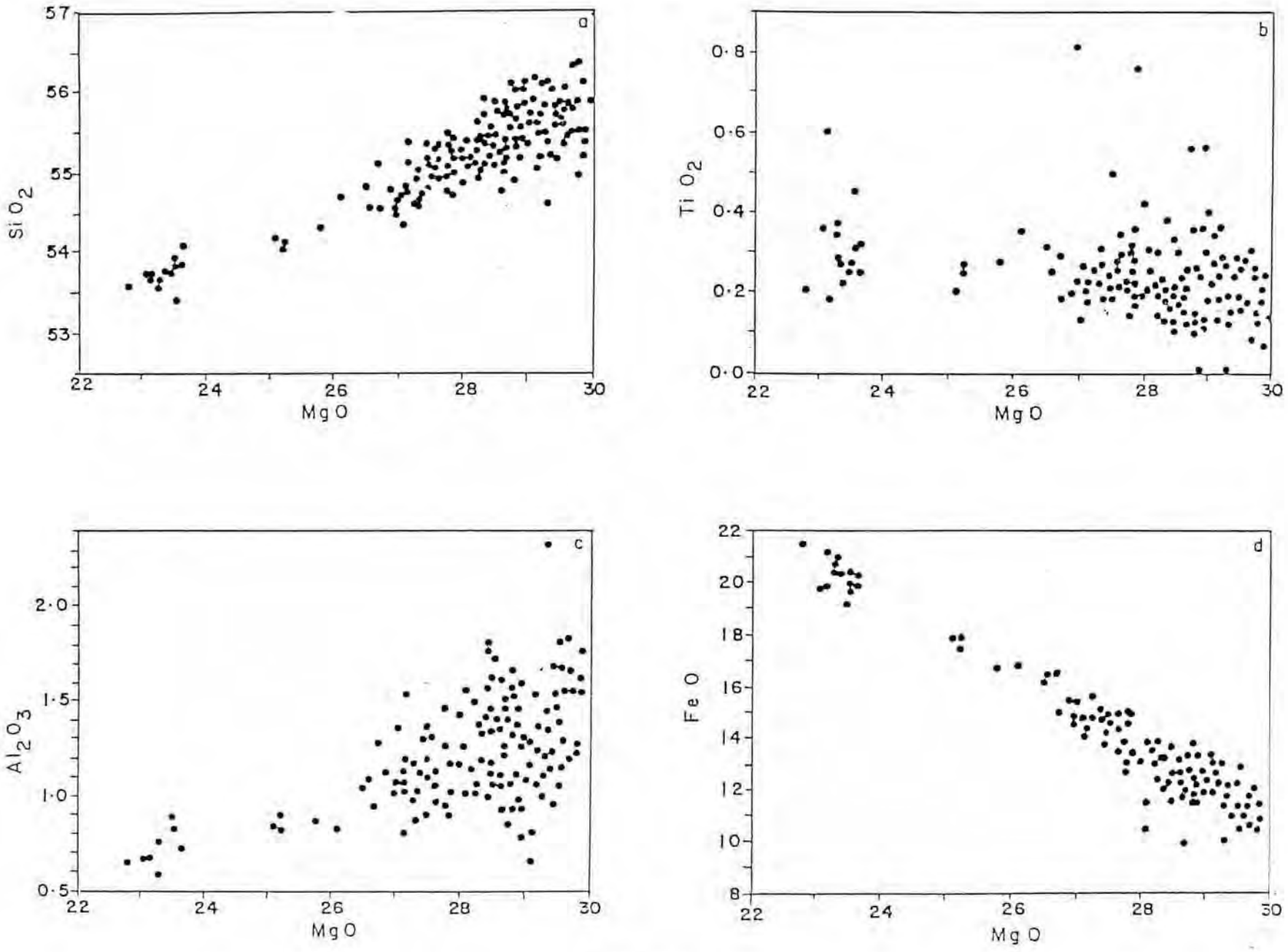
a
Si O2
57
56
55
54
53
22
24
26
28
30
Mg O
b
Ti O2
0·8
0·6
0·4
0·2
0·0
22
24
26
28
30
Mg O
c
Al2O3
2·0
1·5
1·0
0·5
22
24
26
28
30
Mg O
d
Fe O
22
20
18
16
14
12
10
8
22
24
26
28
30
Mg O

FIGURE 4.6

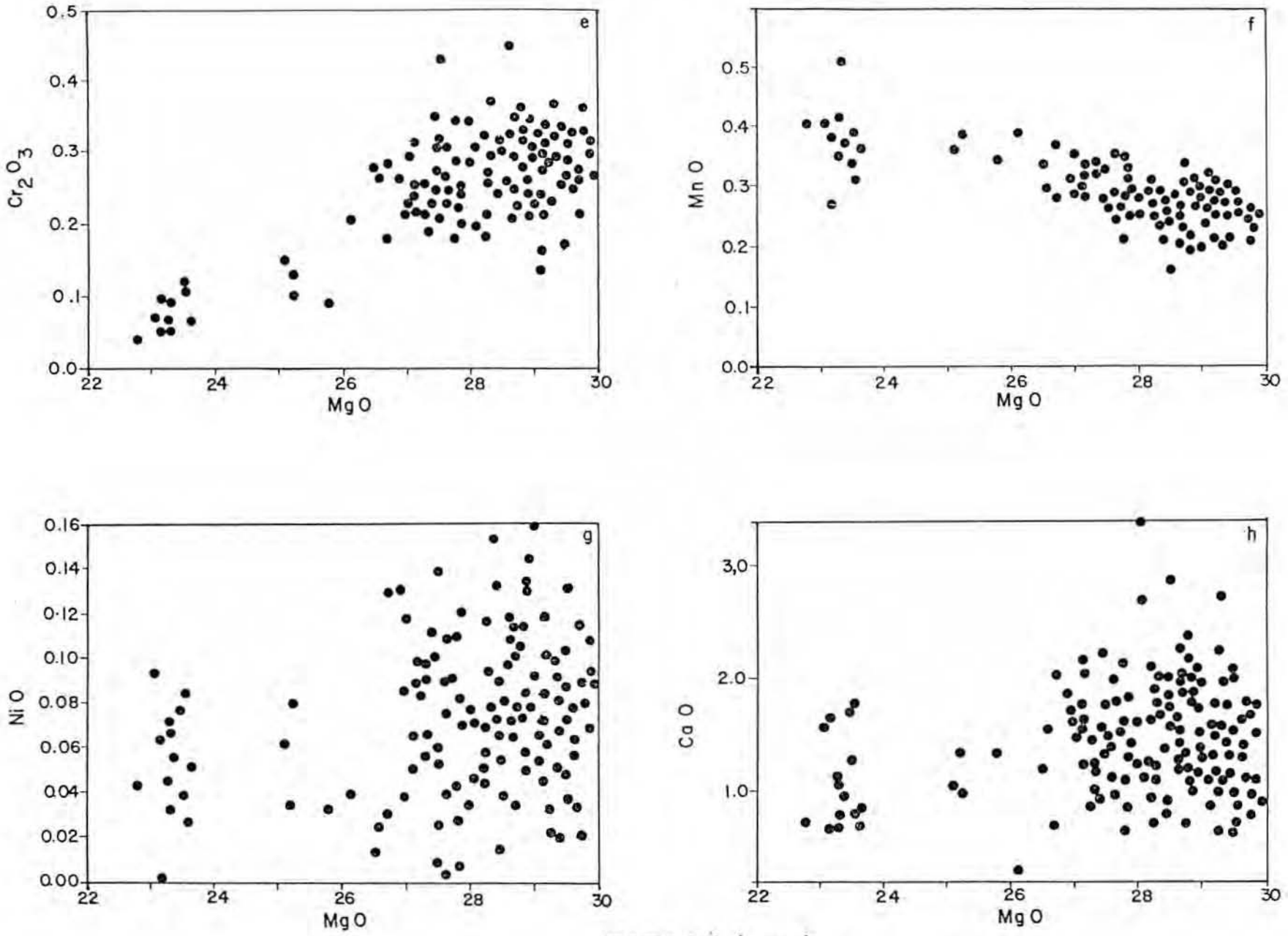

FIGURE 4.6 (Cont.)

to follow successively down the curve. This most probably follows from the postcumulus nature of clinopyroxene.

Variation diagrams representing orthopyroxene compositions, in which element oxides are plotted against MgO, are presented in figure 4.6. Some information concerning the chemical variability of orthopyroxenes can be gleaned from these diagrams.

Linear relationships between MgO and SiO_2, TiO_2, Al_2O_3, FeO, Cr_2O_3 and MnO indicate that these elements behave rationally during fractionation processes. SiO_2, Al_2O_3 and Cr_2O_3 are depleted in sympathy with MgO, while TiO_2, FeO and MnO attain higher levels in grains which are poorer in MgO. Thus MgO-rich grains are clearly more primitive, while MgO-poor grains are more evolved (fractionated).

It is evident from the excellent linear relationship between MgO and FeO in figure 4.6d, that complete diadochy exists between these two elements in orthopyroxene, and that the variation trend from Mg-rich to Fe-rich varieties represents a bona fide fractionation trend, which is confirmed by the saw-tooth variation pattern exhibited in figure 4.7a.

The fact that Al_2O_3 is depleted with fractionation (decreasing MgO) possibly reflects the influence of plagioclase, which is a co-crystallizing phase with intermediate- and low-MgO ortho-pyroxene. When Mg-rich pyroxene crystallizes, it does not have to compete with plagioclase for Al in the melt. The simultaneous lowering of SiO_2 and Al_2O_3 with MgO is a

somewhat unusual feature, for it would be expected that Al^{3+} would substitute for Si^{4+} in more evolved grains, and therefore an increase in Al_2O_3 with decreasing MgO would be expected. Clearly, the removal of Al by plagioclase has a far greater effect on the amount of Al incorporated in orthopyroxene.

Titanium, which has a normal valency of 4+, is more highly concentrated in Mg-poor than in Mg-rich orthopyroxenes (see figure 4.6b). This element's behaviour is apparently influenced by two major factors, namely its tetravalent state, and the fact that it has a crystal field stabilization energy (CFSE) of zero. This means that it will only enter the pyroxene lattice if a charge imbalance exists, for example if two Al^{3+} ions have substituted for two Si^{4+} ions. Furthermore, it will not substitute into the lattice ahead of Cr^{3+}, as this cation has a far higher CFSE than Ti^{4+}. This behaviour is clearly illustrated in figure 4.6, where TiO_2 can be seen to reach its maximum level at low MgO (when Cr_2O_3 is also low), SiO_2 and Al_2O_3 levels, when enough vacant sites are available, and when charge imbalances are most likely.

The common valence state of chromium in earth materials is 3+. Cr^{3+} has been found (Deer et al.,1978) to partition strongly into early formed pyroxene grains. This tendency is best explained by the cation's high CFSE, which is the highest for all the transition metal ions. For Cr^{3+} to substitute into orthopyroxene's octahedral sites, a charge imbalance needs to be created in the tetrahedral site. This condition is usually met through the substitution of Al fo Si (Campbell and Borley, 1974). Campbell and Borley (op.cit) have observed that Cr is

Table 5.4 Some distribution coefficient data, taken from the literature.

D coeff	olivine	orth.pyx	clino.pyx	plagioclase	biotite	spinel
Ni	10(2)	1.1-3.1(1)	2(2)	0.01(2)	3.5(2)	5(2)
	35-3.8(3)	4(2)	4-2(3)	0.2(4)		
	34-4.8(6)	5-3(3)	6.5(5)			
Cu	.47-.27(1)	0.071(7)	2.4-1.5(1)	0.004(7)		
	0.023(7)			0.24(5)		
Cr	0.2(2)	2(2)	10(2)	0.01(2)		10(2)
	2.7(9)		20(9)	0.1(11)		
	3.1-10(13)		40(12)			
V	0.04(1)	0.06-3.4(1)	1.5(3)			38(1)
	0.09(3)	0.3(3)	1.3(9)			
	0.05(9)	0.5-2.3(8)	0.94-4.1(12)			
			0.06-3.4(14)			
Sc	0.37(1)	0.53-1.4(1)	3.1(3)	.017-.065(1)		0.048(1)
	0.33(7)	3.3(7)		0.008(7)		
	0.25(3)	1.1(3)		0.01(23)		
Zn	1.8(7)	0.49(2)		0.13(7)		
Sr	0.003(1)	0.018(1)	0.07(2)	2.2(2)	0.08(2)	0.01(2)
	0.001(2)	0.01(2)	0.067(15)	1.5-2.2(16)		
	0.00019(15)	0.007(15)	0.165(3)	3.06(17)		
	0.016(15)	0.016(15)	0.1(18)	1.75(24)		
	0.1(19)		.16-.28(16)			
Rb	0.001(2)	0.004(1)	0.017(1)	0.94-3.3(19)		
	0.00018(15)	0.0006(15)	0.0011(15)	0.03(19)	3.1(2)	
	0.01(19)		0.001(2)	0.07(2)	1.26-1.58(20)	
	0.01(3)		0.03(18)			
	0.002(18)					
Zr	0.01(21)	0.03(21)	0.12(1)	0.01(21)		
			0.1(21)			
Y	0.002(3)	0.009(3)	0.20(3)	0.031(1)	0.03(21)	
	0.01(21)	0.2(21)	0.5(21)	0.03(21)		
			1.65(22)	0.014(17)		
				0.049(22)		
K	0.001(2)	0.001(2)	0.0026(1)	0.2(1)	2.7(2)	
	0.0018(15)	0.001(5)	0.002(2)	0.2(2)		0.01(2)
			0.002(15)			

References:
(1) Irving(1978),(2) Cox et al.(1979),(3) Frey et al.(1978),(4) De Long(1974),(5) Ewart et al.(1973),(6) Leeman & Lindstrom(1978),(7) Paster et al.(1974),(8)Jensen(1973),(9) Duke(1974),(10) Lindstrom & Weill(1978),(11) .Walker(1979),(12) Campbell & Borley(1974), (13) Flower(1973), (14) Ringwood(1970),(15) Hansen(1977),(16) Sun et al.(1974),(17) Drake(1975),(18) Hart & Brooks(1974),(19) Philpots & Schnetzler(1970),(20) Marsh(1973),(21) Pearce & Norry(1979),(22) Morse & Nolan(1985),(23) Salpas et al.(1983),(24) Morse(1982).

Table 5.4

also preferentially incorporated into clinopyroxene rather than orthopyroxene. Since clinopyroxene is an intercumulus, late-crystallizing phase in the rocks of the succession, this competition is unlikely to have had a significant influence on the distribution of Cr in orthopyroxene, which is preferentially partitioned into Mg-rich grains (see figure 4.6e).

Manganese is a fairly common divalent cation in most magmas, and since it is of a similar size as the Fe^{2+} and Mg^{2+} cations, it could be expected to compete with these ions for lattice sites in orthopyroxene. Strong partitioning is however nullified by the ions' zero CFSE. Some substitution does occur, and since the ionic size of the element more closely resembles that of Fe, Mn is more readily accepted into Fe-rich orthopyroxene. Hence the negative correlation with MgO, in figure 4.6f, can be considered to be normal.

The behaviour of Ni^{2+}, which has a high CFSE and the same charge as Fe and Mg could be expected to be rational with respect to these elements. Consideration of figure 4.6h does not confirm this, and instead a wide scatter of data points is witnessed in which high and low Ni values are recorded for both high and low Mg orthopyroxenes. In general the Ni content of orthopyroxenes can be said to be low. The occurrence of low Ni concentrations in some high-Mg grains may reflect the fact that these grains coexist with olivine and/or sulphides which have a higher affinity for it. High-Ni, high-Mg grains possibly come from non olivine-bearing mafic rocks such as the poikilitic pyroxenites of the UG-1 and Bastard

Units.

Figure 4.6g reveals that a wide variation in the Ca content of orthopyroxenes is apparent. This wide scatter probably reflects the presence of fine exsolution lamellae, whose influence is greater on more Ca-rich analyses.

4.3.3 Fe-Mg Variations in Orthopyroxene Through the Succession.

It is clear from the above discussion that orthopyroxene chemistry can be related to rock type. This is emphasized in figure 4.7 in which the MMF (atomic $Mg/Mg+Fe^{2+}$) ratio of orthopyroxenes is plotted against a stratigraphic column. This diagram shows that in "complete" units, such as the Merensky Unit, the relative proportions of Mg in orthopyroxene decrease systematically upwards reaching lowest values in the anorthosite layer. In the overlying basal layer of the next unit high Mg (primitive) pyroxene is again present. This must represent strong evidence for cryptic cyclicity in these units. There are a number of other features which are worth noting in this diagram. Firstly, in the Bastard unit an initial increase in the MMF ratio is encountered from the base of the unit upwards, and it is only where pyroxenite grades into norite that an upward decrease becomes evident. The other units do not exhibit this feature. Secondly, it is clear that the orthopyroxenes of olivine-bearing layers have considerably higher MMF ratios than those in overlying pyroxenites, and that these values disrupt the smooth curves described through rocks which contain cumulus plagioclase and

Figure 4.7 Variations in orthopyroxene chemistry plotted against a stratigraphic column. In (a) the MMF (atomic Mg/Mg+Fe) ratio is plotted for each individual analysis. In (b) and (c) averaged Cr/Al and Cr/Ti are plotted, where the error bars represent one standard deviation.

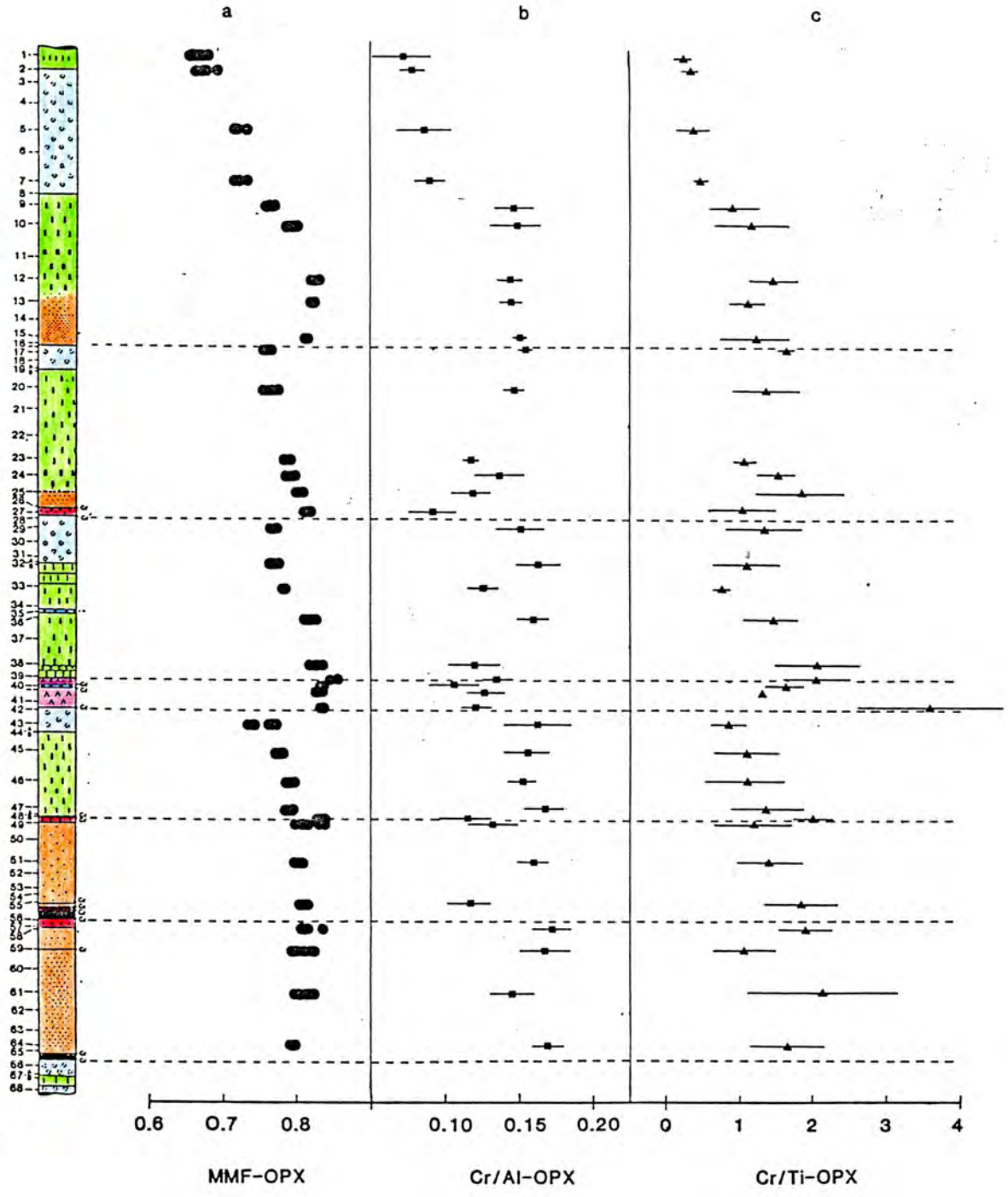

Figure 4.7

cumulus plagioclase and pyroxene e.g., at the base of the Footwall Unit, and within the P1 harzburgite. Thirdly, if the Lower Pseudo Reef horizon were to be ignored, a fairly smooth curve could be drawn through the plagioclase cumulates of the Lower Pseudo Unit, and this could be extrapolated into the UG-2 Unit; and fourthly, a slight upward increase in MMF is apparent through the UG-1 Unit, which is a reversal of the trend encountered in the remainder of the sequence.

No chemical zoning is apparent in these orthopyroxenes, and the spread in MMF values for particular samples represents differences between separate grains. It is noticeable that this spread is greatest in anorthosites, where orthopyroxene is a postcumulus mineral. Any primary zonation which may have existed was probably lost through subsolidus readjustment concomitant with exsolution of clinopyroxene lamellae.

4.3.2 Cr/Al and Cr/Ti Variations in Orthopyroxene.

In columns b and c of Figure 4.7 these ratios are plotted against the stratigraphic column. An upward increase in the Cr/Al of orthopyroxene is evident through the Lower Pseudo, Footwall and Merensky Units, while the UG-2 unit exhibits a reversal in this trend half way up the unit, and, the UG-1 has an initial decrease upwards, followed by an upward increase. Of particular interest however, is the Bastard Unit, in which two well-defined trends are discernible. At the base of the Unit, that is, through the poikilitic pyroxenite and norite, the ratio is roughly constant at around 0.15. However at the base of the Bastard anorthosite (Giant Mottled Anorthosite) the Cr/Al ratio drops markedly to 0.10, and continues to

decrease upwards.

Cr/Ti ratios in orthopyroxene generally decrease upwards through cyclic units, which is what would be expected given that Ti will only enter the pyroxene structure once Cr has been depleted, for it cannot compete successfully with this trivalent cation (Deer et al., 1980). In the Bastard Unit this trend is not as smooth as it is the other units, and a distinct "step" is visible at the base of the Giant Mottled anorthosite, which correlates well with the change in the Cr/Al ratio.

4.3.3 Clinopyroxene.

This mineral occurs either as fine exsolution lamellae in orthopyroxene, or as large intercumulus grains. Microprobe analyses of the latter variety were carried out on 42 grains from various samples (see figure 4.1). These analyses are listed in Table 4.3. Unfortunately, due to the sporadic occurrence of these grains, they are not present in all the polished thin sections, thereby rendering it difficult to establish valid trends.

The chemistry of the clinopyroxenes of the study section is summarized in figure 4.8, where their En (Mg/Mg+Fe+Ca) and Wo (Ca/Mg+Fe+Ca) mole percentages are plotted against the stratigraphic column. The data are scattered, due largely to the limited number of analysed samples, and it is only in the Bastard and Merensky Units that any trends are discernible. En values show a general upward decrease in both units,

Table 4.3 Averaged clinopyroxene analyses. The analyses show weight percent concentrations of element oxides, the number of cations based on 6 cations, and the number of analyses in the average (N).

TABLE 4.3: CLINOPYROXENE ANALYSES BY MICROPROBE

Sample Number:	AE-2	AE-5	AE-7	AE-13	AE-15	AE-16	AE-20	AE-24
Oxides								
SiO_2	52.65	52.51	52.35	53.00	52.80	52.95	52.97	53.19
TiO_2	0.50	0.49	0.47	0.48	0.60	0.50	0.51	0.40
Al_2O_3	1.50	1.23	1.72	2.23	2.08	1.80	1.72	2.16
FeO	8.47	10.93	8.30	5.30	5.19	6.57	6.49	6.55
Cr_2O_3	0.17	0.09	0.16	0.59	0.46	0.36	0.32	0.45
MnO	0.20	0.26	0.23	0.15	0.14	0.19	0.20	0.20
NiO	0.04	0.01	0.04	0.00	0.05	0.12	0.04	0.04
MgO	15.26	14.05	15.78	17.30	16.36	14.73	15.97	17.38
CaO	20.34	20.14	19.98	20.10	21.18	23.01	21.74	19.90
Na_2O	0.28	0.25	0.28	0.35	0.44	0.34	0.32	0.32
Total	99.42	99.94	99.30	99.61	99.37	100.56	100.27	100.60
Cations								
Si^{4+}	1.9619	1.9671	1.9509	1.9938	1.9474	1.9497	1.9479	1.9390
Ti^{4+}	0.0141	0.0137	0.0131	0.0133	0.0166	0.0138	0.0140	0.0110
Al^{3+}	0.0659	0.0541	0.0755	0.0963	0.0903	0.0782	0.0745	0.0930
Fe^{2+}	0.2639	0.3423	0.2588	0.1625	0.1598	0.2024	0.1996	0.1998
Cr^{3+}	0.0051	0.0025	0.0048	0.0170	0.0135	0.0105	0.0094	0.0130
Mn^{2+}	0.0064	0.0082	0.0075	0.0046	0.0044	0.0058	0.0061	0.0063
Ni^{2+}	0.0012	0.0002	0.0010	0.0000	0.0010	0.0034	0.0012	0.0012
Mg^{2+}	0.8477	0.7651	0.8767	0.9451	0.8984	0.8084	0.8754	0.9450
Ca^{2+}	0.8121	0.8086	0.7976	0.7915	0.8362	0.9076	0.8564	0.7773
Na^{+}	0.0206	0.0181	0.0202	0.0249	0.0320	0.0247	0.0232	0.0227
N	3	5	1	3	1	3	1	2

Sample Number:	AE-25	AE-29	AE-35	AE-36	AE-40.1	AE-43	AE-49	AE-55
Oxides								
SiO_2	52.81	53.15	52.44	53.10	52.61	52.55	53.41	52.46
TiO_2	0.63	0.42	0.64	0.49	0.41	0.59	0.55	0.05
Al_2O_3	2.22	1.90	1.65	2.27	2.56	1.82	2.04	2.50
FeO	5.96	6.15	6.74	5.02	5.40	6.71	6.01	6.59
Cr_2O_3	0.47	0.34	0.18	0.45	0.54	0.42	0.50	0.57
MnO	0.15	0.15	0.26	0.18	0.14	0.20	0.18	0.17
NiO	0.08	0.00	0.02	0.02	0.04	0.07	0.03	0.06
MgO	16.77	16.41	14.85	16.41	17.80	15.54	17.01	17.52
CaO	20.84	21.17	22.78	21.92	19.91	21.92	19.90	18.78
Na_2O	0.40	0.31	0.35	0.35	0.50	0.30	0.08	0.45
Total	100.34	99.98	99.68	100.20	99.93	100.10	99.78	99.16
Cations								
Si^{4+}	1.9326	1.9518	1.9469	1.9411	1.9239	1.9408	1.9552	1.9371
Ti^{4+}	0.0173	0.0115	0.0186	0.0134	0.0114	0.0162	0.0153	0.0013
Al^{3+}	0.0956	0.1888	0.0719	0.0978	0.1111	0.0792	0.0881	0.1088
Fe^{2+}	0.1824	0.0096	0.2071	0.1536	0.1651	0.2072	0.1841	0.2036
Cr^{3+}	0.0137	0.0046	0.0054	0.0131	0.0155	0.0123	0.0146	0.0166
Mn^{2+}	0.0047	0.0046	0.0062	0.0056	0.0044	0.0062	0.0054	0.0054
Ni^{2+}	0.0024	0.0000	0.0005	0.0008	0.0012	0.0017	0.0010	0.0018
Mg^{2+}	0.9152	0.8982	0.8213	0.8945	0.9706	0.8556	0.9287	0.9647
Ca^{2+}	0.8172	0.8330	0.9051	0.8580	0.7803	0.8674	0.7838	0.7432
Na^{+}	0.0289	0.0221	0.0241	0.0246	0.0359	0.0217	0.0042	0.0328
N	1	3	1	1	2	1	3	2

Figure 4.8 Clinopyroxene composition, represented by En mole percent (Mg/Mg+Fe+Ca), and Wo (Ca/Mg+Fe+Ca). Here each individual analysis is plotted.

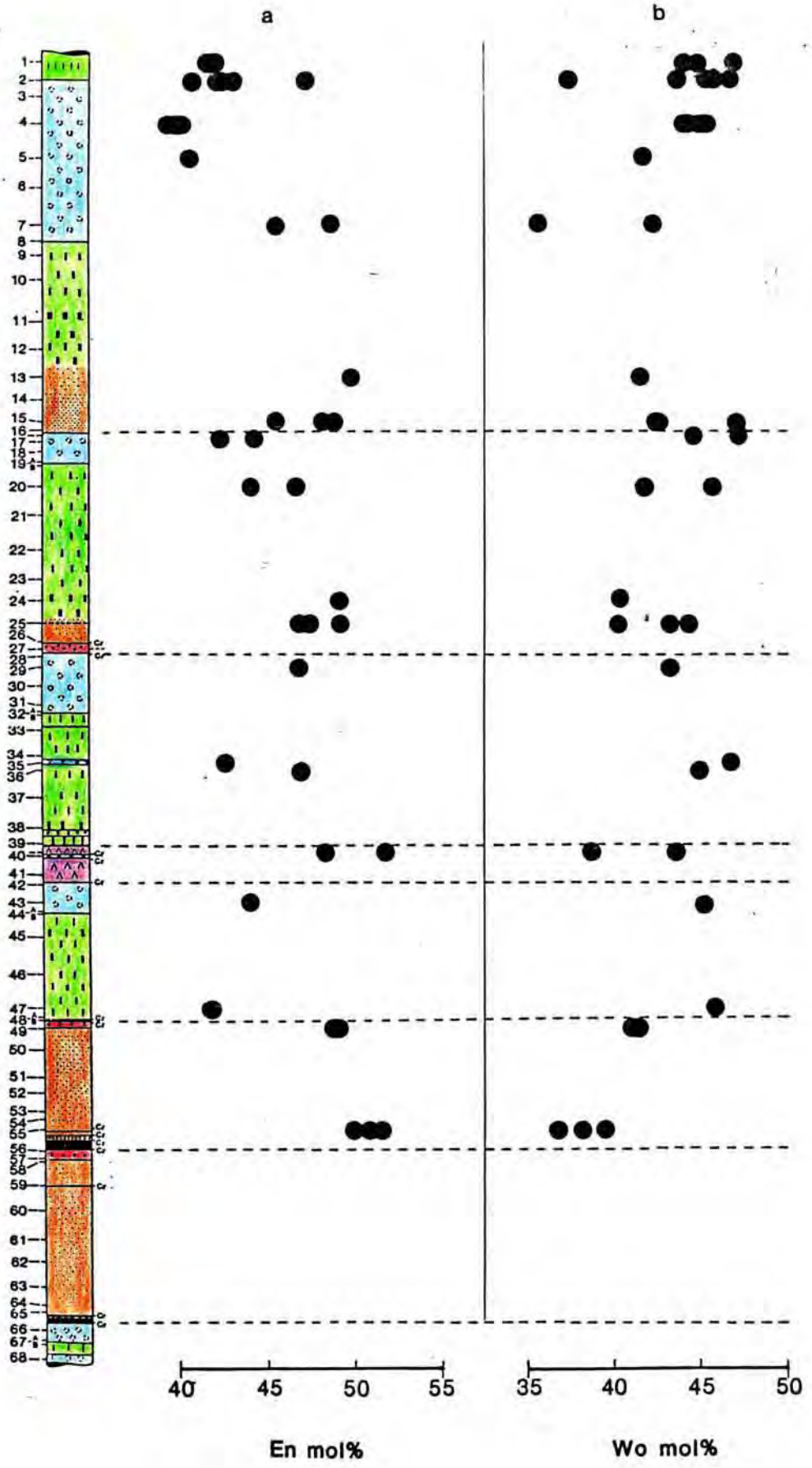

Figure 4.8

although an initial upward increase is apparent at the base of the Bastard Unit. This latter feature matches that exhibited by the MMF ratio of orthopyroxenes. In the remainder of the sequence high En values are recorded for olivine-bearing horizons such as the UG-2 hanging wall and Upper Pseudo Reef, while the reverse is true of clinopyroxenes of anorthositic layers such as the Footwall Marker. Wo values exhibit an upward increase in the Merensky Unit, while an inflection is apparent in the Bastard, where an initial upward decrease becomes reversed at the base of the Giant Mottled Anorthosite. Olivine-bearing horizons have low Wo values, while clinopyroxenes in anorthosites are generally enriched in this molecule.

4.4 Plagioclase.

The common feldspar minerals may be classified in terms of three end-member components, orthoclase ($KAlSi_3O_8$), albite ($NaAlSi_3O_8$) and anorthite ($CaAlSi_2O_8$). Apart from this chemical classification however, it is essential that they also are defined in terms of their structural states. This depends on their temperature of crystallization and subsequent thermal history. Volcanic feldspars are commonly quenched in their high-temperature state, whereas in plutonic rocks, (for example those of the Bushveld Complex) they have evolved to a low temperature state as a result of slow cooling from elevated magmatic temperatures. The feldspars of the Critical Zone of the Bushveld Complex belong almost exclusively to the plagioclase ($NaAlSi_3O_8$ - $CaAlSi_2O_8$) series, while they contain only minor quantities (less than 2 mole percent) of the orthoclase component.

Table 4.4 Representative plagioclase analyses. The analyses show weight percent concentrations of element oxides and the number of cations, based on 32 oxygens. Analysis codes are: R- rim of grain, C- core of grain and RS- restrained grain.

TABLE 4.4: PLAGIOCLASE ANALASES BY MICROPROBE

Sample Number:	AE-1R	AE-1C	AE-2R	AE-2C	AE-2RS	AE-4R	AE-4C	AE-4RS
Oxide								
SiO_2	49.94	49.22	49.95	51.76	50.99	47.26	50.28	49.29
Al_2O_3	30.43	31.98	31.79	30.29	30.65	32.28	30.80	31.50
FeO	0.23	0.19	0.31	0.28	0.19	0.26	0.26	0.36
CaO	14.60	16.09	15.70	14.15	14.19	16.99	14.98	15.56
Na_2O	2.79	2.26	2.69	3.48	2.46	1.79	2.87	2.56
K_2O	0.23	0.14	0.16	0.21	1.56	0.09	0.19	0.17
Total	98.22	99.89	100.60	100.17	100.04	98.67	99.37	99.34
Cations								
Si^{4+}	9.2693	9.0154	9.0846	9.4090	9.3270	8.8013	9.2352	9.0761
Al^{3+}	6.6575	6.9049	6.8152	6.4911	6.6085	7.0861	6.6672	6.8368
Fe^{2+}	0.0357	0.0290	0.0476	0.0423	0.0288	0.0397	0.0395	0.0397
Ca^{2+}	2.9032	3.1581	3.0602	2.7567	2.7801	3.3899	2.9490	3.0693
Na^{+}	1.0185	0.8159	0.9627	1.2451	0.8853	0.6562	1.0369	0.9282
K^{+}	0.0537	0.0334	0.0378	0.0478	0.3636	0.0209	0.0438	0.0390

Sample Number:	AE-5R	AE-5C	AE-5RS	AE-7R	AE-7C	AE-7RS	AE-9R	AE-9C
Oxide								
SiO_2	48.26	49.23	48.43	49.71	48.44	47.98	48.55	48.79
Al_2O_3	32.00	31.39	31.09	31.24	32.14	32.69	32.30	31.82
FeO	0.23	0.19	0.41	0.32	0.32	0.35	0.24	0.21
CaO	16.17	15.14	16.63	15.44	16.38	16.73	16.31	15.90
Na_2O	2.30	2.61	2.46	2.70	2.10	2.09	2.00	2.26
K_2O	0.09	0.18	0.16	0.14	0.12	0.06	0.11	0.14
Total	99.05	99.03	99.17	99.55	99.51	99.90	99.51	99.11
Cations								
Si^{4+}	8.9299	9.0886	8.9838	9.1310	8.9252	8.8200	8.9321	9.0057
Al^{3+}	6.9793	6.8299	6.7981	6.7640	6.9805	7.0829	7.0049	6.9239
Fe^{2+}	0.0357	0.0289	0.0633	0.0493	0.0499	0.0544	0.0369	0.0321
Ca^{2+}	3.2064	3.0548	3.3052	3.0381	3.2339	3.2960	3.2161	3.1446
Na^{+}	0.8359	0.9466	0.8960	0.8960	0.9773	0.7627	0.7553	0.7344
K^{+}	0.0222	0.0419	0.0374	0.0316	0.0270	0.0150	0.0265	0.0325

Sample Number:	AE-9RS	AE-10R	AE-10C	AE-10RS	AE-12R	AE-12C	AE-12RS	AE-13R
Oxide								
SiO_2	49.02	47.78	48.40	48.65	47.99	48.95	48.68	52.23
Al_2O_3	31.79	32.72	31.93	32.16	32.15	31.82	31.73	29.95
FeO	0.31	0.23	0.17	0.19	0.19	0.24	0.28	0.35
CaO	15.93	16.87	16.10	16.34	16.61	15.85	16.05	13.53
Na_2O	2.34	1.84	2.35	2.21	2.05	2.35	2.24	3.69
K_2O	0.13	0.12	0.17	0.18	0.13	0.18	0.19	0.30
Total	99.53	99.55	99.12	99.73	99.12	99.38	99.16	100.19
Cations								
Si^{4+}	9.0165	8.8093	8.9499	8.9499	8.9408	8.8828	9.0143	9.0143
Al^{3+}	6.8925	7.1103	6.9582	6.9670	7.0151	6.9074	6.9096	6.4180
Fe^{2+}	0.0483	0.0353	0.0266	0.0295	0.0300	0.0362	0.0434	0.0528
Ca^{2+}	3.1399	3.3329	3.1894	3.2172	3.2941	3.1273	3.1770	2.6346
Na^{+}	0.8484	0.6686	0.8546	0.7992	0.7451	0.8515	0.8128	1.3199
K^{+}	0.0314	0.0271	0.0392	0.0431	0.0300	0.0421	0.0443	0.0705

Sample Number:	AE-13C	AE-15R	AE-15C	AE-16R	AE-16C	AE-16RS	AE-18R	AE-18C
Oxide								
SiO_2	49.15	54.38	50.06	48.82	49.47	49.44	49.01	49.87
Al_2O_3	31.87	27.75	30.79	32.24	31.75	32.01	32.24	32.40
FeO	0.17	0.48	0.18	0.41	0.27	0.40	0.37	0.41
CaO	16.08	11.30	14.99	16.15	15.53	15.81	16.04	16.16
Na_2O	2.28	4.82	2.98	2.00	2.55	2.37	2.25	2.28
K_2O	0.14	0.31	0.16	0.12	0.17	0.15	0.13	0.15
Total	99.70	99.04	99.16	99.74	99.73	100.19	100.05	101.26
Cations								
Si^{4+}	9.0201	9.9286	9.2173	8.9618	9.0692	9.0312	8.9715	9.0158
Al^{3+}	6.8951	5.9718	6.6814	6.9752	6.8607	6.8922	6.9551	6.9034
Fe^{2+}	0.0262	0.0728	0.0280	0.0636	0.0417	0.0614	0.0569	0.0620
Ca^{2+}	3.1623	2.2105	2.9572	3.1754	3.0504	3.0950	3.1466	3.1299
Na^{+}	0.8237	1.7318	1.0795	0.7216	0.9180	0.8514	0.8111	0.8092
K^{+}	0.0335	0.0717	0.0366	0.0274	0.0388	0.0345	0.0306	0.0337

Sample Number:	AE-18RS	AE-20R	AE-20C	AE-20RS	AE-23R	AE-23C	AE-23RS	AE-24R
Oxide								
SiO_2	49.15	49.74	49.77	49.41	48.06	48.86	48.62	50.24
Al_2O_3	32.08	31.97	31.87	32.04	32.15	31.68	31.74	31.90
FeO	0.39	0.29	0.35	0.26	0.15	0.20	0.23	0.24
CaO	15.90	15.74	15.53	15.59	16.66	15.93	16.10	15.54
Na_2O	2.23	2.18	2.48	2.11	2.06	2.39	2.44	2.68
K_2O	0.15	0.18	0.16	0.21	0.10	0.16	0.14	0.18
Total	99.88	100.10	100.15	99.61	99.18	99.03	99.26	100.78
Cations								
Si^{4+}	9.0051	9.0755	9.0818	9.0556	8.8877	9.0010	8.9783	9.1097
Al^{3+}	6.9273	6.8768	6.8552	6.9215	7.0090	6.9050	6.9091	6.8177
Fe^{2+}	0.0590	0.0435	0.0528	0.0403	0.0234	0.0312	0.0352	0.0361
Ca^{2+}	3.1220	3.0776	3.0370	3.0625	3.3014	3.1558	3.1856	3.0196
Na^{+}	0.8021	0.7830	0.8905	0.7595	0.7485	0.8685	0.8848	0.9561
K^{+}	0.0339	0.0424	0.0370	0.0479	0.0241	0.0382	0.0332	0.0407

Sample Number:	AE-24C	AE-24RS	AE-25R	AE-25C	AE-MRR	AE-MRR	AE-29R	AE-29C
Oxide								
SiO_2	49.13	49.05	56.09	52.97	49.95	49.55	48.05	48.48
Al_2O_3	32.53	32.76	28.24	30.36	31.58	31.67	33.16	32.50
FeO	0.22	0.22	0.32	0.12	0.23	0.25	0.31	0.30
CaO	16.26	16.50	10.81	13.41	15.14	15.35	17.15	16.75
Na_2O	2.10	2.11	5.07	3.75	2.86	2.60	1.83	2.03
K_2O	0.14	0.12	0.37	0.26	0.08	0.12	0.08	0.13
Total	100.38	100.76	100.91	100.86	99.83	99.53	100.57	100.20
Cations								
Si^{4+}	8.9559	8.9171	10.0167	9.5267	9.1334	9.0937	8.7755	8.8795
Al^{3+}	6.9903	7.0187	5.9446	6.4346	6.8059	6.8495	7.1387	7.0169
Fe^{2+}	0.0335	0.0339	0.0479	0.0173	0.0352	0.0375	0.0469	0.0460
Ca^{2+}	3.1770	3.2131	2.0683	2.5843	2.9658	3.0179	3.3561	3.2882
Na^{+}	0.7526	0.7533	1.7818	1.3273	1.0279	0.9370	0.6584	0.7324
K^{+}	0.0316	0.0281	0.0850	0.0592	0.0187	0.0286	0.0175	0.0311

Sample Number:	AE-29RS	AE-32R	AE-32C	AE-32RS	AE-33R	AE-33C	AE-35R	AE-35C
Oxide								
SiO_2	49.22	48.60	49.19	48.68	49.28	47.12	48.42	49.42
Al_2O_3	32.25	32.14	31.75	32.05	31.81	33.27	32.39	31.65
FeO	0.19	0.20	0.26	0.37	0.25	0.26	0.27	0.27
CaO	16.28	16.38	15.65	16.42	15.83	17.54	16.48	15.72
Na_2O	2.12	2.22	2.45	2.28	2.53	1.68	2.10	2.57
K_2O	0.12	0.10	0.12	0.10	0.09	0.05	0.05	0.10
Total	100.18	99.63	99.41	99.91	99.78	99.91	99.70	99.85
Cations								
Si^{4+}	8.9883	8.9391	9.0472	8.9406	9.0368	8.6775	8.9003	9.0628
Al^{3+}	6.9423	6.9676	6.8833	6.9377	6.8747	7.2228	7.0178	6.8382
Fe^{2+}	0.0290	0.0305	0.0401	0.0564	0.0390	0.0393	0.0407	0.0555
Ca^{2+}	3.1856	3.2282	3.0834	3.2319	3.1095	3.4619	3.2454	3.0863
Na^{1+}	0.7625	0.8016	0.8856	0.8253	0.9117	0.6081	0.7603	0.9272
K^{1+}	0.0284	0.0223	0.0289	0.0277	0.0201	0.0110	0.0127	0.0234

Sample Number:	AE-36R	AE-36C	AE-36RS	AE-38R	AE-38C	AE-38RS	AE-39.4R	AE394C
Oxide								
SiO_2	49.49	49.30	49.23	49.04	48.69	50.65	50.20	49.26
Al_2O_3	31.99	32.05	32.12	32.24	32.49	30.94	31.10	31.97
FeO	0.15	0.22	0.20	0.17	0.27	0.55	0.17	0.19
CaO	16.13	15.99	16.14	16.26	16.44	14.60	14.51	15.76
Na_2O	2.48	2.49	2.13	2.47	2.23	3.16	2.98	2.39
K_2O	0.12	0.14	0.12	0.14	0.17	0.18	0.18	0.14
Total	100.37	100.19	99.94	100.32	100.29	100.08	99.14	99.70
Cations								
Si^{4+}	9.0253	9.0091	9.0084	8.9590	8.9052	9.2442	9.2262	9.0318
Al^{3+}	6.8772	6.9024	6.9264	6.9425	7.0041	6.6563	6.7361	6.9099
Fe^{2+}	0.0235	0.0330	0.0309	0.0255	0.0408	0.0839	0.0263	0.0290
Ca^{2+}	3.1519	3.1304	3.1646	3.1831	3.2211	2.8553	2.8573	3.0957
Na^{1+}	0.8881	0.8967	0.7676	0.8860	0.8028	1.1344	1.0769	0.8619
K^{1+}	0.0284	0.0331	0.0285	0.0333	0.0404	0.0412	0.0429	0.0318

Sample Number:	AE-395R	AE-395C	AE-396R	AE-396C	AE396RS	AE-401C	AE-401C	AE-42R
Oxide								
SiO_2	49.00	49.07	49.51	49.15	49.25	54.76	53.20	50.94
Al_2O_3	29.80	31.74	32.18	32.11	32.16	28.65	30.10	31.62
FeO	0.13	0.14	0.28	0.28	0.22	0.26	0.15	0.15
CaO	13.52	15.57	15.93	15.80	15.80	11.46	12.97	14.54
Na_2O	3.92	2.65	2.49	2.42	2.41	4.76	3.95	3.13
K_2O	0.05	0.04	0.15	0.14	0.14	0.30	0.20	0.11
Total	99.41	99.21	100.54	99.90	99.98	100.18	100.57	100.49
Cations								
Si^{4+}	9.2689	9.0405	9.0146	9.0026	9.0086	9.8696	9.5836	9.2282
Al^{3+}	6.6439	6.8931	6.9057	6.9324	6.9341	6.0870	6.3897	6.7511
Fe^{2+}	0.0203	0.0214	0.0422	0.0424	0.0335	0.0389	0.0226	0.0233
Ca^{2+}	2.7409	3.0741	3.1071	3.1014	3.0978	2.2130	2.5033	2.8225
Na^{1+}	1.4583	0.9595	0.8905	0.8711	0.8689	1.6876	1.3985	1.1161
K^{1+}	0.0121	0.0082	0.0353	0.0337	0.0320	0.0688	0.0460	0.0261

Sample Number:	AE-42C	AE-43R	AE-43C	AE-43RS	AE-45R	AE-45C	AE-45RS	AE-46R
Oxide								
SiO_2	48.90	46.25	49.00	49.15	47.36	48.98	48.69	48.39
Al_2O_3	31.97	34.45	32.29	32.27	33.38	32.06	32.41	32.13
FeO	0.30	0.27	0.32	0.29	0.24	0.27	0.36	0.21
CaO	15.64	18.73	16.39	16.27	17.52	16.09	16.42	16.61
Na_2O	2.42	1.06	2.09	2.25	1.62	2.33	2.09	2.20
K_2O	0.10	0.04	0.14	0.14	0.08	0.16	0.10	0.08
Total	99.33	100.79	100.22	100.36	100.18	99.18	100.07	99.63
Cations								
Si^{4+}	9.0047	8.4681	8.9571	8.9704	8.6925	8.9824	8.9183	8.9107
Al^{3+}	6.9381	7.4357	6.9567	6.9426	7.2213	6.9292	6.9974	6.9740
Fe^{2+}	0.0464	0.0406	0.0482	0.0446	0.0367	0.0416	0.0548	0.0328
Ca^{2+}	3.0864	3.6738	3.2106	3.1814	3.4450	3.1610	3.2255	3.2774
Na^{+}	0.8772	0.3830	0.7521	0.8066	0.5847	0.8408	0.7525	0.7960
K^{+}	0.0237	0.0086	0.0317	0.0319	0.0180	0.0367	0.0222	0.0188

Sample Number:	AE-46C	AE-46RS	AE-47R	AE-47C	AE-47RS	AE-48C	AE-48C	AE-49R
Oxide								
SiO_2	48.57	48.52	46.75	49.04	48.41	50.22	51.36	54.51
Al_2O_3	31.88	32.07	33.24	31.69	32.27	31.37	30.67	28.68
FeO	0.25	0.23	0.19	0.23	0.19	0.15	0.18	0.11
CaO	16.21	16.38	17.61	15.96	16.87	14.74	14.15	11.76
Na_2O	2.35	2.24	1.50	2.35	2.17	2.96	3.46	4.85
K_2O	0.12	0.10	0.09	0.21	0.11	0.07	0.07	0.24
Total	99.39	99.54	99.38	99.46	100.03	99.03	99.89	100.14
Cations								
Si^{4+}	8.9596	8.9353	8.6561	9.0270	8.8869	9.1947	9.3544	9.8362
Al^{3+}	6.9318	6.9625	7.2543	6.8759	6.9820	6.7698	6.5830	6.0996
Fe^{2+}	0.0381	0.0350	0.0291	0.0353	0.0296	0.0225	0.0276	0.0169
Ca^{2+}	3.2046	3.2330	3.4930	3.1472	3.3183	2.8914	2.7604	2.2731
Na^{+}	0.8518	0.8124	0.5475	0.8508	0.7845	1.0671	1.2403	1.7224
K^{+}	0.0289	0.0230	0.0208	0.0486	0.0260	0.0168	0.0172	0.0541

Sample Number:	AE-49C	AE-51R	AE-51C	AE-55C	AE-55C	AE-57R	AE-57C	AE-59R
Oxide								
SiO_2	53.59	55.82	53.84	53.18	52.80	54.61	54.07	58.29
Al_2O_3	29.32	28.05	29.11	29.34	29.79	28.80	29.07	26.14
FeO	0.11	0.18	0.10	0.13	0.14	0.14	0.09	0.18
CaO	12.58	10.92	12.51	12.17	12.57	11.85	12.32	8.76
Na_2O	4.23	5.22	4.37	4.20	4.02	4.70	4.52	6.25
K_2O	0.23	0.41	0.29	0.21	0.16	0.24	0.25	0.47
Total	100.16	100.58	100.22	99.22	99.49	100.34	100.32	100.08
Cations								
Si^{4+}	9.6887	10.0090	9.7274	9.6894	9.6044	9.8321	9.7517	10.4337
Al^{3+}	6.2475	5.9272	6.1990	6.2998	6.3877	6.1118	6.1801	5.5142
Fe^{2+}	0.0169	0.0262	0.0154	0.0204	0.0218	0.0208	0.0142	0.0272
Ca^{2+}	2.4374	2.0982	2.4209	2.3752	2.4502	2.2868	2.3816	1.6806
Na^{+}	1.5411	1.8406	1.5549	1.5041	1.4376	1.6647	1.6030	2.2002
K^{+}	0.0531	0.0926	0.0662	0.0479	0.0378	0.0561	0.0584	0.1069

Sample Number:	AE-59C	AE-61R	AE-61C	AE-64R	AE-64C	AE-66R	AE-66C	AE-68
Oxide								
SiO_2	57.96	51.93	50.40	55.12	54.71	49.70	49.50	49.26
Al_2O_3	26.43	30.49	31.56	27.51	28.94	31.91	31.74	31.60
FeO	0.07	0.19	0.17	0.15	0.12	0.30	0.22	0.30
CaO	9.08	14.16	15.12	10.20	12.06	15.82	15.75	15.80
Na_2O	6.03	3.71	2.72	4.81	4.59	2.54	2.38	2.45
K_2O	0.45	0.20	0.15	1.01	0.22	0.17	0.16	0.15
Total	100.02	100.66	100.12	99.82	100.64	100.45	99.74	99.58
Cations								
Si^{4+}	10.3817	9.3952	9.1788	10.0161	9.8209	9.0553	9.0712	9.0561
Al^{3+}	5.5798	6.5026	6.7747	5.8891	6.1237	6.8531	6.8567	6.8478
Fe^{2+}	0.0111	0.0280	0.0257	0.1739	0.0180	0.0457	0.0331	0.0460
Ca^{2+}	1.7481	2.7453	2.9500	1.9839	2.3197	3.0891	3.0926	3.1112
Na^{+}	2.1245	1.3197	0.9750	1.7198	1.6203	0.9098	0.8568	0.8844
K^{+}	0.1026	0.0450	0.0339	0.2331	0.0497	0.0402	0.0369	0.0349

Plagioclase feldspars have triclinic symmetry, and their structure involves a framework of linked (Si,Al) - O tetrahedra (Deer et al.,1982). This framework has large interstices which are filled essentially by Ca and Na ions, while minor quantities of K, Mg, Fe^{3+}, Ti, Mg, Ba and Sr may also be present.

In the study section, three textural varieties of plagioclase are defined. There are "intercumulus" grains which occur in the interstices between pyroxene and olivine grains in pyroxenites and harzburgites. Secondly there are the "cumulus-restrained" grains which are poikilitically enclosed by olivine and/or pyroxene, and finally, the "cumulus-unrestrained" variety whose growth was not inhibited by enclosure. The latter variety are the most common constituents of anorthosites and norites.

An inherent problem in microprobe analysis of plagioclase grains is the extreme chemical zonation exhibited by them (Kruger, 1983; Cameron, 1980). This means that random analyses are unlikely to be representative of the mineral's chemistry. To overcome this problem traverses of whole grains were made to allow their full chemical variation to be displayed. In all, 600 plagioclase analyses were performed. Selected representative analyses are presented in Table 4.4.

4.4.1 Intercumulus Grains.

These grains exhibit wide chemical variations. This is evi-

Figure 4.9 Variations in plagioclase chemistry represented on a portion of the Ab-An-Or diagram. Analyses are presented for each Unit for intercumulus and cumulus grains.

Figure 4.10 Microprobe profiles, in terms An mole percent and potassium in parts per million, across an intercumulus plagioclase grain. The profile represents a complete profile from grain rim to grain rim.

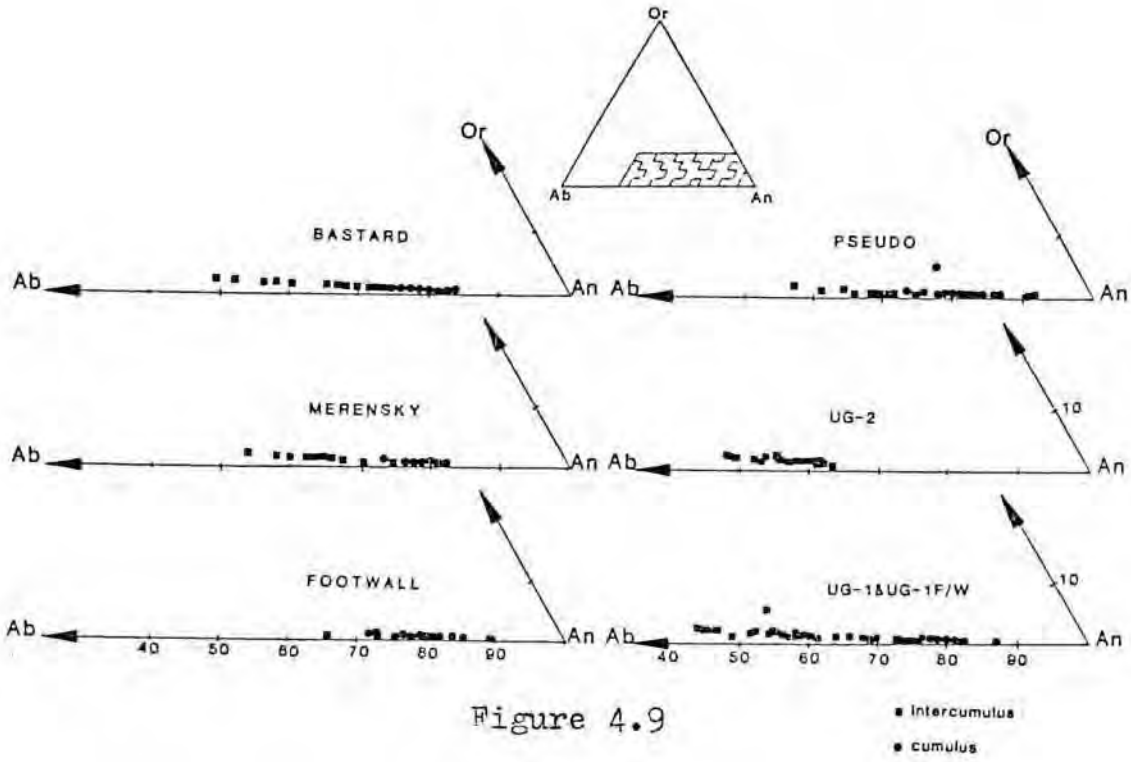

Figure 4.9

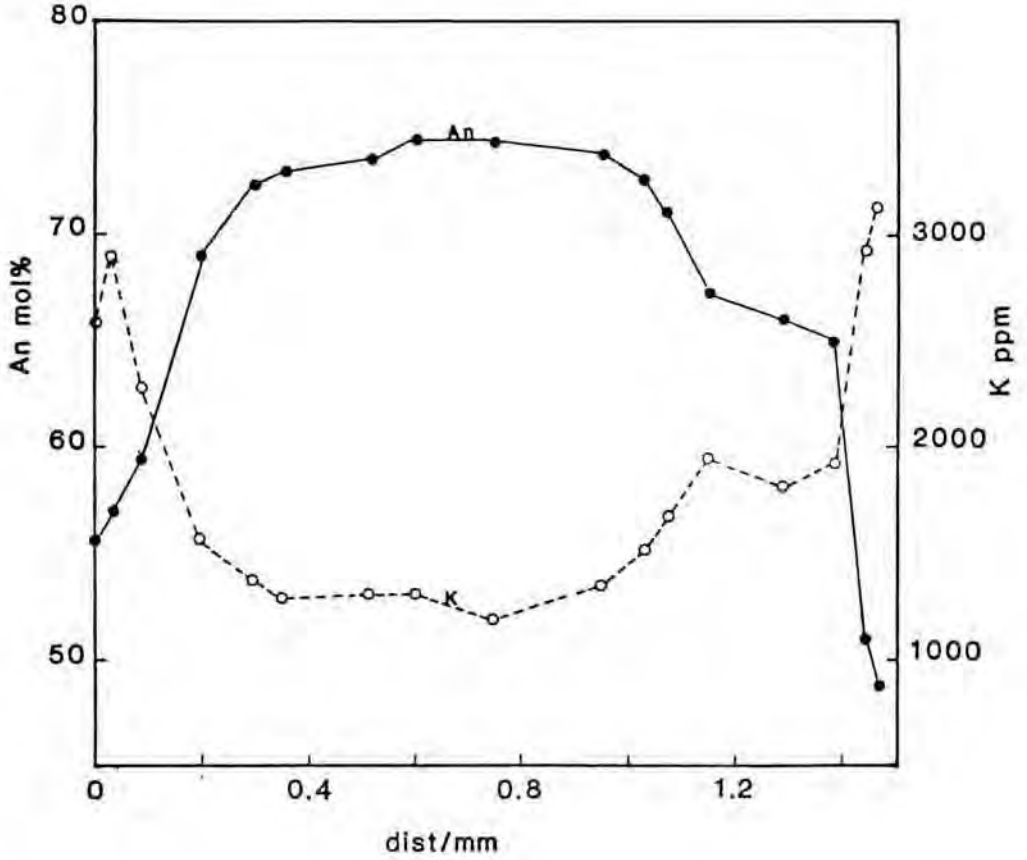

Figure 4.10

dent in figure 4.12 where mole percentage An content is plotted against stratigraphic height. It is clear that this variation is apparent in individual samples as well as from one sample to the next. In figure 4.9, it is clear that intercumulus plagioclase not only has lower An contents than cumulus plagioclase, but it may contain higher levels of K_2O. The chemical variations in single grains are best illustrated by microprobe profiles, such as those in figure 4.10. The most striking feature of these profiles is the marked depletion in An mole percentage of the feldspar at its grain boundaries with cumulus orthopyroxene grains. The central portions of the grains however, may be fairly homogeneous, or they may show weak oscillatory zoning. These strongly sodic zones were recorded in all the grains which were profiled. However, their absolute values vary widely from sample to sample. This chemical zoning is also apparent in the potasium content of the mineral, with highest K concentrations matching highest Ab values.

4.4.2 Unrestrained, Cumulus Grains.

It is evident from figure 4.12 that these grains have a more restricted compositional range than the previous type. Most analyses fall in the An70-An80 range, and it is also evident that successive samples vary more systematically with stratigraphic height. In spite of their more restricted range, these grains do exhibit marked chemical zonation patterns, which is evident in the microprobe profiles of figure 4.11.

A common feature of this chemical zoning is the occurrence of strongly reversed rims on otherwise oscillatory zoned grains.

Furthermore, these rims are irregular features which need not totally envelope the cumulus grains. Commonly they vary considerably in width, while the An-values of the rims, although still higher than those of the core, may differ considerably at opposite ends of a grain. In thin section these rims can be seen as bands which have slightly different extinction angles when compared with the remainder of the grain.

The oscillatory zoning of the inner parts of unrestrained grains is variable, especially in the number of zones which any single grain may possess. Usually, but not always, the core is slightly more calcic and it is surrounded by up to four alternating sodic and calcic zones. Optical observations indicate that more complex zoning patterns, of the type recorded by Maaloe (1976) in Skaergaard rocks may be present in these rocks as well.

Potassium levels in cumulus plagioclase are generally lower than those recorded in intercumulus grains, while the highest levels are recorded in albitic portions of the oscillatory zoned cores of grains. Chemical zonation of potasium is antipathetic to that exhibited by An mole percent.

4.4.3 Restrained Cumulus Grains.

Although these grains are texturally distinct from the unrestrained variety, the compositions of the majority of analysed grains are indistinguishable from those of the latter type. Occasional grains, however, have either higher or lower

Figure 4.11 Three microprobe profiles across cumulus plagioclase grains, in terms of An mole percent and potassium. In (a) an anorthitic core is rimmed by a more albitic margin. In (b) a reversed anorthitic margin is evident at both ends. In (c) a strongly anorthitic margin is apparent on one margin only.

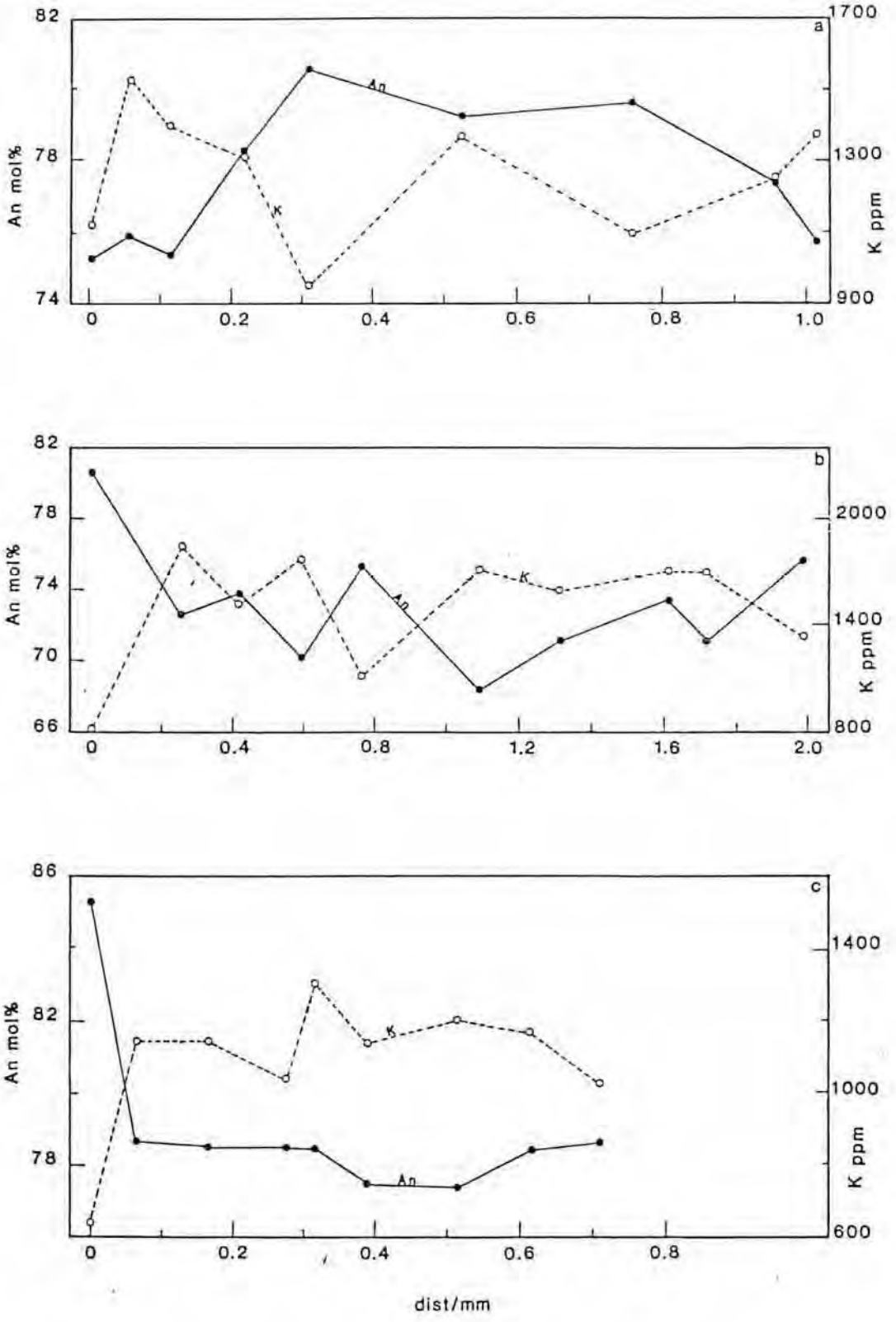
82
78
74
An mol%
1700
1300
900
K ppm
a
An
K
0
0.2
0.4
0.6
0.8
1.0
82
78
74
70
66
An mol%
2000
1400
800
K ppm
b
An
K
0
0.4
0.8
1.2
1.6
2.0
86
82
78
An mol%
1400
1000
600
K ppm
c
K
An
0
0.2
0.4
0.6
0.8
dist/mm

Figure 4.11

An contents than unrestrained grains from the same sample. It is possible that the composition of these grains is dependent on the stage at which they become trapped. Smaller grains generally have higher An values than larger ones, suggesting that they were trapped at any early stage during crystallization. It is evident from figure 4.12, however, that a number of these grains also contain the highly anorthitic reversed rims, evident in unrestrained grains.

4.4.4 Variations in Plagioclase Compositions with Stratigraphic Height.

Upward increase in the average An content of plagioclase is obvious wherever plagioclase-cumulates overlie rocks containing only intercumulus feldspar (Figure 4.12). There is, however, also an upward increase in the An content of cores of cumulus grains through the plagioclase-cumulates of the lower Pseudo, Footwall and Merensky Units. In the Bastard Unit, by contrast, this pattern is only developed through the noritic rocks, while a clear upward decrease in An is apparent through the Giant Mottled Anorthosite.

An-values in the UG-2 and UG-1 Units, where only intercumulus plagioclase occurs, are widely scattered. In the UG-2, the cores of the grains exhibit a vague upward decrease in An with height. A wide range of An-values is apparent in the UG1 Unit, (see Figure 4.12), and no consistent pattern is apparent. The thin chromitite layer which is contained within this unit is distinctive. The sample below the chromitite has high-An plagioclase, when compared to other intercumulus grains, whereas the sample containing the chromitite contains

Figure 4.12 A plot of plagioclase analyses, in terms of An mole percent, against a stratigraphic log. Here squares represent intercumulus grains, circles cumulus unrestrained grains, and triangles cumulus restrained grains. Open symbols represent grain margins, and solid symbols grain cores.

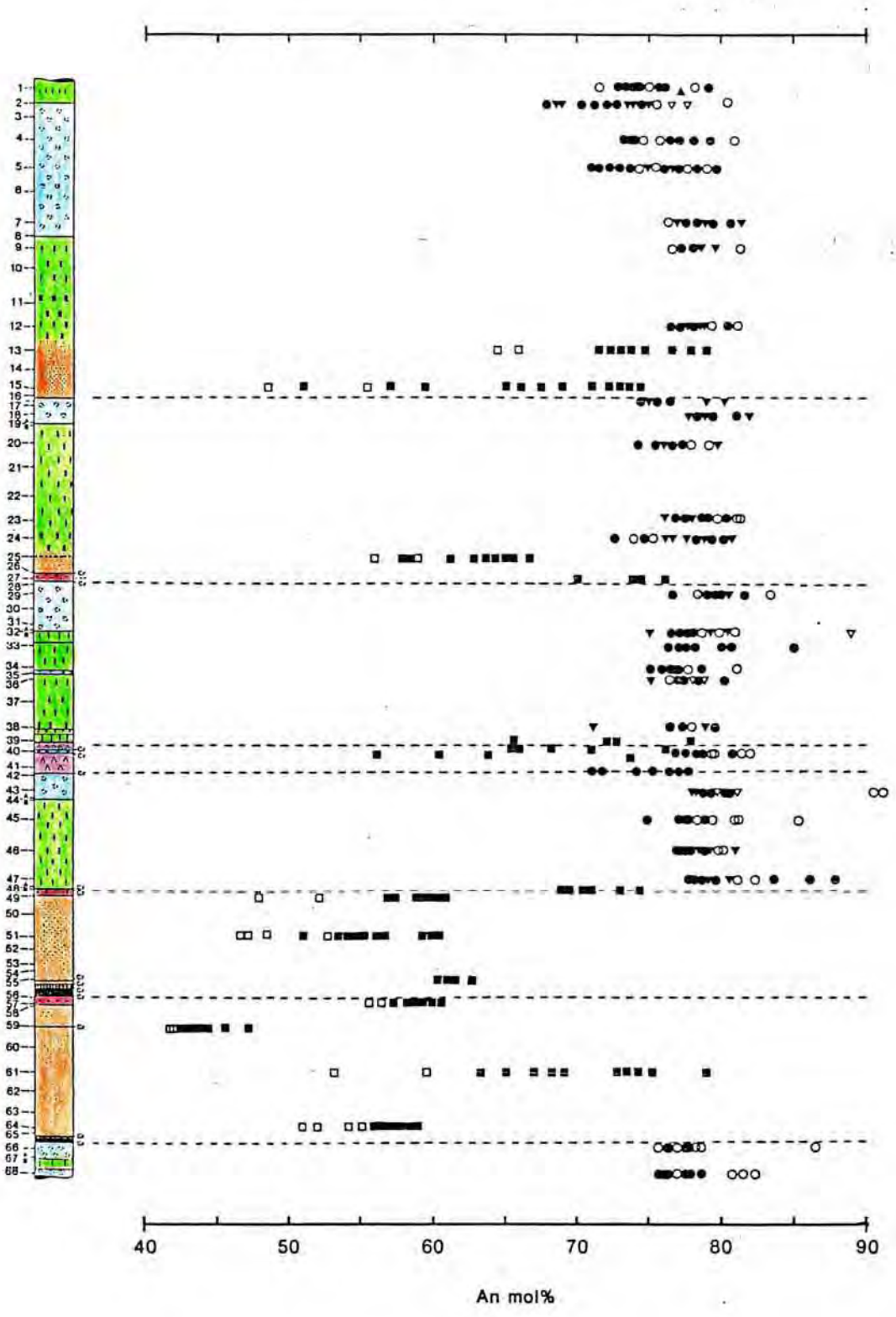

Figure 4.12

plagioclase whichis the most sodic recorded in the entire succession.

4.5 Discussion.

4.5.1 Causes and Implications of Chemical Zoning of Feldspar.

Chemical zonation in plagioclase has been documented from a host of magmatic and metamorphic environments (Smith, 1974). Three varieties of zoning have been recognized by Smith (op.cit), namely "normal", "oscillatory" and "reversed". The origins and genetic significance of zoning have been widely discussed in the literature, and the following five points summarizes the majority of ideas:

(i) the simultaneous crystallization of hornblende with plagioclase leads to the withdrawal of Ca from the melt, which may result in the formation of oscillatory zoning in plagioclase;

(ii) convection results in the movement of growing crystals to and from areas of undepleted magma. This may bring about any one of the three types of zoning, depending on the extent of movement;

(iii) the imbalance which results from differing rates of diffusion of new components to the growth surface may bring about zoning, depending on the availability and nature of such components;

(iv) zoning may be brought about by diffusion in the solid-state, subsequent to crystallization;

(v) volatile loss or pressure changes may lead to the depression or elevation of the Ab-An solidus-liquidus loop, with concomitant changes in feldspar composition.

Morse and Nolan(1984) found An-enriched reversed rims on cumulus plagioclase grains in the Kiglapait intrusion of Labrador. These rims resemble those of this study, although the cores of Bushveld plagioclases are more calcic than those of Kiglapait. These authors believe that the reversed rims may be explained by the "augite-effect", in which a strong correlation has been found between the CIPW-normative An-partition coefficient and the Di-content of a basaltic liquid (Morse, 1979). They show that by increasing the Di-content of a liquid, plagioclase which becomes increasingly Ca-rich, may crystallize. This means that the reversed rims on plagioclase may be brought about by increasing augite components in the residual melt. This explantion may also be invoked to explain the occurrence of calcic rims on cumulus plagioclase in this study because, as has been noted, they resemble late-stage overgrowths on cumulus grains and, they occur in rocks where intercumulus clinopyroxene is common. The intercumulus clinopyroxene may have crystallized at roughly the same time, or just after the highly calcic plagioclase.

4.5.2 Cryptic Cyclical Variations in Mineral Chemistry

The main evidence for cryptic cycles through the sequence comes from variations in the chemistry of orthopyroxene and plagioclase, mainly because both these mineral phases are present in all the samples that were analysed. This meant

that closely spaced samples were analysed, from which valid trends could be described. Olivine chemistry indicates that layers containing primitive minerals are present at the base of each unit, which in turn indicates that new primitive liquids were probably injected into the magma chamber at these levels.

Chemical cyclicity is best illustrated by variations in the Mg-Fe ratio of orthopyroxenes, where in the upper three Units variations from Mg-rich to less magnesian varieties are indicated upwards through all three of these units. Importantly, the lowermost sample of the overlying unit again possesses primitive Mg-rich orthopyroxene. These variations closely match the lithologically recognizable contacts between Units.

The cyclicity reflected by plagioclase chemistry is somewhat more subtle. Here an upward increase in An content is apparent through the three uppermost Units. If Bowen's Reaction Series is taken to indicate valid fractionation trends, then the variations exhibited by plagioclase are of the opposite sense to those of orthopyroxene. The most evolved (sodic) grains occur at the bases of Units, whereas more calcic ones occur at the top. Furthermore, it is apparent that the lowermost samples in some Units, for example the Merensky Unit, have plagioclase compositions which are more akin to those of the underlying Unit.

Differences in composition between cumulus and intercumulus grains may be brought about by their respective positions in the crystallization sequence, where cumulus grains are earlier fractionation products and are resultantly more calcic. The

observation that intercumulus plagioclase is more sodic, and occurs at lower levels in Units, may be explained by the occurence at low levels (in such units) of plagioclase components which are more typical of underlying units. This does still not explain the upward increase in anorthite content through members containing cumulus plagioclase. Vermaak (1976) suggests that this feature can be explained by the flotation of plagioclase. He envisaged the formation of a floating plagioclase mat, onto which later-crystallizing grains would underplate. Early, calcic grains would therefore be located at the top of the Unit, while later, more sodic grains would be found at its base. Eales et al.(in press) suggested that the upward increase results from the mixing of new magma magma impulses with hybrid layers. This has the effect of shifting the liquid into the primary phase-field of plagioclase in the Di-Plag-En+4Q system. Others, for example Ferguson and Wright (1970) have suggested that the upward increase is brought about by by changes in oxygen fugacity, which also have the effect of shifting the liquid into the anorthite field.

The variations which are observed in mineral chemistry through each unit are clearly more complex than those which might be expected from the simple fractional crystallization or bottom crystallization of a single magma batch, as coherent fractionation patterns for pyroxene and feldspar would be expected. It is likely that the observed chemical diversity may also have been brought about by the mixing of chemically different liquids, while processes such as double-diffusive convection are also likely to have been contributory factors.

4.5.3. The Critical Zone-Main Zone Boundary.

The exact position of the boundary between the Main and Critical Zones of the Bushveld Complex is somewhat uncertain, and has not been unequivocally defined. The Giant Mottled Anorthosite is generally regarded as the boundary, probably only because it is such a good marker horizon.

Microprobe analyses of closely spaced samples through this member, and its underlying lithologies, reveal that there is a geochemical inflection through this "anorthosite" layer and that trends which are charcteristic of the lower portion of the study section become reversed at this level. The data which most clearly exhibits this change are the Cr/Al ratio of orthopyroxenes (figure 4.7b) and the An content of plagioclase (figure 4.12).

Eales et al. (in press) have shown that there is a significant shift in Cr/Al of orthopyroxenes at the top of the Upper Critical Zone. They give values of 0.2 to 0.3 for the Critical Zone, and 0 to 0.1 for the Main Zone. Clearly, therefore the pyroxenes of the Giant Mottled anorthosite are more akin to those of the Main Zone, while those of the remainder of the succession are typical of the Critical Zone lineage. Low Cr/Al ratios are also obtained in harzburgite and pegmatoidal pyroxenite layers, but these low values could conceivably be ascribed to the presence of chromite in these rocks, which has depleted Cr in the melt, and has therefore had the effect of reducing this element's abundance in orthopyroxene. No chromite is present in the Giant Mottled

Anorthosite, a fact attested to by low whole-rock values of around 140ppm. Another possibility is that nucleation of plagioclase has depleted the melt in Al, causing Cr/Al to rise. This depletion in Al is not typical of harzburgite, presumably because feldspar was not nucleating, and hence Cr/Al is low.

CHAPTER 5 : WHOLE-ROCK GEOCHEMISTRY

Whole-rock geochemical analyses were performed by X-ray fluorescence spectrometry on 141 samples from boreholes AE and AF. Trace elements Zn Cu, Ni, Co, Cr, V, Sc, Rb, Sr, Y and Zr, and Na were determined on pressed-powder briquettes, while major elements oxides SiO_2, TiO_2, Al_2O_3, Fe_2O_3, MnO, CaO, K_2O and P_2O_5 were determined on fused discs. All the experimental conditions pertinent to each analytical run are summarized in Appendix A, while anhydrous analyses are presented in Table 5.1 and analyses including H_2O and loss-on-ignition, in Table B in this Appendix.

5.1 Major Elements

The Norrish and Hutton (1969) fusion method was employed for these analyses. All the samples from borehole AE were analysed in duplicate, and those whose totals ranged between 99 and 101 weight percent were accepted, while duplicate pairs were checked for compatibility. Total iron was determined as Fe_2O_3, and for purposes of C.I.P.W. normative calculations an Fe_2O_3/FeO ratio of 0.1 was assumed. This value was chosen, because the Irvine and Baragar (1971) equation;

$$\%Fe_2O_3 = \%TiO_2 + 1.5$$

yields unrealistically high percentages of normative magnetite and hematite, which are not in accord with the modes of these rocks. These analyses, together with their trace element analyses, are presented in Table 5.1.

Table 5.1 Whole-rock analyses for samples from borehole AE. These include major elements, without H2O- and LOI, as well as trace elements.

TABLE 5.1 WHOLE-ROCK ANALYSES

Sample No.	AE-1	AE-2	AE-3	AE-4	AE-5	AE-6	AE-7	AE-8
SiO_2	50.08	50.84	50.34	50.40	50.29	50.08	49.35	49.62
TiO_2	0.10	0.13	0.07	0.08	0.10	0.10	0.12	0.12
Al_2O_3	28.70	26.68	28.29	29.56	28.92	28.87	29.12	26.18
Fe_2O_3	0.22	0.27	0.17	0.16	0.17	0.22	0.19	0.32
FeO	2.15	2.65	1.69	1.55	1.65	2.19	1.86	3.33
MnO	0.03	0.04	0.03	0.03	0.03	0.04	0.03	0.06
MgO	2.50	3.42	2.15	1.79	1.58	2.35	2.81	5.04
CaO	13.20	13.83	14.15	13.91	14.65	13.56	14.32	13.30
Na_2O	2.33	2.13	2.25	2.24	2.29	2.30	1.95	1.86
K_2O	0.25	0.26	0.20	0.23	0.25	0.25	0.20	0.22
P_2O_5	0.03	0.06	0.06	0.06	0.06	0.05	0.05	0.06
Total	99.59	100.01	100.00	100.01	99.99	100.01	100.00	100.00
Zn	20	23	17	15	15	19	16	24
Cu	16	15	15	12	12	19	18	28
Ni	46	64	43	36	32	42	53	105
Sc	6.8	10.2	6.9	6.0	7.2	7.6	6.8	9.6
Co	17	21	24	12	11	15	16	25
Cr	131	239	141	106	84	114	193	410
V	35	64	34	29	45	38	35	46
Rb	6.3	5.8	2.7	4.6	3.7	2.6	4.4	6.9
Sr	346	321	353	363	353	351	329	312
Y	1.6	4.5	5.6	3.5	5.4	3.1	2.7	3.2
Zr	10.8	13.6	7.2	8.9	11.2	9.5	8.5	15.2

Sample No.	AE-9	AE-10	AE-11	AE-12	AE-13	AE-14	AE-15	AE-16
SiO_2	50.35	51.40	51.60	52.83	54.10	55.01	54.84	49.41
TiO_2	0.13	0.12	0.12	0.10	0.26	0.25	0.21	0.10
Al_2O_3	23.33	19.70	17.30	13.40	7.15	6.18	5.83	23.40
Fe_2O_3	0.43	0.50	0.56	0.67	0.87	0.89	0.95	0.56
FeO	4.25	5.01	5.63	6.66	8.68	8.93	9.47	5.56
MnO	0.09	0.11	0.11	0.14	0.20	0.20	0.21	0.08
MgO	7.83	11.36	14.28	17.90	23.20	22.92	23.40	7.70
CaO	11.68	10.13	9.08	7.14	4.87	4.57	3.98	11.14
Na_2O	1.66	1.45	1.17	1.10	0.56	0.75	0.73	1.84
K_2O	0.21	0.17	0.09	0.06	0.08	0.24	0.22	0.18
P_2O_5	0.21	0.17	0.05	0.00	0.05	0.05	0.17	0.04
Total	100.01	100.00	99.99	100.00	100.02	99.99	100.01	100.01
Zn	41	45	45	52	76	80	77	36
Cu	37	23	20	22	33	102	239	1676
Ni	177	239	314	387	553	647	871	4295
Sc	12.1	14.5	15.7	19.2	27.4	28.1	26.8	9.8
Co	37	38	56	67	91	107	96	93
Cr	827	1287	1817	2331	3459	2717	2878	971
V	62	65	74	84	125	126	125	44
Rb	6.3	3.8	1.4	4.1	3.2	7.1	4.1	2.6
Sr	273	237	191	228	57	65	63	283
Y	3.7	4.6	5.4	5.8	4.5	4.1	7.2	1.8
Zr	12.3	11.1	5.8	8.3	9.8	17.9	18.2	8.8

Sample No.	AE-18	AE-19A	AE-19B	AE-20	AE-21	AE-23	AE-24	AE-25
SiO_2	49.20	49.24	50.10	50.75	49.96	50.51	51.17	54.89
TiO_2	0.06	0.05	0.08	0.08	0.12	0.08	0.13	0.24
Al_2O_3	31.30	31.46	27.85	26.65	27.55	24.41	17.31	5.42
Fe_2O_3	0.10	0.09	0.22	0.28	0.24	0.37	0.63	0.99
FeO	0.96	0.88	2.19	2.84	2.38	3.66	6.29	9.91
MnO	0.01	0.03	0.04	0.04	0.05	0.07	0.12	0.22
MgO	1.08	1.06	3.40	5.00	4.06	7.04	13.36	23.00
CaO	14.96	14.73	13.86	12.39	12.96	11.86	9.42	4.46
Na_2O	2.11	2.07	2.03	1.78	2.52	1.87	1.43	0.63
K_2O	0.17	0.18	0.19	0.16	0.17	0.13	0.10	0.21
P_2O_5	0.05	0.06	0.06	0.01	0.02	0.01	0.05	0.07
Total	100.01	100.01	100.02	99.98	100.03	100.01	100.01	100.04
Zn	6	7	14	23	21	29	46	81
Cu	41	42	60	54	48	103	167	300
Ni	67	65	139	166	133	280	508	1185
Sc	3.6	3.1	6.3	8.9	8.4	10.0	18.0	30.5
Co	9	8	20	54	21	34	100	99
Cr	102	73	367	547	439	805	1639	3035
V	15	14	29	35	31	46	81	139
Rb	3.8	5.0	4.3	37.4	2.3	2.0	3.3	7.0
Sr	393	394	353	338	350	312	215	62
Y	3.6	0.9	2.5	4.1	1.8	4.6	3.6	8.7
Zr	8.5	6.5	8.6	3.7	7.6	7.4	7.8	23.4

Sample No.	AE-26	AE-28	AE-29	AE-30	AE-31	AE-32A	AE-32B	AE-33
SiO_2	53.97	49.10	49.72	49.78	49.52	49.70	49.83	49.33
TiO_2	0.25	0.09	0.09	0.09	0.08	0.11	0.09	0.07
Al_2O_3	5.35	30.42	29.56	29.86	31.21	31.49	28.11	29.38
Fe_2O_3	1.05	0.16	0.16	0.18	0.12	0.12	0.20	0.17
FeO	10.52	1.64	1.61	1.75	1.20	1.16	2.04	1.68
MnO	0.23	0.03	0.05	0.03	0.03	0.02	0.04	0.03
MgO	23.66	1.67	2.08	2.27	1.28	1.51	3.95	3.06
CaO	3.99	14.44	14.33	13.88	14.14	13.99	13.55	14.01
Na_2O	0.81	2.23	2.18	1.97	2.21	1.71	1.96	2.04
K_2O	0.15	0.17	0.17	0.19	0.20	0.19	0.18	0.17
P_2O_5	0.05	0.06	0.05	0.02	0.02	0.01	0.06	0.06
Total	100.03	100.01	100.00	100.02	100.01	100.01	100.01	100.00
Zn	94	nd	14	14	76	8	19	14
Cu	600	nd	25	25	33	13	21	13
Ni	1151	nd	39	40	553	35	81	65
Sc	27.6	nd	5.4	5.7	27.1	4.7	7.5	6.6
Co	113	11	12	13	91	9	19	14
Cr	4357	87	99	114	3429	144	435	324
V	146	25	23	27	125	16	29	22
Rb	5.5	1.0	4.1	4.4	3.2	4.6	3.7	3.5
Sr	62	449	444	447	457	452	413	416
Y	7.3	5.1	3.2	3.3	4.5	4.0	2.9	3.5
Zr	15.0	7.2	9.1	9.8	9.8	9.5	12.1	6.8

Sample No.	AE-34	AE-35	AE-36	AE-37	AE-38	AE-39	AE-40	AE-41
SiO_2	51.37	48.93	50.90	50.08	50.92	51.51	44.22	42.87
TiO_2	0.12	0.10	0.10	0.08	0.10	0.14	0.13	0.17
Al_2O_3	21.94	30.70	21.62	24.35	16.59	11.73	4.19	5.35
Fe_2O_3	0.40	0.12	0.42	0.34	0.59	0.77	1.25	1.33
FeO	4.04	1.24	4.21	3.37	5.92	7.69	12.48	13.29
MnO	0.09	0.03	0.09	0.08	0.16	0.16	0.22	0.22
MgO	9.31	1.53	10.01	7.08	15.61	19.92	32.78	32.76
CaO	10.91	14.93	10.86	12.18	8.61	6.64	4.04	3.20
Na_2O	1.62	2.16	1.60	1.55	1.33	1.28	0.55	0.59
K_2O	0.16	0.20	0.14	0.13	0.13	0.11	0.11	0.17
P_2O_5	0.05	0.08	0.05	0.05	0.05	0.06	0.05	0.05
Total	99.98	100.02	100.00	100.01	100.01	100.01	100.02	100.00
Zn	29	9	32	25	45	54	nd	98
Cu	20	19	21	22	49	130	nd	52
Ni	210	33	237	189	369	760	nd	1500
Sc	13.1	6.4	12.2	9.7	16.8	17.5	nd	8.7
Co	40	9	42	33	58	81	160	168
Cr	1050	37	1141	848	1975	3006	1583	4081
V	48	20	49	36	67	89	58	85
Rb	3.4	2.0	4.6	2.4	4.3	0.7	1.6	4.6
Sr	315	456	317	346	213	157	60	92
Y	6.6	4.8	4.7	1.5	2.9	5.5	5.0	6.3
Zr	13.7	6.3	9.7	6.6	5.6	8.3	11.4	8.1

Sample No.	AE-42	AE-43	AE-44A	AE-44B	AE-45	AE-46	AE-47	AE-48A
SiO_2	49.34	48.90	48.87	49.11	49.36	49.64	49.26	47.84
TiO_2	0.09	0.06	0.06	0.07	0.06	0.06	0.06	0.06
Al_2O_3	27.98	31.45	31.92	30.38	30.91	29.62	29.71	29.27
Fe_2O_3	0.24	0.11	0.09	0.15	0.12	0.15	0.16	0.23
FeO	2.43	1.11	0.88	1.49	1.15	1.52	1.61	2.26
MnO	0.06	0.03	0.03	0.04	0.03	0.03	0.04	0.06
MgO	4.24	1.41	0.95	2.21	1.62	2.66	2.69	4.32
CaO	13.34	14.64	14.91	14.32	14.50	14.08	14.27	13.97
Na_2O	2.08	2.09	2.08	2.05	2.05	2.03	1.99	1.76
K_2O	0.16	0.15	0.16	0.14	0.15	0.16	0.16	0.19
P_2O_5	0.05	0.05	0.05	0.05	0.05	0.05	0.05	0.05
Total	100.01	100.00	100.00	100.01	100.00	100.00	100.00	100.01
Zn	26	8	7	12	11	13	14	23
Cu	65	18	18	19	18	19	23	71
Ni	279	34	29	55	42	66	63	245
Sc	nd	4.9	4.9	5.6	5.4	5.7	6.1	4.0
Co	25	8	7	12	9	14	14	26
Cr	2392	597	573	588	600	563	603	1180
V	42	17	16	20	19	21	21	22
Rb	4.5	4.3	3.4	1.3	1.0	2.7	3.6	4.0
Sr	339	450	459	435	443	437	430	445
Y	1.5	2.8	4.7	4.3	5.3	nd	0.8	nd
Zr	8.2	5.5	4.5	6.3	5.6	7.7	9.8	7.6

Sample No.	AE-48B	AE-49	AE-50	AE-51	AE-52	AE-53	AE-54	AE-55
SiO_2	43.36	54.53	53.88	55019	55.07	54.13	51.97	49.55
TiO_2	0.08	0.16	0.20	0.26	0.27	0.23	0.29	0.20
Al_2O_3	5.72	6.27	5.77	5.57	4.83	6.17	6.67	5.15
Fe_2O_3	1.39	0.91	0.95	0.95	1.02	0.96	1.09	1.22
FeO	13.86	9.10	9.45	9.53	10.16	9.56	10.92	12.23
MnO	0.23	0.20	0.21	0.21	0.22	0.23	0.22	0.24
MgO	30.22	23.49	23.34	22.76	23.69	22.93	24.18	27.15
CaO	2.71	4.42	3.67	4.49	3.56	4.79	3.99	3.59
Na_2O	2.34	0.77	2.18	0.78	0.81	0.75	0.60	0.52
K_2O	0.09	0.10	0.26	0.22	0.32	0.14	0.08	0.09
P_2O_5	0.02	0.05	0.03	0.05	0.06	0.12	0.05	0.06
Total	100.02	100.00	100.03	100.01	100.01	100.01	100.01	100.00
Zn	84	79	74	75	82	77	95	94
Cu	719	37	34	34	35	63	42	21
Ni	3413	566	550	545	556	573	810	1091
Sc	8.4	24.3	26.4	27.8	28.8	29.0	26.7	20.5
Co	182	90	90	91	93	90	105	126
Cr	4434	3561	3324	3427	3596	4521	6000(+)	6000(+)
V	56	120	129	102	143	188	220	155
Rb	0.0	1.1	9.5	8.5	11.3	3.9	1.7	5.9
Sr	76	83	79	75	61	74	78	68
Y	2.9	4.3	3.8	4.7	5.6	8.3	4.2	2.3
Zr	7.0	6.5	14.3	20.7	26.3	16.8	9.3	10.5

Sample No.	AE-56	AE-58	AE-59	AE-60	AE-61	AE-62	AE-63	AE-64
SiO_2	54.79	54.78	54.20	55.61	55.13	54.64	54.23	54.45
TiO_2	0.25	0.22	0.23	0.22	0.23	0.33	0.17	0.17
Al_2O_3	4.78	5.11	5.06	4.89	4.97	4.19	5.45	5.48
Fe_2O_3	1.04	1.01	1.07	1.01	1.01	1.06	1.02	1.01
FeO	10.35	10.13	10.67	10.09	10.14	10.59	10.19	10.09
MnO	0.23	0.21	0.23	0.22	0.21	0.23	0.22	0.21
MgO	23.04	23.74	23.59	23.85	23.36	24.23	24.21	24.13
CaO	4.51	3.90	4.09	3.59	3.91	3.95	3.76	3.73
Na_2O	0.86	0.68	0.68	0.68	0.71	0.52	0.65	0.64
K_2O	0.11	0.16	0.11	0.27	0.27	0.21	0.06	0.07
P_2O_5	0.05	0.05	0.06	0.07	0.06	0.05	0.05	0.05
Total	100.01	99.99	99.99	100.00	100.00	100.00	100.01	100.03
Zn	80	81	82	82	80	93	81	78
Cu	21	24	24	25	20	19	20	17
Ni	590	557	565	550	550	570	559	552
Sc	28.5	29.0	30.2	28.7	29.0	24.6	28.9	28.0
Co	96	94	96	95	93	95	98	97
Cr	3743	4506	6000(+)	6000(+)	3270	3252	3230	403
V	145	149	206	148	153	163	163	158
Rb	2.3	5.4	4.3	11.5	7.6	5.8	5.1	0.0
Sr	66	69	63	59	60	49	59	69
Y	7.7	6.7	4.7	7.4	4.9	5.1	7.4	5.3
Zr	14.1	10.2	13.1	26.8	20.8	25.3	27.2	6.7

Sample No.	AE-65	AE-66	AE-67A	AE-67B	AE-68	AE-MR1
SiO_2	51.50	49.24	49.19	50.52	49.35	47.10
TiO_2	0.23	0.05	0.05	0.06	0.05	0.12
Al_2O_3	8.79	31.95	32.00	27.43	31.83	10.12
Fe_2O_3	1.09	0.08	0.07	0.23	0.08	1.06
FeO	10.85	0.80	0.70	2.29	0.81	10.62
MnO	0.25	0.03	0.03	0.04	0.03	0.19
MgO	22.51	0.98	0.75	4.33	0.77	24.21
CaO	3.97	14.48	14.80	13.24	14.56	5.65
Na_2O	0.76	2.11	2.18	1.63	2.24	0.67
K_2O	0.06	0.18	0.17	0.19	0.24	0.21
P_2O_5	0.00	0.05	0.05	0.05	0.05	0.05
Total	100.01	99.98	99.99	100.01	100.01	100.00
Zn	123	6	8	11	5	82
Cu	16	11	10	11	16	42
Ni	573	27	17	92	12	1291
Sc	29.2	4.5	5.0	8.2	3.7	9.9
Co	108	6	5	18	5	123
Cr	6000(+)	599	393	718	53	2430
V	443	17	13	35	11	54
Rb	14.8	2.7	3.3	5.0	5.5	5.6
Sr	84	456	463	384	463	156
Y	0.0	5.4	1.2	4.7	3.2	1.5
Zr	6.5	6.8	3.2	6.7	4.7	8.8

Figure 5.1 Variation diagrams in which major element concentrations are plotted against MgO.

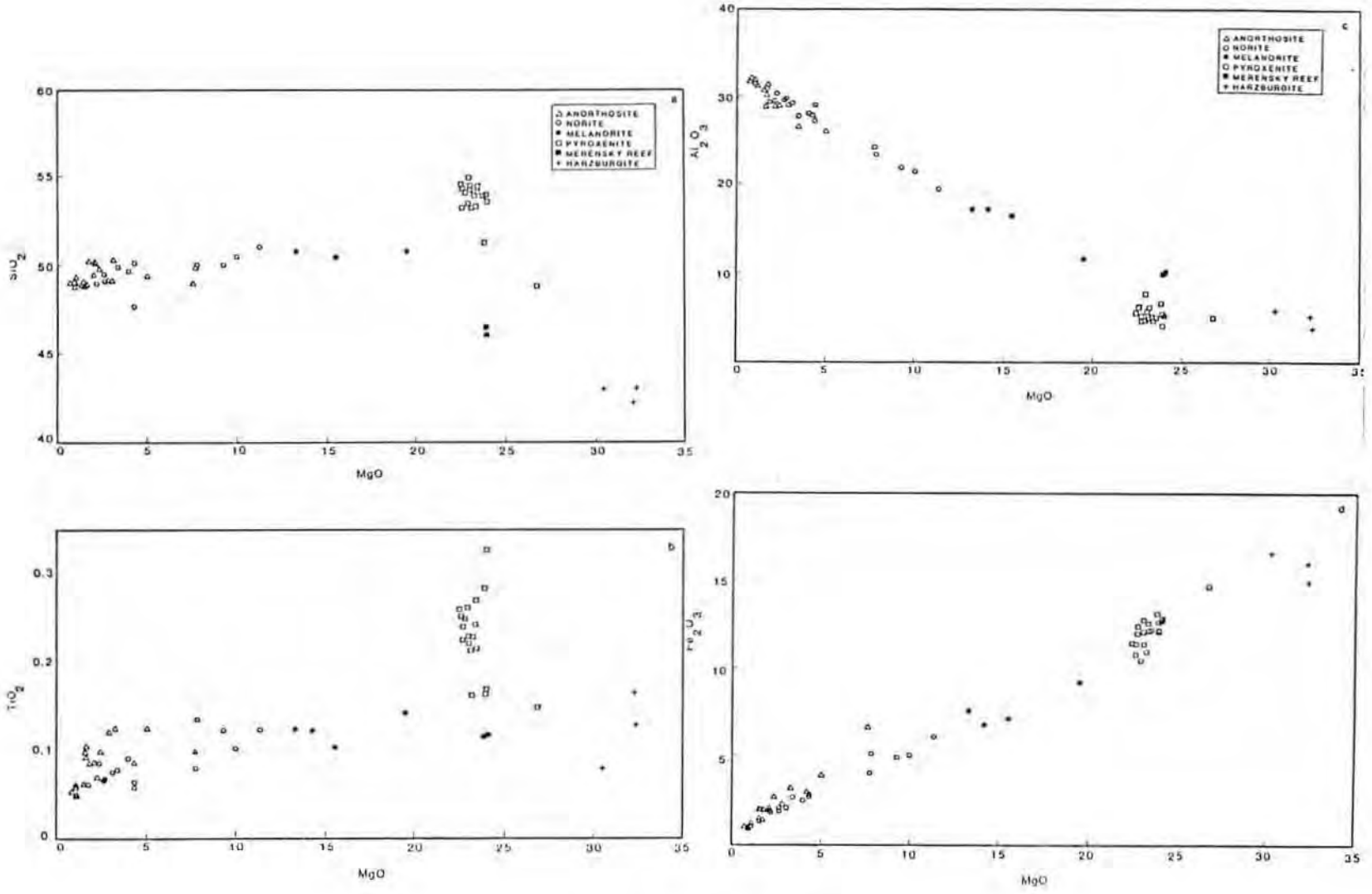
a
b
c
d
ANORTHOSITE
NORITE
MELANORITE
PYROXENITE
MERENSKY REEF
HARZBURGITE
SiO2
TiO2
Al2O3
Fe2O3
MgO

Figure 5.1

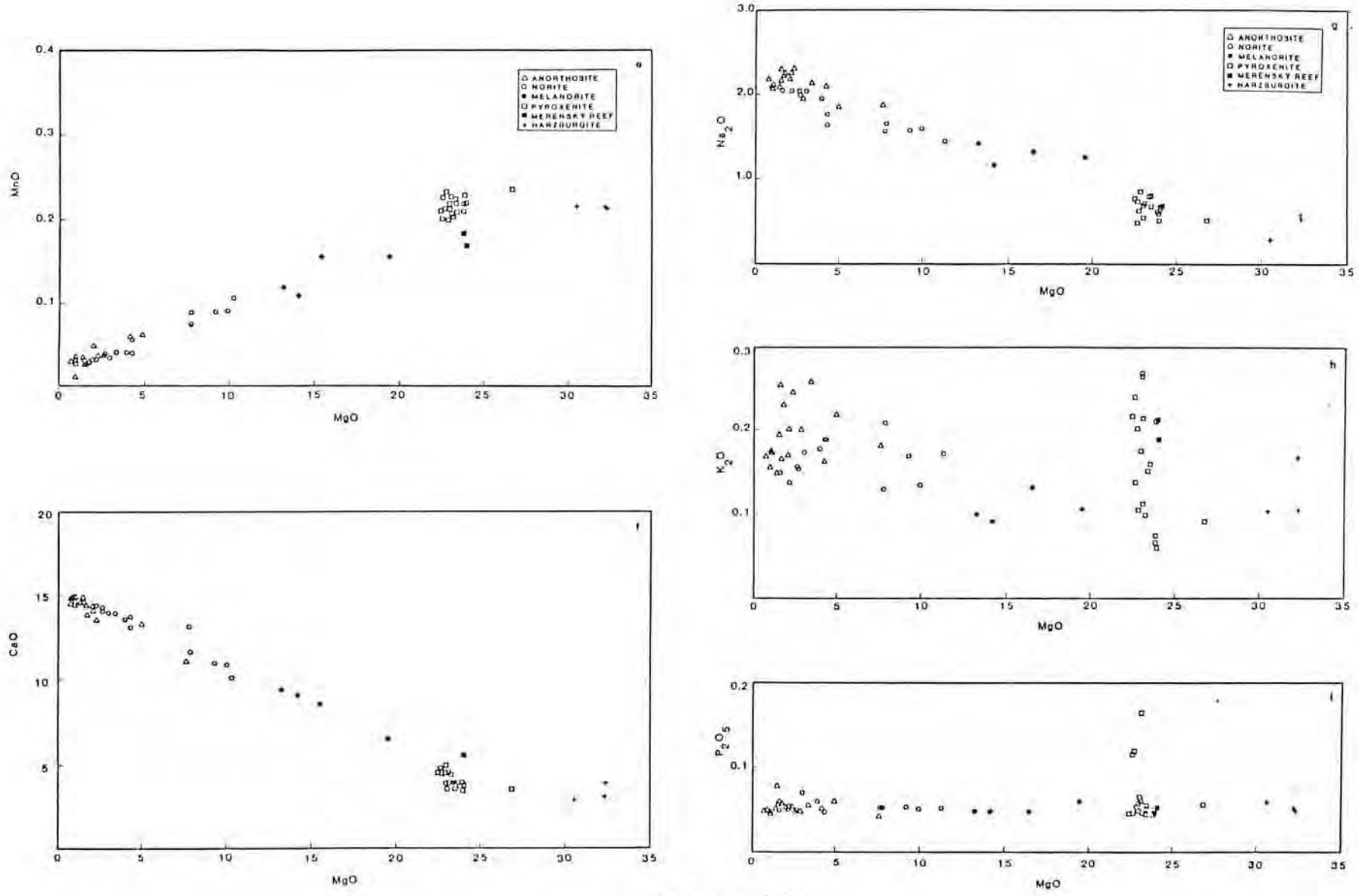
a
MnO
MgO
ANORTHOSITE
NORITE
MELANORITE
PYROXENITE
MERENSKY REEF
HARZBURGITE
g
Na_2O
h
K_2O
f
CaO
i
P_2O_5

Figure 5.1

4.1.1 Variation Diagrams

Binary plots of major element oxides against some index of fractionation have been widely used (Cox et al., 1981) in the interpretation of chemical data of igneous rocks. Although they are more applicable to volcanic rock suites, where whole rock analyses can be directly correlated with liquid compositions, they serve the purpose of displaying the wide chemical variations of the plutonic rocks of the study area In addition, they give some indication of the modal mineral species which controlled the distribution of the different elements.

In the variation diagrams presented in Figure 5.1, MgO is employed as the abscissa because it has been widely used as an index of fractionation, and because it has an extremely wide range in rocks of the study section (from 0.75 weight percent in anorthosites to 35 weight percent in harzburgite). With the exception of K_2O and P_2O_5, rational, near-linear variations exist between other oxides and MgO. This near-linearity is best defined in the Al_2O_3, Fe_2O_3, MnO, CaO and Na_2O diagrams, where data for anorthosites, norites, melanorites and pyroxenites plot along a straight line. Harzburgites, however, lie off this line. In the SiO2 and TiO_2 diagrams the linearity is restricted to plagioclase-cumulates, while pyroxenites define a second, discordant linear trend. The variation diagram for K_2O shows a relatively wide scatter of data. However, one feature which is noticeable in this diagram, is the higher concentration of K_2O in some pyroxenite samples. A similar peak in P_2O_5 concentrations in pyroxenites is also evident.

Interpretation of these diagrams is complicated by the fact that the whole-rock analyses cannot be correlated with original liquid compositions. This means that the concepts of "mixing lines" and "liquid-lines-of-descent", cannot be used in the interpretation of the variation diagrams. In the majority of cases, the rational variations which can be observed merely represent variations in the modal proportions of plagioclase, pyroxene and olivine from sample to sample. The only possible exceptions are P_2O_5 and K_2O, as these oxides are effectively incompatible in the structures of the above-mentioned mineral species. This explains their low concentrations, while the occurrence of higher values in some pyroxenites suggests that these rocks contain actual accumulations of late-stage liquids.

5.1.2 Variations with Stratigraphic Height.

In figure 5.2, whole-rock major element concentrations are plotted against the borehole log. It is clear from these diagrams that a number of discrete layers can be recognized through which element concentrations vary systematically. They are suggestive of the existence of cyclic units, but as Eales et al. (in press,a) point out, are not proof of cyclicity, because the variations are brought about by changes in the modal mineralogy of the layer (unit).

Where the base of a unit is a pyroxenite (for example the Bastard Unit) SiO_2 decreases upwards through that unit, representing an increase in modal plagioclase over pyroxene.

Figure 5.2 Variations in major element oxide levels through the stratigraphic column.

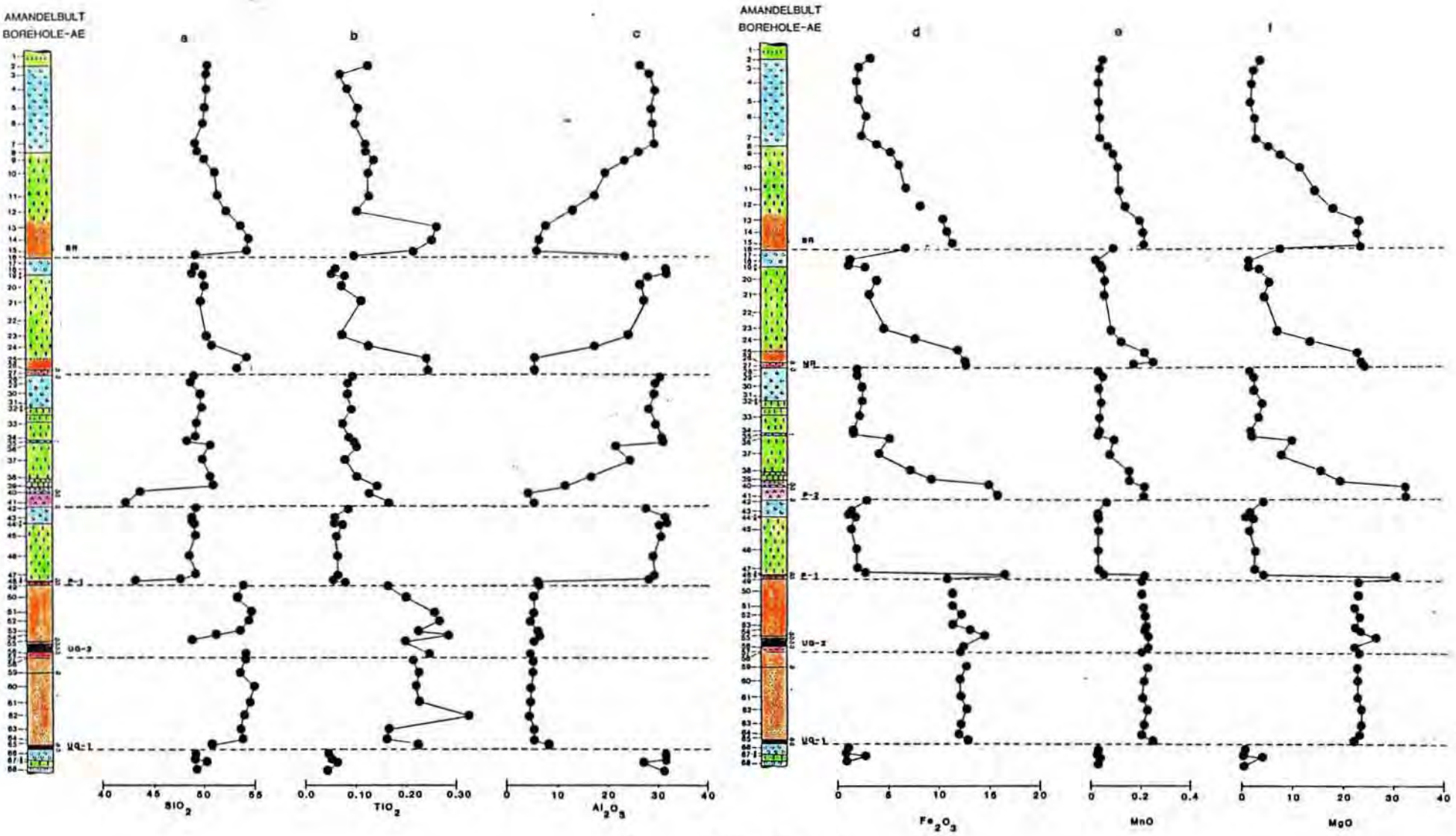

Figure 5.2

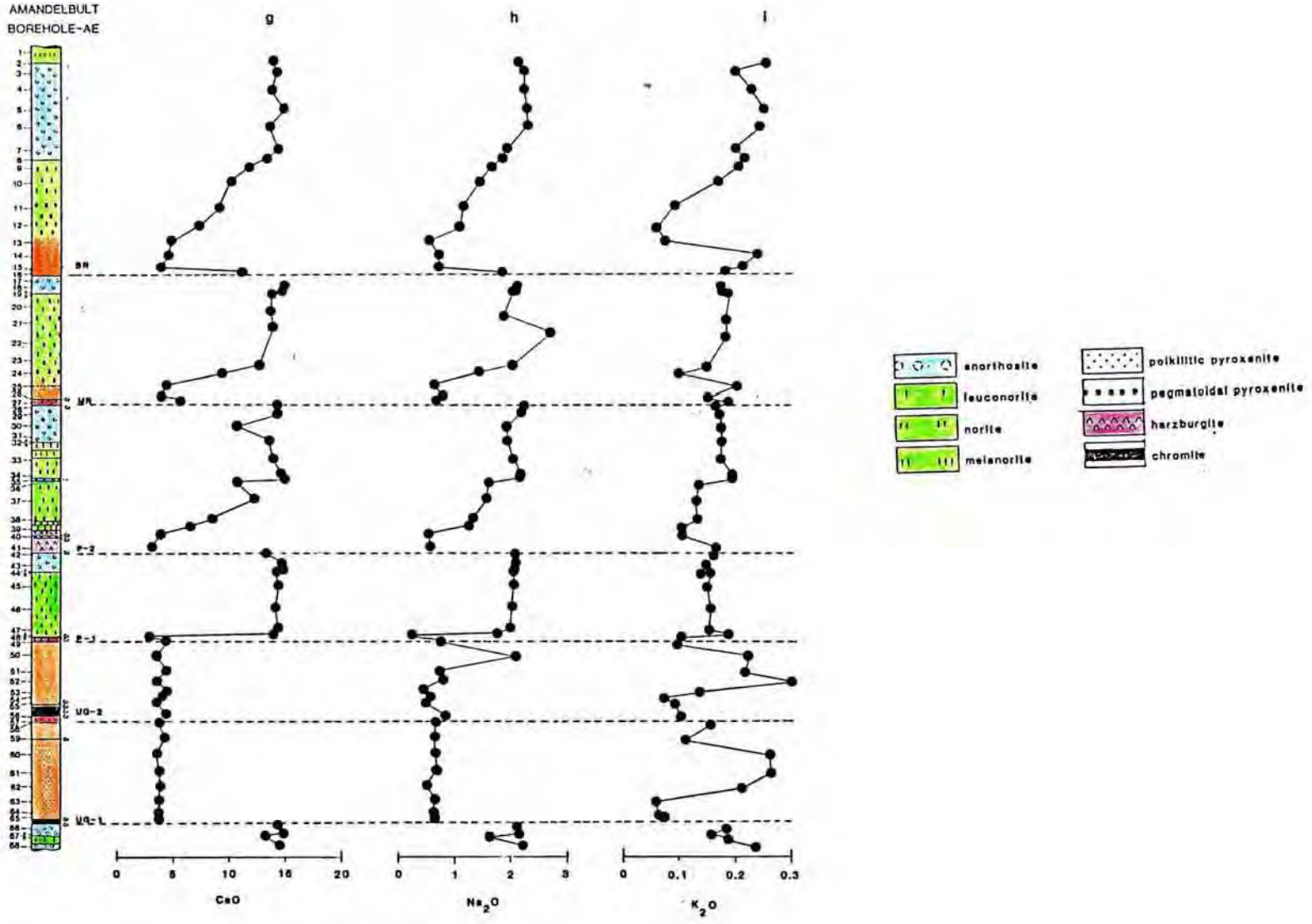

Figure 5.2(cont)

Where the base is chromitite, or an olivine-bearing layer (for example the Merensky Unit) there is an initial increase in SiO_2 upwards, representing an increase in modal pyroxene, and a decrease in modal olivine and/or chromite. Similarly upward increases in Al_2O_3, CaO and Na_2O, and decreases in Fe_2O_3, MnO and MgO are brought about by an increase in modal plagioclase over pyroxene. In non-chromite bearing rocks, TiO_2 levels decrease upwards in sympathy with decreasing modal pyroxene. However TiO_2 - enrichment is evident where chromite is abundant. Variations in K_2O are haphazard, but, as noted in the previous section, maximum concentrations of this element occur in pyroxenite layers, often near the bases of units.

5.1.3 Normative Data

C.I.P.W. weight percent norms were calculated for all samples from anhydrous (L.O.I- and H_2O^- free) major element data using a fortran program available on open-file on the Cyber main frame computer at Rhodes University. This program is based on the method of Kelsey (1965). The resultant norms are listed in Table 5.2.

All the rocks of the study section have normative feldspar (An+Ab+Or) and hypersthene (HyEn+HyFs), while a large number have small percentages of normative diopside (DiEn+DiFs+DiWo). Normative olivine is restricted to the ultramafic rocks, while all those with no normative olivine have normative quartz. Accessory normative constituents (less than 5 weight percent) are apatite, ilmenite, corundum and magnetite.

In figure 5.8 the relative variations of the main normative

Table 5.2 C.I.P.W. weight percent norms for samples from borehole AE. The normative mineral codes are;

Ap - apatite	En - enstatite
Il - ilmenite	Fs - ferrosilite
Or - orthoclase	Wo - wollastonite
An - anorthite	Hy - hypersthene
Ab - albite	Q - quartz
C - corundum	Fo - forsterite
Mt - magnetite	Fa - fayalite
Di - diopside	MgNo is the magnesium number.

Sampl	AE-1	AE-2	AE-3	AE-4	AE-5	AE-6	AE-7	AE-8	AE-9	AE-10	AE-11
Ap	0.07	0.14	0.14	0.14	0.14	0.12	0.12	0.14	0.12	0.12	0.12
Il	0.23	0.24	0.13	0.15	0.19	0.19	0.23	0.23	0.24	0.23	0.23
Or	1.48	1.54	1.18	1.36	1.48	1.48	1.18	1.30	1.24	1.00	0.53
Ab	19.71	18.02	19.04	18.95	19.38	19.46	16.50	15.74	14.05	12.27	9.90
An	61.58	62.47	68.14	58.62	67.90	66.95	70.12	62.44	55.59	46.75	41.69
C				0.48		0.28					
Mt	0.32	0.39	0.25	0.23	0.25	0.32	0.28	0.46	0.62	0.72	0.81
DiEn	0.93	1.48	0.43		1.03		0.16	0.85	0.57	0.93	0.90
DiFs	0.54	0.78	0.23		0.73		0.07	0.38	0.22	0.29	0.25
DiWo	1.55	2.40	0.69		1.83		0.25	1.32	0.85	1.33	1.27
HyEn	5.30	7.04	4.93	4.46	2.90	5.85	6.84	11.70	18.93	27.36	34.66
HyFs	3.90	3.73	2.68	2.64	2.06	3.75	3.05	5.21	7.19	8.51	9.64
Q	3.24	1.78	2.17	2.98	2.11	1.62	1.22	0.25	0.40	0.50	
Fo											
Fa											
MgNo	0.67	0.70	0.69	0.67	0.63	0.66	0.73	0.74	0.77	0.80	0.82

Sampl	AE-13	AE-14	AE-15	AE-16	AE-18	AE-19A	AE-19B	AE-20	AE-21	AE-23
Ap	0.12	0.12	0.40	0.09	0.12	0.12	0.14	0.02	0.05	0.02
Il	0.49	0.47	0.39	0.19	0.11	0.09	0.15	0.15	0.23	0.15
Or	0.47	1.42	1.30	1.06	1.06	1.00	1.12	0.95	1.00	0.77
Ab	4.74	6.35	6.18	15.57	17.85	17.51	17.18	15.06	21.32	15.82
An	16.76	12.79	11.98	55.01	73.69	72.75	66.32	61.40	63.36	57.83
C				0.02	0.56	1.21		1.05		
Mt	1.26	1.29	1.38	0.81	0.14	0.13	0.32	0.41	0.35	0.54
DiEn	2.13	2.85	1.97				0.55		0.22	0.24
DiFs	0.56	0.78	0.56				0.25		0.09	0.10
DiWo	2.95	3.99	2.78				0.85		0.33	0.39
HyEn	55.65	54.22	56.30	15.20	2.69	2.64	7.92	12.45	7.85	17.27
HyFs	14.61	14.85	16.09	7.72	1.60	1.52	3.54	4.99	3.16	6.32
Q	0.28	0.86	0.68		1.98	3.03	1.68	3.56		0.54
Fo				2.79					1.43	
Fa				1.56					0.63	
MgNo	0.83	0.82	0.81	0.71	0.67	0.68	0.73	0.76	0.75	0.77

Sampl	AE-24	AE-25	AE-26	AE-28	AE-29	AE-32A	AE-32B	AE-33	AE-34	AE-35
Ap	0.12	0.17	0.12	0.14	0.12	0.02	0.14	0.14	0.12	0.19
Il	0.24	0.45	0.47	0.17	0.17	0.21	0.17	0.13	0.23	0.13
Or	0.59	1.24	0.89	1.00	1.00	1.12	1.06	1.00	0.95	1.18
Ab	12.10	5.33	6.85	18.87	18.44	14.47	16.58	17.26	13.71	18.28
An	40.52	11.34	10.52	71.25	70.37	69.34	66.83	69.11	52.04	73.49
Mt	0.91	1.44	1.52	0.23	0.23	0.17	0.29	0.25	0.58	0.17
DiEn	1.70	3.03	2.61		0.10				0.51	.02
DiFs	0.96	0.92	0.82		0.05				0.16	0.01
DiWo	2.46	4.31	3.74		0.16				0.73	0.03
HyEn	28.25	54.25	52.35	4.16	5.08	3.76	9.84	7.62	22.67	3.79
HyFs	9.38	16.48	16.42	2.79	2.72	1.89	3.51	2.89	6.91	2.06
Q		1.09		0.94	1.54	5.96	1.39	1.08	1.38	0.62
Fo	2.33		2.77							
Fa	0.85		0.96							
MgNo	0.79	0.81	0.80	0.64	0.70	0.78	0.76	0.80	0.69	0.67

Table 5.2

Smpl	AE-36	AE-37	AE-38	AE-39	AE-40	AE-41	AE-42	AE-43	AE-44A	AE-44B	AE-45	AE-46
Ap	0.12	0.12	0.12	0.14	0.12	0.12	0.12	0.12	0.12	0.12	0.12	0.12
Il	0.19	0.15	0.19	0.26	0.24	0.32	0.17	0.11	0.11	0.13	0.11	0.11
Or	0.83	0.77	0.77	0.65	0.65	1.00	0.95	0.89	0.95	0.83	0.89	0.95
Ab	13.54	13.11	11.25	10.83	4.65	4.99	17.60	17.68	17.60	17.34	17.34	17.18
An	51.40	59.10	38.92	25.94	8.64	11.45	65.85	72.30	73.64	70.72	71.61	69.53
C							0.25	1.35	1.34	0.94	1.13	0.63
Mt	0.61	0.49	0.86	1.12	1.81	1.93	0.35	0.16	0.13	0.22	0.17	0.22
DiEn	0.63	0.29	1.04	1.98	3.31	1.21						
DiFs	0.19	0.09	0.28	0.54	0.90	0.35						
DiWo	0.90	0.42	1.45	2.76	4.62	1.71						
HyEn	24.29	19.13	29.72	34.22	10.60	7.58	10.40	3.51	2.37	5.50	4.03	6.62
HyFs	7.20	5.85	8.04	9.35	2.87	2.18	4.17	1.91	1.50	2.57	1.97	2.63
Q	0.11	0.50						1.97	2.25	1.64	2.62	2.03
Fo			5.69	9.40	47.46	51.01	0.11					
Fa			1.70	2.83	14.15	16.15	0.05					
MgNo	0.81	0.80	0.82	0.82	0.82	0.81	0.76	0.69	0.66	0.73	0.72	0.76

Smpl	AE-47	AE-48A	AE-48B	AE-49	AE-50	AE-51	AE-52	AE-53	AE-54	AE-55	AE-56	AE-58
Ap	0.12	0.12	0.14	0.12	0.07	0.12	0.14	0.28	0.12	0.14	0.12	0.12
Il	0.11	0.11	0.15	0.30	0.38	0.49	0.51	0.43	0.54	0.38	0.47	0.41
Or	0.95	1.12	0.65	0.53	1.54	1.30	1.89	0.83	0.47	0.53	0.65	0.95
Ab	16.84	14.89	2.28	6.51	18.44	6.60	6.95	6.35	5.08	4.40	7.28	5.75
An	70.47	68.98	14.14	13.36	5.19	11.05	8.60	13.06	15.27	11.45	8.86	10.42
C	0.44	0.89	0.36									
Mt	0.23	0.33	2.02	1.32	1.38	1.38	1.48	1.39	1.58	1.77	1.51	1.45
DiEn				2.46	3.80	3.21	2.55	2.83	1.22	1.73	3.84	2.53
DiFs				0.68	1.08	0.95	0.77	0.86	0.39	0.55	1.21	0.76
DiWo				3.44	5.35	4.55	3.62	4.14	1.75	2.49	5.51	3.59
HyEn	5.70	7.71	19.18	55.46	34.50	53.47	56.45	53.13	48.14	38.07	53.54	56.59
HyFs	2.80	2.85	6.11	15.24	9.80	15.74	17.02	15.65	15.30	12.15	16.96	17.04
Q	1.35					1.17	0.14				0.08	0.37
Fo		2.14	40.69	0.41	14.05			0.74	7.52	19.49		
Fa		0.87	14.28	0.12	4.51			0.24	2.63	6.85		
MgNo	0.75	0.77	0.80	0.82	0.81	0.81	0.81	0.81	0.80	0.80	0.80	0.81

Smpl	AE-59	AE-60	AE-61	AE-62	AE-63	AE-64	AE-65	AE-66	AE-67A	AE-67B	AE-68	AE-MR
Ap	0.14	0.17	0.14	0.12	0.12	0.12		0.12	0.12	0.12	0.12	0.12
Il	0.43	0.41	0.43	0.62	0.32	0.32	0.43	0.09	0.09	0.11	0.09	0.23
Or	0.65	1.60	1.60	1.24	0.35	0.41	0.35	1.06	1.00	1.12	1.42	1.24
Ab	5.75	5.75	6.01	4.40	5.50	5.41	6.43	17.85	18.44	13.79	18.95	5.67
An	10.43	9.49	9.58	8.48	11.78	11.87	19.69	71.51	73.10	65.36	71.91	23.99
C							0.26	2.08	1.44	0.59	1.53	
Mt	1.55	1.46	1.46	1.54	1.48	1.46	1.52	0.12	0.10	0.33	0.12	1.54
DiEn	2.75	2.30	2.76	3.16	1.93	1.86						1.08
DiFs	0.76	0.88	0.70	0.84	0.97	0.58						0.34
DiWo	3.95	3.28	3.94	4.51	2.74	2.63						1.55
HyEn	54.84	55.85	55.41	57.18	56.83	57.95	45.69	2.44	1.87	10.78	1.92	23.00
HyFs	17.52	17.05	16.96	17.50	16.97	17.18	15.58	1.43	1.20	3.99	1.40	7.17
Q		1.34	0.67	0.30				3.28	2.62	3.81	2.56	
Fo	0.81				1.07		7.27					25.37
Fa	0.29				0.35		2.73					8.71
MgNo	0.80	0.80	0.80	0.80	0.81	0.81	0.68	0.68	0.66	0.77	0.63	0.80

Table 5.2 (cont)

Figure 5.3 Variations in normative constituents. In (a) the relative variations of the four major normative constituents are presented. In (b) variations in the level of Sr in normative plagioclase are shown.

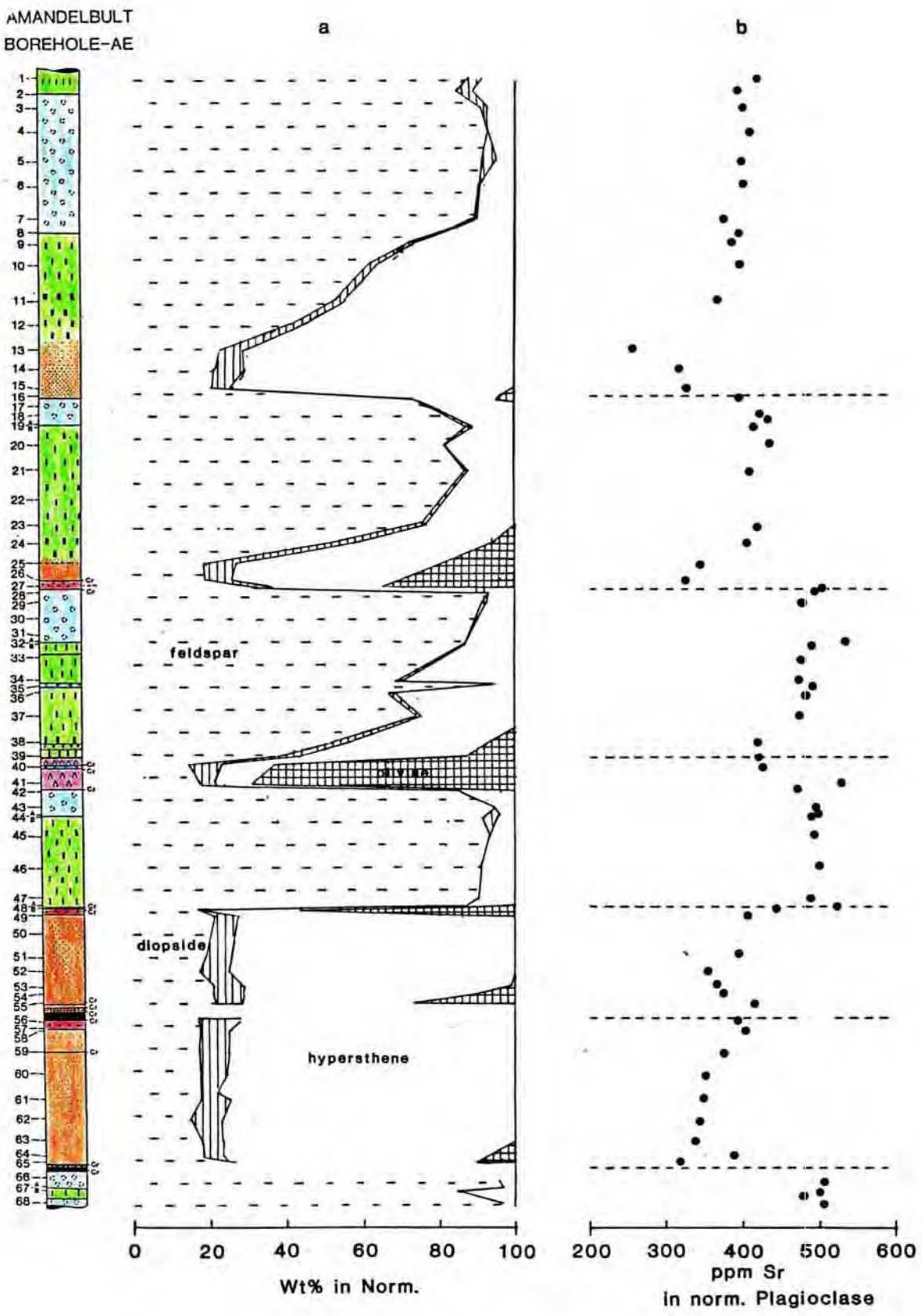
AMANDELBULT
BOREHOLE-AE
a
b
feldspar
diopside
hypersthene
0
20
40
60
80
100
Wt% in Norm.
200
300
400
500
600
ppm Sr
in norm. Plagioclase

Figure 5.3

constituents, namely olivine, hypersthene, diopside and feldspar, are plotted against a stratigraphic column. Variations exhibited in this diagram compare favourably with those of the mode, with a few exceptions. These include the occurrence of normative olivine in the Bastard poikilitic pyroxenite and the Merensky poikilitic pyroxenite, not matched in the mode, and the relative amount of normative clinopyroxene (diopside) which is greater in the norm than in the mode. Several features of this diagram are worth noting. First, the normative feldspar content of the Merensky Reef is higher than its overlying poikilitic pyroxenite. Second, normative diopside decreases upwards in the Bastard, Merensky and Footwall Units. Third, the normative feldspar content of the norite of the Lower Pseudo Unit is high when compared to other norite layers, and finally, the UG-2 and UG-1 units show little variation. These points will be used in later arguments.

5.2 Trace Elements.

Trace element analyses of 141 samples are listed in Tables 5.1 (for borehole AE) and 5.3 (for boreholes AF, AW, AX and AZ), while the experimental conditions for each set of determinations are summarized in Appendix B. Variation diagrams in which individual trace element concentrations (in parts per million) are plotted against MgO (in weight percent) are presented in figure 5.4, while variations in trace element levels with stratigraphic height are depicted in plots against borehole logs in figure 5.5. For convenience of discussion, the elements have been grouped into five groups, namely Ni, Cu, Co - the "chalcophile" elements; Cr a "spinel-compatible"

Table 5.3 Trace element analyses for boreholes AF, AW, AX and AZ.

TABLE 5.3 TRACE ELEMENT ANALYSES

Sample No.	AF-1	AF-2	AF-3	AF-4	AF-5	AF-6	AF-7	AF-8	AF-8b	AF-9
Element										
Zn	26	23	11	15	20	72	25	26	29	44
Cu	9	14	10	8	14	16	30	16	18	15
Ni	78	51	20	40	37	41	81	72	108	215
Sc	11.2	6.5	5.4	5.4	6.3	8.1	10.9	7.1	9.6	15.5
Co	25	15	8	14	12	26	25	20	40	48
Cr	174	136	58	146	87	129	372	278	549	1207
V	65	32	21	31	33	41	58	33	66	69
Rb	2.6	2.6	2.8	1.7	4.9	3.3	nd	4.5	6.5	1.8
Sr	329	352	369	343	353	352	nd	330	306	243
Y	3.4	1.8	1.8	nd	2.5	3.7	nd	2.4	3.3	3.9
Zr	8.5	7.9	5.7	3.9	9.4	14.7	nd	15.7	17.3	10.8

Sample No.	AF-10	AF-11	AF-12	AF-13	AF-14	AF-15	AF-16	AF-17	AF-18	AF-19
Element										
Zn	46	44	53	61	76	76	82	19	43	18
Cu	20	48	18	28	104	135	165	81	328	60
Ni	267	301	393	503	669	728	1165	126	924	116
Sc	14.3	15.8	17.8	23.9	25.9	26.5	23.8	7.7	5.5	6.8
Co	48	56	71	83	91	84	97	19	25	13
Cr	1398	1803	2363	3109	2676	2911	3572	463	145	206
V	65	70	85	113	125	129	122	27	18	21
Rb	2.4	0.9	1.8	1.3	11.2	8.0	6.6	2.7	4.1	2.0
Sr	229	195	145	92	92	65	77	354	526	376
Y	2.5	2.7	1.1	4.6	8.0	5.7	0.1	2.6	4.6	1.6
Zr	6.8	5.2	3.3	5.2	27.8	22.1	17.6	9.2	4.3	4.7

Sample No.	AF-20	AF-21	AF-22	AF-23	AF-24	AF-25	AF-26	AF-27	AF-30	AF-31
Element										
Zn	24	22	26	31	63	91	79	82	12	18
Cu	51	37	49	69	148	454	99	923	21	23
Ni	176	137	169	265	617	1375	636	2382	30	48
Sc	10.3	8.1	8.9	12.7	21.0	25.6	26.2	27.7	5.3	7.1
Co	28	22	24	38	73	100	93	129	6	13
Cr	628	429	531	932	2072	2844	2882	3024	30	124
V	43	32	33	52	98	128	145	137	16	27
Rb	3.2	3.8	1.7	2.8	5.4	4.2	13.1	4.8	2.9	3.0
Sr	335	354	345	302	167	87	70	61	465	444
Y	2.1	1.9	nd	2.2	4.7	6.9	8.9	7.9	1.4	1.9
Zr	8.6	7.5	5.6	4.5	8.4	15.4	38.7	18.4	5.5	7.2

Sample No.	AF-32	AF-33	AF-34	AF-35	AF-36	AF-37	AF-38	AF-39	AF-40	AF-41
Element										
Zn	10	19	23	41	35	10	38	30	27	55
Cu	13	20	28	1347	1075	248	22	19	20	32
Ni	30	93	107	4006	2664	653	153	174	161	378
Sc	6.7	5.8	5.9	7.4	10.4	6.4	11.6	10.5	10.1	17.1
Co	7	15	nd	96	71	16	33	82	83	64
Cr	97	454	nd	1238	1144	106	908	838	890	2007
V	nd	22	nd	46	54	16	46	40	37	74
Rb	3.0	5.1	3.7	4.8	3.7	6.7	4.1	2.6	1.5	1.9
Sr	453	416	406	316	340	457	355	309	347	208
Y	2.5	3.1	1.7	4.4	6.3	3.2	6.3	2.7	2.1	3.2
Zr	7.0	8.5	6.0	12.5	16.0	7.1	7.1	7.8	3.6	4.8

Sample No.	AF-42	AF-43	AF-44	AF-45	AF-46	AF-47A	AF-47B	AF-48	AF-49	AF-50
Element										
Zn	67	74	122	66	12	10	23	16	18	23
Cu	97	17	82	14	10	11	13	11	10	14
Ni	958	1590	2002	32	30	22	60	65	92	107
Sc	16.6	9.5	9.0	7.0	7.4	7.0	7.8	8.4	9.1	9.8
Co	97	147	143	10	8	15	14	15	19	20
Cr	7310	1097	712	264	452	539	390	407	523	553
V	110	89	48	19	21	23	23	24	27	29
Rb	2.9	1.6	13.1	2.8	3.1	2.7	1.5	nd	1.9	1.0
Sr	154	67	63	446	452	465	482	422	405	395
Y	5.0	2.1	3.4	2.1	6.0	3.6	1.5	3.1	2.8	3.2
Zr	9.7	3.9	12.6	5.0	6.9	11.6	5.7	7.3	5.9	6.9

Sample No.	AF-51	AF-52	AF-53A	AF-53B	AF-54	AF-56	AF-57	AF-58	AF-59	AF-60
Element										
Zn	16	17	19	106	109	52	78	80	87	71
Cu	18	19	48	959	671	43	31	30	30	23
Ni	105	102	114	3293	3760	590	540	557	580	804
Sc	9.6	9.5	10.1	20.0	8.7	27.6	26.7	27.1	28.9	26.4
Co	22	21	19	155	182	93	94	96	91	107
Cr	589	577	568	6000	6000	3431	331	372	3446	6141
V	20	28	28	204	190	137	126	146	139	133
Rb	2.8	3.0	nd	7.6	2.7	9.3	6.2	11.8	12.6	3.0
Sr	401	400	393	114	78	57	75	65	61	85
Y	2.4	21.8	nd	nd	1.4	7.1	4.1	8.4	7.0	4.4
Zr	5.7	5.5	3.6	nd	4.2	22.2	11.4	22.3	29.0	17.1

Sample No.	AF-61	AF-62	AF-63	AF-64	AF-65	AF-66	AF-67	AF-68	AF-69	AF-72
Element										
Zn	61	94	62	119	83	74	79	87	52	19
Cu	32	25	24	22	18	20	18	22	10	8
Ni	1004	609	606	635	602	548	540	573	80	31
Sc	25.5	30.0	31.0	30.6	12.9	27.6	27.4	28.3	8.1	6.3
Co	120	101	100	108	96	96	95	99	27	nd
Cr	3717	4702	6900	6000	3595	3572	3855	3481	6000	nd
V	118	162	167	270	124	137	141	141	225	nd
Rb	13.3	9.9	3.5	3.4	4.4	9.5	3.1	4.9	3.9	2.9
Sr	51	39	57	63	68	58	61	61	437	443
Y	9.3	7.9	5.5	5.6	6.8	6.4	4.8	5.6	2.9	0.8
Zr	30.7	33.5	18.6	12.3	15.9	21.2	14.7	16.5	4.4	0.9

Sample No.	AF-73	AW-1	AW-2	AW-3	AW-4	AW-5	AW-6	AW-7	AW-8	AW-9
Element										
Zn	22	88	116	65	82	89	87	80	100	83
Cu	16	753	27	19	14	20	15	25	44	22
Ni	30	1469	603	522	558	623	582	638	794	1099
Sc	4.9	43.5	31.1	33.3	26.5	29.1	27.9	25.5	29.0	18.2
Co	9	147	89	89	94	96	96	94	101	130
Cr	6514	3440	3324	3124	3302	3593	5371	6178	6905	4064
V	78	162	118	109	120	139	155	137	156	nd
Rb	3.1	1.8	1.8	0.4	3.2	2.4	4.2	nd	7.4	1.4
Sr	458	43	75	117	68	71	60	82	54	86
Y	1.2	12.0	10.5	6.8	6.7	9.9	8.7	5.1	5.4	4.9
Zr	nd	10.7	11.5	5.2	15.5	8.0	11.7	6.1	10.6	5.9

Sample No.	AW-10	AX-1	AX-2	AX-3	AX-4	AX-5	AX-6	AX-7	AX-9	AZ-1
Element										
Zn	384	130	23	93	98	87	77	86	85	78
Cu	69	125	63	31	30	nd	18	21	26	101
Ni	4068	867	632	557	563	499	547	623	1321	804
Sc	21.2	35.8	28.5	29.1	29.2	27.5	26.4	27.9	16.7	26.7
Co	124	108	97	99	95	96	93	94	147	101
Cr	6674	3411	3391	3201	3231	3532	5934	5863	3922	3667
V	117	161	138	144	137	143	144	147	91	127
Rb	1.4	4.2	2.4	6.1	4.1	5.6	2.3	8.3	0.2	4.4
Sr	70	41	67	59	38	48	74	57	57	63
Y	2.6	8.4	22.0	7.2	nd	8.9	5.1	6.7	6.9	5.1
Zr	7.9	11.8	22.8	19.1	8.4	20.1	8.6	29.1	10.5	9.9

Sample No.	AZ-2	AZ-3	AZ-4	AZ-5	AZ-6	AZ-9	AZ-10
Element							
Zn	85	77	80	90	83	88	102
Cu	26	22	21	28	31	24	66
Ni	573	528	542	588	603	1152	1338
Sc	25.9	27.4	27.4	29.8	28.6	19.4	19.9
Co	92	102	94	94	99	133	130
Cr	3460	3327	3506	3624	6300	6000	4634
V	113	134	128	nd	190	108	109
Rb	1.6	4.9	3.6	6.1	4.9	5.3	2.4
Sr	82	83	59	54	48	56	57
Y	3.8	7.8	8.1	7.9	8.3	6.6	5.7
Zr	5.2	11.7	11.6	23.7	11.7	12.7	7.2

element, Sr - a plagioclase compatible" element; V, Sc, Zn - "pyroxene-compatible" elements; and Rb, Zr, Y - the "incompatible" elements.

The recent treatment of trace element behaviour in magmatic systems is based largely on the concept of distribution coefficients (Cox et al., 1981). This concept leans heavily on the Henry's law assumption (see Atkins, 1979, p.213) that at low concentrations, the following relationship holds:

$$D_i^A = \text{conc of i in crystal} / \text{conc i in liquid}$$

Where D_i^A is a constant, known as the distribution coefficient of element i in crystal A. Numerous determinations of distribution coefficients of elements in common silicate phases have been made on natural and synthetic systems. Some published distribution coefficient data are summarized in Table 5.4.

5.2.1 Nickel, Copper and Cobalt.

These elements have been grouped together because of their well documented dual chalcophilic-lithophilic behaviour in magmatic systems. Maclean and Shimizaki (1976) investigated the distribution of these elements between silicate and sulphide melts. Their observations that the relative chalcophile affinity decreases in the order Ni > Cu > Co > Fe > Zn, are confirmed to a large degree by the analyses presented here.

Distribution coefficients for Cu in silicate minerals are generally low (see table 5.4). This means that Cu^{2+} ions in the melt will be excluded from crystallizing silicate phases.

In most instances this element will be preferentially concentrated in any immiscible sulphide droplets in the silicate melt. This fact is confirmed in both the variation diagram (figure 5.4) and the stratigraphic plot, where higher Cu concentrations are found for samples known to contain sulphide. In other samples, Cu concentration are low, generally less than 50ppm.

Nickel displays a more complex geochemical behaviour, for apart from its affinity for sulphides, it may also substitute readily into olivine and less readily into orthopyroxene (see Table 5.4). The variation diagram, figure 5.4c, indicates that good linear correlation exists between MgO and Ni, but that a small number of samples plot above, but never below, this linear trend. The correlation with MgO is indicative of Ni substituting into ferromagnesian silicate minerals, while the higher values indicate the presence of sulphide in these sample. This feature has been noted by Naldrett et al. (1986) and Scoon and de Klerk (in press) at Rustenburg and Union Section of R.P.M. The latter authors suggest that sulphide control on Ni concentrations becomes evident when Ni exceeds 1800 ppm in harzburgite, and 700-800 ppm in pyroxenite. Where olivine and sulphide do not control Ni, this element is seen to decline rapidly upwards through any unit, and although distribution coefficients in excess of unity are quoted for Ni in orthopyroxene (see Table 5.4), microprobe analyses of this mineral (see previous chapter) yield low Ni concentrations (generally less than 0.1 weight percent).

Variations in whole-rock cobalt concentrations are evident in

the variation diagram (figure 5.4d) and stratigraphic column (figure 5.5c). The former diagram shows that a good linear correlation exists between Co and MgO, which indicates that it substitutes readily into silicate minerals. Lowest Co values occur in anorthosites, but concentrations increase successively in norite, pyroxenites and harzburgites. The higher Co values in harzburgite indicate that this element may be preferentially incorporated within olivine. The occurrence of data points above the linear trend in Figure 5.4d, may indicate that sulphides contain only minor proportions of this element. This is confirmed in Figure 5.5c, where maximum concentrations of Cu and Ni correspond with those of Co, but, enrichment factors of Ni and Cu are significantly greater than for Co. The opposite, however, is not always true, that is, samples with high Cu concentrations do not always have corresponding high Co concentrations. This could represent differences in the compositions of sulphides, and differences in the chalcophile affinity of copper and cobalt.

To summarize, the stratigraphic column may be divided into three regions in terms of the relative concentrations of Ni, Co and Cu: (i) those regions where sulphides are present, which are represented by higher concentrations of all three elements, or of only Ni and Cu. (ii) Olivine-bearing horizons, where high Ni and Co values are recorded, and (iii) regions where Ni, Co and Cu levels are low, and whole rock values are apparently controlled by the relative abundance of orthopyroxene, which may incorporate low levels of all three elements, and plagioclase, which effectively excludes them. Regions (i) and (ii) may be coincident.
.pa

Figure 5.4 Varaition diagrams of trace elements, plotted against MgO.

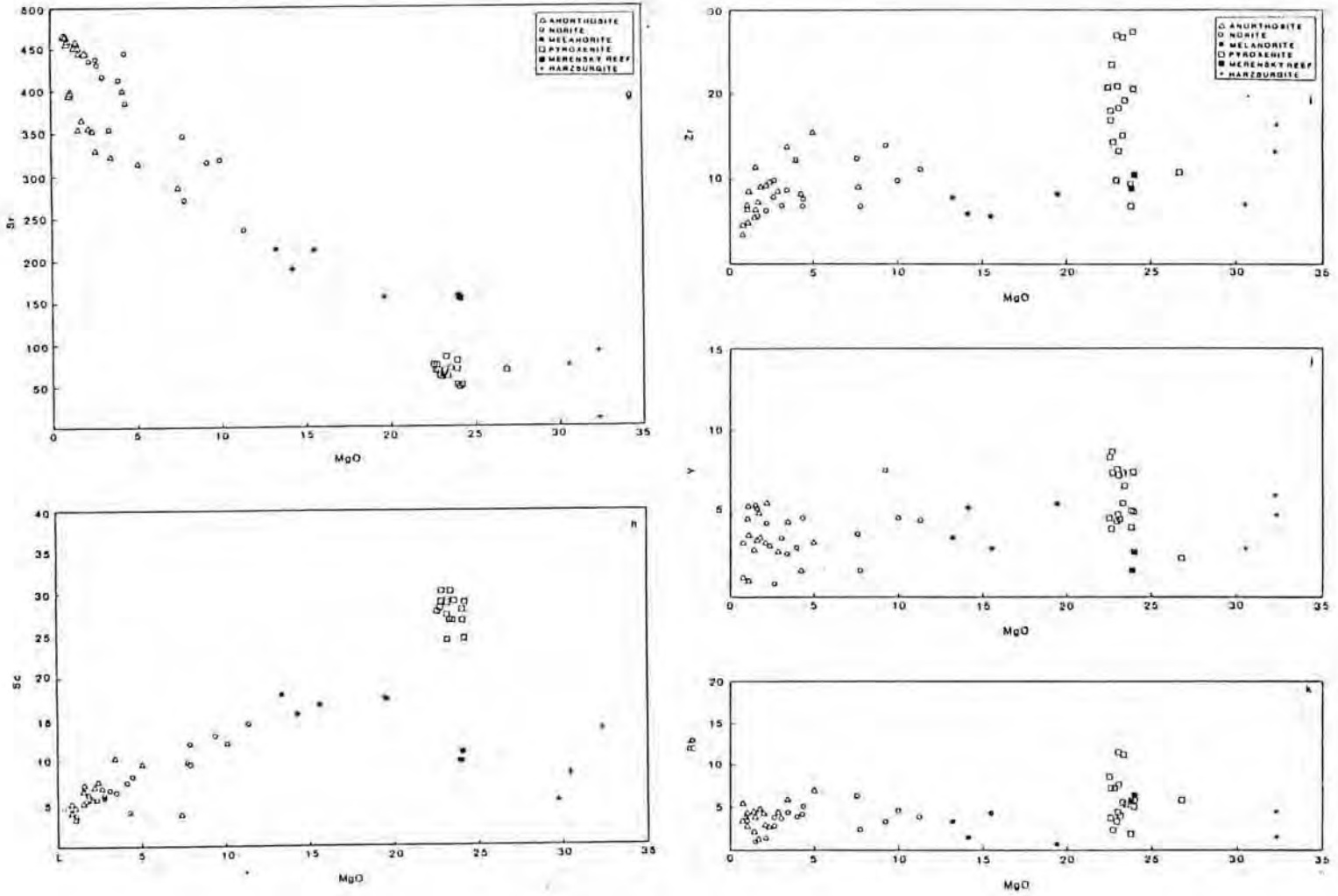

Figure 5.4(cont)

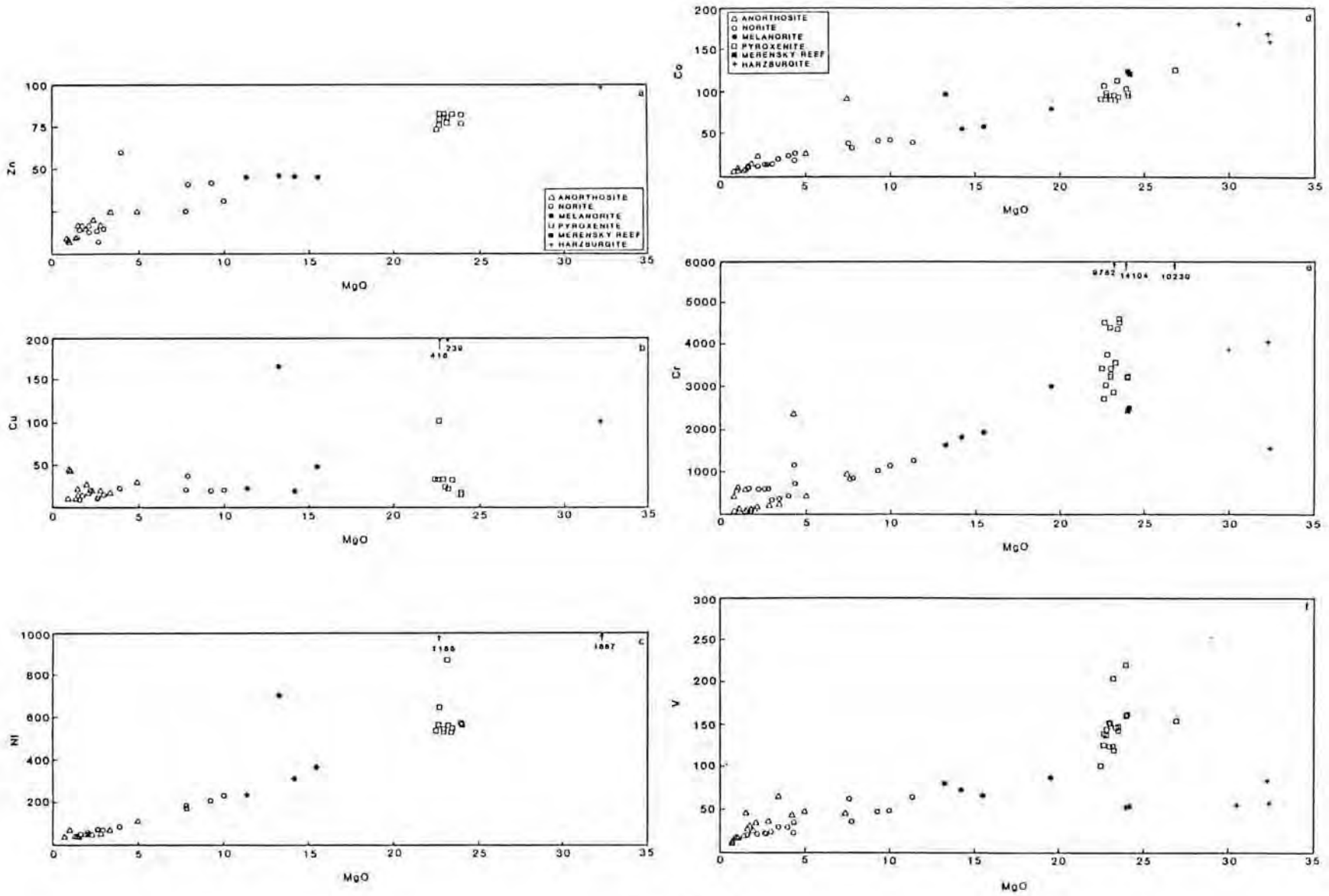
a
Zn
MgO
ANORTHOSITE
NORITE
MELANORITE
PYROXENITE
MERENSKY REEF
HARZBURGITE
b
Cu
MgO
239
410
c
Ni
MgO
1188
1887
d
Co
MgO
e
Cr
MgO
9782
14104
10230
f
V
MgO

Figure 5.4

Figure 5.5 Variations in trace element levels through boreholes AE and AF.

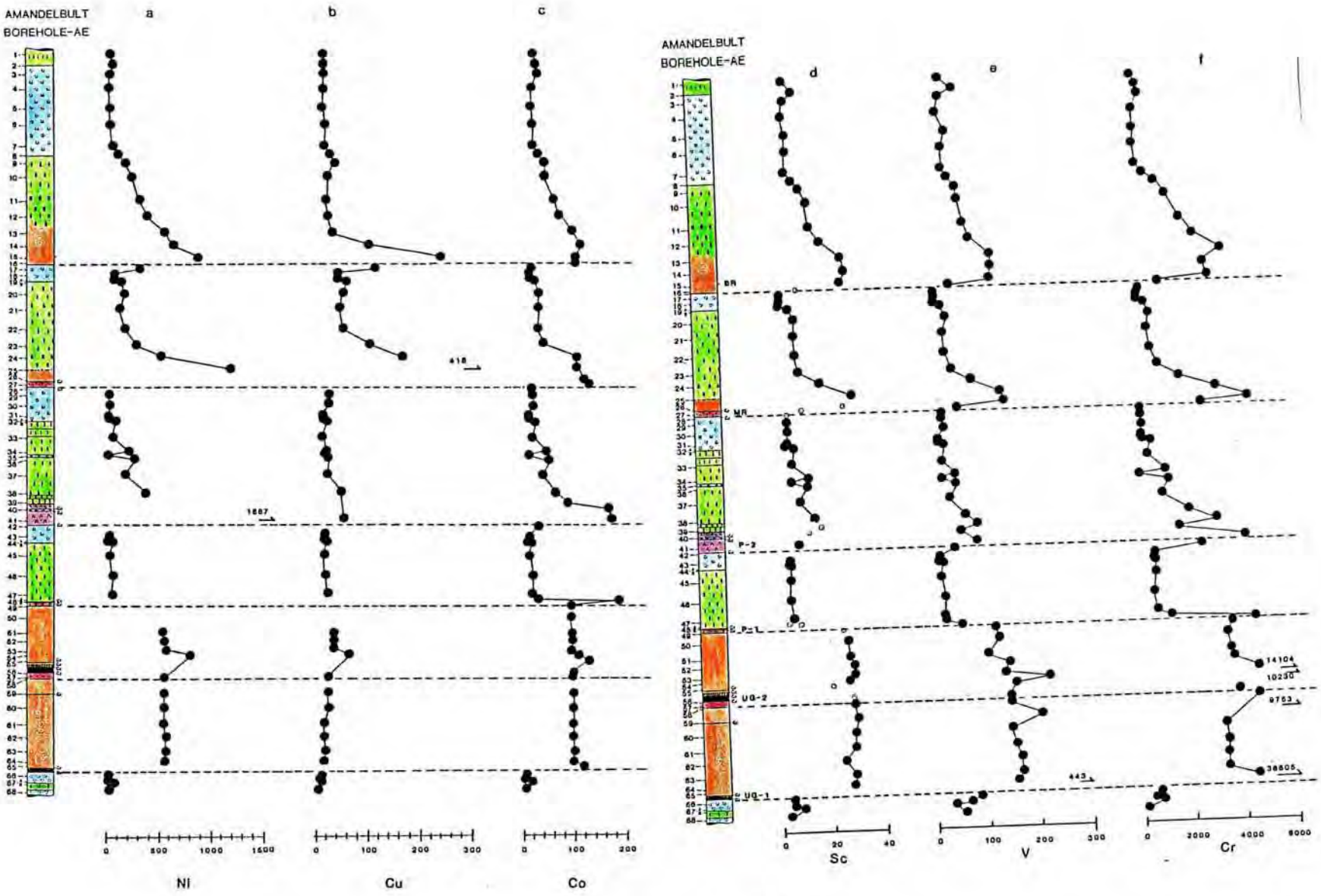
AMANDELBULT
BOREHOLE-AE
a
b
c
1887
418
0
500
1000
1500
Ni
0
100
200
300
Cu
0
100
200
Co
AMANDELBULT
BOREHOLE-AE
d
e
f
BR
MR
P-2
P-1
UG-2
UG-1
14104
10230
9753
38805
443
0
20
40
Sc
0
100
200
300
V
0
2000
4000
6000
Cr

Figure 5.5

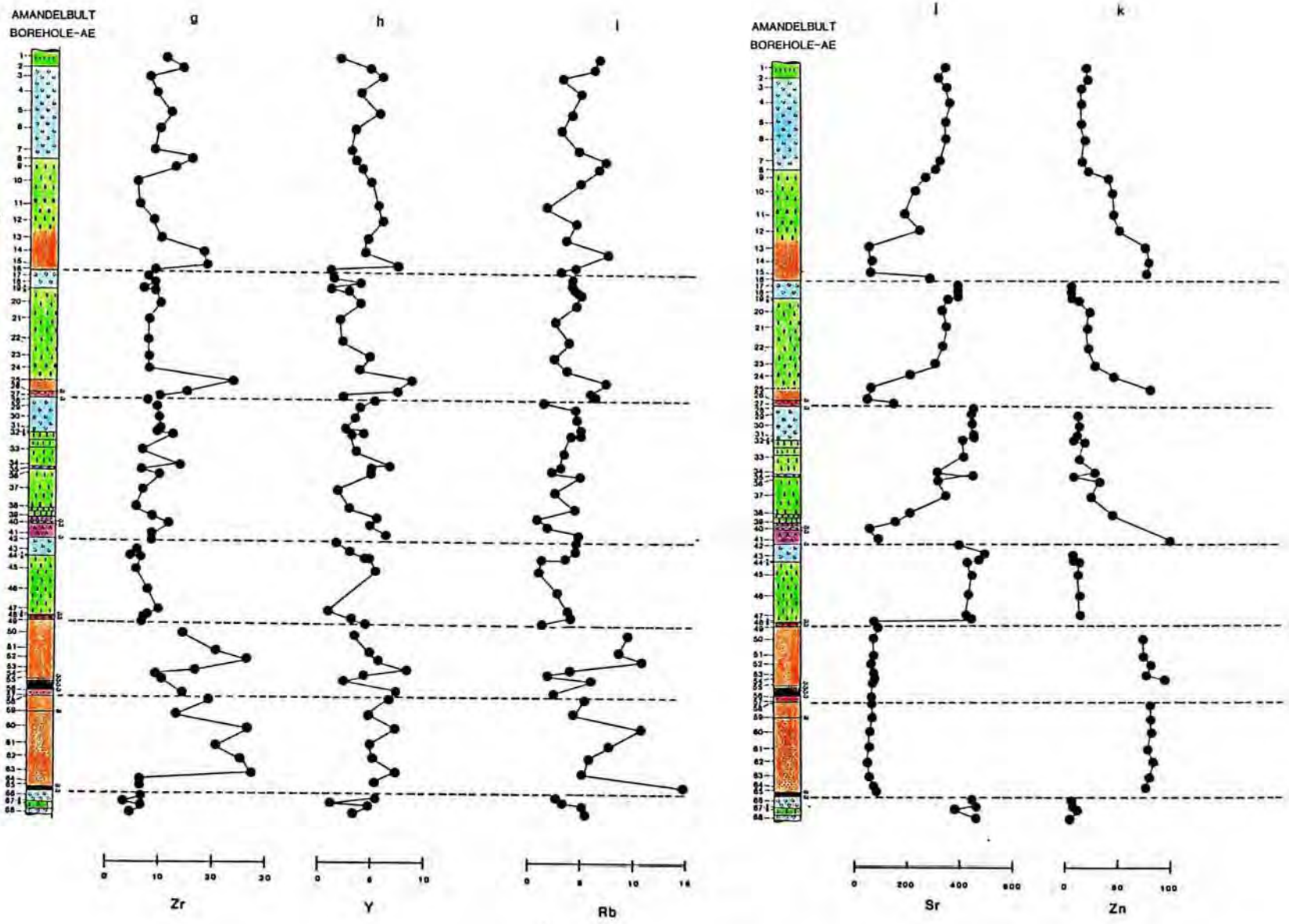

Figure 5.5(cont)

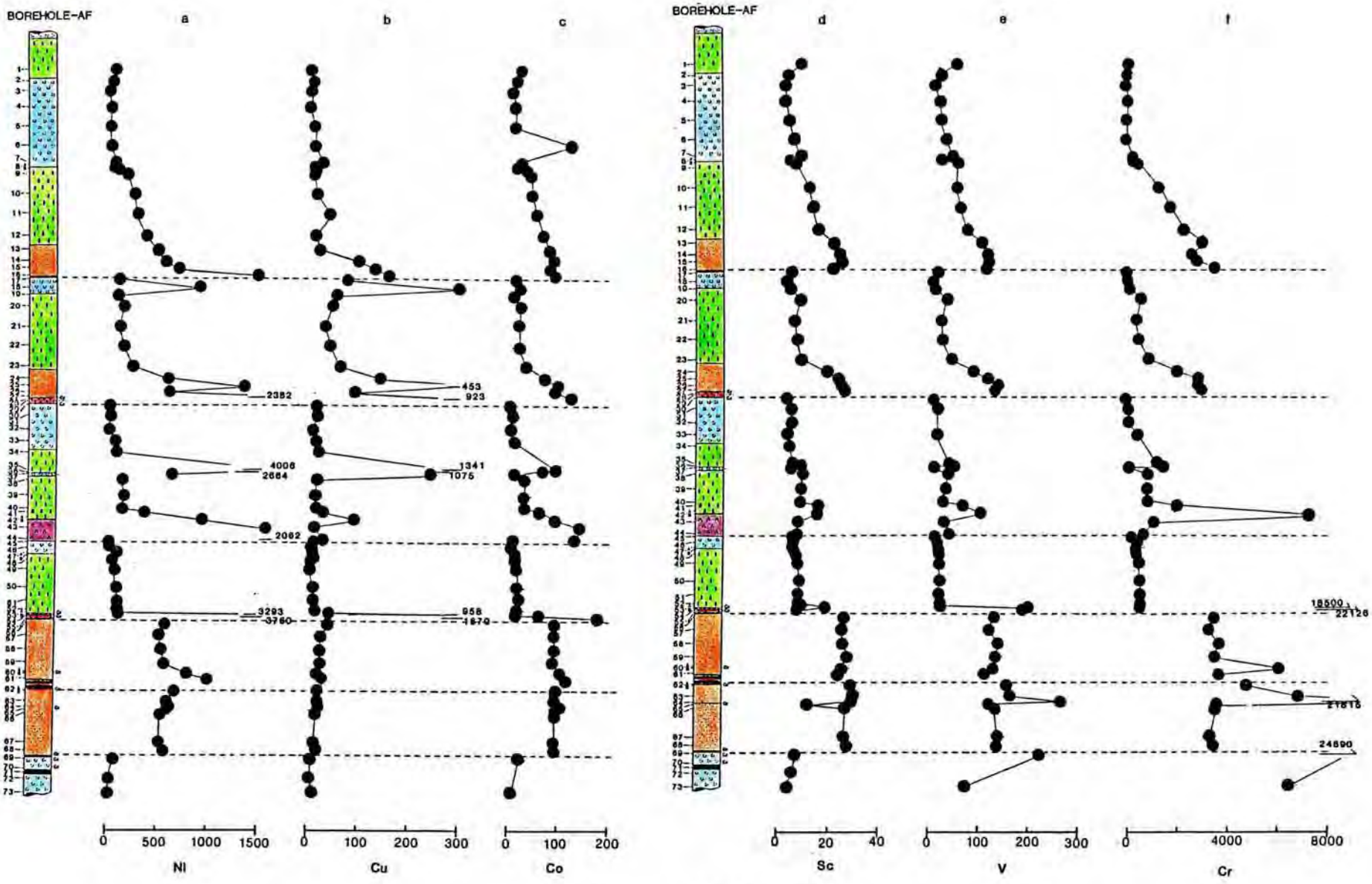

Figure 5.5(cont)

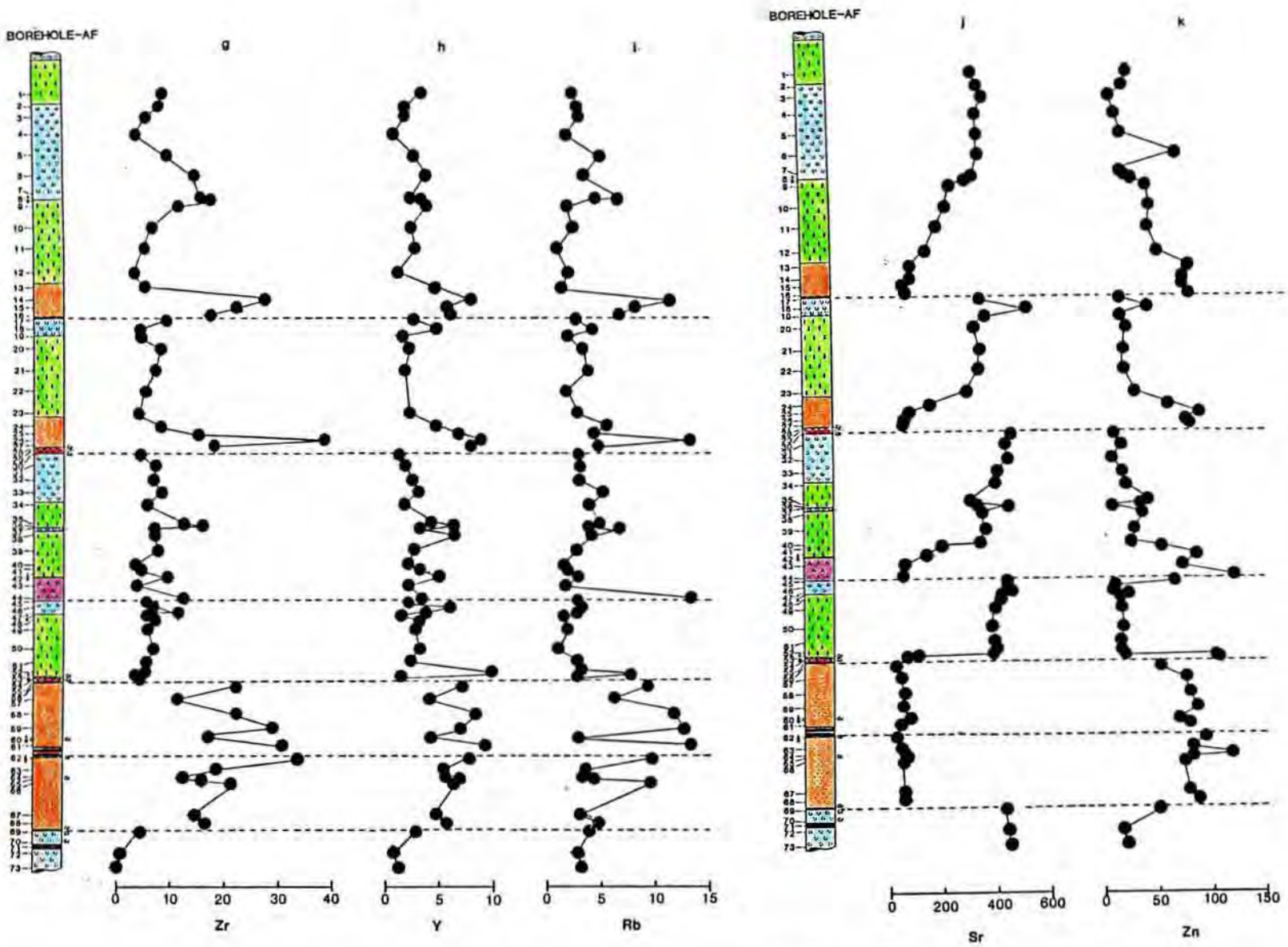

Figure 5.5(cont)

5.2.2 Vanadium, Scandium and Zinc

These three elements display similar distribution patterns through the study sections. This is clearly evident in figures 5.4f,h and a, and 5.5e,d and k respectively.

According to the distribution coefficient data in Table 5.4, vanadium is incompatible with respect to olivine and plagioclase, while it is favourably partitioned into clinopyroxene and spinel. This behaviour is well illustrated in both the variation diagram and the stratigraphic log. A linear correlation with MgO is evident for anorthosites, norites and pyroxenites, which reflects the partitioning of vanadium into increasing modal proportions of orthopyroxene. Those points which lie above the straight line represent chromite-bearing pyroxenites, while olivine-bearing samples plot below the line. The higher levels of whole-rock vanadium, brought about by the presence of chromite, is also evident from the stratigraphic log, where maxima in vanadium concentrations can be seen to correspond with the stratigraphic positions of chromitite layers. The upward decrease in V content through units corresponds to an upward decrease in modal pyroxene.

Scandium concentrations through the study section vary from around 3ppm for anorthosites to around 30ppm for pyroxenites, while all other rock types exhibit intermediate concentrations. These relative variations indicate that the behaviour of this element is well accounted for by the distribution coefficients quoted in Table 5.4. These data

indicate that Sc is most likely to be incorporated into the crystal lattices of orthopyroxene and clinopyroxene, while it should be excluded from olivine, plagioclase and spinel. The variation diagram (figure 5.4h) confirms this, as pyroxene-bearing rocks plot on a straight line, while olivine-bearing rocks plot below it. In the stratigraphic column, Sc concentrations decrease upwards through "complete" units, representing an increase in modal plagioclase over pyroxene. Where olivine-bearing rock forms the base of such a unit, for example the Merensky unit, an initial upwards increase is encountered.

With the exception of some olivine-bearing horizons in borehole AF, all the samples analysed for zinc yielded values below 100 ppm. Zinc levels appear to vary systematically within each "complete" unit (figure 5.5k) with highest values being recorded at the base of each unit, followed by a systematic decrease upwards. Furthermore, the variation diagram (figure 5.4a) reveals a good linear relationship between Zn and MgO. These factors indicate that this element`s distribution is controlled by silicate phases, but the possible inclusion of Zn within sulphide must be considered. Liebenberg (1970) investigated the sulphide species present in the Complex, and reported that Zn in magmatic environments has a limited chalcophile affinity, and that although minor sphaleritic inclusions occur in chalcopyrite and cubanite, the element generally behaves lithophilically. Distribution coefficients (Table 5.4) indicate that zinc would be incorporated most readily within olivine, and to a lesser extent in orthopyroxene, but that it would be

excluded by plagioclase. This behaviour is clearly confirmed in figures 5.4k and 5.5a.

The partitioning of V,Sc and Zn is therefore controlled to a large degree by the crystallization of pyroxene, whereas vanadium may be locally concentrated in chromite-bearing members, and zinc in olivine-bearing layers. Systematic variations are clearly related to the modal abundance of pyroxene in each sample.

5.2.3 Chromium

Chromium concentrations of rocks in the study section are both high and variable, ranging from percentage level concentrations in chromite-bearing pyroxenites to around 100 ppm in anorthosites. The variation diagram (figure 5.4e) shows that a linear correlation exists between MgO and Cr, particularly for rocks containing cumulus plagioclase, and cumulus plagioclase and orthopyroxene. Furthermore, Cr variations through the stratigraphic column (figure 5.5f) show that a rapid depletion is displayed upwards through a complete unit, whereas high levels are maintained throughout the UG-2 and UG-1 units. It is clear therefore that high Cr levels are brought about by the presence of chromite, while where this mineral is absent, whole rock concentrations are controlled by the modal proportion of pyroxene in the rocks. Distribution coefficients for silicate minerals (table 5.4) indicate that this element could be incorporated within both olivine and pyroxene. The occurrence of lower Cr levels (1000 ppm) in harzburgite samples, suggests that pyroxene is the main phase into which Cr is substituted. Microprobe analyses (see

Chapter 4) confirm this suggestion.

5.2.4 Strontium

Distribution coefficients for this element in common silicate phases have been determined by a number of workers (see table 5.4). All of these show emphatically that strontium is incompatible in ferromagnesian silicates but that it is strongly compatible in plagioclase. This behaviour is clearly discernible in the stratigraphic column in figure 5.5j where Sr levels can be seen to increase upwards through complete cyclic units, which are characterized by an upward increase in modal plagioclase. In Figure 5.4g a negative linear correlation is evident between MgO and Sr. Closer observation of this diagram reveals that a number of converging linear trends are discernible. Each of these trends corresponds to a different Unit, which contains cumulus plagioclase-bearing rocks. The Mg-rich rock types, namely pyroxenite and harzburgite are clustered together, with no apparent differences recognizable for rocks from the different units. These separate trends for plagioclase cumulates have important genetic implications, which will be discussed in the final chapter.

5.2.5 Zirconium, Yttrium and Rubidium.

These elements may be defined as incompatible, because they have distribution coefficients which are considerably smaller than unity for all the mineral phases represented in the study section. This means that during crystallization they will be

excluded from lattices of crystallizing minerals and enriched in the residual liquid. This process will continue until the final liquid has crystallized, with the result that the mineral or rock that crystallized last will contain the highest concentration of incompatible elements.

Incompatible element concentrations in these rocks are low (zirconium ranging from 3 to 35 ppm, yttrium from 0 to 10, and rubidium from 0 to 15 ppm). Variation diagrams, in which these elements are plotted against MgO (figure 5.4i-k) show a wide scatter of data points in which no definite trends are discernible. A common feature of all three diagrams is the occurrence of maximum concentrations of incompatible elements in pyroxenites. Variations with stratigraphic height (figure 5.5g-i) show also that the data are widely scattered, however, it is also clear that maximum concentrations for all three elements occur in the same samples, and that these maxima occur at low stratigraphic levels in complete units. The occurrence of maximum incompatible trace-element concentrations in rocks which contain mafic ferromagnesian minerals, would appear to be an enigma. However, these rocks do contain greater intercumulus space than those with cumulus plagioclase, and it would appear that it was in this intercumulus space that the final, incompatible element-enriched liquid crystallized.

5.3 Trace Element Variations Through the UG-2 Poikilitic Pyroxenite.

Samples were taken at closely spaced (approximately 1 metre) intervals through the poikilitic pyroxenite layer of the UG-2

Figure 5.6 Trace element varaitions through the poikilitic pyroxenite of the UG-2 Unit. Symbols for the five boreholes are; AE- solid triangles, AF- solid squares, AW- open circles, AX- solid circles, and AZ- open triangles.

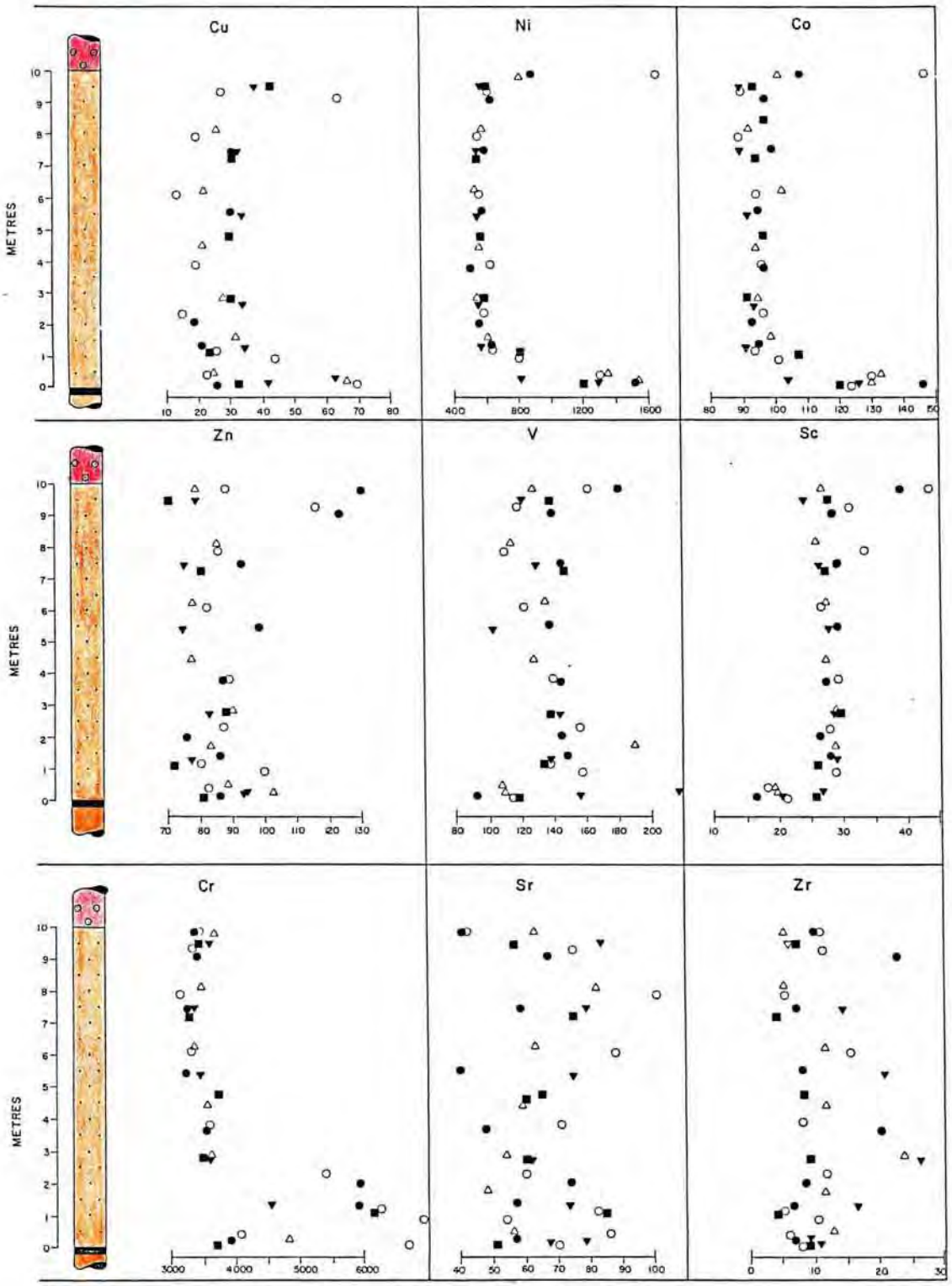

Figure 5.6

Unit in five widely separated boreholes. The rationale of the excercise was to investigate lateral trace element variations in a single layer. This particular layer was chosen because it is fairly homogeneous, because it contains only a few thin chromitite layers, and because it is not affected by pothole structures. The layer is underlain by the UG-2 leader chromitite and overlain by the olivine-bearing pegmatoidal pyroxenite/harzburgite of the Lower Pseudo Reef. Apart from the presence of scattered cumulus olivine grains in the basal parts of the layer, it is a fairly homogeneous poikilitic bronzitite with intercumulus plagioclase.

Selected trace elements were analysed and their concentrations through a generalized log are presented in figure 5.6. The fairly tightly constrained distribution patterns of pyroxene-compatible elements such as Ni, Co, Sc and Cr reflect the cumulus nature of orthopyroxene, whereas increases in Ni and Co and a decrease in Sc at the base of the layer, reflect the presence of cumulus olivine. An increase in Cr near the base reflects the influence of chromite close to the UG-2 leader chromitite. Corresponding increases in Ni, Cu and Co at the top of the layer possibly reflect the influence of sulphides associated with the Lower Pseudo Reef. The extremely irregular distribution of Sr values through the layer reflect the intercumulus nature of plagioclase and its' irregular distribution. Zr levels also exhibit a fairly irregular distribution, which is in accord with its incompatible nature, but it is noticeable that maximum concentrations of this element occur at low levels of the layer in at least four of the boreholes.

Figure 5.7 Variations of selected trace element ratios through the UG-2 pokilitic pyroxenite. The symbols are the same as for figure 5.6.

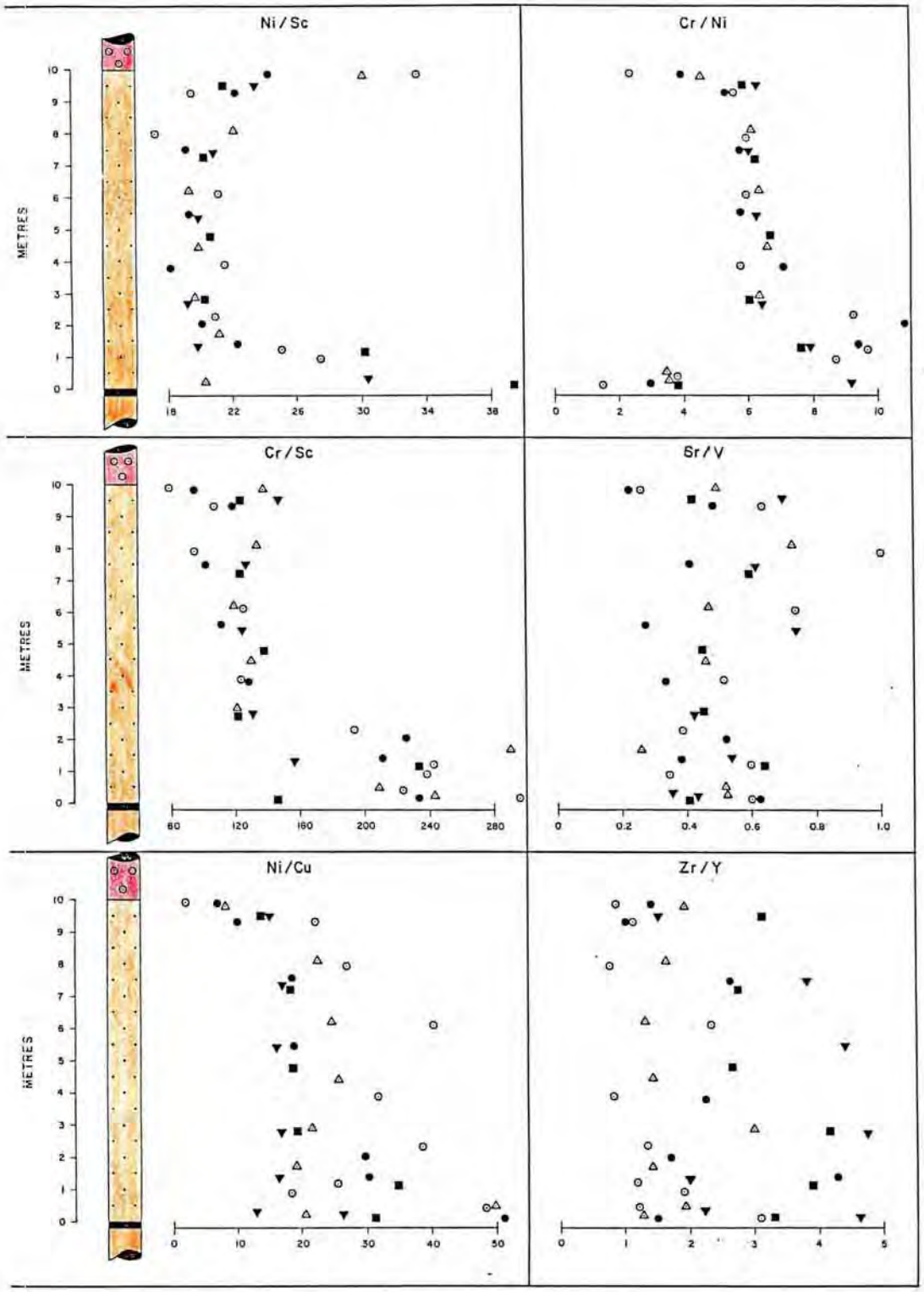

Figure 5.7

Figure 5.8 Plan-diagrams of Amandelbult showing averaged Ni/Sc and Co/Sc values for the UG-2 poikilitic pyroxenite in each of five boreholes. These values only reflect samples which do not contain olivine, chromite, or base metal sulphides.

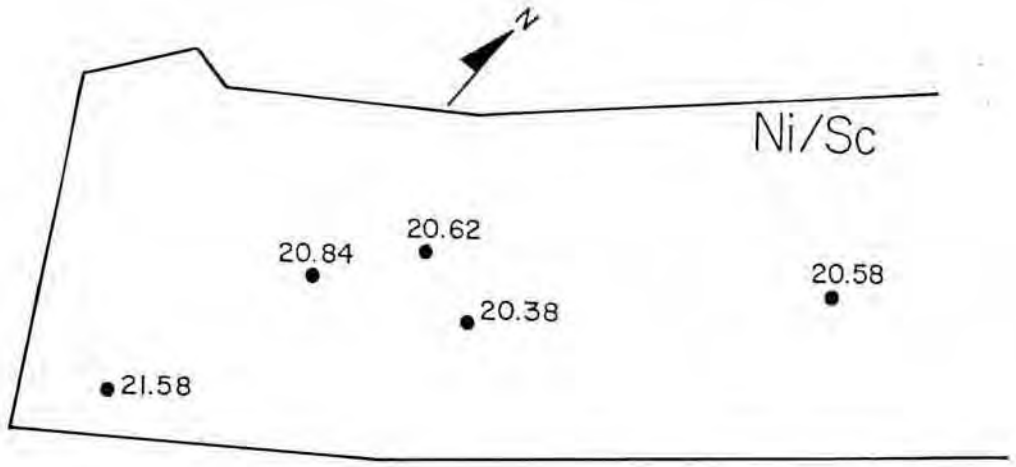

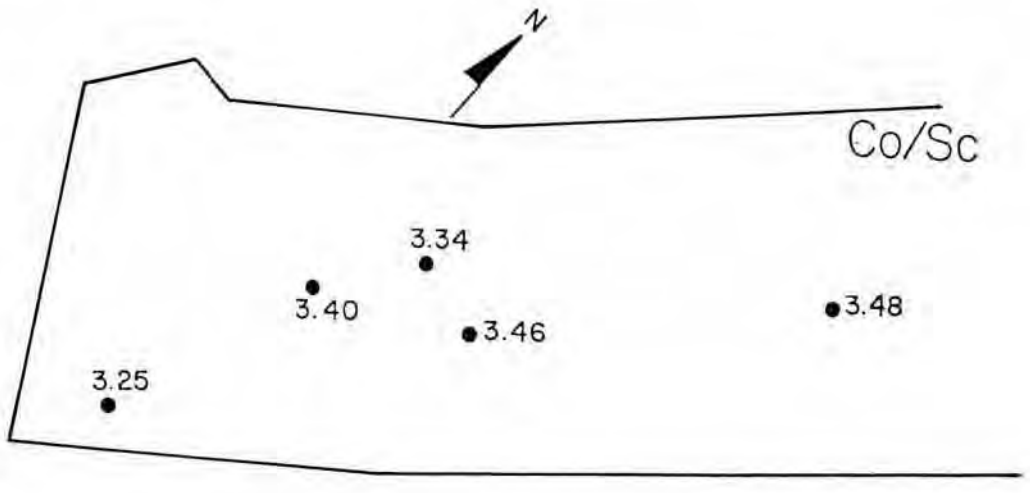

Figure 5.8

In an attempt to overcome the modal influence on whole-rock concentrations, selected inter-element ratios were calculated and plotted against the stratigraphic log (Figure 5.7). In these diagrams, the modal affects of olivine, chromite and sulphides cannot be entirely eliminated, but it is apparent that fairly constant values are maintained in the central portions of the layer, where petrographic observations have shown that the above mentioned mineral species are absent. In order to test whether different levels of these ratios are apparent in each borehole, the values of centrally located samples in each borehole were averaged, and these values plotted on a lease-area plan in figure 5.8. This diagram shows that a decrease in Ni/Sc and Cr/Sc occur from the southwest to the northeast, which is suggestive of a fractionation trend in this direction. The obvious failure of these diagrams is the paucity of sufficient data points from which to draw more definite conclusions. This trend is in accord with the observations of Eales et al. (in press b) who found that rocks at Union Section are more primitive in nature than their equivalents at Amandelbult. This is taken to mean that Union is more proximally, and Amandelbult more distally situated with respect to a feeder zone.

5.4 Discussion.

5.4.1 Compatible Elements - Evidence for Cyclicity.

It is clearly apparent from the preceding sections that the modal mineralogy of these rocks controls the distribution of compatible elements to such a degree that cyclical variations

in their concentrations cannot be taken as prima facie evidence for the existence of repetitive cycles of crystallization or fractionation. Eales et al. (in press), have investigated the geochemical parameters which may be used to define such cycles, particularly as to where the bases and tops of such units should be placed. They conclude that cycles may be defined by either (a) some parameter that is constant in each cycle, but different in successive cycles, or (b) a parameter that evolves progressively from some primitive initial value in each cycle, displaying a saw-tooth pattern through the succession. Furthermore, they recommend that since element concentrations are modally controlled, ratios of selected elements, based on their occurrence in one phase, and virtual exclusion from others, should be used instead of absolute values, as these ratios should be independent of modal control. If these ratios show a progressive change from some primitive value through the sequence, this will constitute evidence for the consanguinity of the sequence. A geochemical discontinuity would indicate a lithological hiatus.

In figure 5.9 there is evidence of both types of cycles as defined in (a) and (b) above. In column (a) of this diagram, the $Sr/Al_2O_3^*$ ratio, where

$$Al_2O_3^* = Al_2O_3 \text{ rock} - [(MgO \text{ in rock}/MgO \text{ in pyroxene}) \times Al_2O_3 \text{ in pyroxene}]$$

(after Eales et al., in press,a) is plotted against the stratigraphic column, this parameter is seen to have a fairly constant value for each unit, but differs from one unit to another, in the manner of (a) above. These data groups

Figure 5.9 Geochemical variations through the succession which indicate cyclicity. In (a), the $Sr/Al_2O_3^*$ ratio is designed to eliminate the presence of Al in pyroxene (see text for details), so that the ratio indicates variations in plagioclase components. In (b) and (c) variations reflect changes in pyroxene components.

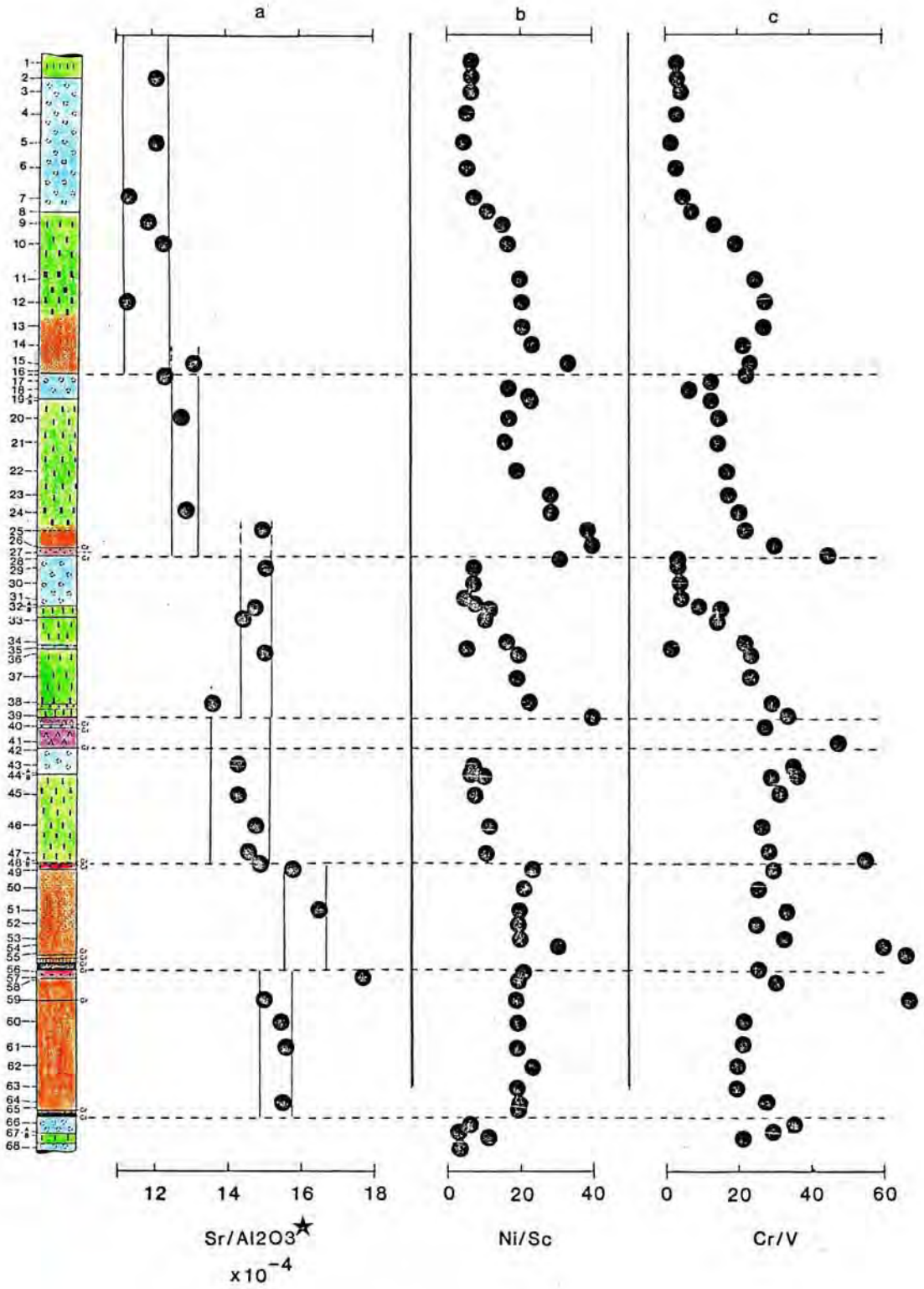

Figure 5.9

correspond closely with the lithologically recognizable units separated by the defined contacts between units (the dashed lines in figure 5.9). However, a common feature is that the ratio for the lowest sample in each unit corresponds more closely with the value of the underlying unit, than with that of other samples in the unit within which it is contained. This pattern has proved to be almost identical to that described Eales et al. (in press,a) for the same successions at Union and Rustenberg sections of R.P.M. A similar cyclicity is exhibited in figure 5.8b, where the concentration of Sr in normative feldspar is plotted against a stratigraphic column.

Cyclicity in the Amandelbult section is also evidenced by ratios of pyroxene-compatible elements. In columns (b) and (c) of figure 5.9, Ni/Sc and Cr/V ratio exhibit a saw-tooth pattern, in the manner of (b) above. The rationale for using Ni/Sc and Cr/V ratios exists in the distribution coefficients relevant to pyroxene, being Ni > Sc and Cr > V. Accordingly, these ratios may be expected to decrease with fractionation, or with increased proportions of residual liquid in the rocks concerned. Rocks containing excess Ni and Cr, by virtue of their containing sulphides and/or chromite, can be recognized from variation diagrams such as figures 5.4c and, and these samples were excluded from the plot in figure 5.9. The cyclicity is most prominently displayed in the "complete" Footwall, Merensky and Bastard units, but is not as clearly discernible in the "incomplete" Pseudo and "beheaded" UG-2 and UG-1 units.

Further evidence for cyclicity is also displayed in figure

Figure 5.10 A plot of MgO against Sr for the Footwall, Merensky and Bastard Units, which shows that a unique linear trend can be defined for norite and anorthosite rocks of each Unit.

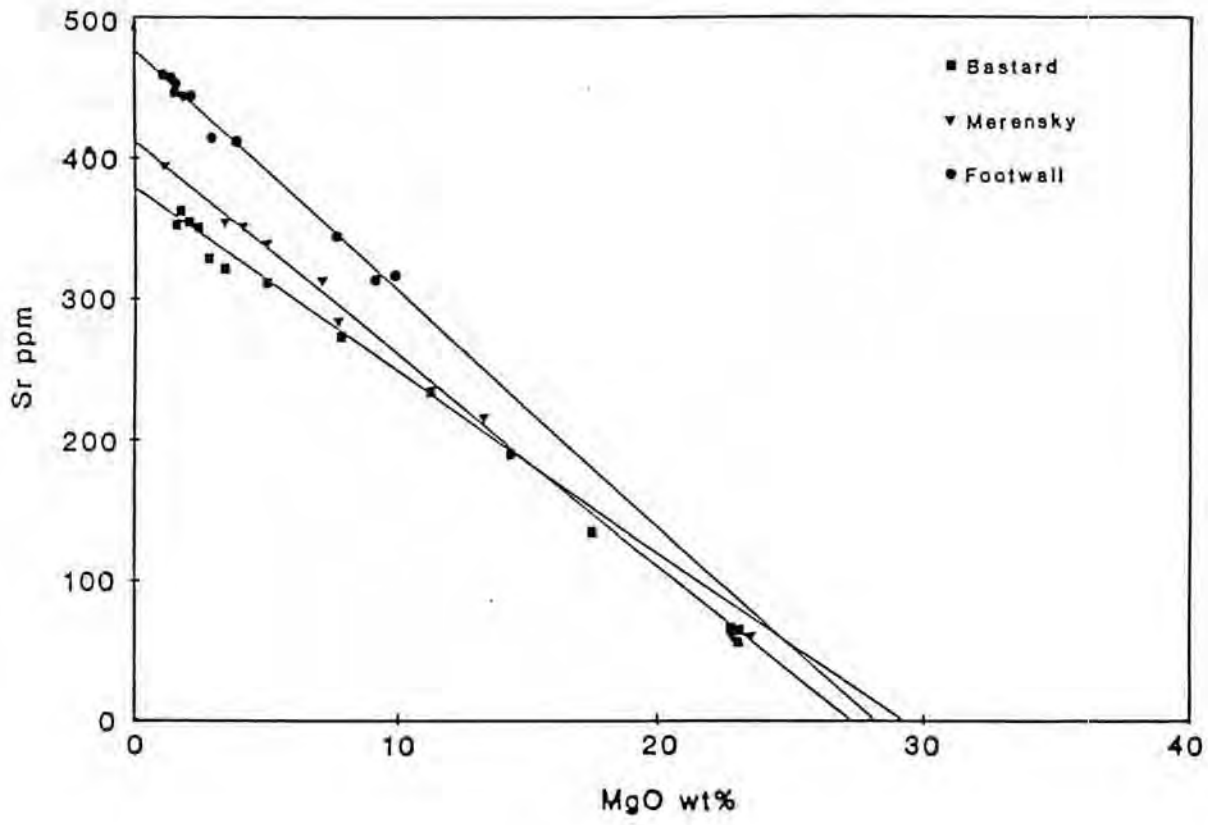
500
400
300
200
100
0
Sr ppm
0
10
20
30
40
MgO wt%
Bastard
Merensky
Footwall

Figure 5.10

5.10 where analyses of rocks from the three "complete" units have been plotted on a Sr versus MgO variation diagram. Each unit plots on a different linear trend, and linear regressions through each group have different slopes and intercepts. This must strongly favour a suggestion that each of these units represents a different population of cumulus plagioclase grains, differing subtly in their composition. Furthermore, the slopes of each of the linear regressions increase upwards, following the stratigraphic succession, which is suggestive of an evolutionary change from one unit to the next. The fact that these straight lines converge at high MgO values is indicative that the bases of each unit represent geochemically similar starting materials, a fact supported by the reversion to primitive values of Ni/Sc and Cr/V at the base of it each unit in figures 5.9b and c.

A striking feature of the cyclicity diagrams is that the cycles defined by plagioclase components differ from that described by ferromagnesian components. The lithological contacts between cycles correspond exactly to those of pyroxene-components while plagioclase-components define cycles which penetrate the lower layers of overlying cycles.

5.4.2 Incompatible Elements

A number of authors, including Henderson (1968), Lee (1983) and Cawthorn and McCarthy (1985) have used incompatible element concentrations in cumulate rocks to calculate the proportion of intercumulus liquid retained in the cumulus framework and to reflect the position in the sequence where

this liquid crystallized.

The distributions of K2O, P2O5, Rb, Zr and Y through the succession, (figures 5.2i and j, 5.5g, h and i,) indicate that the highest concentrations of the elements occur in pyroxenites at or near the bases of units. This poses a problem, as figures 5.9b and c clearly indicate upward fractionation trends through each unit, on the grounds of which the residual liquid would have been expected to crystallize at the top of the unit. It must be borne in mind however, that higher incompatible element concentrations probably occur in rocks which contained the greatest amount of intercumulus space. Because orthopyroxenes form a less effective close-packed structure, than plagioclase was probably in poikilitic pyroxenites that the last residual liquid was accommodated. The question which therefore arises is, does this incompatible-enriched fluid represent the last vestiges of the unit within which it is contained, or did this fluid originate from the unit below?

Consideration of figure 5.9a strongly supports the latter possibility, as the feldspar components of the lowest sample in each unit commonly correspond to those of the underlying unit, and it is together with these feldspar components, now represented as intercumulus plagioclase, that incompatible elements are concentrated. This situation is reminiscent of the "infiltration metasomatism" model of Irvine (1980a), but it differs in one very important respect namely, that the compositions of cumulus minerals in the lower layers do not appear to have been affected by reaction with the intercumulus liquid, to any great degree. One case in which such a

reaction may have occurred is in the Bastard Unit, where the MMF ratio of orthopyroxene (see chapter 4, figure 4.6a) at the lower levels of the reef increases upwards, in a reverse trend to that evident in the remainder of the succession. Kerr and Tait (1985) have recently documented experiments in which pore fluid between cumulus grains may be convectively exchanged with an overlying magma reservoir. The effects of such exchange could be considerable, particularly if residual liquids could bemoved by this convective process, as their final crystallization position could then be entirely random within a given Unit.

A second possibility is that the incompatible elements were originally concentrated at the top of the underlying unit, and that as a result of melting of this (feldspathic) layer, induced by the inflow of a new hot ultramafic liquid, they become incorporated into the new liquid. The incompatible elements were then probably inhibited from rising, by newly crystallized rocks containing cumulus plagioclase. This could also explain the occurrence of more sodic plagioclase at the base of such Units.

CHAPTER 6 : DISCUSSION

6.1 Introduction

This chapter consists of three parts. In the first, some recent ideas on, and models for the formation of layered complexes, particularly the layered rocks of the Bushveld Complex, are considered. In the second section, the factual data recorded in the preceding chapters are evaluated in terms of these models, and in the third, a genetic model is developed, which attempts to explain the origins of most of the features recorded in earlier chapters.

6.2 Existing Models

Six existing models are summarized here in order to emphasize the diversity of ideas concerning the origins of layered igneous rocks. These are considered seperately below.

6.2.1 The Wager and Brown (1968) Model

Wager, Brown and Wadsworth (1960) developed the "cumulus theory" to explain the layering present in igneous intrusions such as Skaergaard. They postulated that crystals would nucleate and grow within a magmatic liquid until downward gravitational forces acting upon them exceed upward bouyancy forces exerted by the magma and they would then settle through the magma under the influence of gravity and would be deposited on the chamber floor as sediment-like deposits. Sorting processes would be controlled by density and size fluctuations, and would result in the formation of layers. This theory was applied by Wager and Brown (1968), to account

for layering in the Bushveld Complex as well.

For the Bushveld, they visualized the existence of two significantly different stages, namely an "integration" and a "differentiation" stage. They suggested, also, that a very large volume of basaltic magma was injected into the crust, but that this did not occur as a single event. Rather, the magma filled four interconnected chambers during a number of discrete pulses of magma injection.

During their integration stage, bronzite and Mg-olivine were the main mineral phases to crystallize. These dense grains settled through the residual magma to form the pyroxenite and dunite layers of the Basal Series (their terminology). Although crystal settling was regarded as being the dominant process reponsible for the formation of such layers, a minor role is ascribed to convection currents in the magma as well. Later, Cr-spinel became an important liquidus phase, and it crystallized as great swaths which settled periodically to form the chromitites of the Critical Series. Upwards through the accumulating crystal pile, olivines and pyroxenes were becoming increasingly Fe-rich, and plagioclase more sodic. These trends are complicated by occasional fluctuations in cumulus compositions, which were brought about by periodic flooding of the chamber with fresh supplies of parental magma. These fresh pulses mixed with the residues of previous influxes. They visualized that towards the close of the integration stage, a major replenishment of fresh magma was introduced. This new liquid mixed with the pre-existing residue, and led to the formation of an immiscible sulphide

liquid from which platinoid and sulphide minerals crystallized. The sulphide crystallized together with chromite and bronzite, to form the Merensky Reef horizon. The turbulence of this mixing event led to the formation of channel and scour structures, which brought about the formation of potholes. The integration stage was therefore characterized by tectonic instability.

Their differentiation stage, by contrast, was characterized by relative tectonic stability, in which cryptic layering developed in preference to rhythmic layering. Here ortho-pyroxene, clinopyroxene and plagioclase crystallized, to form the weak rhythmic layering observed in the Main Zone. A return to strong rhythmic layering is envisaged in the Upper Zone, where dense Fe-rich oxides and Fe-rich olivine began to crystallize. Wager and Brown therefore view the layered rocks of the Bushveld Complex as the product of the complete fractional crystallization of a single parental magma, which has intruded as a number of pulses into the magma chamber. They extend this fractional crystallization process to include the granophyric roof rocks as well.

6.2.2 Irvine's (1980b) Model

Following the crystal settling hypotheses of Wager and Brown (1968), a number of workers presented evidence that plagioclase would be less dense than its parental liquid, and that it would float rather than settle through basaltic liquids. Foremost amongst these workers were Campbell (1978), who found such evidence in the Jimberlana intrusion of Western Australia, McBirney and Noyes (1979) working on Skaergaard and

Campbell et al. (1978) who provided experimental evidence to support this view. In light of this, Irvine (1980b) explored possible mechanisms whereby the mechanical aspects of magmatic currents could bring about the deposition of low-density minerals at or near the floors of such intrusions. Two of his proposed mechanisms, namely density currents, and double diffusive convection are worthy of more detailed consideration.

Density currents, Irvine postulated, are formed when liquids with suspended crystals move down the side walls of an intrusion in the form of a surge. When such surges contain only mafic minerals, coarser crystals would advance preferentially by virtue of their greater momentum and would be enriched in the lower fringes of the flow. This fringe would be continuously left behind along the floor as the surge passed over it, with the coarser crystals being concentrated along the bottom. Finer crystals would be enriched at the top rear of the surge, from where they would be transferred to the top of the trailing layer. The resulting trailing layer would therefore be graded in terms of grain size. If the surge contained both plagioclase and mafic minerals, there would be little tendency for the plagioclase to be enriched at its head, because of its lower density. Consequently, plagioclase would concentrate behind the head of the surge and mafic minerals at its head. Mafic minerals would then be deposited at the base of the trailing layer and plagioclase at the top. Consequently a mineral-graded layer would be produced. The plagioclase, deposited at the top of the layer, would be trapped by the overlying magma and could not float upwards

through it.

The second mechanism considered by Irvine (1980b) was that of layer formation by bottom crystallization, which invokes the theory of double-diffusive convection. This process involves both heat and mass transfer by a mechanism of coupled diffusion and convection. There are generally two manifestations of the process, the so-called "finger" and "diffusive" cases. The latter is applicable where a high-temperature magmatic liquid underlies a less dense, lower-temperature liquid of different composition. These liquids become gravitationally stratified as horizontal layers, each of which contain numerous, highly irregular convection cells. There is a stepwise upward decrease in density from one layer to the next, with similar steps in composition and temperature. The interfaces (boundary layers) between the layers have finite thicknesses, and the liquid within them is static, while rapid heat but less rapid chemical transfer occurs through them by diffusion. This diffusion results from steep temperature and composition gradients between individual layers. The boundary layers are maintained because heat diffusivity through the liquid exceeds chemical diffusivity. As a result, the upward movement of heat causes a reduction in the density of the liquid above each boundary layer. This causes gravitational instability which drives convection. Three zones can be distinguished in such intrusions. At the base a zone of bottom crystallization occurs, where the liquidus temperature profile of the magma intersects the adiabatic temperature profile. In the central portions of the chamber, a zone of strong liquid blending occurs, where the fresh primitive magma mixes with the overlying residual magma.

In the upper portions of the intrusion, the residual magma may be contaminated through interactions with roof rocks. In the zone of bottom crystallization olivine and chromite would be the first minerals to crystallize as a result of their higher liquidus temperatures, but with continued heat loss and chemical transfer upwards, the liquidus temperature gradients could be shifted so that pyroxenes and plagioclase could also crystallize, while chromite and olivine would cease to do so. In this way each layer would yield a separate, modally graded layer, and by this process of bottom crystallization plagioclase would not float through its parental liquid.

6.2.3 Vermaak's (1976) Model

Vermaak investigated the Merensky reef and its enclosing units in the Western lobe of the Bushveld Complex. He suggested that the lower parts of the Critical Zone, which is composed of thick isomodal pyroxenites, interspersed with chromitite layers, crystallized from an ultrabasic magma. Essential to his model, however, is the repeated flotation of plagioclase in the evolved melt residue of this crystallization event, to temperature-, density- and composition- inversions. The floating plagioclase would form a mat, which would have grown by underplating of later crystallized grains. This would effectively account for the upward An-enrichment trend documented for anorthosites in these rocks. Furthermore, the presence of this mat would greatly affect the continued evolution of the magma below it. If the mat formed an effective trap, volatiles would be trapped in the magma, which would lead to a lowering of its viscosity and bring about the

rapid growth of ferromagnesian phases. Rapid crystallization, Vermaak postulated, would lead to the aggregation of ferromagnesian minerals to form "boulder-like" masses, and would create an "acidification trend" in the residual magma. Superimposed on this would be a "basification trend" created by the removal of plagioclase through flotation. Both these trends would be manifested in the chemistry of the boulders, as these would have mafic rims, and altered centres, in addition to which olivine and quartz could be found as co-existing phases within them.

In the Boulder Bed at Rustenburg, the boulders are postulated to have frozen before they coalesced, whereas at Union Section they coalesced to form the Pseudo reef. At both localities their coalescence resulted in the formation of the Merensky reef. Vermaak claims that the outlines of such boulders can be seen in weathered outcrops of Merensky reef.

To explain the finer details of the Merensky reef horizons, Vermaak suggests that just prior to its deposition, the floor of the Complex was tectonically readjusted. This caused turbulence and erosion of the pre-existing crystalline pile, as well as assimilation of country rocks. The former led to the formation of pothole structures while the latter brought about the crystallization of chromite, either by increasing oxygen fugacity (Cameron and Desborough, 1969) or by increasing the silica activity of the magma, in the manner described by Irvine (1975). This chromite settled to form the lower Merensky chromitite. The removal of Fe from the melt (into chromite) led to an increase in sulphur activity and the concomitant formation of immiscible sulphide droplets, which

collected P.G.E. from the melt. This was followed by the flotation of plagioclase to form a mat, and the formation of boulders, which settled under gravitational forces to form the Merensky Reef. These heavy boulders dimpled the underlying chromitite layer and still-plastic Footwall anorthosite. These events were followed by a second crystallization sequence which commenced with chromite and was followed by pyroxene and plagioclase, to complete the Merensky Unit. In the case of the Bastard Unit, an effective volatile trap was not formed, and the sequence of events, described above, did not evolve to completion.

6.2.4. The Model of Irvine, Keith and Todd (1983).

This model is based largely on observations made in the Stillwater Complex, which have been extrapolated to include the Bushveld as well. These authors have evidence which suggests that the Stillwater Complex crystallized from two parent liquids, an ultramafic (U-type) and an anorthositic (A-type) liquid, and that their crystallization and mixing were controlled by double-diffusive convection. In double-diffusive convection systems two types of interfaces may be developed between two different liquids. Diffusive interfaces develop where a hot liquid underlies a relatively cooler, but less dense liquid of different composition. Through such interfaces thermal and chemical exchanges occur only by diffusion, while they also tend to inhibit mechanical mixing of the liquids. Finger interfaces are formed when relatively hot liquid floats on a cooler liquid that is denser only because it is cooler. These interfaces develop because

diffusive exchanges cause mechanical mixing.

The two parental liquids, the authors claim, differed sufficiently in density for separate liquid layers to exist in the chamber. The whole sequence of cumulates then developed concurrently by downdip accretion from a column of liquid layers that were separated by diffusive interfaces. Each layer grew from one or more liquid layers, with its lower cumulates growing in advance of the upper in accordance with their higher crystallization temperatures. If the liquid residua that fractionated along the crystallization front had lower densities than their parent liquids, they would be continuously transferred step-by-step up the front. This would eventually lead to the elimination of liquid layers that occupied the bottom of the column, but would also ensure that new layers were produced at the top. Intermediate layers would subside into the chamber, and cumulate strata would form, inclined into the chamber, with primary dips.

These authors' calculations show that anorthositic layers would be more dense than ultramafic ones, and hence that anorthositic liquid layers were emplaced beneath mixed derivatives.

In this case "finger-mixing" would occur along the interface between the two liquids. Mixing would lower the liquidus temperature and produce hybrid liquids capable of dissolving earlier cumulates. This process they use to account for the formation of potholes. Furthermore, mixing would lead to the precipitation of immiscible sulphide liquids, which would collect PGE. The repetition of cyclic units could be

explained by having periodic additions of dense (anorthositic) magma beneath a subsiding column of crystallizing liquid layers, thus raising them repeatedly so they could crystallize repeated pulses of the same cumulates.

In their extrapolation to the Bushveld Complex, Irvine et al.(op.cit) suggest that the anorthositic liquid was somewhat more siliceous than its Stillwater counterpart, while the Bushveld's U-liquids were somewhat less evolved. To explain the great lateral persistence of layers it is suggested that the layered liquid succession extended across the whole of a single lobate lopolith, so that similar sequences of rocks could crystallize at widely seperated points. Cyclic repititions in the Bushveld, especially in the upper Critical Zone are ascribed to re-elevation of continuously fractionating liquid layer successions, in which compositional changes from zone to zone reflect progressive differentiation of parent liquids.

6.2.5 The Models of Campbell et al. (1983) and Naldrett et al. (1986).

These two models are essentially the same, with Naldrett and Barnes being authors in both. They have considered the Bastard, Merensky and Footwall units at Union and Rustenburg mines, and they point out that the base of each unit is marked by an increase in the Mg-number of orthopyroxene, and by pockets, or a layer of sulphide which have a higher Ni/Cu and much higher Pt/Cu ratios than sulphides from the remainder of the Units. Furthermore, they show that the Pt-tenor

alternates from high to low through each unit, which may be taken as evidence that the sulphides and the Pt-tenor were established with the stratigraphy, and not by later post-depositional processes.

Campbell et al. (1983) show that the Pt-rich horizons of both the Bushveld and Stillwater complexes have high Pt/S and Pd/S ratios when compared to other ultramafic rocks, and that a close correlation exists between P.G.E. and sulphides. The high P.G.E. content of these sulphides is problematic, because it would mean either that a high distribution coefficient for platinum in sulphide would be required or, that the sulphides would have to have been in equilibrium with a very large volume of liquid. They show that, a silicate/sulphide mass ratio (R-factor) greater than the distribution coefficient would have to be attained, and that very special conditions would have to prevail for this requirement to be met.

Their model visualizes a residual magma, which has crystallized plagioclase, and therefore has a higher density than a fresh magma input. This fresh input would rise through the fractionated magma, and seek out its own density level, where it would spread out as a layer. It would rise through the residual magma as a turbulent plume, entraining old magma into itself. If both these magmas were close to saturation with respect to sulphur, sulphide droplets would separate from the silicate melt, and they would be swirled around in the plume. The sulphide droplets would thereby attain a high R-factor. On reaching its density level the new magma would form a rapidly convecting layer, which would lose heat rapidly through its upper surface. At some critical stage convection

would change from being turbulent to laminar, and suspended crystals of olivine and orthopyroxene, together with sulphide droplets and entrained liquid, would sink through the underlying magma as downspouts to spread over the crystalline floor, to form the Merensky Reef. Chromite would be precipitated as a result of the mixing of the two liquids, in the manner described by Irvine (1977), to form the lower Merensky chromitite. At a later stage, the new layer would have cooled sufficiently, so that its density would match that of the older magma, allowing them to mix. The crystallization sequence from this mixture would be orthopyroxene; orthopyroxene + plagioclase, and finally plagioclase alone, and this would account for the formation of the entire unit. The upper Merensky chromitite would be formed by diffusion and reaction between the new hybrid magma, and the underlying Merensky Reef. The sulphides precipitating from the hybrid would have lower Ni/Cu ratios than their Merensky counterparts.

The Footwall and Bastard Units are proposed to have been produced by similar mechanisms, but in each case slightly different circumstances are thought to have prevailed. In the Pseudo Reef (at the base of the Footwall Unit), the proportion of sulphide/silicate liquids was very much lower than was the case in the Merensky Reef, while the Boulder Bed at Rustenburg resulted from differences in viscosities between the down-spouting material and the host magma. These differences were such that the down-spouts broke up into droplets. In the Bastard Unit, a high sulphide/silicate liquid volume ratio was attained, but no down-spouting occurred. Instead, the immiscible sulphide droplets settled on their own, and became

modified in the process.

6.2.6 The Model of Eales, Marsh, Mitchell, De Klerk, Kruger and Field (1986: in press).

These authors present geochemical data for the upper Critical - Main Zone intersection at Rustenburg and Union sections of R.P.M. The geochemical trends presented by them for the Bastard Unit - UG1 Unit intersection are closely matched by those documented in earlier chapters of this thesis. Important additional data presented include Sr-isotope systematics through the same sequence at Union Section, and chemical data pertaining to the Main Zone and the lower Critical Zone.

Initial Sr-isotope ratios (Sr_o) are seen to be constant at ca. 0.7063 through the lower portions of the succession, but they rise rapidly through the Merensky and Bastard Units, and only become relatively constant again 350m above the Giant Mottled Anorthosite, at the level of the Porphyritic Gabbro Marker, where a value of 0.7087 is attained. These high values chracterize most of the Main Zone up to the Pyroxenite Marker (2240m above the Bastard Reef). Here the initial Sr ratio drops to 0.7077 - 0.7073. It is important to note that the sustained increase in Sr_o through the Merensky and Bastard Units occurs irrespective of rock type.

The analyses of the rocks 340 to 570 metres above the Bastard Unit indicate that they are homogeneous and geochemically coherent with respect to compatible element ratios. Within the first 1200m of the Main Zone however, a number of highly feldspathic intervals occur. Amongst these are anorthosites

which have geochemical characteristics typical of the upper Critical Zone. A further parameter of interest is the Cr/Al ratio of orthopyroxene, which exhibits a clear break between the upper Critical and Main Zones (see section 4.3.2), as well as a similar break at the top of Main Subzone B, above which it reverts to values typical of the upper Critical Zone.

The presentation of the model of Eales et al. (in press,a) begins with a column of residual, evolved magmatic liquid above the UG-2 pyroxenite. This liquid has an Sr_o of 0.7063. They visualize that a layer of hot, dense, primitive liquid was emplaced at the base of the residual liquid column. Mafic cumulates, with geochemical affinities akin to those of the underlying crystal pile, precipitated from the new liquid. With crystallization, the density of this liquid was lowered, until it equalled that of the overlying residue, at which point mixing commenced, and norites and anorthosites were precipitated. This represents the Footwall Unit.

These events were followed by the emplacement of a wedge of Main Zone liquid, hundreds of metres above the crystalline floor, which had a Sr_o close to 0.7090 . Progressive mixing between the new wedge and the underlying residual liquid produced a hybrid liquid, which possessed isotope ratios which increased upwards, as a result of mixing.

Further emplacements of primitive Critical Zone liquids then followed. The first of these produced the Merensky Unit. This liquid was initially above the feldspar liquidus, which led to the resorption of the anorthositic floor and the

dimpling of the lower surface. Assimilation of this feldspathic material brought about changes in the bulk composition of the new layer and lowered its density. Heat balance requirements caused accelerated crystal growth of mafic cumulates and the formation of the pegmatoidal Merensky Reef and pyroxenite. Once mixing with the overlying residue was achieved, precipitation of norites and anorthosites occurred. The Bastard Unit represents, essentially, a repetition of this process, while the remainder of the liquid column crystallized as norite and gabbro. It is possible that the anorthosites of the Main Zone included feldspathic crystal mushes or schlieren of upper Critical Zone material which became entangled with, or uplifted by, the influx of new Main-Zone magma.

6.3 Evaluation of Models.

The most obvious failure of the Wager and Brown (1968) model is the plagioclase-flotation problem, which was discussed under Irvine's (1980b) model. A further objection arises from their interpretation of the Main Zone, for recent studies by Harmer and Sharpe (1985) and Eales et al. (in press,a) have shown that it is geochemically and isotopically distinct from both the Critical and Upper zones, and is therefore most likely to represent the intrusion of a new liquid above the Critical Zone. Their model also does not explain the finer details of the upper Critical zone, particularly the origin of repetitive cyclic units. They do, however recognize that the Bushveld magma was intruded as a number of pulses, and that complexities could be brought about by the mixing of fresh influxes with the residua of previous influxes.

The applicability of Irvine`s (1980) density current hypothesis to the Bushveld is somewhat dubious. It is difficult to visualize how a sufficiently large volume of liquid could build up on the sidewalls of an intrusion with the dimensions and shape of the Bushveld, so that the resultant density current could deposit layers that exhibit the lateral persistentce of those recorded in the Complex. Furthermore, the size-graded layers typical of the Skaergaard and Muskox bodies are not evident in the study section, particularly in rocks free of cumulus plagioclase, where one would expect this phenomenon to be most prominent. Irvine`s (1980) double-diffusive convection model would seem to be more plausible, particularly in explaining the chemical cyclicity exhibited by the rocks of the study section. A problem with this model is that it does not explain the occurrence of primitive mafic minerals at the base of each unit.

Vermaak (1976) makes maximum use of the plagioclase-flotation hypothesis and, although it offers a viable explanation as to why plagioclase becomes more calcic with height, his model fails on a number of accounts. Firstly, the model does not account for the existence of primitive mafic minerals at the base of each unit, for no new liquid inputs are envisaged. Secondly, his model does not explain the presence of P.G.E.-bearing sulphides beyond the confines of the Merensky Reef, as he states that the separation of immiscible sulphide liquid was indirectly, but essentially, brought about by the assimilation of country rock as a result of tectonic re-adjustment just prior to the deposition of the Merensky Reef.

This tectonic readjustment is implied to be the cause of pothole structures, so that a correlation may exist between potholes and P.G.E.-bearing sulphides. This correlation most certainly is not applicable to the UG-2 chromitite layer, where high and mineable P.G.E. values occur. Clearly, sulphur-isotope work is required to ascertain the origin of the sulphur in the P.G.E.-rich sulphide.

Irvine et al.'s (1983) model is particularly complex, but it has several aspects which are of considerable merit. Of particular merit are the explanations for the presence of P.G.E. in layers such as the Merensky and J-M Reefs, and the extreme lateral persistence of individual cumulate layers. A serious objection however arises when the model is extrapolated to the Bushveld Complex, particularly with regard to the intrusion of A-type liquids beneath U-type derivatives. Evidence from Harmer and Sharpe (1985) and Eales et al.(in press) clearly shows that the Main Zone of the Complex appears to represent a major new influx of A-type liquid, and this is obviously placed above typical Critical Zone U-type liquids. The geochemical data presented in this thesis indicate that fractionation trends define cycles which commence in ultramafic layers and pass upwards through the sequence harzburgite-pyroxenite-melanorite-norite-anorthosite, and that it would be inappropriate to place anorthosite at the bases of such units. It could be that the crystallization of the Bushveld Complex proceeded in a similar to that described by these authors, but that the A-type liquid was emplaced above U-type derivatives, instead of vice versa. Cyclicity could have been brought about by re-elevation of existing layers as a result of the intrusion of new batches of U-type, rather

than A-type liquids. If this possibility is to be entertained, relative density considerations would have to evaluated. Another aspect of this model which may be questioned, is the growth of layers with primary dips. Hattingh (1984), has shown through palaeomagnetic studies of the Merensky Reef footwall rocks, that they cooled from the floor upwards, and later (Hattingh, 1986), that parts of the Main Zone acquired their remanent magnetization while the igneous layering was in a horizontal position, which is in conflict with the idea of accretionary growth of a dipping layer.

The models of Campbell et al.(1983) and Naldrett et al.(1986) satisfy a number of the constraints provided by the data of this thesis. Particularly, they explain the occurrence of primitive mafic minerals at the bases of each of the Footwall, Merensky and Bastard Units, and provide a viable explanation for the wide range in Ni contents of olivines in single layers. Furthermore, the failure of downspouting in the Bastard Unit may explain the initial upward increase in mafic nature of pyroxenes in this unit, which does not occur elsewhere. There are however, some difficulties with the model. For example, do the turbulent plumes invoked by these authors bring about pothole structures, as is suggested by Buntin et al. (1985)? If this is the case, then why are these structures only associated with the Merensky plumes, and never with those of the Bastard and Footwall? Furthermore, was the important P.G.E. mineralization in the UG-2 chromitite brought about by a similar mechanism, and if so, why was so much more chromite precipitated here than from the other events? It

should be not be overlooked that the UG-2 chromitite wholly overshadows the Merensky Reef as a future reserve of P.G.E.

The model of Eales et al. (in press,a) is favoured here, for it considers in detail the chemical characteristics of rocks underlying and overlying the Merensky Unit, in addition to which it meets the important constraints imposed by initial Sr-isotope ratios, whose variations cannot be attributed to fractionation processes. This model may also be used to explain some of the features recorded in this thesis. For example, the abrupt changes in trends of the Cr/Al ratio of orthopyroxene and the An-content of plagioclase at the base of the Giant Mottled Anorthosite, may be brought about by the first major mixing event between typical Critical zone liquid residua and Main zone-type liquid. The continued re-elevation of Critical zone residua, brought about by new influxes of primitive Critical zone liquid, may be invoked to explain the complex zoning patterns in plagioclase grains, while An-rich, reversed rims may be a direct manifestation of the mixture of evolved liquid with a new Ca-rich liquid. The model is particularly applicable to the Bastard, Merensky and Footwall units, but the interpretation of the lower parts of the study section are more problematic. Foremost amongst these problems, is an adequate explanation for the Pseudo reef horizons. The upper Pseudo reef has sharp contacts with its P2 middling leucotroctolite and underlying anorthosite, while the lower reef has a sharp contact with the overlying norite. In all three cases the contacts are undulatory, suggesting resorption, and the associated felsic rocks are recrystallized. These relationships suggest that the mafic layers were intruded as hot liquids or crystal mushes into a

Figure 6.1 A conceptual model which describes the seqeunce of events which led to the formation of the study section. Refer to the text for details.

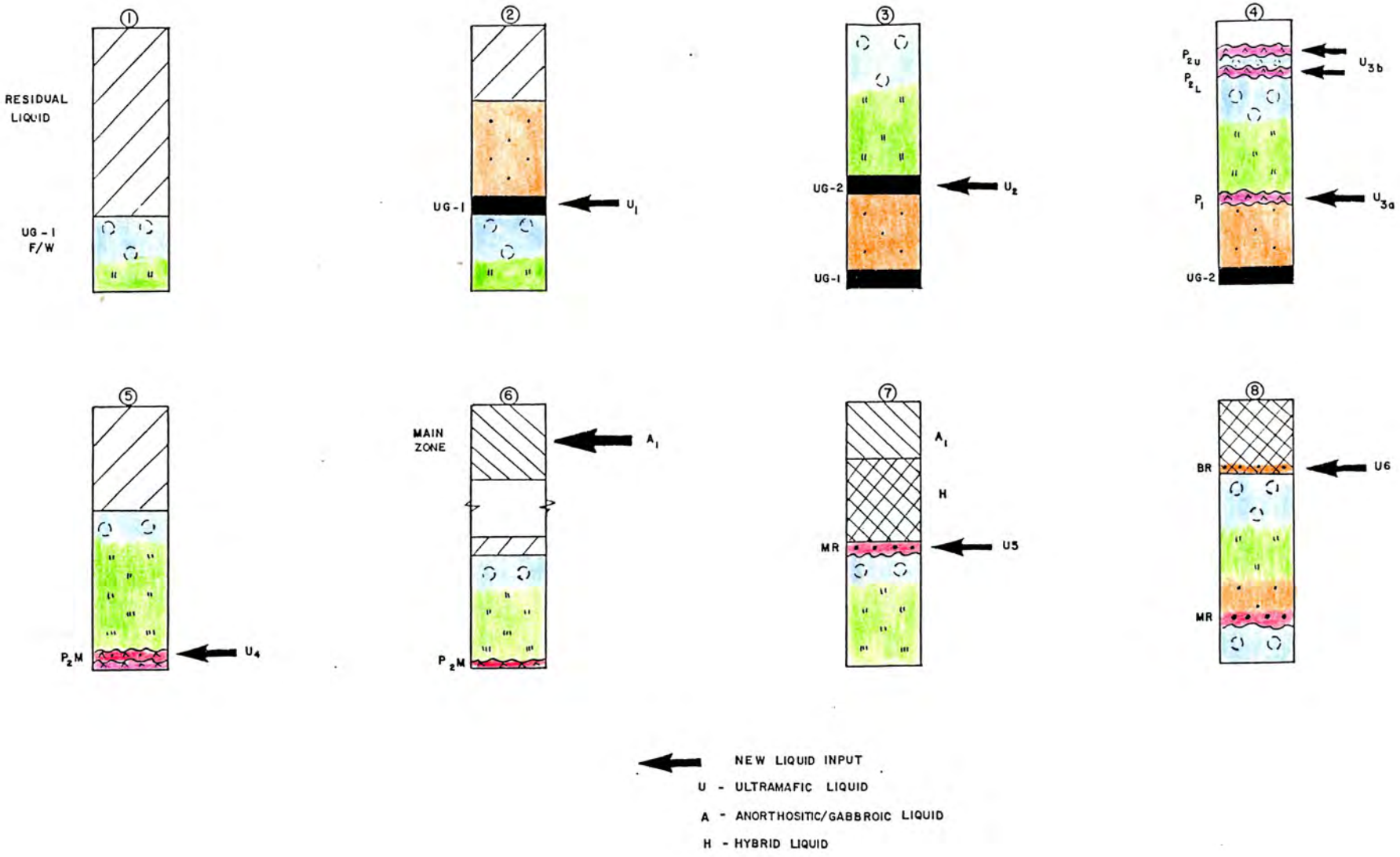
①
RESIDUAL LIQUID
UG-1 F/W
②
UG-1
U1
③
UG-2
U2
UG-1
④
P2U
P2L
U3b
P1
U3a
UG-2
⑤
P2M
U4
⑥
MAIN ZONE
A1
P2M
⑦
A1
H
MR
U5
⑧
BR
U6
MR
NEW LIQUID INPUT
U - ULTRAMAFIC LIQUID
A - ANORTHOSITIC/GABBROIC LIQUID
H - HYBRID LIQUID

Figure 6.1

crystalline pile. The associated heat brought about re-crystallization of plagioclase, while the only evidence of melting and subsequent mixing lies in P-2 middling leuco-troctolite. This intrusive theory is problematic, in that no small-scale cross-cutting features are apparent, and the lateral persistence of these layers is difficult to reconcile with an intrusive origin. It should nevertheless be noted that the wedging-out of the P2 middling anorthosite along strike is in reality a low angle transgression that would be consistent with an intrusive origin for the P2 harzburgite. It is also likely that the upper Pseudo reef predated the Merensky event, because it forms the refractory layer on which pothole Merensky reef is deposited.

A further complication is the apparently beheaded nature of the UG-1 and UG-2 Units for no adequate explanation exists to expain the whereabouts of their complementary feldspathic components. The sharp contact of the Lower Pseudo Reef with its overlying norites suggest that it may be intrusive with respect to them, and that the norites and anorthosites of the Lower Pseudo Unit may in fact belong to the UG-2 Unit. A problem with this theory is that it does not fit the cryptic cycles described by the $Sr/Al_2O_3^*$ ratio (see Fig.5.9a), which indicate that the UG-2 and Lower Pseudo Units have significantly different values.

6.4 Towards a Model.

In conclusion therefore, the layered sequence of upper Critical Zone rocks at Amandelbult was most likely formed in

the following manner: (refer to Figure 6.1)

(i) A primitive Critical Zone-type liquid (U1) was intruded at the base of a column of residual liquid. Chromite crystallized from this liquid, to form the UG-1 chromitite layer, and was followed by the crystallization of bronzite. If any olivine did crystallize at the base of this Unit it is likely that it became unstable and was resorbed. Stage 2 in figure 6.1.

(ii) A second pulse of primitive liquid (U2) was intruded into the liquid residue above the floor. This pulse crystallized chromite, followed by olivine and bronzite, bronzite alone, then bronzite and plagioclase, and finally plagioclase alone to, produce the chromitite and poikilitic pyroxenite of the UG-2 Unit as well as the norite and anorthosite layers of the Lower Pseudo Unit. Stage 3 in figure 6.1.

(iii) A third pulse of primitive magma (U3) intruded the unconsolidated crystal pile between the newly crystallized pyroxenite and norite layers. Its high temperature brought about recrystallization of feldspar in the overlying norite, but little or no melting. This layer of liquid crystallized chromite, olivine and bronzite to form the lower Pseudo Reef (P-1). Penecontemporaneously similar liquids (U3a and b) intruded at the top of the layer of anorthosite. This liquid melted some of the anorthosite which then recrystallized as leucotroctolite (the P2 middling leucotroctolite), while the bulk of it crystallized as harzburgite to form the upper Pseudo reef (P2). Stage 4 in figure 6.1.

(iv) A fourth pulse of primitive liquid (U4) precipitated a thin layer of olivine and bronzite, before mixing with the overlying liquid column to crystallize the bronzite and

plagioclase-bearing layers which constitute the Footwall Unit. Mixing of the new pulse with the pre-existing residue occurred rapidly as no pyroxenites were developed here. Stage 5 in figure 6.1.

(v) A major influx of anorthositic or gabbroic liquid (A1) followed a few hundred metres above the crystalline floor. This was the Main-Zone liquid which had a higher initial Sr-isotope ratio then Critical zone liquid (see the model of Eales et al. (in press,a)). This liquid mixed with the underlying residua of preceding Critical zone pulses, to create a hybrid liquid (H). Stages 6 and 7 in figure 6.1.

(vi) This was followed by a fifth pulse of primitive Critical zone material (U5). The liquid was at a temperature higher than the liquidus temperature of the underlying crystalline anorthosite, and as a result, the upper portions of the latter melted. This material was assimilated into the primitive magma. The melting episode accounts for the undulatory basal contact of the Merensky Reef, while the assimilated material brought about the precipitation of chromite through the contamination mechanism of Irvine (1975). The presence of this felsic material also brought about the rapid crystallization of mafic minerals (Eales et al., in press,a) as a result of changing the heat-balance requirements of the magma, and hence the pegmatoidal nature of the Merensky Reef. Once density and temperature conditions had been modified sufficiently, mixing with the overlying hybrid liquid occurred and bronzitite, norite and anorthosite crystallized. Stage 7 in figure 6.1.

(viii) The final input of primitive Critical zone liquid (U6) occurred at the base of the Bastard Unit. Here however, no

assimilation of underlying anorthosite occurred, and only bronzite crystallized from the primitive liquid, and mixing occurred soon afterwards. The hybrid liquid which now mixed with the new primitive batch, had a considerable Main zone signature, which is most clearly manifested in the chemical attributes of the Giant Mottled Anorthosite.

It is likely that with each new pulse of Critical zone liquid, a certain amount of pre-existing residual material was entrained into the primitive pulse. It was from this material that low An-intercumulus plagioclase crystallized. This material also carried slightly higher incompatible element abundances.

It should be borne in mind that during each of the above stages, that a great number of complex physical processess were probably operative. For example, it is likely that the residual liquid column was stratified, and that double diffusive convection was occurring in each of the layers. Furthermore, important rheological factors, such as viscosity and density, probably controlled the mixture, or separation of different liquids.

CHAPTER 7: CONCLUSIONS.

The following points summarize the more important geological and geochemical features of the study section at Amandelbult.

1. The succession can be divided into a number of repetitive "Units", only two of which, namely the Merensky and the Bastard, appear to contain the full spectrum of rock types possible in any unit. The others lack upper, intermediate or basal members of the sequence harzburgite and/or pyroxenite-melanorite-norite-leuconorite-anorthosite.

2. Considerable lateral stratigraphic variations occur, but these are restricted to the sequence between the base of the Lower Pseudo Reef and the base of the Merensky Reef. Pothole features also occur only within this interval.

3. The rocks of the study section may be classified in terms of the relative abundances of their cumulus mineral constituents according to an existing I.U.G.S. scheme and, more rigidly, using chemical criteria based on normative data calculated from whole-rock analyses.

4. The presence of annealed anorthosites immediately below ultramafic layers, and the presence of undulatory contacts between these members in the Pseudo, Footwall and Merensky Units indicates that the ultramafic layers of each of these Units were probably intruded as hot liquids over pre-existing crystalline anorthositic floors, and that some remelting of this floor probably took place. This remelted material was then incorporated into the new, mafic liquid.

5. Variations in mineral chemistry through the succession indicate unique trends for each of the species investigated. Olivines exhibit wide chemical variations both within single layers and from one layer to the next. These variations are shown to reflect subsolidus re-equilibration processes with species such as chromite and sulphides, rather than being indicative of chemical distinctive mother-liquids. Ortho-pyroxenes exhibit well-defined fractionation trends through individual Units, particularly where such appear to be complete. Here Mg-rich values are recorded in basal members, and these become progressively Fe-rich upwards through the sequence. Primitive compositions are re-instated at the base of the next Unit. Plagioclase grains exhibit chemical variations of the opposite sense, with an upward increase in An content through Units. These grains also exhibit extreme chemical zonation patterns.

6. Whole-rock chemical variations, of most elements, exhibit pseudo-cyclical variaition patterns, which in fact represent changes in modal mineralogy rather than cryptic cycles. Through the use of selected interelement ratios, bona fide cyclical variations can be shown. Ratios of pyroxene-compatible elements such as Ni/Sc exhibit a sawtooth cyclical variation pattern through the uppermost three Units. Ratios of the plagioclase-compatible elements $Sr/Al_2O_3^*$ (see section 5.3.1) display a different form of cyclicity in which individual Units have near constant values, but succesive Units have uniquely different values.

7. Variations in the trace elements of an individual layer in several boreholes, indicate that there may be some evidence

for a fractionation trend from the southwest towards the northeast, but that a greater number of data points are required to show this convincingly.

8. Sudden changes in the Cr/Al ratio of orthopyroxene and a reversed upward decrease in the An content of plagioclase, sets the Giant Mottled Anorthosite layer geochemically apart from other anorthosite layers in the succession. These parameters suggest that this member is closely akin to the Main Zone than its upper Critical Zone counterparts from the lower six Units.

APPENDIX A
X-Ray Flourescence Spectrometry

Rock samples were broken into match box-sized pieces using a rock splitter before being crushed in a mechanical jaw crusher, and then milled to a fine powder in a swing mill. The grain size of this powder was reduced to -300 mesh in an automatic pestle and mortar. Five grams of this material was then compressed to 12 tons pressure to make a "pressed-powder-briquette", on which trace element and sodium analyses were carried out. A further two grams was accurately weighed, heated in an oven at 110 ^{o}C for six hours, and then reweighed. Weight loss after this procedure was recorded as H_2O^-. Each sample was then heated in a furnace at 1000 ^{o}C for 8 hours, and subsequent mass changes were recorded as LOI (loss on ignition). 0.28 grams of this material was then accurately weighed out (to five decimal places of a gram) and mixed with 1.5 grams of lithium tetraborate flux. This mixture was melted in Pt-Au alloy crucibles, at high temperatures. While still molten it was poured onto an aluminium disc and compressed and rapidly quenched, to form Norrish and Hutton (1969) fusion discs. Two discs were prepared per sample, and these were analysed for major elements.

The instrumental settings used on the Phillips 1410 X-ray spectrometer are summarized in the table below. Mass absorption coefficients were determined using the Mo-compton/Fe-K-alpha technique described by Nesbitt et al. (1976). Standard calibration and data reduction was achieved by using computer programs available on XRFFILE on the Rhodes University Cyber main frame computer. These programs allow for

position, dead-time and background corrections, instrumental drift and spectral line interferences.

Calibration curves were determined from the following international and in-house standards.

Major elements	-	NIM-N, BCR, GSP, AGV, DTS, G-2.
Na	-	G-2, PCC, BCR, AGV, GSP, NIM-G.
Zn, Cu, Ni	-	PCC, BHVO, DTS, BCR, AGV.
Sc	-	BCR, AGV, GSP, NIM-N.
Co, Cr, V	-	QLO, PCC, SDC, BHVO, KRF-13, BCR.
Rb, Sr, Zr, Y	-	BCR, G-2, S-12, AGV, SDC.
MAC`s	-	DTS, BHVO, GSP, BCR, G-2, AGV.

Table A Running conditions used for the various X.R.F. analyses

ELEMENT	TUBE	kV	MA	CRYSTAL	TIME (SECS)	COUNTER	COLLIMATOR	SPECIMEN
Si	Cr	55	40	PET	40	flow	coarse	fusion disc
Ti	Cr	55	40	LiF(200)	10	flow	fine	fusion disc
Al	Cr	55	40	PET	40	flow	coarse	fusion disc
Fe	Cr	55	40	LiF(200)	20	flow	fine	fusion disc
Mn	Cr	55	40	LiF(200)	20	flow	coarse	fusion disc
Mg	Cr	55	40	TLAP	100	flow	fine	fusion disc
Ca	Cr	55	40	LiF(200)	10	flow	fine	fusion disc
Na	Cr	55	40	TLAP	100	flow	fine	powder pellet
K	Cr	55	40	LiF(200)	10	flow	fine	fusion disc
P	Cr	55	40	Ge	20	flow	coarse	fusion disc
Sr	W	55	40	LiF(220)	200	scint.	fine	powder pellet
Rb	W	55	40	LiF(220)	200	scint.	fine	powder pellet
Zr	W	55	40	LiF(220)	200	scint.	fine	powder pellet
Y	W	55	40	LiF(220)	200	scint.	fine	powder pellet
Co	W	55	40	LiF(220)	200	flow	fine	powder pellet
Cr	W	55	40	LiF(220)	200	flow	fine	powder pellet
V	W	55	40	LiF(220)	200	flow	fine	powder pellet
Zn	Mo	55	40	LiF(220)	200	flow + scint.	fine	powder pellet
Cu	Mo	55	40	LiF(220)	200	flow + scint.	fine	powder pellet
Ni	Mo	55	40	LiF(220)	200	flow + scint	fine	powder pellet
Sc	Cr	55	40	LiF(200)	200	flow	fine	powder pellet

Table B: Whole rock major element analyses for samples from borehole AE, including LOI and H_2O^-.

SAMPLE NO:	AL-1	AL-2	AL-3	AE-4	AL-5		AL-6	AL-7	AE-8	AE-9
ALL FE AS FE2O3										
SIO2	50.09	50.93	51.19	50.08	50.03	.00	51.16	46.42	49.47	50.42
TIO2	.100	.125	.097	.044	.104	.000	.099	.117	.119	.135
AL2O3	28.79	28.07	29.38	29.89	29.12	.00	29.50	28.57	28.10	29.28
FE2O3	2.08	2.21	2.09	1.89	2.02	.00	2.71	2.62	3.90	3.15
MNO	.03	.03	.03	.03	.03	.00	.04	.03	.06	.04
MGO	2.50	2.42	2.14	1.81	1.59	.00	2.40	2.70	5.03	7.84
CAO	13.20	12.83	13.34	14.05	14.75	.00	13.85	14.03	13.28	11.84
NA2O	2.33	2.13	2.29	2.69	2.31	.00	2.35	1.91	1.85	1.66
K2O	.25	.26	.21	.23	.26	.00	.25	.20	.22	.21
P2O5	.03	.06	.00	.06	.06	.00	.00	.05	.06	.06
LOI	.973	.052	.127	.165	.130	.000	.048	.092	.074	-.054
H2O	.07	.07	.07	.06	.06	.00	.04	.03	.06	.05
	99.97	100.40	102.06	101.22	101.05	.00	102.60	99.04	100.19	100.61

SAMPLE NO:	AE-10	AL-11	AE-12	AL-13	AL-14	AE-15	AL-16	AL-17	AE-17A	AE-17B
ALL FE AS FE2O3										
SIO2	51.73	52.04	51.52	54.10	54.65	54.03	46.76	49.56	49.68	49.31
TIO2	.163	.165	.104	.262	.250	.218	.096	.059	.051	.075
AL2O3	17.62	17.45	19.32	7.45	8.14	5.01	23.10	31.33	31.62	27.41
FE2O3	8.10	8.07	8.02	10.32	10.75	11.42	8.04	1.17	1.07	2.01
MNO	.21	.21	.14	.20	.20	.21	.06	.01	.03	.04
MGO	11.44	11.43	17.00	23.28	22.77	23.30	7.34	1.09	1.07	3.33
CAO	10.19	9.26	7.10	4.07	4.04	3.37	11.00	13.07	14.81	13.03
NA2O	1.90	1.98	1.07	.25	.79	.73	1.01	2.13	2.08	1.99
K2O	.27	.27	.06	.03	.24	.22	.18	.13	.18	.18
P2O5	.03	.05	.09	.05	.05	.17	.04	.05	.05	.05
LOI	-.063	-.225	.913	-.272	.132	-.242	.084	.300	.211	.122
H2O	.07	.13	.04	.07	.07	.04	.04	.06	.08	.06
	101.25	101.32	100.65	100.76	100.95	100.47	100.83	101.26	100.91	98.85

SAMPLE NO:	AE-20	AL-21	AE-23	AE-24	AL-25	AE-26	AE-27	AL-28	AL-29	AE-30
ALL FE AS FE2O3										
SIO2	50.01	49.62	50.62	51.29	50.42	52.29	49.46	49.48	49.40	49.69
TIO2	.074	.119	.079	.127	.249	.242	.112	.093	.065	.068
AL2O3	28.44	27.47	28.27	17.34	9.38	5.48	9.75	30.65	29.37	29.80
FE2O3	3.27	2.07	3.91	7.04	11.40	12.58	12.27	2.00	1.79	2.11
MNO	.09	.22	.07	.12	.21	.22	.16	.03	.05	.03
MGO	4.79	4.04	7.03	13.36	22.77	23.36	23.32	1.68	2.07	2.27
CAO	12.23	12.92	11.77	9.44	9.42	5.44	5.40	14.23	14.23	13.66
NA2O	1.84	2.21	2.10	1.93	.63	.00	.05	2.29	2.16	1.97
K2O	.18	.17	.23	.10	.20	.15	.18	.17	.17	.19
P2O5	.01	.02	.01	.05	.07	.05	.05	.00	.05	.02
LOI	.102	.049	.060	-.108	.025	-.123	2.545	.272	.128	.117
H2O	.05	.05	.03	.09	.05	.03	.21	.06	.05	.06
	100.17	100.14	99.41	100.83	100.35	99.20	99.76	101.26	99.70	100.17

SAMPLE NO:	AL-31	AE-32	AE-33	AL-34	AL-35	AL-36	AL-37	AE-38	AE-39
ALL FE AS FE2O3									
SIO2	48.73	49.04	48.98	48.57	50.40	49.17	50.74	49.77	49.90	50.40
TIO2	.074	.101	.061	.072	.120	.099	.101	.078	.100	.141
AL2O3	30.71	31.45	30.17	28.93	21.71	30.66	21.57	29.20	10.28	11.01
FE2O3	1.49	1.40	2.48	2.00	4.65	1.51	5.04	4.05	7.03	9.22
MNO	.03	.02	.04	.03	.04	.03	.04	.06	.15	.16
MGO	1.25	1.21	3.46	3.01	9.22	1.24	9.45	7.75	15.32	14.71
CAO	13.41	13.77	13.54	13.60	10.81	13.00	10.24	12.11	8.45	8.57
NA2O	2.18	1.71	1.96	2.01	1.61	2.17	1.60	1.54	1.30	1.26
K2O	.19	.19	.18	.17	.17	.20	.14	.13	.13	.11
P2O5	.02	.01	.00	.06	.05	.08	.05	.05	.05	.06
LOI	.106	.171	.141	.015	.243	.241	.040	.503	1.040	.161
H2O	.05	.00	.07	.11	.10	.07	.06	.04	.22	.04
	98.78	100.05	100.76	99.37	99.86	101.00	100.34	100.45	100.03	100.15

Table B

SAMPLE NO:	AE-40	AE-41	AE-42	AE-43	AE-44A	AE-44B	AE-45	AE-46	AE-47	AE-48A
ALL FE AS FE2O3										
SIO2	43.28	[illegible]	44.12	46.43	46.59	44.58	46.85	44.07	44.14	46.44
TIO2	.167	.268	.064	.059	.058	.074	.060	.062	.064	.054
AL2O3	4.11	[illegible]	27.86	31.47	31.74	30.66	30.54	29.68	29.04	28.75
FE2O3	14.60	15.62	2.43	1.34	1.06	1.62	1.38	1.49	1.44	2.64
MNO	.21	.21	.06	.03	.03	.04	.03	.03	.04	.06
MGO	32.64	[illegible]	9.22	1.41	.44	2.23	1.61	2.03	2.09	9.24
CAO	3.75	3.12	13.28	14.05	14.02	14.46	14.35	13.42	14.24	13.72
NA2O	.54	.27	2.07	2.04	2.06	2.07	2.03	2.01	1.94	1.73
K2O	.11	.16	.10	.15	.16	.14	.15	.15	.15	.14
P2O5	.05	.03	.05	.05	.05	.05	.05	.05	.05	.03
LOI	.419	.409	.342	.136	.217	.116	.291	.290	.296	1.803
H2O	.21	.23	.03	.06	70.00	.05	.06	.06	.08	.14
	100.16	[illegible]	100.20	100.29	104.74	101.39	99.49	98.73	100.31	100.41

SAMPLE NO:	AE-49B	AL-50	AL-50	AE-51	AL-52	AL-53	AE-54	AE-55	AL-56	AE-58
ALL FE AS FE2O3										
SIO2	40.34	52.24	53.03	54.75	54.76	53.56	50.39	47.99	54.68	54.34
TIO2	.072	.162	.202	.259	.269	.225	.277	.194	.247	.215
AL2O3	5.27	[illegible]	9.79	9.53	9.60	8.41	8.47	9.99	9.74	9.67
FE2O3	15.79	[illegible]	11.99	11.48	12.23	11.97	12.03	14.35	12.42	12.17
MNO	.19	.20	.21	.21	.22	.23	.21	.23	.23	.21
MGO	24.81	[illegible]	23.42	22.58	23.56	22.70	23.39	20.30	22.03	23.35
CAO	2.50	[illegible]	3.09	3.05	3.24	4.75	3.27	3.93	4.47	3.06
NA2O	.25	.76	2.18	.77	.80	.75	.58	.50	.85	.07
K2O	.09	.20	.26	.22	.32	.14	.07	.09	.11	.16
P2O5	.03	.05	.03	.03	.03	.17	.04	.03	.05	.05
LOI	4.432	.078	.231	-.300	-.452	-.499	-.341	-.062	-.475	-.124
H2O	.09	.13	.05	.05	.05	.05	.08	.02	.03	.08
	99.36	[illegible]	101.29	99.43	100.15	99.66	97.86	98.12	99.76	100.25

SAMPLE NO:	AE-59	AL-60	AL-61	AL-62	AL-63	AL-64	AE-65	AE-67A	AE-67B	AE-68
ALL FE AS FE2O3										
SIO2	54.60	55.17	54.74	53.76	53.58	54.42	46.54	44.67	50.40	46.54
TIO2	.267	.260	.230	.265	.168	.165	.048	.053	.062	.046
AL2O3	[illegible]	[illegible]	9.43	9.23	[illegible]	8.47	31.72	31.92	27.36	31.61
FE2O3	12.83	12.12	12.14	12.03	12.18	12.21	1.60	.65	2.77	.56
MNO	.23	.22	.21	.27	.22	.21	.03	.03	.04	.03
MGO	23.51	23.26	22.17	23.04	23.08	24.22	.98	.75	4.52	.75
CAO	4.68	3.97	5.68	4.09	5.71	5.73	14.32	14.77	13.21	14.27
NA2O	.63	.63	.71	.51	.69	.64	2.10	2.18	1.63	2.19
K2O	.21	.27	.27	.21	.06	.07	.15	.17	.14	.23
P2O5	.06	.07	.09	.05	.05	.03	.05	.03	.05	.05
LOI	-.373	-.265	-.291	.177	.060	-.023	.544	.447	1.506	.500
H2O	.07	.21	.01	.09	.05	.09	.07	.05	.09	.08
	100.92	100.01	100.12	99.97	99.92	100.33	99.05	100.33	101.61	98.70

Table B (contd.)

APPENDIX B.

Electron Microprobe Analyses.

Microprobe analyses were carried out on Rhodes University`s new Jeol 733 Superprobe instrument. Highly polished thin sections were coated under vacuum to 250 angstroms with carbon. The thickness of this coat was monitored by observing the interference colours produced by the carbon on a polished brass strip.

The energy excitation potential of the microprobe was set at 15kv, while a beam current of 25nA was maintained. The beam current was continually monitored by reference to a Faraday cage. The instrument has four crystal spectrometers, two of which are gas flow counters, while the others are sealed xenon counters. Counting times of 30 seconds on element K-alpha peaks and 10 seconds on background positions on both sides of the peak were instituted for all elements.

Data reduction was achieved by using the PACX program supplied by the manufacturers of the instrument. This program applies the ZAF correction scheme, that is, an Atomic number (Z) correction using Philibert-Tixier`s formula, an Absorption (A) correction using Philibert-Heinrich`s formula and a Fluorescence (F) correction using Reed`s formula. See Philibert and Tixier (1968), and the Jeol Operations manual.

The instrumental settings and standards used for each of the three mineral species that were analysed, are presented the tables overleaf;

TABLE C . Instrumental settings and standards used for microprobe analyses

TABLE C.1. OLIVINE ANALYSES

ELEMENT	STANDARD	CRYSTAL	TYPICAL STANDARD C.P.S.
SiO_2	SiO_2 (U.K.)	TAP	25 245
MgO	MgO (U.K.)	TAP	22 338
CaO	Wollastonite (R.U.)	PET	6 310
NiO	NiO (U.K.)	LiF	3 925
FeO	Rhodonite (U.K.)	LiF	431
MnO	Rhodonite (U.K.)	PET	8 699

TABLE C.2. PYROXENE ANALYSES

ELEMENT	STANDARD	CRYSTAL	TYPICAL STANDARD C.P.S.
SiO_2	SiO_2 (U.K.)	TAP	25 337
TiO_2	TiO_2 (U.K.)	PET	10 852
Al_2O_3	Al_2O_3 (U.K.)	TAP	26 791
FeO	Rhodonite (U.K.)	LiF	439
Cr_2O_3	Cr_2O_3 (U.K.)	PET	33 516
MnO	Rhodonite (U.K.)	LiF	1 276
NiO	NiO (U.K.)	LiF	3 837
MgO	MgO (U.K)	TAP	22 560
CaO	Wollastonite (R.U.)	PET	6 227

Na_2O	Jadeite (R.U.)	TAP	1

TABLE C.3. PLAGIOCLASE ANALYSES

ELEMENT	STANDARD	CRYSTAL	TYPICAL STANDARD
SiO_2	SiO_2 (U.K.)	TAP	25 08
Al_2O_3	Al_2O_3 (U.K.)	TAP	26 59
FeO	Rhodonite (U.K.)	LiF	431
CaO	Wollastonite (R.U.)	PET	6 30
Na_2O	Omphacite (R.U.)	TAP	576
K_2O	Orthoclase (R.U.)	PET	1 77

Note:- The standards denoted (U.K.) were obtained from Polarqn Equipment limited, Watford, England, while those denoted (R.U.) are Rhodes University in-house standards which have acquired fr various operating laboratories, and are well characterized.

REFERENCES.

Atkins, F.B. (1969) Pyroxenes of the Bushveld Complex Intrusion, South Africa. J.Pet., 10, 222-249.

Atkins, P.W. (1979). Physical chemistry. Oxford University Press, Oxford. 1022pp.

Barnes, S.J. and Naldrett, A.J. (1985). Geochemistry of the J-M (Howland) reef of the Stillwater Complex, Minneapolis adit area. I. Sulfide chemistry and sulphide-olivine equilibrium. Econ.Geol., 80, 627-645.

Biesheuvel, K. (1970). An interpretation of a gravimetric survey in the area west of the Pilansberg in the western Transvaal. geol.Soc.S.Afr.Spec. Publ., 1, 266-283.

Buntin, T.J., Grandstaff, D.E., Ulmer, G.C. and Gold, D.P. (1985). A pilot study of geochemical and redox relationships between potholes and adjacent normal Merensky reef of the Bushveld Complex. Econ.Geol., 80, 975-987.

Burns, R.G and Fyfe, W.S. (1966). Behaviour of nickel during magmatic crystallization . Nature, 210, 1147-1148.

Cameron, E.N. (1971). Problems of the eastern Bushveld Complex. Fortschr.Min., 48, 86-108.

Cameron, E.N. (1980). Evolution of the lower Critical zone, central sector eastern Bushveld Complex, and its chromite deposits. Econ.Geol., 75, 845-871.

Cameron, E.N. and Desborough, G.A. (1969). Occurrence and characteristics of chromite deposits- eastern Bushveld Complex. Econ.Geol.Monogr., 4, 23-40.

Campbell, I.H. (1978). Some problems with the cumulus theory. Lithos, 11, 311-323.

Campbell, I.H. and Borley, G.D. (1974). The geochemistry of pyroxenes from the lower layered series of the Jimberlana intrusion, Western Australia. Contrib. Mineral.Pet., 47, 281-297.

Campbell, I.H., Roeder, P.L. and Dixon, J.M. (1978). Plagioclase bouyancy in basaltic liquids as determined with a a centrifuge furnace. Conrib.Mineral.Pet., 67, 369-377.

Campbell, I.H., Naldrett, A.J., and Barnes, S.J. (1983). A model for the origin of the Pt-rich sulfide horizons in the Bushveld and Stillwater Complexes. J.Pet., 24, 133-165.

Cawthorn, R.G. and McCarthy, T.S. (1985). Incompatible trace element behaviour in the Bushveld Complex. Econ. Geol., 80, 1016-1026.

Cox, K.G., Bell, J.D. and Pankhurst, R.J. (1981). The interpretation of igneous rocks. George Allen and Unwin, London. 450pp.

Deer, W.A., Howie, R.A. and Zussman, J. (1963). Rock-forming minerals: Vol.4, framework silicates. Longmans, London. 435pp.

Deer, W.A., Howie, R.A. and Zussman, J. (1978). Rock-forming minerals: Vol.2A, single-chain silicates. 2nd Ed. Longmans, London. 668pp.

Deer, W.A., Howie, R.A., and Zussman, J. (1982). Rock-forming minerals : Vol.1A, orthosilicates. 2nd Ed. Longmans London. 919pp.

De Klerk, W.J. (1982). The geology, geochemistry and silicate mineralogy of the upper Critical zone of the Bush-

veld Complex at Rustenburg Platinum Mines, Union Section. M.Sc. thesis (unpubl.), Rhodes Univ., Grahamstown.

De Long, S.E. (1974). Distribution of Rb, Sr and Ni in igneous rocks, central and western Aleutian islands, Alaska Geochim. Cosmochim. Acta., 38, 245-266.

Drake, M.J. (1975). Partition of Sr, Ba, Ca, Y, Eu2+, Eu3+ and other REE between plagioclase feldspar and magmatic liquid: an experimental study. Geochim. Cosmochim. Acta., 39, 689-712.

Duke, J.M. (1976). Distribution of the period four transition elements among olivine, calcic clinopyroxene and mafic silicate liquid: experimental results. J.Pet., 17, 499-521.

Eales, H.V. and Reynolds, I.M. (1986). Cryptic variations within chromitites of the upper Critical zone, northwestern Bushveld Complex. Econ.Geol. 81, (in press).

Eales, H.V., Marsh, J.S., Mitchell, A.A., De Klerk, W.J., Kruger, F.J. and Field, M. (in press, a). Some geochemical constraints upon models for the crystallization of the upper Critical zone- Main zone interval, northwestern Bushveld Complex. Min. Mag., (in press)

Eales, H.V., Field, M., De Klerk, W.J. and Scoon, R.N. (in press, b). Geochemical features and comparison of the upper Critical Zone sequences at R.P.M. Union and Amandelbult Sections, northwestern Bushveld : A preliminary assessment.

Engelbrecht, J.P. (1985). The chromitites of the Bushveld Complex in the Nietverdiend area. Econ.Geol., 80, 896-924.

Evans, B.R. and Wright, T.L. (1972). Composition of liquidus chromite from the 1959 and 1965 eruptions of Kilauea volcano, Hawaii. Amer.Min., 57, 217-230.

Ewart, A., Bryan, W.B. and Gill, J.B. (1973). Mineralogy and geochemistry of the younger volcanic islands of Tonga, S.W. Pacific. J.Pet., 14, 429-465.

Ferguson, J. and Wright, J. (1970). Composition variation of plagioclase in the Critical series, Bushveld Complex: In, Visser, D.J.L. and von Gruenewaldt, G. (eds), Symposium on the Bushveld Igneous Complex and other layered intrusions. geol.Soc.S.Afr.Spec.Publ., 1, 59-66.

Flower, M.J. (1973). Trace element distribution in lava flows from Anjouan and Grande Comore, western Indian ocean Chem.Geol., 12, 81-98.

Frey, F.A., Green, D.H. and Roy, S.D. (1978). Intergrated models for basalt petrogenesis: a study of quartz tholeiite to olivine melilitites from southeastern Australia, utilizing geochemical and experimental petrological data. J.Pet., 19, 463-513.

Hall, A.L. (1932). The Bushveld igneous complex of the central Transvaal. S.Afr.Geol.Surv.Mem. No. 28.

Hamilton, P.J. (1970). Bushveld Complex - product of impacts? Spec.Publ. geol.Soc.S.Afr., 1, 367-379.

Hanson, G.N. (1977). Geochemical evaluation of the suboceanic mantle. J.Geol.soc.Lond., 134, 235-253.

Harmer, R.E. and Sharpe, M.R. (1985). Field relations and strontium isotope sytematics of the marginal rocks of the eastern Bushveld Complex. Econ.Geol., 80, 813-837.

Hart, S.R. and Brooks, C.J. (1977). The geochemistry and evolution of the Precambrian Mantle. Contrib. Mineral. Petrol., 61, 109-128.

Hart, S.R and Davis, K.E. (1978). Nickel partitioning between olivine and silicate melt. Earth Planet. Sci. Lett., 40, 203-219.

Hattingh, P.J. (1984). The paleomagnetism of the Merensky reef footwall rocks. Institute for geological research on the Bushveld Complex, University of Pretoria. Research report No. 52, 23pp.

Hattingh, P.J. (1986). The paleomagnetism of the Main zone of the eastern Bushveld Complex. Tectonophysics, 124, 271-295.

Henderson, P. (1968) The distribution of phosporus in the middle stages of fractionation of some basic layered intrusions. Geochim. Cosmochim. Acta., 32, 897-911.

Hunter, D.R. (1976). The regional setting of the Bushveld Complex. Econ. Geol. Res. Unit, Univ. Witwatersrand, Johannesburg.

Hunter, D.R. and Hamilton, P.J. (1978). The Bushveld complex: In, Tarling, D.H. (ed), The evolution of the earth's crust. Academic press. London, 107-172.

Irvine, T.N. (1974). Chromitite layers in stratiform intrusions. Carnegie Inst. Washington, Yearbook, 73, 300-316.

Irvine, T.N. (1975). Crystallization sequences in the Muskox intrusion and other layered intrusions: II. Origin of chromitite layers and similar deposits of other magmatic ores. Geochim. Cosmochim. Acta., 39, 991-1020.

Irvine, T.N. (1977). Origin of chomite layers in the Muskox intrusion and other stratiform intrusions, a new interpretation. Geology, 5, 273-277.

Irvine, T.N. (1980a). Magmatic infiltration metasomatism, double-diffusive fractional crysallization, and adcumulus growth in the Muskox intrusion and other layered intrusions: in, Hargreaves, R.B. (ed). Physics of magmatic processes. Priceton. Univ. Press, 325-383.

Irvine, T, N. (1980b). Magmatic density currents and cumulus processes. Amer. J. Sci., 280, 1-58.

Irvine, T.N. (1982). Terminology for layered intrusions. J. Pet., 23, 127-162.

Irvine, T.N., Keith, D.W. and Todd, S.G. (1983). The J-M Pt-Pd reef of the Stillwater complex, Montana: II. Origin by double-diffusive convective magma mixing, and implications for the Bushveld Complex. Econ. Geol., 78, 1287-1330.

Irvine, T.N. and Baragar, W.R.A. (1971). A guide to the chemical classification of the common volcanic rocks. Can. J. Earth. Sci., 8, 523-548.

Irving, A.J. (1978). A review of experimental studies of crystal/liquid trace element partitioning. Geochim. Cosmochim. Acta., 42, 743-770.

Jackson, E.D. (1969). Chemical variation in coexisting chromite and olivine in chromitite zones of the Stillwater Complex. Econ. Geol. Monogr., 4, 41-71.

Jensen, B.B. (1973). Patterns of trace element partitioning. Geochim. Cosmochim. Acta., 37, 2227-2242.

Kelsey, C.H. (1965). Calculation of the C.I.P.W. norm. Min. Mag., 34, 276-282.

Kerr, R.C. and Tait, S.R. (1985). Convective exchange between pore fluid and an overlying resevoir of denser

fluid: a postcumulus process in layered intrusions. Earth.PLanet.Sci.Lett., 75, 147-156.

Kruger,F.J.(1983). The petrology of the Merensky cyclic unit and associated rocks and their significance in the evolution of the western Bushveld Complex. Ph.D thesis (unpub.), Rhodes Univ., Grahamstown.

Lee,C.A.(1983). Trace element and platinum-group element geochemistry, and the development of the Merensky unit of the western Bushveld Complex. Mineralium Deposita, 18, 173-190.

Lee,C.A. and Sharpe,M.R.(1986). The stuctural setting of the Bushveld Complex - an assessment aided by Landsat imagery. In Anhausser,C.R. and Maske,S. (eds), Mineral deposits of southern Africa, Vol II, geol. Soc.S.Afr.

Leeman,W.P. and Lindstrom,D.J.(1978). Partitioning of Ni2+ between basaltic and synthetic melts and olivines: an experimental study. Geochim.Cosmochim.Acta., 42, 801-816.

Lindstrom,D.J. and Weill,D.F.(1978). Partitioning of transition metals between diopside and coexisting silicate liquids: I. Nickel, cobalt and manganese. Geochim. Cosmochim., 42, 817-832.

Liebenberg,L.(1970). The sulphides in the layered sequence of the Bushveld Igneous Complex: In Visser,D.J.L. and von Gruenewaldt,G.(eds), Symposium on the Bushveld Igneous complex and other layered complexes. Geol. Soc.S.Afr.Spec.Publ., 1, 108-207.

Maaloe.S.(1976). The zoned plagioclase of the Skaergaard intrusion, east Greenland. J.Pet., 17, 398-419.

Maclean,W.H. and Shimizaki,H.(1976). The partition of Co, Ni, Cu and Zn between sulfide and silicate liquids. Econ. Geol., 71, 398-419.

McBirney,A.R. and Noyes,R.M.(1979). Crystallization and layering of the Skaergaard intrusion. J.Pet., 20, 487-554.

Molyneux,T.G. and Klinkert,P.S.(1978). A structural interpretation of part of the eastern mafic lobe of the Bushveld Complex and its surrounds. Trans. geol.Soc.S.Afr., 81,359-368.

Morse,S.A.(1979). Influence of augite on plagioclase fractionation. J.Pet., 87, 202-208.

Morse,S.A.(1982). Kiglapait geochemistry, V: strontium. Geochim.Cosmochim.Acta., 46, 223-234.

Morse,S.A. and Nolan,K.M.(1984). Origin of strongly reversed rims on plagioclase in cumulates. Earth.Planet.Sci. Lett., 68, 485-498.

Morse,S.A. and Nolan,K.M.(1985) Kiglapait geochemistry VII: yttrium and rare earth elements. Geochim.Cosmochim. Acta., 49, 1621-1644.

Naldrett,A.J., Gasparrini,E.C., Barnes,S.J., von Greunewaldt,G. and Sharpe,M.R.(1986) The upper Critical zone of the Bushveld Complex and origins of Merensky-type ores. Institute for geological research on the Bushveld complex, Univ.Pretoria, Research report No. 60, 30pp.

Nesbitt,R.W, Mastings,H., Stolz,G.W. and Bruce,D.R.(1976). Matrix corrections in trace element analysis by X-ray fluoresence: an extension of the Compton scattering technique to long wavelengths. Chem. Geol., 18, 203-213.

Norrish, K. and Hutton, J.T. (1969). An accurate x-ray spectrographic method for the analysis of a wide range of geological samples. Geochim. Cosmochim. Acta, 33, 431-453.

Paster, T.P., Schauwecker, D.S. and Haskin, L.A. (1974). The behaviour of some trace elements during solidification of the Skaergaard layered series. Geochim. Cosochim. Acta., 38, 1549-1577.

Pearce, J.A. and Norry, M.J. (1979). Petrogenetic implications of Ti, Zr, Y and Nb variations in volcanic rocks. Contrib. Minerl. Petrol., 69, 33-47.

Philibert, J. and Tixier, R. (1968). Brit. J. App. Phys., 1685-1964.

Phillips, D. (1984). Mineralogy and petrography of the Townlands iron-rich ultramafic pegmatite. M.Sc thesis (unpubl.), Rhodes Univ., Grahamstown.

Philpotts, J.A. and Schnetzler, C.C. (1970). Phenocryst-matrix partition coefficients for K, Rb, Sr and Ba with applications to anorthosite and basalt genesis. Geochim. Cosmochim. Acta., 34, 307-332.

Pretorius, D.A. (1973). The crustal architecture of southern Africa. A.L. du Toit Memorial Lecture No. 13, Annex. Trans. geol. Soc. S. Afr., 76, 60pp.

Rhodes, R.C. (1975). New evidence for impact origin of the Bushveld Complex. Geology, 3, 549-554.

Ringwood, A.E. (1956). Melting relationships of Ni-Mg olivines and some geochemical implications. Geochim. Cosmochim. Acta., 10, 297-303.

Ringwood, A.E. (1970). Petrogenesis of Apollo 11 basalts and implications lunar origin. J. Geophys. Res., 75, 6453-6479.

Roeder, P.L., Campbell, I.H. and Jamieson, H.E. (1979). A re-evaluation of the olivine-spinel geothermometer. Contrib. Min. Pet., 68, 325-334.

Salpas, P.A., Haskin, L.A. and McCallum, I.S. (1983). Stillwater anorthosites: a lunar analogue? J. Geophys. Res., 88, suppl. B27-B39.

Scoon, R.N. (1985). Discordant bodies of postcumulus, ultramafic rock in the upper Critical zone of the Bushveld Complex: iron-rich ultramafic pegmatite bodies at Amandelbult and the Driekop platiniferous ultramafic pipe. Ph.D thesis (unpubl.), Rhodes Univ., Grahamstown.

Scoon, R.N. and De Klerk, W.J. (in press). The relationship between olivine cumulates, mineralization and cyclic units in the upper Critical zone of the northwestern Bushveld complex.

Sharpe, M.R. (1985). Strontium isotope evidence for preserved density stratification in the Main Zone of the Bushveld Complex. Nature, 316, 119-126.

Sharpe, M.R. and Snyman, J. (1980). A model for the emplacement of the eastern compartment of the Bushveld Complex. Tectonophysics, 65, 85-110.

Smith, J.V. (1974). Feldspar minerals. Vol. 2, chemical and textural properties. Springer-Verlag, Berlin, Heidelberg, New York, 690pp.

Smit, P.J., Hales, A.L. and Gough, D.I. (1962). The gravity survey of the Republic of South Africa. Geol. Surv. S. Afr. Handb., 3, 354pp.

South African Committee for Stratigraphy (SACS) (1980). Stratigraphy of South Africa. Part 1. Geol. Surv. S. Afr. Handb. 8, 223-241.

Streckeisen, A. (1976). To each plutonic rock its proper name. Earth. Sci. Rev., 12, 1-23.
Sun, C. O., Williams, R. J. and Sun, S. S. (1974). Distribution coefficients of Eu and Sr for plagioclase-liquid and clinopyroxene-liquid equilibria in ocean ridge basalt - an experimental study. Geochim. Cosmochim. Acta., 38, 1415-1433.
Tankard, A. J., Jackson, M. P. A., Erikson, K. A., Hobday, D. K., Hunter, D. R. and Minter, W. E. L. (1982). Crustal evolution of southern Africa. Springer-Verlag, New York, 523pp.
Truter, F. C. (1955). Modern concepts of the Bushveld Igneous Complex. C. C. T. A. South Reg. Com. Geol., 1, 77-92.
Van Biljon, W. J. (1976). Goud is nie waar dit gevind word nie. Trans. geol. Soc. S. Afr., 79, 155-167.
Vermaak, C. F. (1976). The Merensky reef- thoughts on its environment and genesis. Econ. Geol., 71, 1270-1298.
Vermaak, C. F. and Hendriks, L. P. (1976). A review of the mineralogy of the Merensky reef, with specific reference to new data on the precious metal mineralogy. Econ. Geol., 71, 1244-1269.
Viljoen, M. J. and Scoon, R. N. (1985). The distribution and main geological features of discordant bodies of iron-rich pegmatite in the Bushveld Complex. Econ. Geol., 80, 1109-1128.
Viljoen, M. J., Theron, J., Underwood, B., Walters, B., Weaver, I. and Peyerl, W. (1986). The Amandelbult section of Rustenburg Platinum Mines Limited, with reference to the Merensky Reef. In; Anhaeusser, C. R. and Maske, S., Geol. Soc. S. Afr. Spec. Publ., 12, 1041-1060.
von Gruenewaldt, G. (1979). A review of some recent concepts of the Bushveld, with particular reference to sulphide mineralization. Can. Min., 17, 223-256.
Wager, R. L. and Brown, G. M. (1968). Layered igneous rocks. Oliver and Boyd, London, 588pp.
Wager, R. L and Mitchell, R. L. (1951). The distribution of trace elements during strong fractionation of basic magma. Geochim. Cosmochim. Acta., 1, 129-270.
Wager, R. L, Brown, G. M. and Wadsworth, W. J. (1960). Types of igneous cumulates. J. Pet., 1, 73-85.
Walker, K. R. (1970). The Palisade sill, New Jersey. A reinvestigation. Geol. Soc. Amer. Spec. paper, 111, 178.
Walraven, R. and Darracott, B. W. (1976). Quantitative interpretation of a gravity profile across the western Bushveld Complex. Trans. geol. Soc. S. Afr., 79, 22-26.
Wells, A. K. (1952). Textural features of some Bushveld norites. Min. Mag., 29, 913-924.
Willemse, J. (1969). The geology of the Bushveld igneous complex, the largest repository of magmatic ore deposits in the world. Econ. Geol. Monogr., 4, 1-22.

ACKNOWLEDGEMENTS

The author would like to thank the following organizations and persons, without whom this thesis would never have come to fruition.

Johannesburg Consolidated Investment Company is thanked for allowing access to their property, and making available costly core material. The Council for Scientific and Industrial Research is thanked for providing funds, and for organizing the yearly C.S.P. meetings, at which a great deal was learnt.

Professor Hugh Eales is thanked for involving the author in the project, and for his never-ending source of encouragement during the course of the research. The other staff members of the Geology Department at Rhodes University, particularly Dr Goonie Marsh, Dr Ivan Reynolds and Mr Rob Skae, who assisted greatly with analytical techiques and computer applications, are also thanked. Colleague Billy De Klerk is thanked for his assistance, particularly in the field, where his intimate knowledge of the western Bushveld proved to be invaluable.

Thanks are also extended to all the undergraduate students who helped with sample preparation and XRF analyses, while Faried Joseph and John Gillam are thanked for developing and printing photographs. Finally the author would also like to thank his wife, Michelle for her patience and encouragement.